SHOCK-WAVE STRUCTURE IN AN IONIZED GAS

A THESIS

Presented to

The Faculty of the Graduate Division

by

Chien - Shiong Lu

In Partial Fulfillment

of the Requirements for the Degree

Doctor of Philosophy

in the School of Aerospace Engineering

Georgia Institute of Technology

July, 1971

SHOCK-WAVE STRUCTURE IN AN IONIZED GAS

Approved:

Chairman

Date approved by Chairman: Aug. 13, 1971

ACKNOWLEDGMENTS

I would like to express my deepest gratitude to Dr. A. Ben Huang, my thesis advisor, for his constructive guidance, invaluable criticism, and continuing assistance throughout the duration of the study.

My sincere appreciation is extended to Dr. D. P. Giddens for his encouragement, fruitful discussions, and friendship during my doctorate program in the School of Aerospace Engineering.

Special thanks go to Dr. M. P. Stallybrass for his libral contributions of time spent in reading the manuscript and in discussing problems in applied mathematics.

I am grateful to Mr. P. F. Hwang for discussions on the "new quadrature" as well as problems related to kinetic theory. I thank Mr. R. Srinivasan, Mr. W. R. Lawrence, Mr. H. F. Barbarika, and Mr. Victor Y. C. Young for their assistance in their individual ways.

Special thanks go to Mrs. Mattie Jo Sims for her deligent and expedient typing of the entire manuscript.

Funds for this work were provided by the National Aeronautics and Space Administration through grant NGL 11-002-062.

I thank my mother, Mrs. Fong-Shiang Lu, for her guidance, encouragement, and unselfish sacrifice in helping me pursue my education. My appreciation is also extended to Dr. and Mrs. K. H. Chang for their help and encouragement. Finally, I wish to thank my wife Hue-Shiang for her constant encouragement, understanding, patience, assistance, and unselfish sacrifice.

TABLE OF CONTENTS

LIST OF TABLES

Table Page

Table Page

LIST OF ILLUSTRATIONS

Figure Page

Figure Page

Figure Page

Figure Page

LIST OF SYMBOLS

a_x	acceleration or deceleration in x-direction
C_p	specific heat at constant pressure
E	electric field
e	electric charge
F	local Maxwellian equilibrium distribution function
F'_{13}	local Maxwellian equilibrium distribution function, defined by Equation (7) in Chapter V
f	local distribution function
g	reduced distribution function
G	reduced equilibrium distribution function
h	reduced distribution function, or enthalpy
H	reduced equilibrium distribution function
H(x)	Heaviside function
k	Boltzmann constant
I	location in physical space
J	location in velocity space
L	reference length
L*	reference length
M	Mach number
m	mass of a particle
n	number density
n'	number density, defined by Eq. (8-a) in Chapter V
p	pressure

P_B probability due to Bleakney [41]

P_I ionization probability

Q collision cross section

R gas constant

t time

T temperature

T'_{13} temperature, defined by Eq. (8-b) in Chapter V

$T_a(0)$ atom temperature at downstream of a frozen shock

u macroscopic velocity in x-direction

V most probable velocity

$\vec{v}$ microscopic velocity with components v_x, v_y, v_z

v_o electron speed corresponding to ionization potential of a neutral particle

W weighting coefficients

x x-direction in physical space

α degree of ionization

β mass ratio, $(m_e/m_i)^{\frac{1}{2}}$

β_{13} inverse thermal speed, $m_1/2kT_{13}$

γ ratio of specific heats

δ thermal conductivity

ϵ_o permitivity of vacuum

Λ quantity defined by Eq. (11) in Chapter II

λ_D Debye length

μ viscosity

ρ density

σ collision prarmeter

ν_{ij} collision frequency

ν_{13_I} collision frequency, $P_I n_3/\sigma_{13}$

$\hat{\xi}$ physical coordinate

τ relaxation time

Φ electrostatic potential

Superscripts

$\hat{}$ nondimensionalization by downstream equilibrium condition

$*$ characterization, or normalization by freestream condition

Subscripts

a neutral particles

e electrons

i ions or index number, 1, 2, 3 for electrons, ions, neutral particles, respectively

j index number, 1, 2, 3 for electrons, ions, neutral particles, respectively

k index number, 1, 2, 3 for electrons, ions, neutral particles, respectively

ℓ index number, 1, 2, 3 for electrons, ions, neutral particles, respectively

m mixture

p plasma

s index number 1, 2 for upstream, downstream, respectively

x x-direction in physical space

$()_2$ downstream equilibrium condition

0 stagnation condition

1 freestream condition

2	downstream equilibrium condition
∞	freestream condition

SUMMARY

The discrete ordinate method is applied to the solutions of a shock-wave structure in fully or partially ionized argon and the relaxation zone of a shock-wave. The effects of the electric field induced by the charge separation on the shock-wave structure are also investigated. The Boltzmann equations with a kinetic model type of collisions are employed as the governing equations. The present results are compared with limited experimental measurements and other theoretical treatments, either by continuum approaches or by the Mott-Smith method.

The findings of the present investigation may be summarized as follows:

In the shock structure of a fully ionized gas the ion temperature can exceed their downstream value. The temperature overshoot becomes greater as the Mach number increases. However, in a weak shock the overshoot of the ion temperature was not observed. The electron temperature follows the ion temperature very closely in a weak shock of a fully ionized gas. However, for a strong shock-wave the electron temperature rise preceeds the ion temperature during the compression process of the shock. The overshoot of the electron temperature was not observed in fully ionized gas. The present results agree well with the results obtained by the continuum approach for weak shocks. The discrete ordinate method gives smooth and continuous results for high Mach numbers. On the other hand the results from the continuum approach contain discontinuities in slope.

No overshoot of upstream velocity has been observed in the shock structure of a partially ionized gas with a frozen degree of ionization. Although the three species of an ionized gas travel with approximately the same macroscopic velocity, the individual distribution functions can be very different and distinguishable. In a strong shock the atom distribution function may have double peaks, while the ion distribution function has only one peak. The electron local Maxwellian distribution function can be considered as an approximation to its actual local distribution function for weaker shocks in both partially and fully ionized gases. Electrons are heated up much earlier than ions and atoms in a partially ionized gas. Because the interactions of electrons with atoms and with ions are different in nature, the ion temperature can be different from the atom temperature. Thus, it can be very misleading to group atoms and ions as a single species merely on the basis of their insignificant differences in mass. In other words, the contribution from other physical properties can be significant. For all cases investigated no undershoot of the upstream temperature has been found. The present results for neutral particles and electrons are generally in fairly good agreement with the continuum solutions at the low Mach number and with the Mott-Smith solutions at the high Mach number. However, it appears that the discrete ordinate method has the advantage over the Mott-Smith method and the continuum approach in obtaining the results for ions.

The induced electric field due to the charge separation in a shock structure tends to equilibrate the flow locally. However, these effects on the structure of a shock-wave are very insignificant for all cases investigated and can be neglected. Thus, the results obtained without

the consideration of the effects of the induced electric field give very good approximations. It has been experiences that when the E field effects are included in the kinetic model equations, the numerical accuracy and the capacity limitation in the available computer facility can cause a great deal of trouble in obtaining correct solutions.

The discrete ordinate method can yield reasonable results to the kinetic model equations for the structure of the relaxation zone if the shock Mach numbers are not very high. The local Maxwellian distribution functions can be used to approximate the actual local distribution functions of atoms, ions, and electrons in the relaxation zone where electrons are not as equilibrium as atoms and ions due to the ionizing effects. Only very slight ionization is generated in the early part of the relaxation zone, while most ionization occurs in the last one-third of the region. The ion temperature is about the same as the atom temperature in the entire relaxation zone. Both atom and ion temperatures drop sharply in the rear part of the relaxation zone where the electron temperature increases rapidly. The thickness of a frozen shock front is negligibly small in comparison with the thickness of its relaxation zone for the cases investigated.

In view of the results presented in this dissertation it is concluded that the discrete ordinate method has the consistency and the flexibility in dealing with plasmagasdynamic problems.

CHAPTER I

INTRODUCTION

Review of Recent Literature

The interest in the shock structure in ionized gases was stimulated by astrophysicists in connection with astrophysical problems. Later, the importance of the shock wave in an ionized gas was realized in other areas. Some of the thermonuclear devices have relied on shock waves in achieving high temperatures and densities simultaneously. In front of an entry vehicle a plasma sheath is formed due to the conversion of the high kinetic energy of the flow to the thermal energy through a shock. As a result, the communication and the guidance to the vehicle are affected seriously. Since the shock wave is extremely nonequilibrium and it does not involve the complexity of the interaction between fluid particles and solid boundaries, the shock wave structure is an ideal problem for testing the kinetic theory approaches toward nonequilibrium flow phenomena in rarefied gasdynamics and plasmagasdynamics.

When a neutral gas goes through a reasonably strong shock a slight degree of ionization will be generated inside the shock by atom-atom collisions. If Mach numbers are less than 20 this atom-atom shock front is much thinner than the relaxation zone which is the region behind the shock front. For purposes the true shock front can be replaced by a shock wave with a frozen degree of ionization. Studies of shock structures in ionized gases have been conducted by many investigators.

Among them only those which are closely related to the present study will be reviewed. Jukes [1] used an iterative method to obtain numerical solutions of the Navier-Stokes equations through a shock wave in a fully ionized gas. The charge separation and the induced electric field inside the shock were estimated to be small. Thus, electrostatic effects were neglected in comparison with those due to pressure and convection. Electron viscosity and proton thermal conductivity were not included. His results predict a broad electron thermal layer in front of the proton shock. Inside the shock the proton temperature overshoots the downstream equilibrium value for Mach number 10.

Petschek and Byron [2] made the assumption that the electron-atom interaction dominated the ionization process in the relaxation zone. Results show that time required to reach downstream equilibrium from their prediction agrees with experimental measurements. Rate of ionization is relatively insensitive to the inelastic ionization cross sections for electron-atom collisions. The degree of ionization during the initial process is about 10% of the final value at the downstream equilibrium condition.

Greenberg, et al. [3], used a diffusion equation and three conservation equations to study the shock structure in fully ionized hydrogen. However, effects of viscosity and thermal conductivity were neglected in their momentum and energy equations. Later Greenberg and Tréve [4] chose the Mott-Smith distribution [5] for protons and assumed that the electron distribution was locally Maxwellian. In both studies the charge separation and the electric field were included. For small and moderate ratio of Debye length to the mean free path, their results show

that the electric field oscillates throughout the entire shock structure and the peak of the obtained electric field is large. For Mach numbers greater than 2.19 no continuous solutions were found. These difficulties may be associated with neglecting the effects of viscosity and thermal conductivity and the inaccuracy of numerical computations, which is to be discussed in Chapter IV.

Truitt [6] investigated the ionization in the relaxation zone applying the method which had been used in the study of an ideal dissociating gas through a normal shock. The initial degree of ionization was assumed. The governing equations were made up of a rate equation of ionization and a set of Rankine-Hugoniot equations including the energy of ionization. The results show that the electron temperature and the temperature of atoms and ions approximately remain constant in most parts of the relaxation region. At the rear portion of this region, both temperatures drop significantly while the degree of ionization increases.

The structure of a shock wave in slightly ionized argon with constant degree of ionization was investigated by Grewal and Talbot [7]. They assumed that the structure of the shock wave of the heavy particles, atoms and ions, could be described by the Mott-Smith solution of a neutral monatomic gas [5]. These results were then used to solve the electron governing equations. As Jukes [1], they found a broad thermal layer of the electron existing ahead of the shock. They also stated that the charge separation was small and the effects of the induced electric field could be neglected in the calculations of the electron temperature.

Jaffrin and Probstein [8] applied the Navier-Stokes equations to

the shock structure in a fully ionized gas. The electron viscosity and ion thermal conductivity were taken into consideration. They assumed that the difference between the ion number density and the electron number density was very small and that the Debye length was much smaller than the ion-ion mean free path downstream of the shock. Thus, the governing equations were very much simplified and the equations related to the electric field and the charge separation could be uncoupled from the other governing equations. For Mach number 10, their profiles for electrons and ions look similar to those of Jukes [1] without the electric effects. Unfortunately the detailed comparison was not presented.

Morgan and Morrison [9] basically followed the work of Petschek and Byron [2] and included the rate of ionization due to atom-atom collisions. It was found that the ionization mechanism was dominated by electron-atom elastic collisions when the degree of ionization began with 10^{-4} for 10^{4}°K and kept increasing with initial temperature of the relaxation zone.

Jaffrin [10] extended his previous work with Probstein [8] to partially ionized argon with frozen degrees of ionization. Electron viscous and inertia effects were neglected. The electron temperature inside the shock was assumed to be constant. Electrons were set to move together with ions at the same macroscopic velocity. Yet the charge separation was included. Other assumptions were made in such a fashion that the electric field could easily be evaluated by the gradient of the ion velocity. His results show that the velocity and temperature differences between atoms and ions become greater as the degree of ionization

increases and that the atom temperature and the ion temperature overshoot their downstream values.

The shock structure of the relaxation zone in a stellar atmosphere was investigated by Skalafuris [11]. It was shown that the electron-atom collisions dominated the ionizing process. The energy of excitation was neglected. The boundary conditions at the beginning of the relaxation region were evaluated by shock equations with an assigned degree of ionization. Thus, temperatures of all species are the same initially. Results indicate that the temperature changes of atoms and protons are large in the rear portion of the relaxation region. Temperature gradients of the electron rely strongly on the Mach number. The differences between the atom and the proton temperature profiles are small.

The relaxation zone was also studied by Hoffert and Lien [12]. Both atom-atom and electron-atom ionization and recombination were considered. They treated the atom-atom shock as a chemically frozen discontinuity. The initial conditions of the relaxation zone were evaluated by the jump conditions at the downstream of the discontinuity. Effects of the electric field were not considered. The energy of the created electrons was included. It was assumed that atoms and ions had the same temperature and all species moved with the same macroscopic velocity. They concluded that for Mach numbers less than 20 only the front portion of the relaxation zone was affected by different initial electron temperatures.

Chubb [13] included the energy transfer due to the electron temperature gradients in the study of atom-atom shock and the relaxation zone. In atom-atom shock a bimodal Mott-Smith velocity distribution [5] was

assumed for atoms. It was also assumed that ions and electrons were in locally Maxwellian distributions. No electron-atom interactions were included in this region. He further made an assumption that all three species had locally Maxwellian distributions in the relaxation zone. It was shown that contributions from the induced electric field were small and could be neglected. The initial degree of ionization was set at 10^{-6} and initial electrons were assumed in thermal equilibrium with upstream atoms. He observed that for freestream Mach number less than 20 the relaxation zone was much thicker than the atom-atom shock and negligible ionization was generated in the atom-atom shock.

Discussion of the Physical Model

In dealing with problems in rarefied gas dynamics the relaxation model suggested by Bhatnager, Gross, and Krook [14] can be used to approximate the troublesome collision integral of the Boltzmann equation. The model equation is simple enough for applications, yet it retains some of the gross features of the full Boltzmann equation. The kinetic model for a mixture proposed by Gross and Krook [15] will be used in Chapter II for a fully ionized gas, in Chapters III for a partially ionized gas with a frozen degree of ionization, and in Chapter IV for electric field effects on the shock structure. Hu and Ziering [16] have extended the works of References [14] and [15] to include ionizing effects into the statistical model equation. In Chapter V the model equations proposed by Hu and Ziering [16] will be used to study the structure of the relaxation zone of a shock wave.

Discussion of the Method

The method of discrete ordinates was applied to solve the problems associated with radiative transfer by Chandrasekhar [17]. Huang and Giddens applied the method of discrete ordinates to the linearized Boltzmann equation with BGK model for steady and unsteady linearized Couette flow problem [18, 19], the linearized channel flow problem [20], and the linearized Rayleigh problem [21, 22]. It was found that this technique with an appropriate quadrature gives more accurate results over a wider range of Knudsen numbers for a given amount of computational effort than any of the other existing approximate analytical techniques for the linearized rarefied gas dynamic problems. The method has been generalized for more complicated gas dynamic problem by Huang [23]. For a monatomic gas, Huang and Hartley used the method to solve nonlinear Couette flow problem [24] with heat transfer and nonlinear Rayleigh problem [25]. Recently, this technique has been applied to a polyatomic gas by Huang and Hwang [26]. For extremely nonequilibrium flow conditions this method has also been used for the shock structure problems in both monatomic and rotationally relaxing diatomic gases [27, 28]. These efforts have demonstrated that the discrete ordinate method has the flexibility to solve complicated practical problems.

The technique discretizes the distribution function of the Boltzmann equation and replaces integrations of distribution functions over velocity space by appropriate quadratures. The velocity dependence of distribution functions is thus approximated by a set of functions, each evaluated at appropriate discrete points in velocity space. A sufficient number of discrete points has to be taken to ensure the desired accuracy.

Thus, instead of solving a set of integro-differential equations for functions of time, space, and velocity, one solves a system of first order partial differential equations for a set of functions which are continuous in time and space, but are point-functions in velocity space. Thus, the solution of this system of first order partial differential equations is an approximation to the true distribution functions in the sense of numerical truncations.

Purpose of the Research

To the best of the author's knowledge, the problems of the shock structure have been treated either by the continuum approaches or by the Mott-Smith method. This thesis will be concerned with the structure of a steady plane shock in ionized argon from the microscopic point of view. The Boltzmann equations with the Bhatnagar-Gross-Krook type model [14] are used as the governing equations. The discrete ordinate method [23] is applied in this thesis as a tool for the solutions. The investigation will be conducted in the following phases:

(1) To investigate the shock-structure in fully ionized argon, without the effects of the induced electric field;

(2) To investigate the shock-structure in partially ionized argon without the effects of the induced electric field;

(3) To investigate the effects of the induced electric field on the shock-structure in ionized argon;

(4) To investigate the structure of a relaxation zone where most ionization occurs due to the electron-atom elastic collisions.

CHAPTER II

SHOCK-WAVE STRUCTURE IN FULLY IONIZED ARGON

Introduction

In this chapter the discrete ordinate method is applied to the solution of the shock-wave structure in fully ionized argon. Similar problems have been investigated by several other investigators. Jukes [1] treated a case for Mach number 10 and found a broad thermal layer of electrons extending ahead of the shock. A similar problem was attacked by Tidman [29], using the Fokker-Planck equation. He assumed that the protons had a bimodal Maxwellian distribution and the electrons were in locally Maxwellian. Thus, the effects of the thermal conductivity of electrons have been neglected and the preheated thermal layer of electrons was not obtained. As mentioned in Chapter I, Greenberg, et al. [3] and Greenberg and Tréve [4] could not obtain continuous solutions for Mach numbers greater than 2.19. Jaffrin and Probstein [8] applied the Navier-Stokes equations to the problem for a wide range of Mach numbers. Previous studies in the problem of the shock structure in a neutral monatomic gas indicate that the Navier-Stokes solutions are considered to be accurate for weak shocks. In view of lack of experimental data the present results will be compared with those obtained by Jaffrin and Probstein [8] in order to check the consistency of the solution obtained and the applicability of the method.

Due to the non-equilibrium nature of the shock-wave structure,

the charge separation of ions and electrons inside the shock may occur. Jukes [1] and Tidman [29] estimated that the effects of the charge separation would be small and were therefore neglected in their studies. If the induced electric field of the charge separation is ignored, then the problem of the shock-wave structure in fully ionized argon can be attacked in the light that the plasma becomes a binary mixture of ion gas and electron gas. The study of this problem not only will give an insight into the structure of a completely ionized shock, but also can bring out some of the general features of the shock-wave problem in a binary mixture.

Formulation of the Problem

For a two-component system, Gross and Krook [15] proposed a kinetic model (BGK model) to represent the collision integral in the Boltzmann equation. The model equation is much simpler than the Boltzmann equation, yet it satisfies the conservations of the number of particles, the total momentum, and the total energy. In the absence of the induced electric field due to the separation of charged particles, the governing BBGK equations for a steady plane shock wave of a fully ionized gas are given as follows:

$$v_{x_1}\frac{\partial f_1}{\partial x} = \frac{n_1}{\sigma_{11}}(F_{11} - f_1) + \frac{n_2}{\sigma_{12}}(F_{12} - f_1) \tag{1}$$

and

$$v_{x_2}\frac{\partial f_2}{\partial x} = \frac{n_1}{\sigma_{21}}(F_{21} - f_2) + \frac{n_2}{\sigma_{22}}(F_{22} - f_2) \tag{2}$$

where, the local Maxwellian distribution functions $F_{k\ell}$ in Equations (1) and (2) are defined as

$$F_{k\ell} = n_k \left(\frac{m_k}{2\pi k T_{k\ell}}\right)^{3/2} \exp\left\{-\frac{m_k\left[(v_x - u_{k\ell})^2 + v_y^2 + v_z^2\right]}{2k T_{k\ell}}\right\}. \tag{3}$$

Subscripts k, ℓ = 1, 2 stand for electrons and ions, respectively. The $\sigma_{p\beta}$ are collision parameters. The quantities $\frac{n_\ell}{\sigma_{1\ell}}$ and $\frac{n_\ell}{\sigma_{2\ell}}$ have the dimensions of a frequency.

The macroscopic properties can be obtained by taking the moments of the distribution functions.

$$n_k = \int_{-\infty}^{\infty}\int_{-\infty}^{\infty}\int_{-\infty}^{\infty} f_k \, dv_x \, dv_y \, dv_z \,, \tag{4}$$

$$n_k u_k = n_k u_{kk} = \int_{-\infty}^{\infty}\int_{-\infty}^{\infty}\int_{-\infty}^{\infty} v_x f_k \, dv_x \, dv_y \, dv_z \,, \tag{5}$$

and

$$\begin{aligned} 3 n_k k T_k &= 3 n_k k T_{kk} \\ &= m_k \int_{-\infty}^{\infty}\int_{-\infty}^{\infty}\int_{-\infty}^{\infty} \left[(v_x - u_k)^2 + v_y^2 + v_z^2\right] f_k \, dv_x \, dv_y \, dv_z \,. \end{aligned} \tag{6}$$

It is noted that the summation convention does not apply in the present investigation whenever the repeated indices appear.

If $\ell \neq k$ for gas mixtures [30, 31],

$$(m_k + m_\ell)\, u_{k\ell} = m_k u_k + m_\ell u_\ell \tag{7}$$

and

$$T_{k\ell} = T_k + \frac{2 m_k m_\ell}{(m_k+m_\ell)^2}\left[(T_\ell - T_k) + \frac{m_\ell}{6k}(u_\ell - u_k)^2 \right]. \tag{8}$$

It is understood that for this problem all these macroscopic flow properties are functions of x alone, while the local distribution function is a function of x, v_x, v_y, and v_z.

The collision frequencies between k species and ℓ species $\frac{n_\ell}{\sigma_{k\ell}}$, can be calculated by the following formulas [32]

$$\frac{n_\ell}{\sigma_{k\ell}} = \nu_{k\ell} = 2\left(\frac{2K}{\pi}\right)^{1/2} n_\ell Q_{k\ell}\left(\frac{T_k}{m_k} + \frac{T_\ell}{m_\ell}\right)^{1/2} \tag{9}$$

where $Q_{k\ell}$ are the collision cross sections.

By limiting the scattering to charged particles within a Debye length of a test charge, it can be derived [33] that

$$Q_{\ell\ell} = \frac{e^4 \ln \Lambda}{36\pi\epsilon_0^2 (k T_{\ell\ell})^2}, \qquad (\ell = 1, 2) \tag{10}$$

where

$$\Lambda = \frac{12\pi (\epsilon_0 k T_{\ell\ell}/e^2)^{3/2}}{n_\ell^{1/2}} \tag{11}$$

Since $\frac{T_1}{m_1} >> \frac{T_2}{m_2}$, it is appropriate to assume that

$$Q_{12} = Q_{11} . \tag{12}$$

In order to make numerical computation more manageable the following reduced distribution functions are defined

$$g_k(x, v_x) = \int_{-\infty}^{\infty}\int_{-\infty}^{\infty} f_k(x, \vec{v}) \, dv_y \, dv_z \tag{13}$$

and

$$h_k(x, v_x) = \int_{-\infty}^{\infty}\int_{-\infty}^{\infty} (v_y^2 + v_z^2) f_k(x, \vec{v}) \, dv_y \, dv_z . \tag{14}$$

Similarly, reduced local equilibrium distribution functions can be defined as

$$G_{kl}(x, v_x) = \int_{-\infty}^{\infty}\int_{-\infty}^{\infty} F_{kl}(x, \vec{v}) \, dv_y \, dv_z \tag{15}$$

and

$$H_{kl}(x, v_x) = \int_{-\infty}^{\infty}\int_{-\infty}^{\infty} (v_y^2 + v_z^2) F_{kl}(x, \vec{v}) \, dv_y \, dv_z . \tag{16}$$

Integrating Equations (15) and (16) gives

$$G_{kl}(x, v_x) = \frac{n_k}{(2\pi R_k T_{kl})^{1/2}} \exp\left[-\frac{1}{2R_k T_{kl}} (v_x - u_{kl})^2\right] \tag{17}$$

and

$$H_{kl}(x, v_x) = 2 R_k T_{kl} G_{kl} \tag{18}$$

where R_k is the gas constant of species k.

If Equations (1) and (2) are multiplied by unity and integrated with respect to v_y and v_z, the following equations are obtained

$$v_{x_1} \frac{\partial g_1}{\partial x} = \nu_{11}(G_{11} - g_1) + \nu_{12}(G_{12} - g_1) \tag{19}$$

and

$$v_{x_2} \frac{\partial g_2}{\partial x} = \nu_{21}(G_{21} - g_2) + \nu_{22}(G_{22} - g_2) \tag{20}$$

If the multiplying factor is $v_y^2 + v_z^2$, then the corresponding set of equations yields

$$v_{x_1} \frac{\partial h_1}{\partial x} = \nu_{11}(H_{11} - h_1) + \nu_{12}(H_{12} - h_1) \tag{21}$$

and

$$v_{x_2} \frac{\partial h_2}{\partial x} = \nu_{21}(H_{21} - h_2) + \nu_{22}(H_{22} - h_2). \tag{22}$$

The moment equations for the macroscopic properties are

$$n_k = \int_{-\infty}^{\infty} g_k \, dv_x \,, \tag{23}$$

$$n_k u_k = \int_{-\infty}^{\infty} v_x g_k \, dv_x \,, \tag{24}$$

and

$$3 n_k R_k T_k = \int_{-\infty}^{\infty} (v_x^2 g_k + h_k) \, dv_x - n_k u_k^2 \,. \tag{25}$$

Other macroscopic properties can be obtained from Equations (7) and (8).

Using the most probable velocity of individual species at the downstream equilibrium conditions, $V_k = \sqrt{2 R_k (T_k)_2}$, and the mean free path of ion-ion collisions, $(\ell_{22})_2 = 1/\sqrt{2}\,(n_2 Q_{22})_2$, the definitions of nondimensional quantities are introduced as follows

$$\hat{x} = \frac{x}{(\ell_{22})_2} \,; \qquad \hat{n}_k = \frac{n_k}{(n_k)_2} \,; \qquad \hat{v}_{x_k} = \frac{v_{x_k}}{(V_k)_2} \,;$$

$$\hat{u}_{kl} = \frac{u_{kl}}{(V_k)_2} \,; \qquad \hat{T}_{kl} = \frac{T_{kl}}{(T)_2} \,; \qquad \hat{g}_k = \frac{(V_k)_2}{(n_k)_2} g_k \,;$$

$$\hat{G}_{kl} = \frac{(V_k)_2}{(n_k)_2} G_{kl} \,; \qquad \hat{h}_k = \frac{h_k}{(n_k V_k)_2} \,; \qquad \hat{H}_{kl} = \frac{H_{kl}}{(n_k V_k)_2} \,;$$

$$\hat{\nu}_{kl} = \frac{(\ell_{22})_2}{(V_k)_2} \nu_{kl}$$

Consequently, Equations (19) - (22) in nondimensional forms become

$$\hat{v}_{x_1} \frac{\partial \hat{g}_1}{\partial \hat{x}} = \hat{\nu}_{11} (\hat{G}_{11} - \hat{g}_1) + \hat{\nu}_{12} (\hat{G}_{12} - \hat{g}_1) \,, \tag{26}$$

$$\hat{v}_{x_2}\frac{\partial \hat{g}_2}{\partial \hat{x}} = \hat{\nu}_{21}(\hat{G}_{21} - \hat{g}_2) + \hat{\nu}_{22}(\hat{G}_{22} - \hat{g}_2), \tag{27}$$

$$\hat{v}_{x_1}\frac{\partial \hat{h}_1}{\partial \hat{x}} = \hat{\nu}_{11}(H_{11} - \hat{h}_1) + \hat{\nu}_{12}(\hat{H}_{12} - \hat{h}_1), \tag{28}$$

and

$$\hat{v}_{x_2}\frac{\partial \hat{h}_2}{\partial \hat{x}} = \hat{\nu}_{21}(H_{21} - \hat{h}_2) + \hat{\nu}_{22}(\hat{H}_{22} - \hat{h}_2), \tag{29}$$

where,

$$\hat{G}_{ij} = \frac{\hat{n}_i}{(\pi \hat{T}_{ij})^{1/2}} \exp\left[-\frac{1}{\hat{T}_{ij}}(\hat{v}_x - \hat{u}_{ij})^2\right] \tag{30}$$

and

$$\hat{H}_{ij} = \hat{T}_{ij}\hat{G}_{ij}. \tag{31}$$

When the discrete ordinate method outlined in Chapter I is applied, Equations (26) - (29) at the discrete points in velocity space are given as follows

$$\hat{v}_{j_1}\frac{d\hat{g}_{j_1}}{d\hat{x}} = \hat{\nu}_{11}(\hat{G}_{j_{11}} - \hat{g}_{j_1}) + \hat{\nu}_{12}(\hat{G}_{j_{12}} - \hat{g}_{j_1}), \tag{32}$$

$$\hat{v}_{j_2}\frac{d\hat{g}_{j_2}}{d\hat{x}} = \hat{\nu}_{21}\left(\hat{G}_{j_{21}} - \hat{g}_{j_2}\right) + \hat{\nu}_{22}\left(\hat{G}_{j_{22}} - \hat{g}_{j_2}\right), \tag{33}$$

$$\hat{v}_{j_1}\frac{d\hat{h}_{j_1}}{d\hat{x}} = \hat{\nu}_{11}\left(\hat{H}_{j_{11}} - \hat{h}_{j_1}\right) + \hat{\nu}_{12}\left(\hat{H}_{j_{12}} - \hat{h}_{j_1}\right), \tag{34}$$

and

$$\hat{v}_{j_2}\frac{d\hat{h}_{j_2}}{d\hat{x}} = \hat{\nu}_{21}\left(\hat{H}_{j_{21}} - \hat{h}_{j_2}\right) + \hat{\nu}_{22}\left(\hat{H}_{j_{22}} - \hat{h}_{j_2}\right), \tag{35}$$

where

$$\hat{G}_{j_{kl}} = \frac{\hat{n}_k}{\left(\pi\hat{T}_{kl}\right)^{1/2}}\exp\left[-\frac{1}{\hat{T}_{kl}}\left(\hat{v}_j - \hat{u}_{kl}\right)^2\right] \tag{36}$$

and

$$\hat{H}_{j_{kl}} = \hat{T}_{kl}\,\hat{G}_{j_{kl}}. \qquad (j = 1, 2, \cdots, n) \tag{37}$$

Notations $\hat{g}_{j_k}$, $\hat{h}_{j_k}$, $\hat{G}_{j_{kl}}$, and $\hat{H}_{j_{kl}}$ represent $\hat{g}_k$, $\hat{h}_k$, $\hat{G}_{kl}$, and $\hat{H}_{kl}$ evaluated at the discrete velocity points $\hat{v}_{j_k}$, respectively.

The nondimensionalized flow properties can be evaluated from the following relations:

$$\hat{n}_k = \int_{-\infty}^{\infty}\hat{g}_k\,d\hat{v}_{x_k} \cong \sum_{s=1}^{n} W_s\,\hat{g}_{s_k}, \qquad (k = 1, 2), \tag{38-a}$$

$$\hat{u}_k = \hat{u}_{kk} = \frac{1}{\hat{n}_k} \int_{-\infty}^{\infty} \hat{v}_{x_k} \hat{g}_k \, d\hat{v}_{x_k} \cong \frac{1}{\hat{n}_k} \sum_{s=1}^{n} W_s \hat{v}_{s_k} \hat{g}_{s_k} , \tag{38-b}$$

and

$$\hat{T}_k = \hat{T}_{kk} = \frac{2}{3\hat{n}_k} \int_{-\infty}^{\infty} \left(\hat{v}_{x_k}^2 \hat{g}_k + \hat{h}_k \right) d\hat{v}_{x_k} - \frac{2}{3} \hat{u}_k^2$$

$$\cong \frac{2}{3} \left[\sum_{s=1}^{n} W_s \frac{\left(\hat{v}_{s_k}^2 \hat{g}_{s_k} + \hat{h}_{s_k} \right)}{\hat{n}_k} - \hat{u}_k^2 \right] , \tag{38-c}$$

where W_s are the weighting coefficients for the quadrature to be used.

If $\ell \neq k$, nondimensionalization of Equations (7) and (8) gives

$$\hat{u}_{k\ell} = \frac{\hat{u}_{kk} + \left(\frac{m_\ell}{m_k} \right)^{1/2} \hat{u}_{\ell\ell}}{1 + \frac{m_\ell}{m_k}} , \quad (k = 1, 2 \; ; \ell = 1, 2) , \tag{39-a}$$

and

$$\hat{T}_{k\ell} = \hat{T}_{kk} + \frac{2 \frac{m_\ell}{m_k}}{\left(1 + \frac{m_\ell}{m_k} \right)^2} \left[\left(\hat{T}_{\ell\ell} - \hat{T}_{kk} \right) + \frac{1}{3} \left(\hat{u}_{\ell\ell} - \sqrt{\frac{m_\ell}{m_k}} \, \hat{u}_{kk} \right)^2 \right] . \tag{39-b}$$

Boundary Conditions

In gasdynamics, the shock wave is very often treated as a discontinuity. From the microscopic point of view, the shock wave has a finite

thickness in which the changes of flow properties vary continuously. In order to determine the structure of a shock wave, the conditions at the upstream and downstream equilibrium states of the shock must be related through the conservation equations and the thermal equation of state. The following relations which are derived in Appendix I are to be used for the boundary conditions at the upstream and downstream equilibrium states of a shock-wave structure in a fully ionized gas. With a given upstream Mach number M_1,

$$M_2^2 = \frac{M_1^2 + \frac{2}{\gamma-1}}{\frac{2\gamma}{\gamma-1} M_1^2 - 1} .$$

$$(\hat{n}_K)_1 = \frac{(\gamma-1)M_1^2 + 2}{(\gamma-1)M_1^2} , \quad (K = 1, 2) .$$

$$(\hat{n}_K)_2 = 1 .$$

$$(\hat{T}_K)_1 = \frac{(\gamma+1)^2 M_1^2}{[2\gamma M_1^2 - (\gamma-1)][(\gamma-1)M_1^2 + 2]} .$$

$$(\hat{T}_K)_2 = 1 .$$

$$(\hat{u}_1)_S = (\hat{u}_2)_S \left(\frac{m_1}{m_2}\right)^{1/2} , \quad (S = 1, 2) .$$

$$(\hat{u}_2)_S = \left[\frac{\gamma}{2}(1+\alpha)(\hat{T})_S\right]^{1/2} M_S ,$$

where, α is the degree of ionization, and m_i is the mass of a molecule of species i.

After obtaining $(\hat{n}_k)_s$, $(\hat{u}_k)_s$, and $(\hat{T}_k)_s$, the reduced equilibrium distribution functions $\hat{G}_{j_{k\ell}}$ and $\hat{H}_{j_{k\ell}}$, at both upstream and downstream equilibrium states can be calculated.

Computational Procedures

It was mentioned previously that when the discrete ordinate method is applied to Equations (26) - (31), then functions $\hat{g}_k$, $\hat{h}_k$, $\hat{G}_{k\ell}$, and $\hat{H}_{k\ell}$ can be replaced by a series of point functions $\hat{g}_{j_k}$, $\hat{h}_{j_k}$, $\hat{G}_{j_{k\ell}}$ and $\hat{H}_{j_{k\ell}}$, respectively, evaluated at the discrete velocity points $\hat{v}_{j_k}$. The location of these discrete velocity points depends on the quadrature to be used. Thus, instead of dealing with a system of first order partial differential equations (Equations (26) - (29)), one solves a system of first order ordinary differential equations (Equations (32) - (35)). The numerical scheme which was successfully applied to the study of the shock-structure problem in a monatomic gas by Giddens, et al. [27] and Young [34] still can be applied in the present investigations. The governing equations are to be rewritten in finite difference form. In physical space, a central difference scheme will be used to approximate the derivatives with respect to $\hat{x}$ in Equations (32) - (35), e.g.,

$$\frac{d\hat{q}_{j_k}}{d\hat{x}} \simeq \left(\hat{q}_{i+1,j_k} - \hat{q}_{i-1,j_k} \right) / 2\Delta\hat{x} \quad , \quad (i = 1, 2, \cdots, N),$$

where, i is the index for variable $\hat{x}$ in physical space. Then Equations (32) and (33) in finite difference form become

$$\left(\hat{\nu}_{i,K1}+\hat{\nu}_{i,K2}\right)\hat{g}_{i,j_K}+\frac{\hat{v}_{j_K}}{2\Delta\hat{x}}\hat{g}_{3,j_K}=\hat{\nu}_{i,K1}\hat{G}_{i,j_{K1}}+\hat{\nu}_{i,K2}\hat{G}_{i,j_{K2}}$$

$$+\frac{\hat{v}_{j_K}}{2\Delta\hat{x}}\hat{G}_{1,j_{KK}}\quad,\ \text{for } i=2,$$

$$-\frac{\hat{v}_{j_K}}{2\Delta\hat{x}}\hat{g}_{i-1,j_K}+\left(\hat{\nu}_{i,K1}+\hat{\nu}_{i,K2}\right)\hat{g}_{i,j_K}+\frac{\hat{v}_{j_K}}{2\Delta\hat{x}}\hat{g}_{i+1,j_K}=\hat{\nu}_{i,K1}\hat{G}_{i,j_{K1}}$$

$$+\hat{\nu}_{i,K2}\hat{G}_{i,j_{K2}}\quad,\ \text{for } i=3,4,\cdots,N-2,$$

and

$$-\frac{\hat{v}_{j_K}}{2\Delta\hat{x}}\hat{g}_{N-2,j_K}+\left(\hat{\nu}_{N-1,K1}+\hat{\nu}_{N-1,K2}\right)\hat{g}_{N-1,j_K}=\hat{\nu}_{N-1,K1}\hat{G}_{N-1,j_{K1}}$$

$$+\hat{\nu}_{N-1,K2}\hat{G}_{N-1,j_{K2}}-\frac{\hat{v}_{j_K}}{2\Delta\hat{x}}\hat{G}_{N,j_{KK}}\quad,\ \text{for } i=N-1.$$

Similar equations can be written for Equations (34) and (35). Thus, four tridiagonal coefficient matrices can be generated.

In the study of shock structure, proper choices of velocity spacing have to be made in order to ensure that the profiles of the calculated distribution functions will accurately describe the actual ones. Sufficient velocity points are needed to make certain that both ends of the actual distribution functions are well covered. In physical space, sufficient physical points are required so that the equilibrium states upstream and downstream of a shock structure will be recovered asymptotically. For the present calculations the equally spaced discrete velocity points vary from 96 for a shock Mach number of 1.1 to 240 for a shock

Mach number of 10. As the Mach number increases, a smaller physical spacing is used.

To initiate the iterative process, the initial values of the macroscopic properties throughout the shock structure must be guessed. Hyperbolic tangent forms are used for normalized number density, velocity, and temperature profiles of ions and for number density and velocity profiles of electrons. It has been observed that at high shock Mach numbers the hyperbolic tangent form is not a convenient approximation for the temperature profile of electrons in so far as the computing time is concerned. Therefore, the initial values of the electron temperature are assumed keeping in mind that with their higher thermal conductivity electrons can be heated up earlier than heavy particles during the compression process of the shock. The initial guesses are used to evaluate all the reduced equilibrium distribution functions throughout the shock. Systems of equations in finite difference form are solved by the tridiagonal matrix technique to give $\hat{g}_{i,j_k}$ and $\hat{h}_{i,j_k}$ for all i and k at each j. To integrate these calculated distribution functions for the flow properties, a new equally spaced quadrature of order $n = 8$ is used [35]. The spacing and the corresponding weighting coefficients of the quadrature have to be properly selected for each case. If the newly calculated macroscopic properties are different from the initial guessed values, then new reduced equilibrium distribution functions can be computed. The above procedure is repeated over and over until the differences in flow properties at every physical point between successive iterations is less than 0.0005. This requires about thirty iterations for a shock Mach number of 1.1 and about twenty iterations for a shock

Mach number of 10. For each individual shock Mach number convergence in the regions close to the upstream and downstream equilibrium conditions is relatively slower.

Results

The numerical solutions of the shock structure in fully ionized argon have been obtained on the UNIVAC 1108 digital computer at the Rich Electronic Computer Center, Georgia Institute of Technology. The results show the direct collisional interactions between electrons and ions. Figure 1 gives the velocity profile of ions and electrons for $M_1 = 1.1$. The upstream flow temperature is set at 3×10^4 °K. The number density of electrons of $1.5 \times 10^{16}/cm^3$ is used at the upstream equilibrium condition. The electron velocity profile is identical with the ion velocity profile. In other words, due to the assumption of single ionization and neglecting the charge separation of ions and electrons inside the shock, electron-gas move together with ion-gas at the same macroscopic velocity. The figure also shows a comparison of the present results with that of Jaffrin and Probstein [8]. The center of the shock, $\rho^* / \ell_{i_2} = 0$, is taken to be where the velocity of heavy particles is at the mean value of upstream and downstream velocities. The velocity profile of Jaffrin and Probstein appears slightly steeper than the present result in the central part of the shock structure. The profiles of the temperature and number density are presented in Figure 2. Because of the assumptions mentioned before, the number density of electrons is equal to that of ions everywhere in the shock. The present results show that the differences between the electron and ion temperatures are too small to be distinguished on

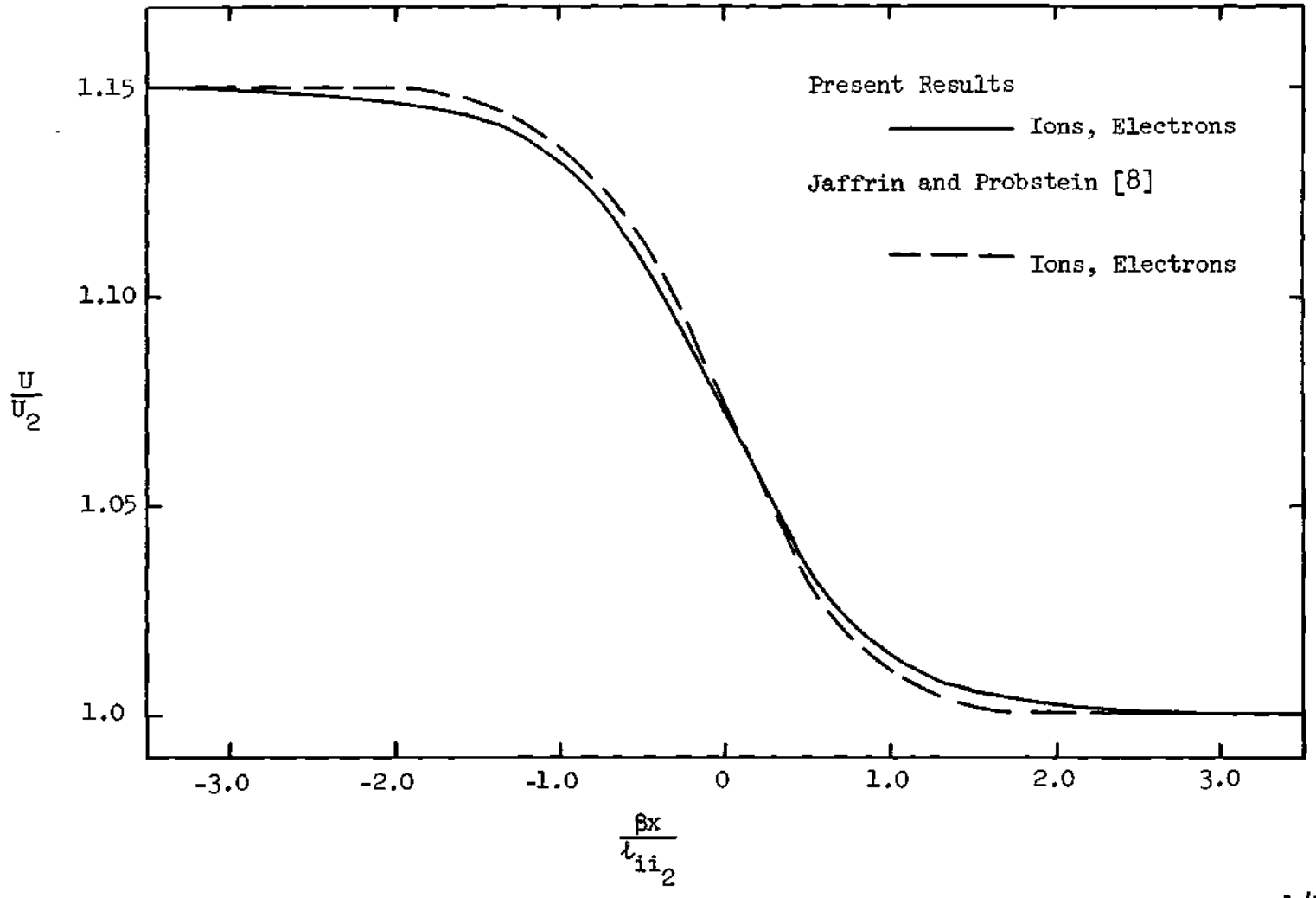

Figure 1. Velocity Profile for $M_1 = 1.1$, $\alpha = 1.0$, $\hat{E} = 0$, $\beta = (m_e/m_i)^{1/2}$.

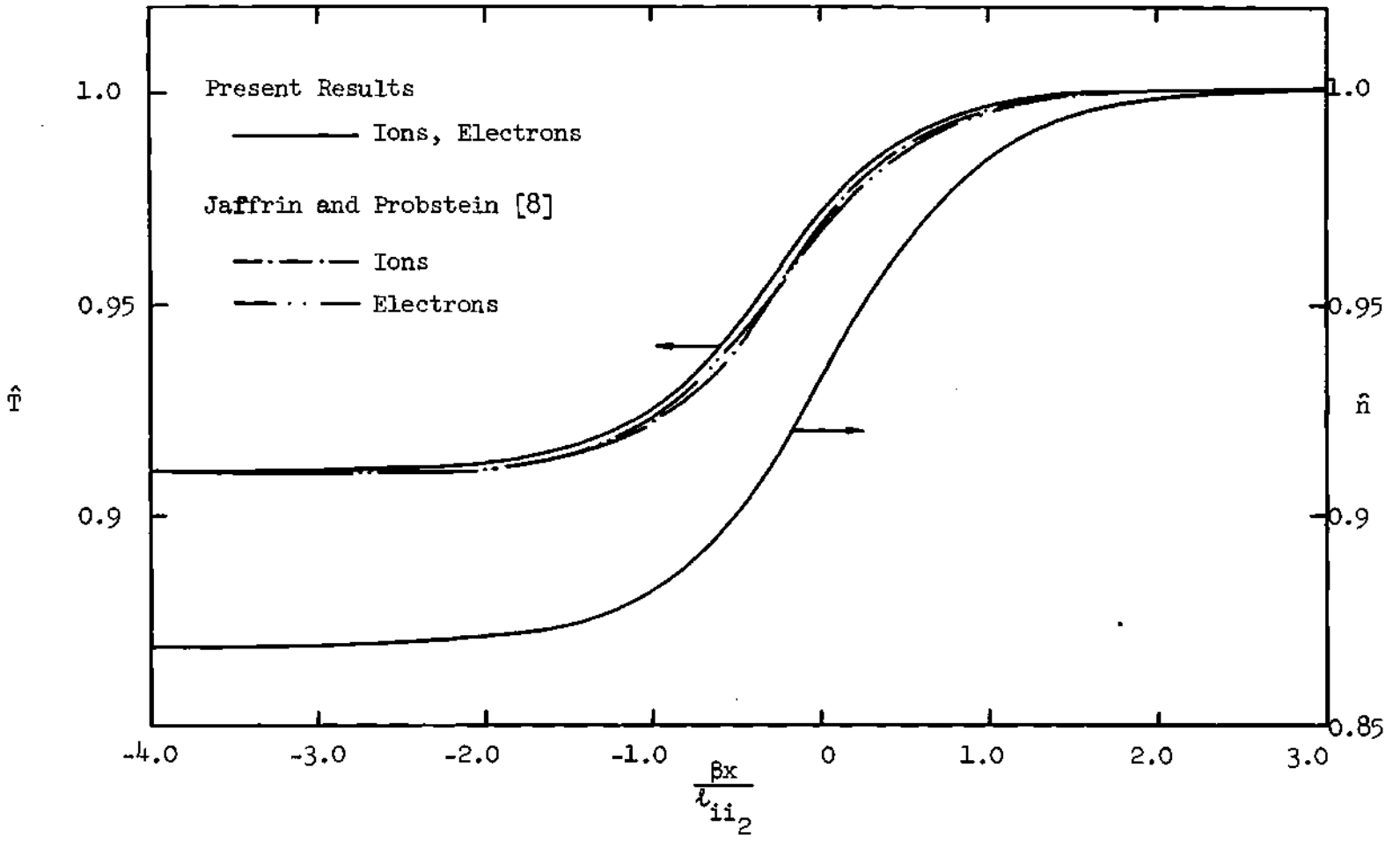

Figure 2. Temperature and Number Density Profiles for $M_1 = 1.1$, $\alpha = 1.0$, $\hat{E} = 0$, $\beta = (m_e/m_i)^{1/2}$.

the graph. Present temperature values are slightly greater than those of Jaffrin and Probstein [8]. In general, the present results agree well with the Navier-Stokes results of Jaffrin and Probstein [8] for the low Mach number. It is known that the Navier-Stokes solutions give good approximations to the shock structure at low Mach numbers. Thus, the applicability and consistency of the discrete ordinate method to the nonequilibrium problems of gas mixtures is indirectly and partially justified. One of the features of the discrete ordinate method is that this method gives the results for the distribution function throughout the shock structure. Figure 3 shows the local distribution functions of ions at various locations across the shock. Since the shock is weak, the shift of these curves is small. The local distribution functions of electrons are shown in Figure 4. The shift of these curves can barely be recognized, because the electron velocity has been normalized by its most probable velocity. The details of the comparison of ion and electron local distribution functions with their local Maxwellian distribution functions are listed in Tables 1 and 2, respectively. The local distribution functions of ions and electrons are indeed very close to their local Maxwellian values. For ions, the absolute value of the differences between $\hat{g}$ and $\hat{G}$ is everywhere in the order of 10^{-5} or less. Electrons, as expected, are even closer to their local Maxwellian values. The absolute value of the differences between their $\hat{g}$ and $\hat{G}$ is everywhere in the order of 10^{-6} or less. Thus, for weak shocks, the electron local Maxwellian distribution function can be considered as an approximation to its actual distribution function.

As the strength of the shock increases, many nonequilibrium

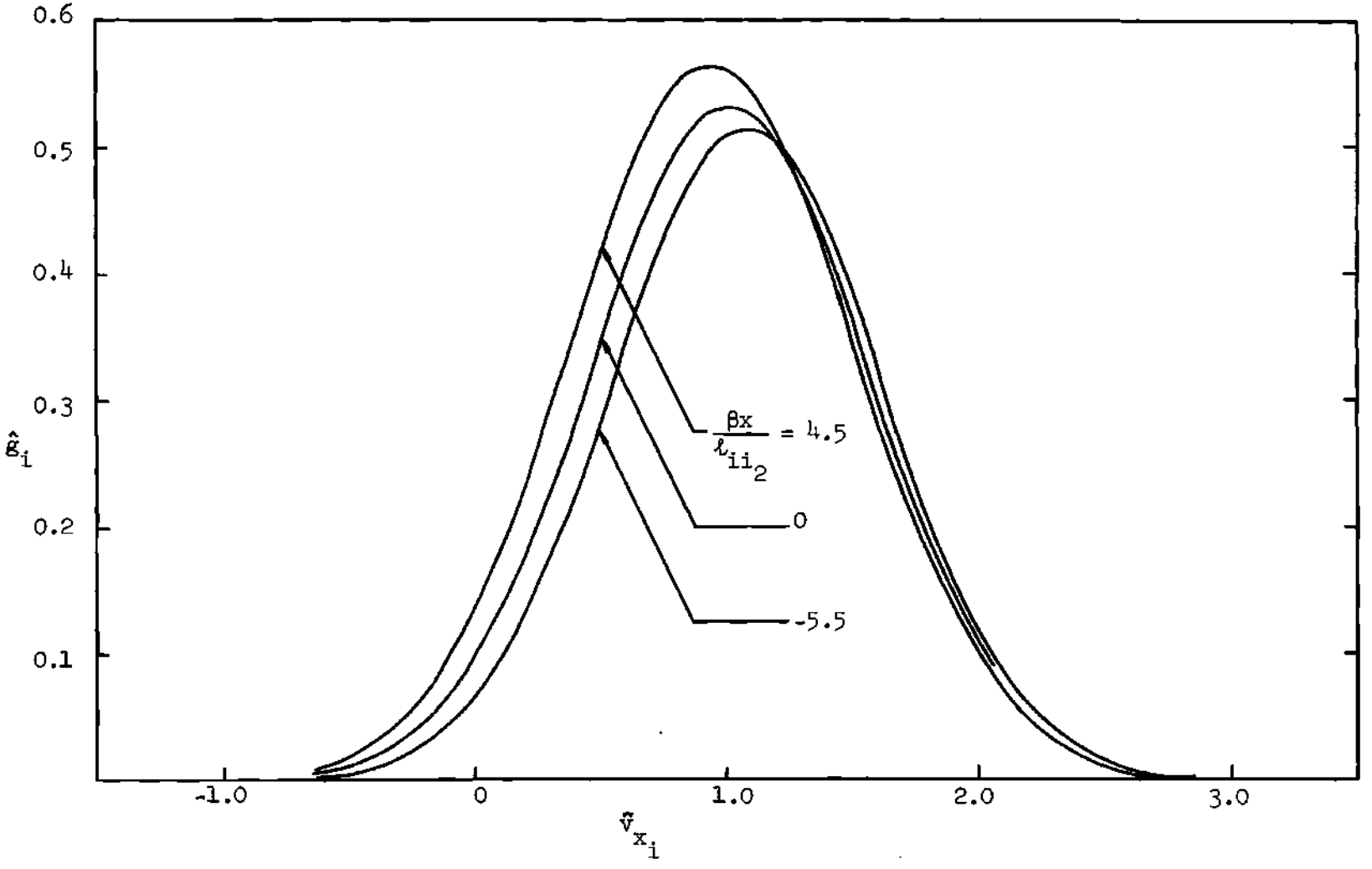

Figure 3. Ion Distribution Functions at Various Locations Across the Shock for $M_1 = 1.1$, $\alpha = 1.0$, $\hat{E} = 0$, $\beta = (m_e/m_i)^{1/2}$.

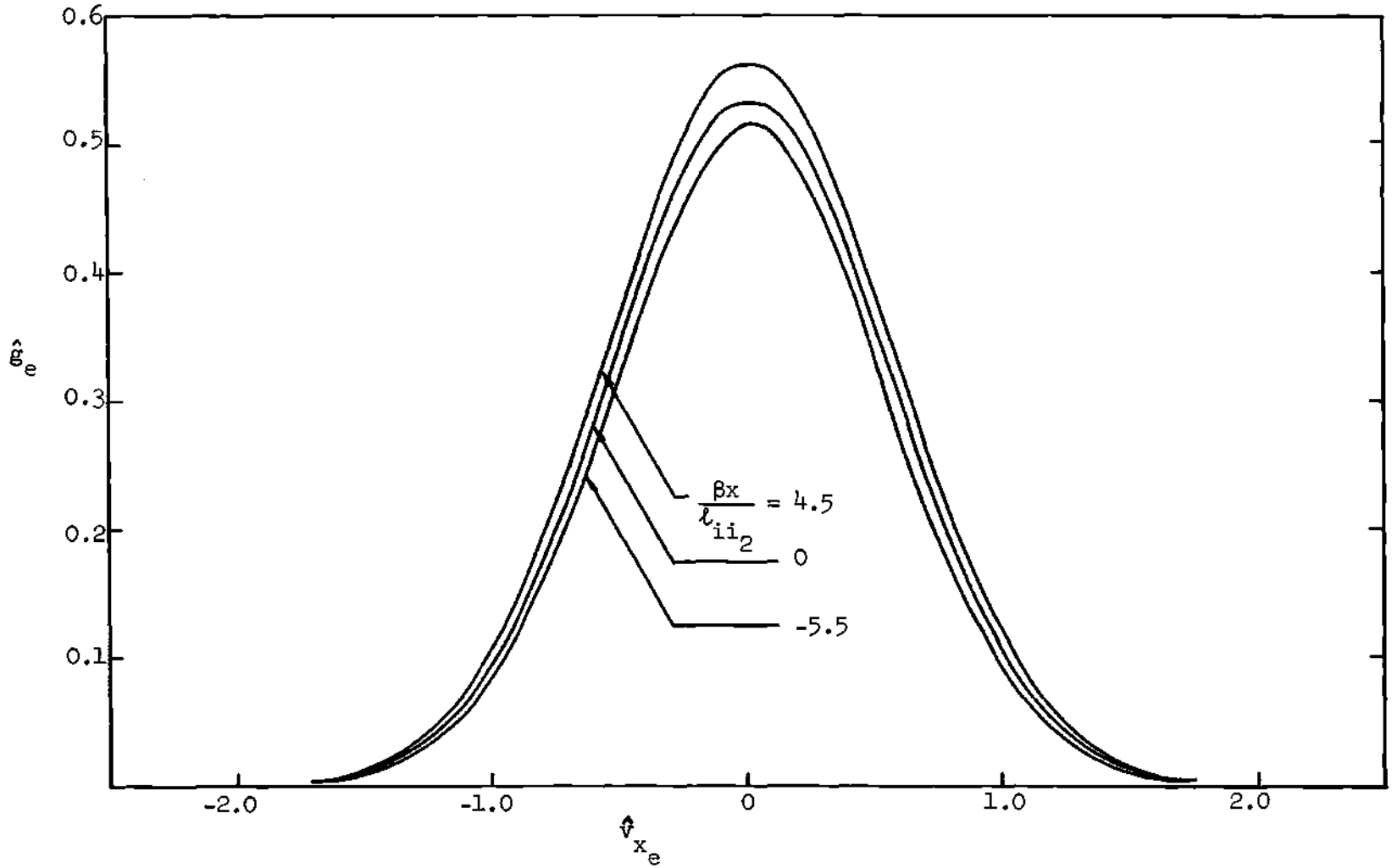

Figure 4. Electron Distribution Functions at Various Locations Across the Shock for $M_1 = 1.1$, $\alpha = 1.0$, $\hat{E} = 0$, $\beta = (m_e/m_i)^{1/2}$.

Table 1. Comparison of Ion Local Distribution Functions with Local Maxwellian Distribution Functions for $M_1 = 1.1$, $\alpha = 1.0$, $\hat{E} = 0$

I	J	$\hat{g}$	$\hat{G}$
25	38	.42578920-03	.42577669-03
	48	.82193480-01	.82192820-01
	58	.51331520+00	.51331563+00
	68	.10371330+00	.10371311+00
	78	.67793450-03	.67792457-03
50	38	.69861120-03	.69741713-03
	48	.99942630-01	.99935954-01
	58	.52200310+00	.52201661+00
	68	.99404930-01	.99398597-01
	78	.68977080-03	.68993719-03
75	37	.11159330-02	.11159152-02
	47	.11968280+00	.11968233+00
	57	.56299580+00	.56299606+00
	67	.11616040+00	.11616016+00
	77	.10512110-02	.10512004-02

Table 2. Comparison of Electron Local Distribution Functions with Local Maxwellian Distribution Functions for $M_1 = 1.1$, $\alpha = 1.0$, $\hat{E} = 0$

I	J	$\hat{g}$	$\hat{G}$
25	28	.73526050-03	.73525507-03
	38	.10792550+00	.10792531+00
	48	.51247340+00	.78719418-01
	58	.78719550-01	.78719418-01
	68	.39116290-03	.39116071-03
50	28	.89367380-03	.89341342-03
	38	.11472860+00	.11472803+00
	48	.52234810+00	.52234495+00
	58	.84314680-01	.84317170-01
	68	.48261220-03	.48255342-03
75	28	.14387390-02	.14387247-02
	38	.13582420+00	.13582387+00
	48	.56129310+00	.56129290+00
	58	.10153550+00	.10153551+00
	68	.80400680-03	.80400983-03

phenomena become more obvious. The velocity profile for a shock Mach number of 2 is shown in Figure 5. The upstream conditions of temperature and number density in the previous case are again used for Mach number of 2. In the low-pressure region, the present curves deviate significantly from the Navier-Stokes solutions of Jaffrin and Probstein [8]. In the vicinity of the center of the shock both methods yield about the same results. In the high-pressure region, the present results again deviate from the results of Jaffrin and Probstein. However, the deviation in the high-pressure region is much smaller than that in the low-pressure region. Figure 6 gives the distributions of temperature and number density in the shock structure. It is noted that the ion temperature overshoots its downstream value. However, the electron temperature does not overshoot and approaches its downstream value asymptotically. These phenomena are similar to those which have been observed in the shock-wave structure in binary mixtures. The present ion temperature deviates from the results of Jaffrin and Probstein except in the vicinity of the center of the shock where both methods give about the same slope. Both methods also predict about the same value of the maximum temperature. It is observed that the electron temperature rise precedes the ion temperature rise. Jaffrin and Probstein [8] keep the electron temperature constant in the most significant portion of the ion shock in their analyses. Thus, their electron temperature profile contains points of discontinuities in slope. However, the discrete ordinate method gives a smooth and continuous electron temperature profile as shown in Figure 6. Ion and electron distribution functions at various locations for $M_1 = 2$ are presented in Figures 7 and 8 respectively. Figure 7 clearly indicates the shift of ion distribution

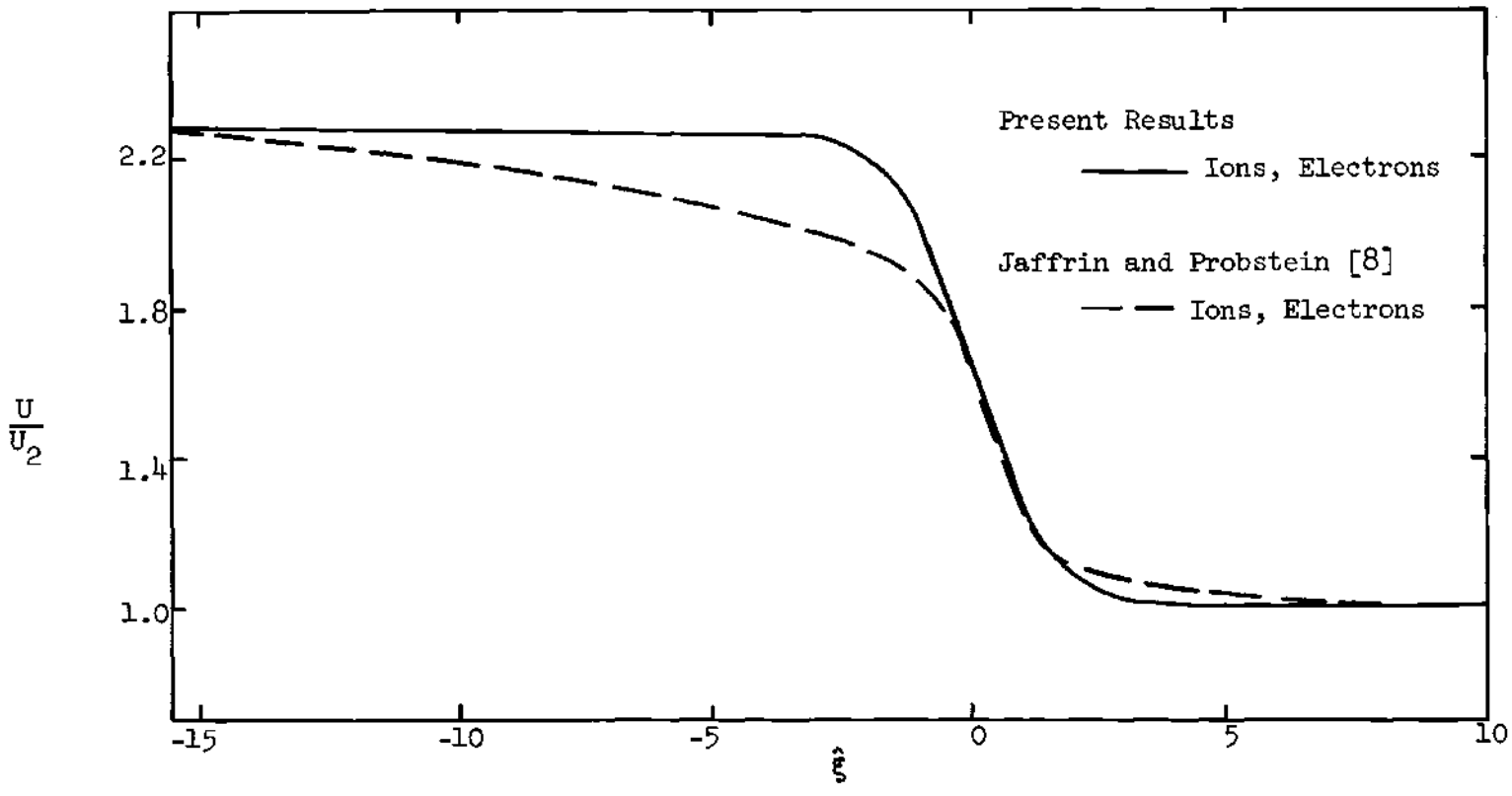

Figure 5. Velocity Profile for $M_1 = 2.0$, $\alpha = 1.0$, $\hat{E} = 0$, $\hat{\xi} = 10x/\ell_{ii_2}$.

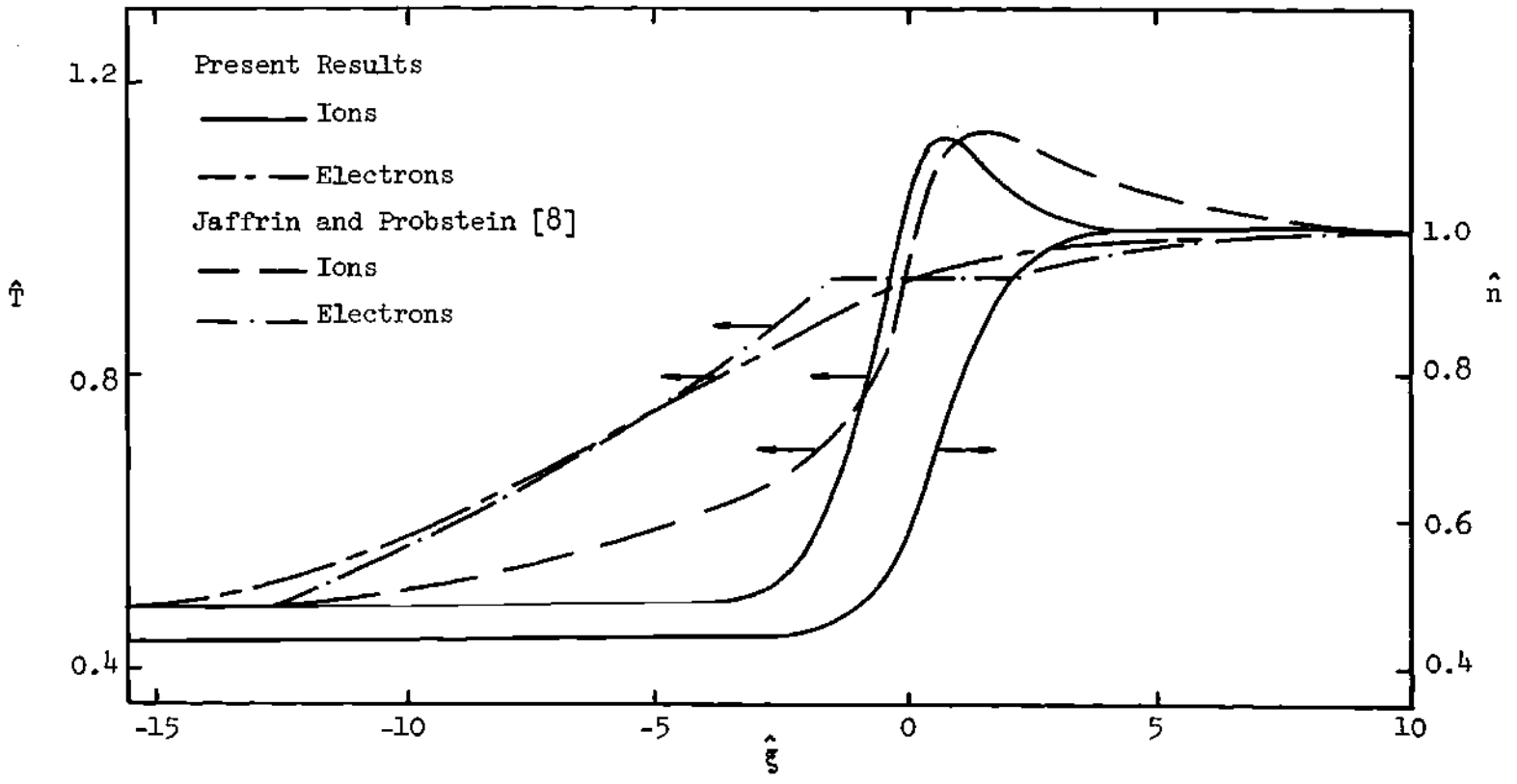

Figure 6. Temperature and Number Density Profiles for $M_1 = 2.0$, $\alpha = 1.0$, $\hat{E} = 0$, $\hat{\xi} = 10x/\ell_{ii_2}$.

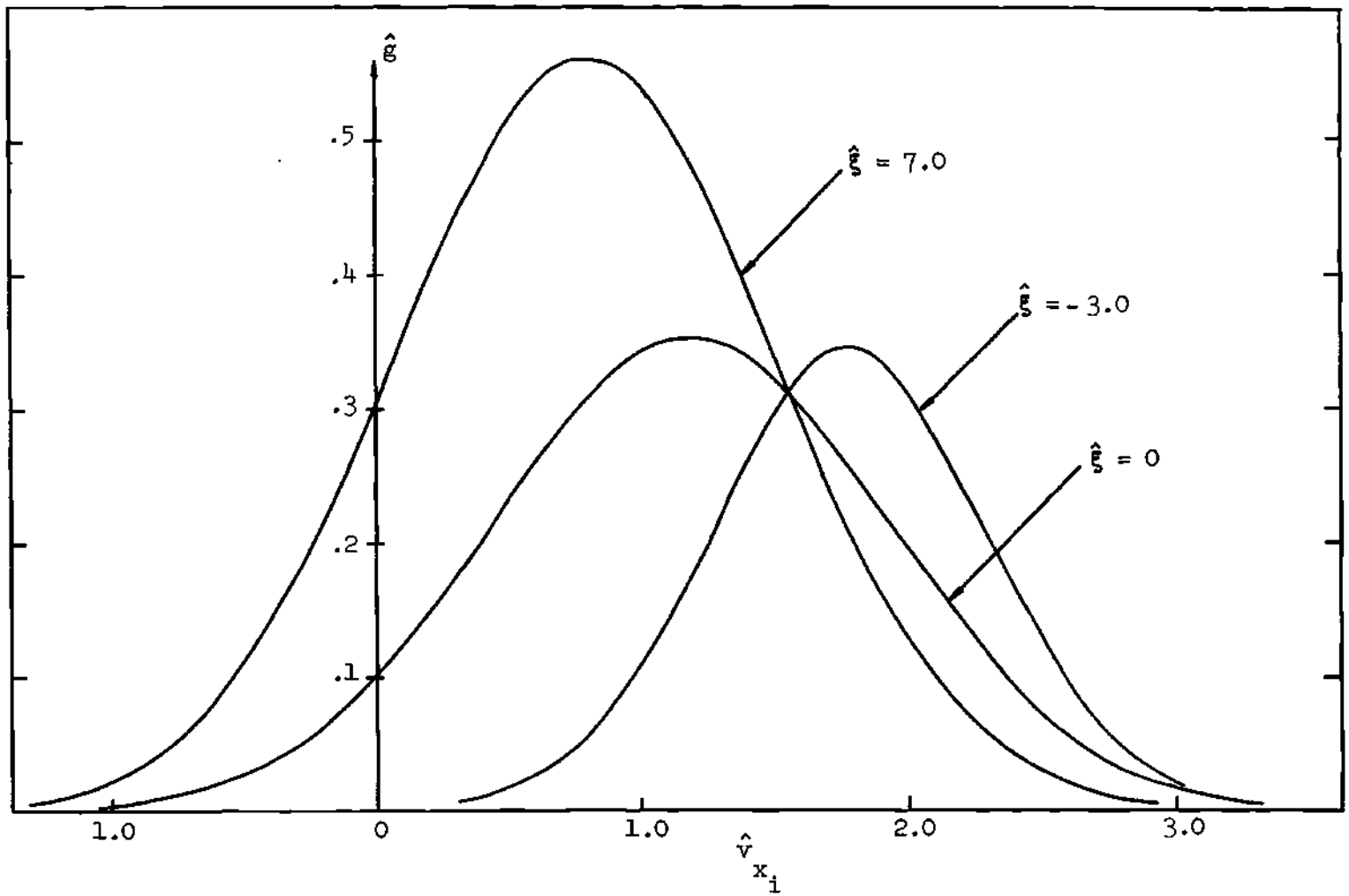

Figure 7. Ion Distribution Functions at Various Locations Across the Shock for $M_1 = 2.0$, $\alpha = 1.0$, $\hat{E} = 0$, $\hat{\xi} = 10x/\ell_{ii_2}$.

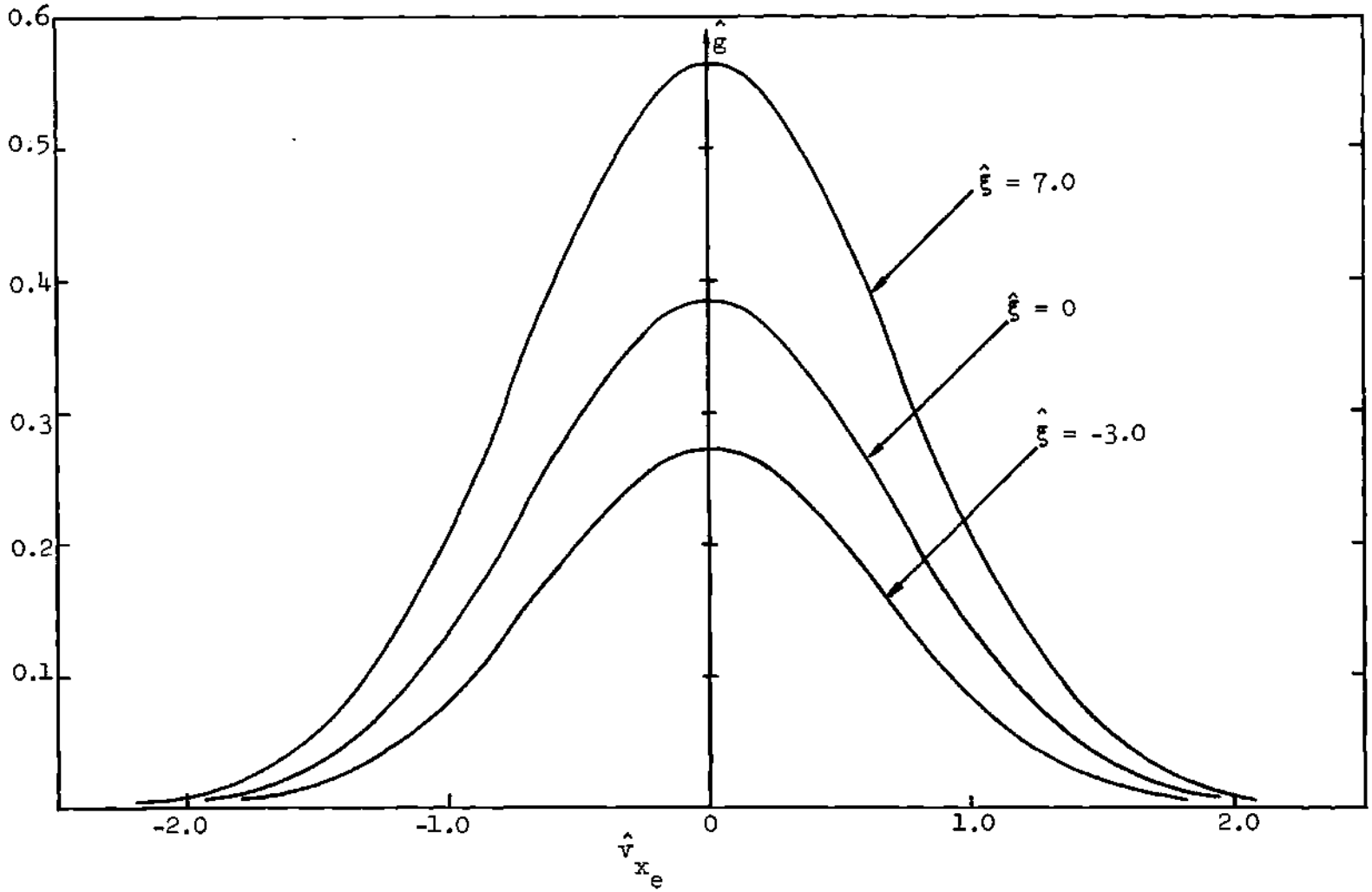

Figure 8. Electron Distribution Functions at Various Locations Across the Shock for $M_1 = 2.0$, $\alpha = 1.0$, $\hat{E} = 0$, $\hat{\xi} = 10x/\ell_{ii_2}$.

functions according to the velocities of the ion-gas at the corresponding locations. The detail comparisons of ion and electron actual distribution functions inside the shock with their local Maxwellian values are listed in Tables 3 and 4, respectively. The maximum absolute value of the differences between $\hat{g}$ and $\hat{G}$ of ions is now in the order of 10^{-4}. For electrons, the maximum absolute value of the differences is of the same order of magnitude as that of ions. Therefore, the true distribution functions are still close to the local Maxwellian. Figure 9 gives a comparison between $\hat{T}_{ie}$ and $\hat{T}_{ei}$. These curves indicate that $\hat{T}_{kk}$ has a great deal of contribution to $\hat{T}_{k}$.

The solutions of the shock structure at $M_1 = 10$ have also been obtained. A comparison of the present velocity profile and that of Jaffrin and Probstein is given in Figure 10. In this case, the results of Jaffrin and Probstein have a discontinuity in the low-pressure region of the shock. But the present results give smooth and continuous profile. The temperature distributions are presented in Figure 11. The maximum $\hat{T}_i$ is 1.2493313. Thus, in a fully ionized gas the overshoot of the ion temperature increases as the shock Mach number increases. Again, the present ion temperature agrees quantitatively with the results of Jaffrin and Probstein in the high-pressure region. As in the previous case of $M_1 = 2$, they assume the electron temperature to be constant in the most significant portion of the ion shock structure. The slope of present electron temperature profile is smaller than that of Jaffrin and Probstein in most part of the low-pressure region. Figures 12 and 13 show the ion and electron distribution functions at various locations across the shock. All these profiles are with single peak. The profiles of downstream

Table 3. Comparison of Ion Local Distribution Functions with Local Maxwellian Distribution Functions for $M_1 = 2.0$, $\alpha = 1.0$, $\hat{E} = 0$

I	J	$\hat{g}$	$\hat{G}$
25	42	.10268020-05	.10271770-05
	52	.15472570-01	.15473104-01
	62	.35523680+00	.35522723+00
	72	.12426620-01	.12428868-01
	82	.66232050-06	.66275549-06
50	40	.10176300-03	.64988862-04
	50	.35544680-01	.34885839-01
	60	.31348950+00	.31353252+00
	70	.46871850-01	.47177966-01
	80	.11970180-03	.11885540-03
75	33	.12565470-02	.12565404-02
	44	.12692080+00	.12692051+00
	54	.56351810+00	.56351776+00
	64	.10997740+00	.10997749+00
	74	.94345250-03	.94345325-03

Table 4. Comparison of Electron Local Distribution Functions with Local Maxwellian Distribution Functions for $M_1 = 2.0$, $\alpha = 1.0$, $\hat{E} = 0$

I	J	$\hat{g}$	$\hat{G}$
25	28	.27494880-04	.26541511-04
	38	.33178820-01	.33069326-01
	48	.30754110+00	.30752986+00
	58	.21250440-01	.21345752-01
	68	.10638050-04	.11058542-04
50	28	.40004170-03	.38416519-03
	38	.60227670-01	.59705396-01
	48	.28903150+00	.28911986+00
	58	.43187350-01	.43622551-01
	68	.19715540-03	.20507511-03
75	28	.13769050-02	.13753560-02
	38	.13535260+00	.13533854+00
	48	.56512070+00	.56511944+00
	58	.10011730+00	.10013166+00
	68	.75188430-03	.75286130-03

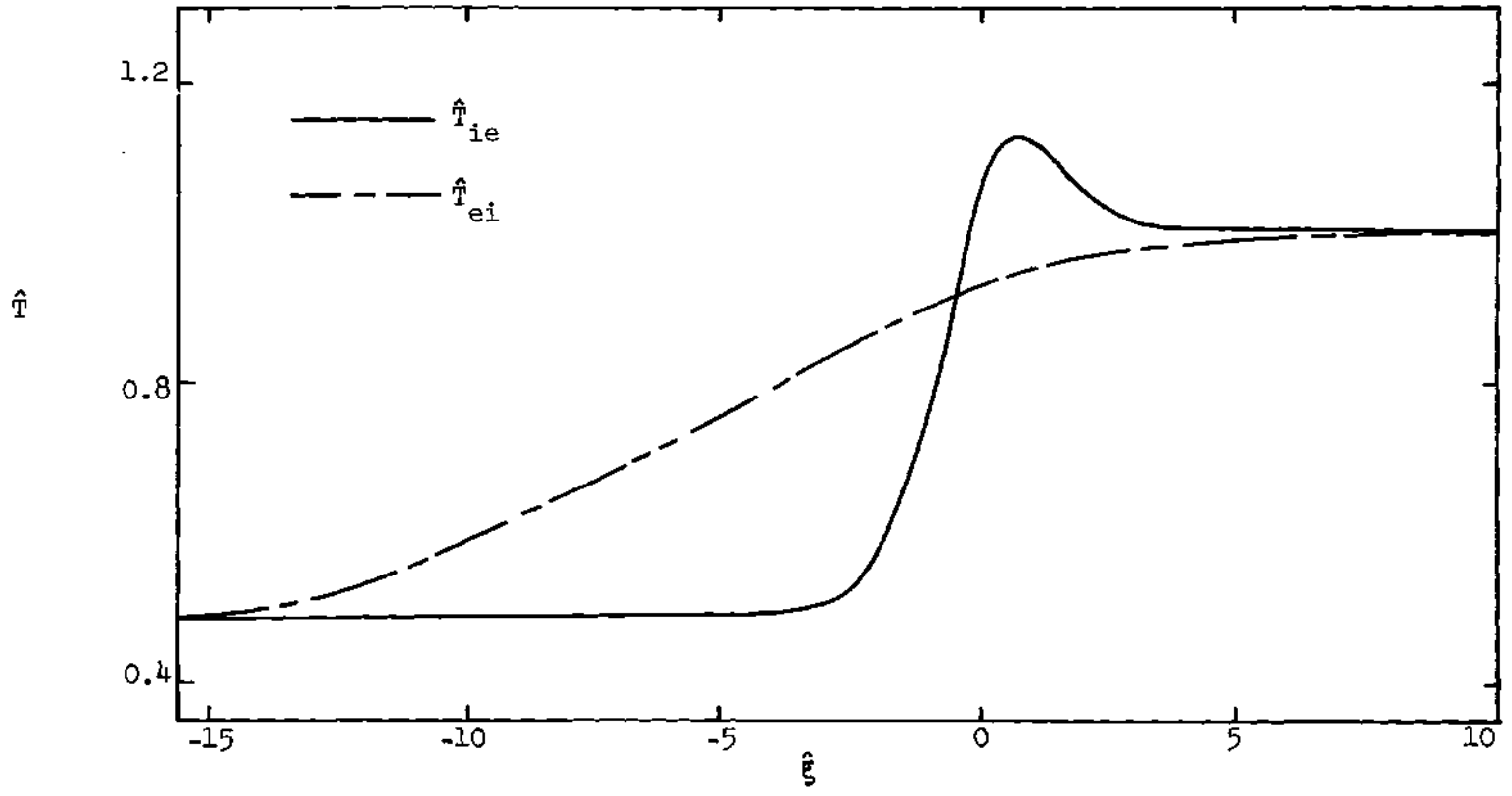

Figure 9. $\hat{T}_{ie}$ and $\hat{T}_{ei}$ for $M_1 = 2.0$, $\alpha = 1.0$, $\hat{E} = 0$, $\hat{\xi} = 10x/\ell_{ii_2}$.

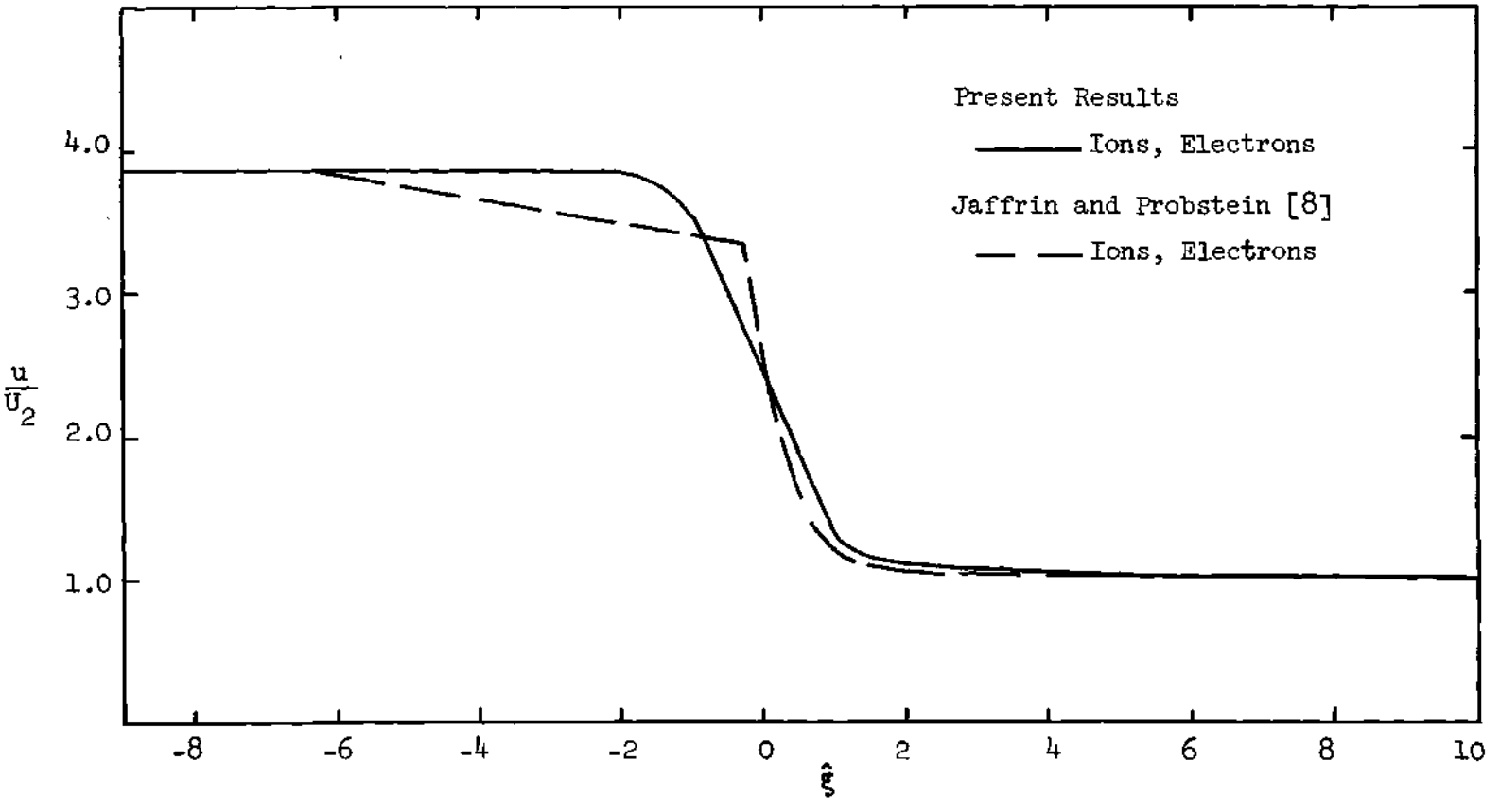

Figure 10. Velocity Profile for $M_1 = 10$, $\alpha = 1.0$, $\hat{E} = 0$, $\hat{\xi} = 10x/\ell_{ii_2}$.

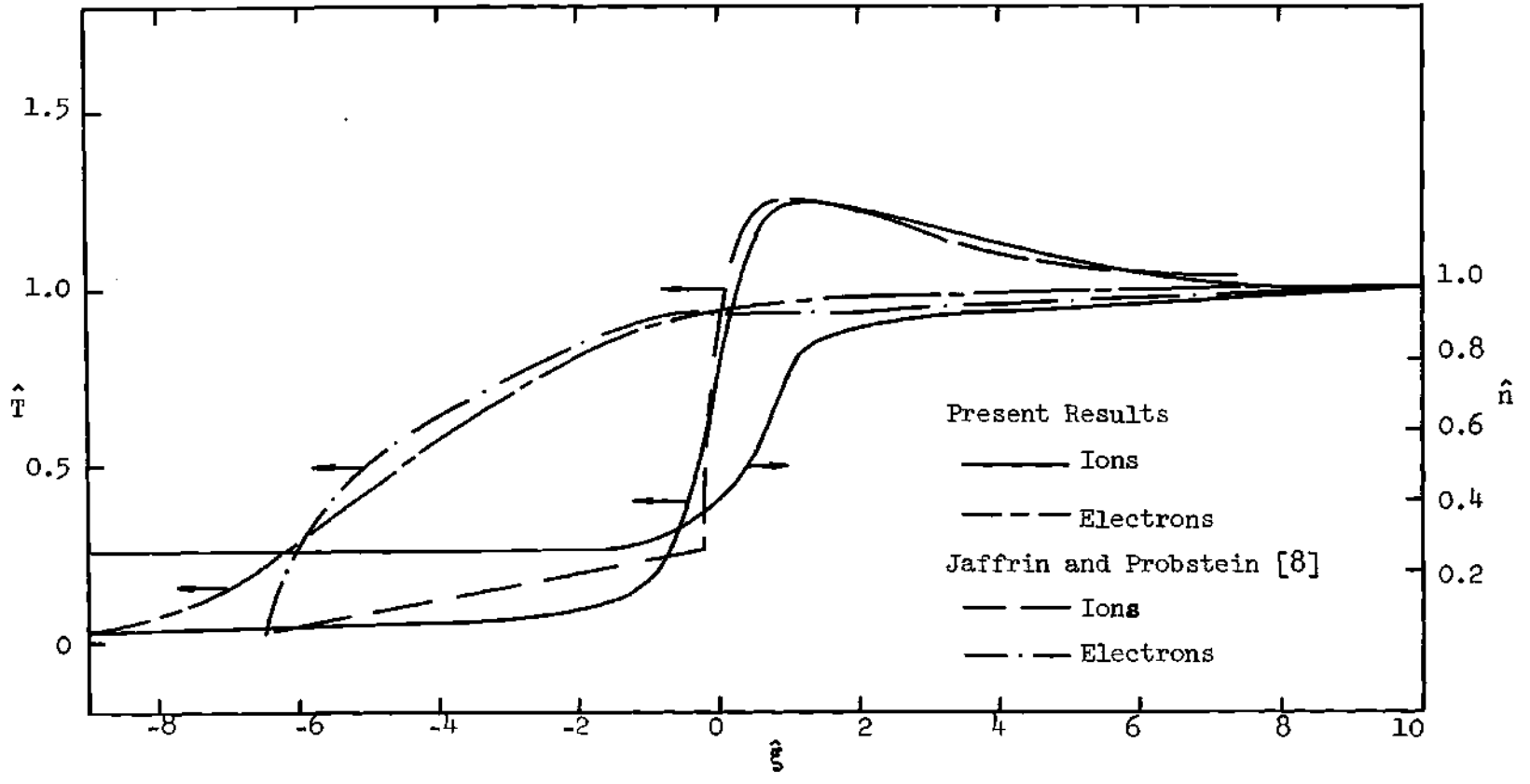

Figure 11. Temperature and Number Density Profiles for $M_1 = 10$, $\alpha = 1.0$, $\hat{E} = 0$, $\hat{\xi} = 10x/\ell_{ii_2}$.

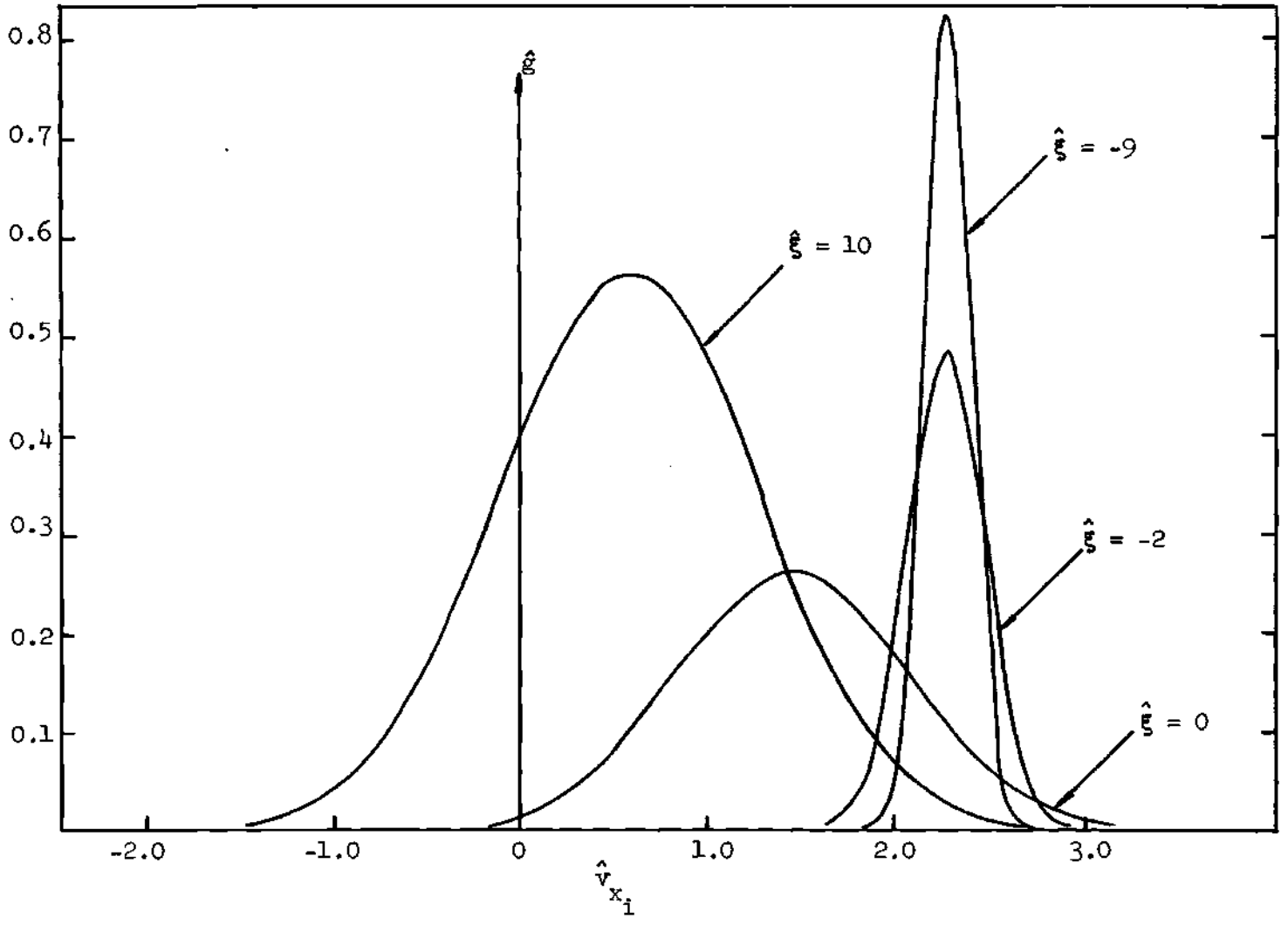

Figure 12. Ion Distribution Functions at Various Locations Across the Shock for $M_1 = 10$, $\alpha = 1.0$, $\hat{E} = 0$, $\hat{\xi} = 10x/\ell_{ii_2}$.

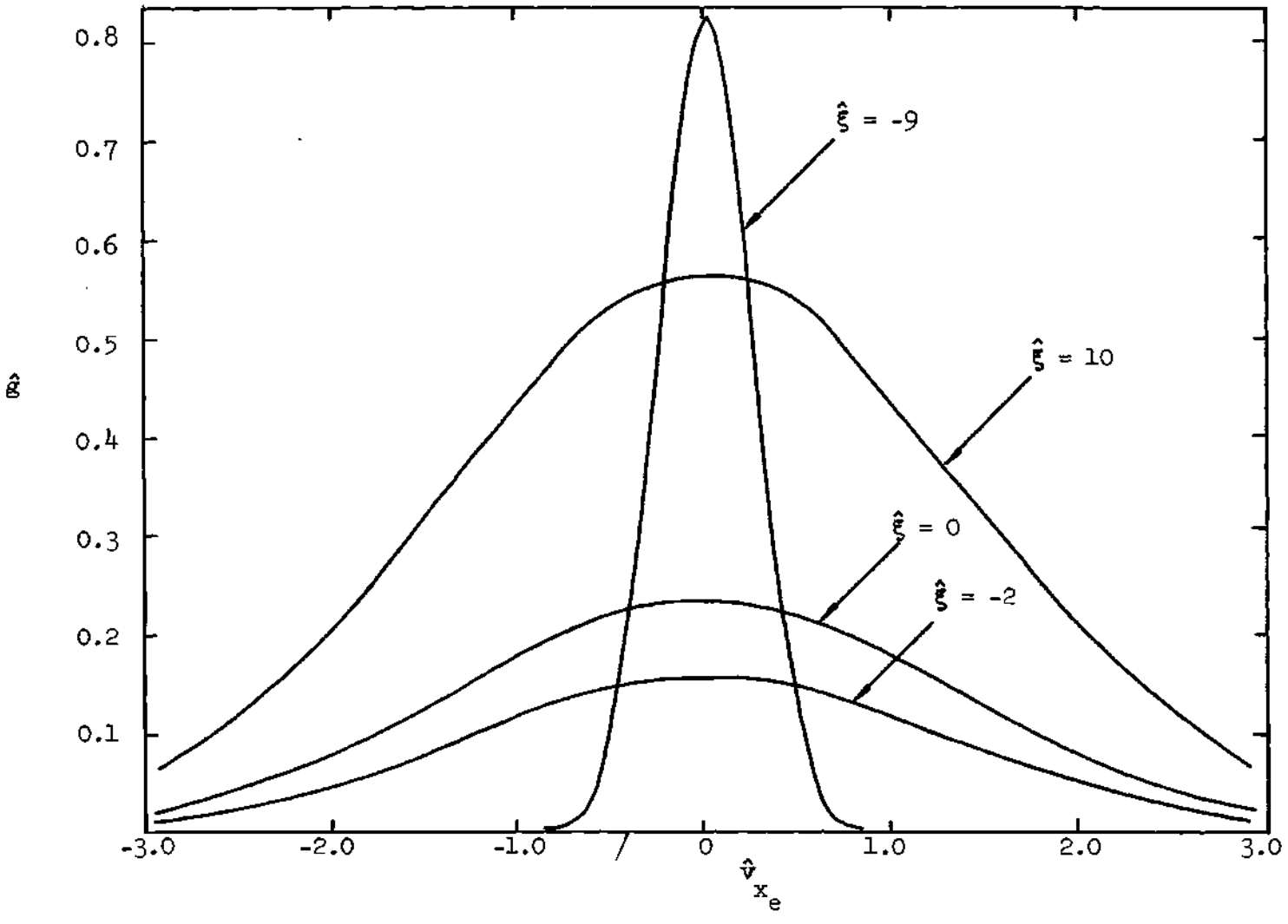

Figure 13. Electron Distribution Functions at Various Locations Across the Shock for $M_1 = 10$, $\alpha = 1.0$, $\hat{E} = 0$, $\hat{\xi} = 10x/\ell_{ii_2}$.

distribution functions are much wider than those of upstream. It is observed that electrons require more velocity points to cover the end points than ions do. Figure 14 gives the comparison of $\hat{T}_{ie}$ and $\hat{T}_{ei}$. These curves also indicate that $\hat{T}_{kk}$ has a great deal of contribution to $\hat{T}_{k}$.

In view of the present results, the author believes that the discrete ordinate method can be applied to other nonequilibrium rarefied gasdynamic and plasmagasdynamic problems in two-component fluids. In the next chapter attempts will be made to apply the discrete ordinate method to a highly nonequilibrium problem in a three-component fluid.

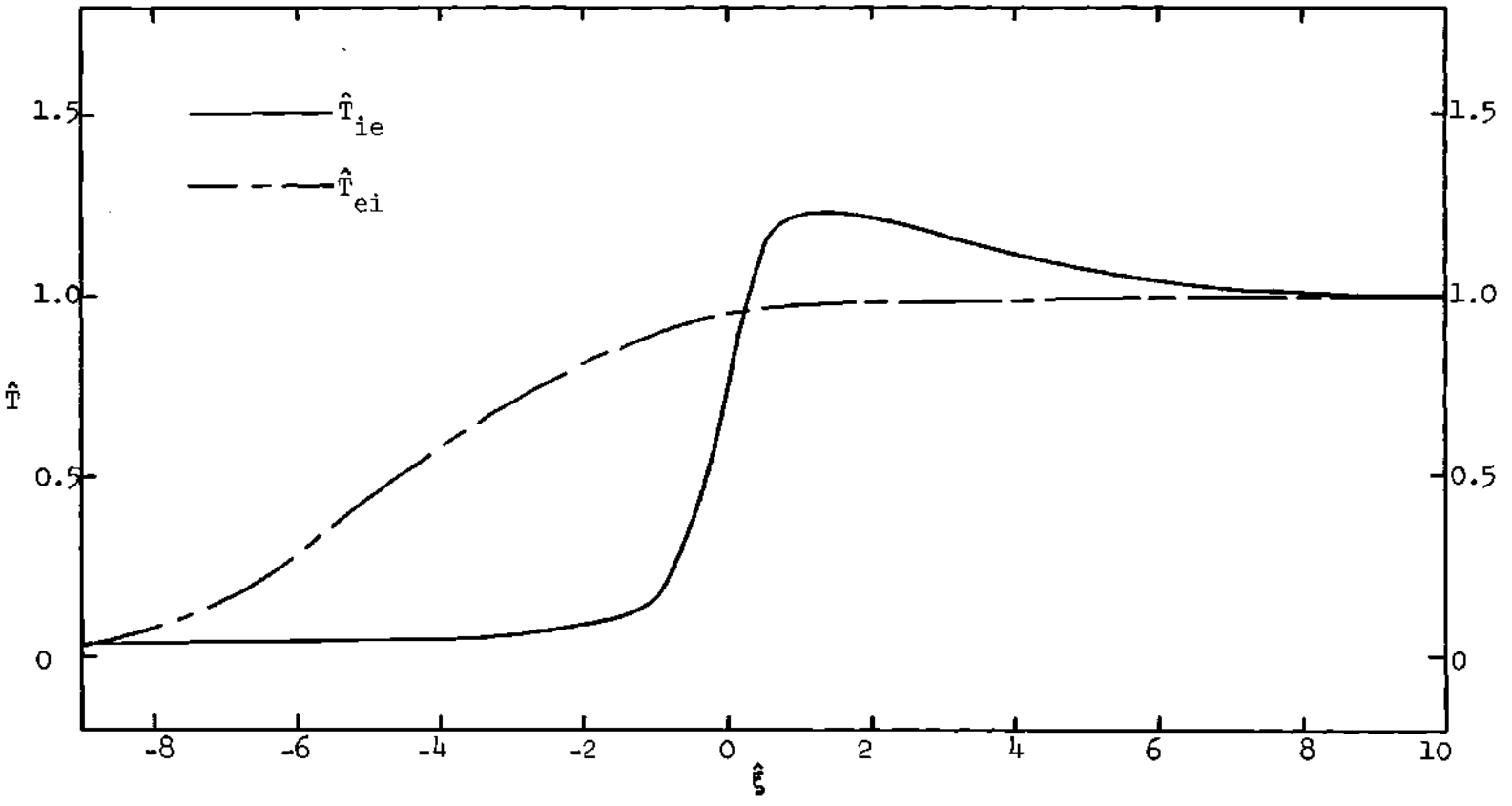

Figure 14. $\hat{T}_{ie}$ and $\hat{T}_{ei}$ for $M_1 = 10$, $\alpha = 1.0$, $\hat{E} = 0$, $\hat{\xi} = 10x/\ell_{ii_2}$.

CHAPTER III

SHOCK-WAVE STRUCTURE IN PARTIALLY IONIZED ARGON

Introduction

As an extension of the work presented in the previous chapter, the shock-wave structure in partially ionized argon is to be studied in this chapter. Again, the discrete ordinate method is used as a tool for the solution of the problem. Similar problems of shock-wave structure have been previously treated by other authors. Grewal and Talbot [7] grouped atoms and ions into one species, the heavy particles. It was assumed that the shock structure of the heavy particles could be described by the Mott-Smith solution of a neutral monatomic gas. Then, these results were used to obtain the solution for another species, the light particles of electrons. It is obvious that they have actually treated the slightly ionized argon as a two-component plasma. Jaffrin [10] applied the Navier-Stokes equations to the problem for a wide range of Mach numbers with various frozen degrees of ionization. Electron viscous and inertia effects were ignored. The electron temperature inside the shock was kept constant. However, as mentioned in Chapter II, the Navier-Stokes approach provides accurate solutions for weak shocks. Therefore, the present results for weaker shocks will be compared with those obtained by Jaffrin [10] as the experimental data are not available for comparison. Previous studies in the problem of the shock structure in a neutral monatomic gas indicate that the Mott-Smith approach yield good results for high Mach numbers.

Thus, the present results for the strong shock will be compared with those obtained by Grewal and Talbot [7].

Similar to Jukes [1] and Tidman [29], Grewal and Talbot [7] estimated that the effects of the charge separation inside the shock-wave structure should be small and were not included in their investigations. If the induced electric field due to the charge separation is neglected, the problem of the shock-wave structure in a partially ionized plasma with a frozen degree of ionization can be treated as if the plasma is a mixture of three components, namely, atoms, ions, and electrons. The results of this problem not only can give an insight into the structure of a partially ionized gas, but also can bring out some of the general features of the shock-wave problem in a three-component mixture.

Formulation of the Problem

The kinetic model for a binary mixture proposed by Gross and Krook [15] can be extended to a three-component system. The resulting model equations still satisfy the conservation equations. In the absence of the induced electric field, the governing BBGK equations for a steady plane shock wave of a partially ionized gas are given as follows:

$$v_{x_1}\frac{\partial f_1}{\partial x} = \frac{n_1}{\sigma_{11}}(F_{11}-f_1)+\frac{n_2}{\sigma_{12}}(F_{12}-f_1)+\frac{n_3}{\sigma_{13}}(F_{13}-f_1), \qquad (1)$$

$$v_{x_2}\frac{\partial f_2}{\partial x} = \frac{n_1}{\sigma_{21}}(F_{21}-f_2)+\frac{n_2}{\sigma_{22}}(F_{22}-f_2)+\frac{n_3}{\sigma_{23}}(F_{23}-f_2), \qquad (2)$$

and

$$v_x \frac{\partial f_3}{\partial x} = \frac{n_1}{\sigma_{31}} (F_{31} - f_3) + \frac{n_2}{\sigma_{32}} (F_{32} - f_3) + \frac{n_3}{\sigma_{33}} (F_{33} - f_3). \tag{3}$$

where the local Maxwellian distributions $F_{k\ell}$ in Equations (1) - (3) are defined as

$$F_{k\ell} = n_k \left(\frac{m_k}{2\pi K T_{k\ell}} \right)^{3/2} \exp\left\{ - \frac{m_k [(v_x - u_{k\ell})^2 + v_y^2 + v_z^2]}{2K T_{k\ell}} \right\}. \tag{4}$$

Subscripts k, ℓ = 1, 2, 3 stand for electrons, ions, and atoms, respectively.

The $\sigma_{r\ell}$ are collision parameters. The quantities $\frac{n_\ell}{\sigma_{1\ell}}$, $\frac{n_\ell}{\sigma_{2\ell}}$, and $\frac{n_\ell}{\sigma_{3\ell}}$ have the dimensions of a frequency.

The macroscopic properties can be obtained by taking the moments of the distribution functions as mentioned in Chapter II.

It is understood that for this problem all macroscopic flow properties are functions of x alone, while the local distribution function is a function of x, v_x, v_y, and v_z.

Expressions for Q_{11}, Q_{12}, and Q_{22} in Chapter II will be used again in this chapter. The other collision cross sections depend on the gas considered. Q_{33} can be obtained from the experimental data of the viscosity coefficient of argon at high temperatures due to Amdur and Mason [36] and is given [10] as

$$Q_{33} = 170 \times 10^{-16} / T_3^{1/4}, \ cm^2, \tag{5}$$

Experimental data for argon show that Q_{23} is only a weak function of temperature and can be considered as a constant [10], i.e.,

$$Q_{23} = 140 \times 10^{-16} \ , \ cm^2 . \tag{6}$$

The approximate relations for Q_{13} of argon from Shkarofsky, et al. [37] are

$$Q_{13} = (-0.35 + 0.775 \times 10^{-4} T_1) \times 10^{-16} \ , \ cm^2 \ ,$$

$$10^4 < T_1 < 5 \times 10^5 \ ^\circ K \ , \tag{7-a}$$

$$Q_{13} = (0.39 - 0.551 \times 10^{-4} T_1 + 0.595 \times 10^{-8} T_1^2) \times 10^{-16} \ , \ cm^2 \ ,$$

$$T_1 < 10^4 \ ^\circ K . \tag{7-b}$$

Similar to Chapter II, the reduced distribution functions g_k, h_k, $G_{k\ell}$, and $H_{k\ell}$ are defined. The macroscopic properties can be obtained by taking the moments of g_k and h_k as described in the previous chapter.

Using the most probable velocities of individual species at the downstream equilibrium conditions, $V_\kappa = \sqrt{2 R_\kappa (T_\kappa)_2}$, and the mean free path of atom-atom collisions, $(\ell_{33})_2 = 1/\sqrt{2}\,(n_3 Q_{33})_2$, the definitions of nondimensional quantities $\hat{x}$ and $\hat{\nu}_{k\ell}$ are introduced as follows

$$\hat{x} = \frac{x}{(\ell_{33})_2} \ ; \quad \hat{\nu}_{k\ell} = \frac{(\ell_{33})_2}{(\bar{V}_k)_2} \nu_{k\ell} .$$

The other nondimensional quantities are defined as before.

Following the procedure presented in Chapter II, the nondimensional governing equations of $\hat{g}_k$ and $\hat{h}_k$ in discrete ordinate form can be obtained.

$$\hat{v}_{j_1}\frac{d\hat{q}_{j_1}}{d\hat{x}} = \hat{\nu}_{11}(\hat{G}_{j_{11}} - \hat{q}_{j_1}) + \hat{\nu}_{12}(\hat{G}_{j_{12}} - \hat{q}_{j_1}) + \hat{\nu}_{13}(\hat{G}_{j_{13}} - \hat{q}_{j_1}), \tag{8}$$

$$\hat{v}_{j_2}\frac{d\hat{q}_{j_2}}{d\hat{x}} = \hat{\nu}_{21}(\hat{G}_{j_{21}} - \hat{q}_{j_2}) + \hat{\nu}_{22}(\hat{G}_{j_{22}} - \hat{q}_{j_2}) + \hat{\nu}_{23}(\hat{G}_{j_{23}} - \hat{q}_{j_2}), \tag{9}$$

$$\hat{v}_{j_3}\frac{d\hat{q}_{j_3}}{d\hat{x}} = \hat{\nu}_{31}(\hat{G}_{j_{31}} - \hat{q}_{j_3}) + \hat{\nu}_{32}(\hat{G}_{j_{32}} - \hat{q}_{j_3}) + \hat{\nu}_{33}(\hat{G}_{j_{33}} - \hat{q}_{j_3}), \tag{10}$$

$$\hat{v}_{j_1}\frac{d\hat{h}_{j_1}}{d\hat{x}} = \hat{\nu}_{11}(\hat{H}_{j_{11}} - \hat{h}_{j_1}) + \hat{\nu}_{12}(\hat{H}_{j_{12}} - \hat{h}_{j_1}) + \hat{\nu}_{13}(\hat{H}_{j_{13}} - \hat{h}_{j_1}), \tag{11}$$

$$\hat{v}_{j_2}\frac{d\hat{h}_{j_2}}{d\hat{x}} = \hat{\nu}_{21}(\hat{H}_{j_{21}} - \hat{h}_{j_2}) + \hat{\nu}_{22}(\hat{H}_{j_{22}} - \hat{h}_{j_2}) + \hat{\nu}_{23}(\hat{H}_{j_{23}} - \hat{h}_{j_2}), \tag{12}$$

and

$$\hat{v}_{j_3}\frac{d\hat{h}_{j_3}}{d\hat{x}} = \hat{\nu}_{31}(\hat{H}_{j_{31}} - \hat{h}_{j_3}) + \hat{\nu}_{23}(\hat{H}_{j_{32}} - \hat{h}_{j_3}) + \hat{\nu}_{33}(\hat{H}_{j_{33}} - \hat{h}_{j_3}). \tag{13}$$

where

$$\hat{G}_{j_{kl}} = \frac{\hat{n}_k}{(\pi\hat{T}_{kl})^{1/2}}\exp\left[-\frac{1}{\hat{T}_{kl}}(\hat{v}_j - \hat{u}_{kl})^2\right] \tag{14}$$

and

$$\hat{H}_{j_{kl}} = \hat{T}_{kl}\hat{G}_{j_{kl}},$$

$$(k, l = 1, 2, 3;\ j = 1, 2, \cdots, n.) \tag{15}$$

The moment equations (Equations (38-a) - (39-b) in Chapter II) with k, ℓ = 1, 2, 3 can be used to calculate the flow properties.

Boundary Conditions

The following relations which are derived in Appendix I are to be used for the boundary conditions at the upstream and downstream equilibrium states of a shock-wave structure in a partially ionized gas with a frozen degree of ionization. With a given upstream Mach number M_1,

$$M_2^2 = \frac{M_1^2 + \frac{2}{\gamma-1}}{\frac{2\gamma}{\gamma-1} M_1^2 - 1}$$

$$(\hat{n}_k)_1 = \frac{(\gamma-1) M_1^2 + 2}{(\gamma-1) M_1^2}, \quad (k = 1, 2, 3).$$

$$(\hat{n}_k)_2 = 1.$$

$$(\hat{T}_k)_1 = \frac{(\gamma+1)^2 M_1^2}{[2\gamma M_1^2 - (\gamma-1)][(\gamma-1) M_1^2 + 2]}.$$

$$(\hat{T}_k)_2 = 1.$$

$$(\hat{u}_1)_s = (\hat{u}_2)_s \left(\frac{m_1}{m_2}\right)^{1/2} \qquad (s = 1, 2).$$

$$(\hat{u}_2)_s = \left[\frac{\gamma}{2}(1+\alpha)(\hat{T})_s\right]^{1/2} M_s.$$

By the assumption that $m_2 \cong m_3$, then,

$$(\hat{u}_2)_s \cong (\hat{u}_3)_s$$

With these $(\hat{n}_k)_s$, $(\hat{u}_k)_s$, and $(\hat{T}_k)_s$, the reduced equilibrium distribution functions, $\hat{G}_{j_{k\ell}}$ and $\hat{H}_{j_{k\ell}}$ at upstream and downstream equilibrium states can be calculated.

Computational Procedure and Results

Even though the mass difference between the neutral particle and the ion is very small, their physical properties are very different. Taking Q_{22}, Q_{23}, and Q_{33}, for example, it is seen immediately that there is no simple relations among them. From the expressions of collisions cross section $Q_{k\ell}$ given in this chapter, one can imagine that the collisional interactions of the present problem are complicated. It is expected that under certain flow conditions, ion-electron interactions will be very much different from atom-electron interactions.

The governing equations to be solved are Equations (8) - (15). Again, the discrete ordinate method is applied to the governing equations. A central difference scheme is used to approximate the derivatives with respect to $\hat{x}$, the variable in physical space. Then, the governing equations in finite difference form are set up in such a way that the tridiagonal matrix technique can be applied. If i is the index for variable $\hat{x}$ in physical space and k is the index for species, Equations (8) - (10) can be rewritten as follows

$$\left(\hat{\nu}_{i_{K1}} + \hat{\nu}_{i_{K2}} + \hat{\nu}_{i_{K3}}\right)\hat{q}_{i,j_K} + \frac{\hat{v}_{j_K}}{2\Delta\hat{x}}\hat{q}_{3,j_K} = \hat{\nu}_{i_{K1}}\hat{G}_{i,j_{K1}}$$

$$+ \hat{\nu}_{i_{K2}}\hat{G}_{i,j_{K2}} + \hat{\nu}_{i_{K3}}\hat{G}_{i,j_{K3}} + \frac{\hat{v}_{j_K}}{2\Delta\hat{x}}\hat{G}_{1,j_{KK}},$$

for $K = 1, 2, 3$ and $i = 2$,

$$-\frac{\hat{v}_{j_K}}{2\Delta\hat{x}}\hat{g}_{i-1,j_K}+(\hat{v}_{i_{K1}}+\hat{v}_{i_{K2}}+\hat{v}_{i_{K3}})\hat{g}_{i,j_K}+\frac{\hat{v}_{j_K}}{2\Delta\hat{x}}\hat{g}_{i+1,j_K}$$

$$=\hat{v}_{i_{K1}}\hat{G}_{i,j_{K1}}+\hat{v}_{i_{K2}}\hat{G}_{i,j_{K2}}+\hat{v}_{i_{K3}}\hat{G}_{i,j_{K3}},$$

$$\text{for } i=3,4,\cdots,N-2,$$

and

$$-\frac{\hat{v}_{j_K}}{2\Delta\hat{x}}\hat{g}_{N-2,j_K}+(\hat{v}_{N-1_{K1}}+\hat{v}_{N-1_{K2}}+\hat{v}_{N-1_{K3}})\hat{g}_{N-1,j_K}$$

$$=\hat{v}_{N-1_{K1}}\hat{G}_{N-1,j_{K1}}+\hat{v}_{N-1_{K2}}\hat{G}_{N-1,j_{K2}}+\hat{v}_{N-1_{K3}}\hat{G}_{N-1,j_{K3}}-\frac{\hat{v}_{j_K}}{2\Delta\hat{x}}\hat{G}_{N,j_{KK}},$$

$$\text{for } i=N-1.$$

Similar equations can be written for $\hat{h}_{i,j_k}$. Thus, six tridiagonal coefficient matrices are obtained.

Proper choices in velocity spacing and velocity points still play an important role in obtaining accurate results. Four different flow cases have been investigated in this chapter. In low shock Mach number of 2.0, 96 equally spaced discrete velocity points were used. However, in high shock Mach number of 10.0, velocity points have been increased to 240 in order to obtain the desired accuracy. It is still true that a smaller physical spacing has to be used as the shock Mach number increases.

Experiences obtained from the study of the shock-wave structure in a fully ionized gas give benefit to the investigations in this chapter.

Results of the electron temperature in Chapter II can serve as a guideline for making initial guessed values of the electron temperature in a partially ionized gas. For other macroscopic flow properties, hyperbolic tangent forms are still good and convenient for the first approximations. The reduced equilibrium distribution functions throughout the shock can be evaluated by using the initial guessed values of flow properties. Then the tridiagonal matrix technique is applied to yield the numerical solutions for $\hat{g}_{i,j_k}$ and $\hat{h}_{i,j_k}$ of atoms, ions, and electrons throughout the shock at each discrete velocity point. The quadrature of order n = 8 mentioned in Chapter II has been used to integrate the distribution functions for the flow properties. The convergent criteria of flow properties were set at 0.0005 for every physical point between successive iterations.

The purpose of this study are not only to obtain the overall flow properties throughout the shock-wave structure at various flow conditions but also to look into the behavior of particles of different species. It is one of the beauties of the discrete ordinate method which can achieve the latter purpose without extra efforts. Unlike the interactions between charged particles alone in the previous chapter, the present problem involves interactions among negative charged particles, positive charged particles, and neutral particles. It has been generally adopted in the literature that, due to the small difference in mass, ions and neutral particles could be grouped into one category as heavy particles in the study of the shock-wave structure in slightly or partially ionized gases, but, surprisingly, the present study will draw an opposite conclusion to this assumption.

The first case investigated in this chapter is the shock structure

with a shock Mach number of 2.0 and a frozen degree of ionization 0.1. The total number density of neutral particles and electrons at the upstream equilibrium conditions is equal to 10^{15} cm^{-3}. The upstream temperature is 10^{4} °K. Figure 15 gives the velocity profile for atoms. The present results are compared with that of Jaffrin [10]. The center of the shock, x/ℓ_{aa_2}, is taken to be where the velocity of neutral particles is at the mean value of upstream and downstream velocities. Jaffrin's profile is steeper than the present profile in the central portion of the shock structure. Since the ion and electron results are different from the values of neutral particles in the order of 10^{-3}, their profiles are not shown in Figure 15. Due to the assumption of single ionization and neglecting the charge separation of ions and electrons inside the shock, the electron velocity profile is identical with the ion velocity profile and the number density of electrons is equal to that of ions everywhere in the shock. Since the difference between the number density of ions and the number density of atoms is in the order of 10^{-3}, only the profile of the number density of atoms is shown in Figure 16. Present temperature profiles and Jaffrin's results [10] are compared in Figure 16. Both methods predict the same general trend. With their higher thermal conductivity electrons are heated up earlier than both atoms and ions during the compression process of the shock. However, Jaffrin's electron temperature profile contains two discontinuities in slope inside the shock structure, because the electron temperature was kept constant inside the shock structure of atoms in his analyses. The ion temperature profile is not shown in Figure 16 since its deviation from the atom temperature profile is only by an order of 10^{-3}. However, it is worthwhile

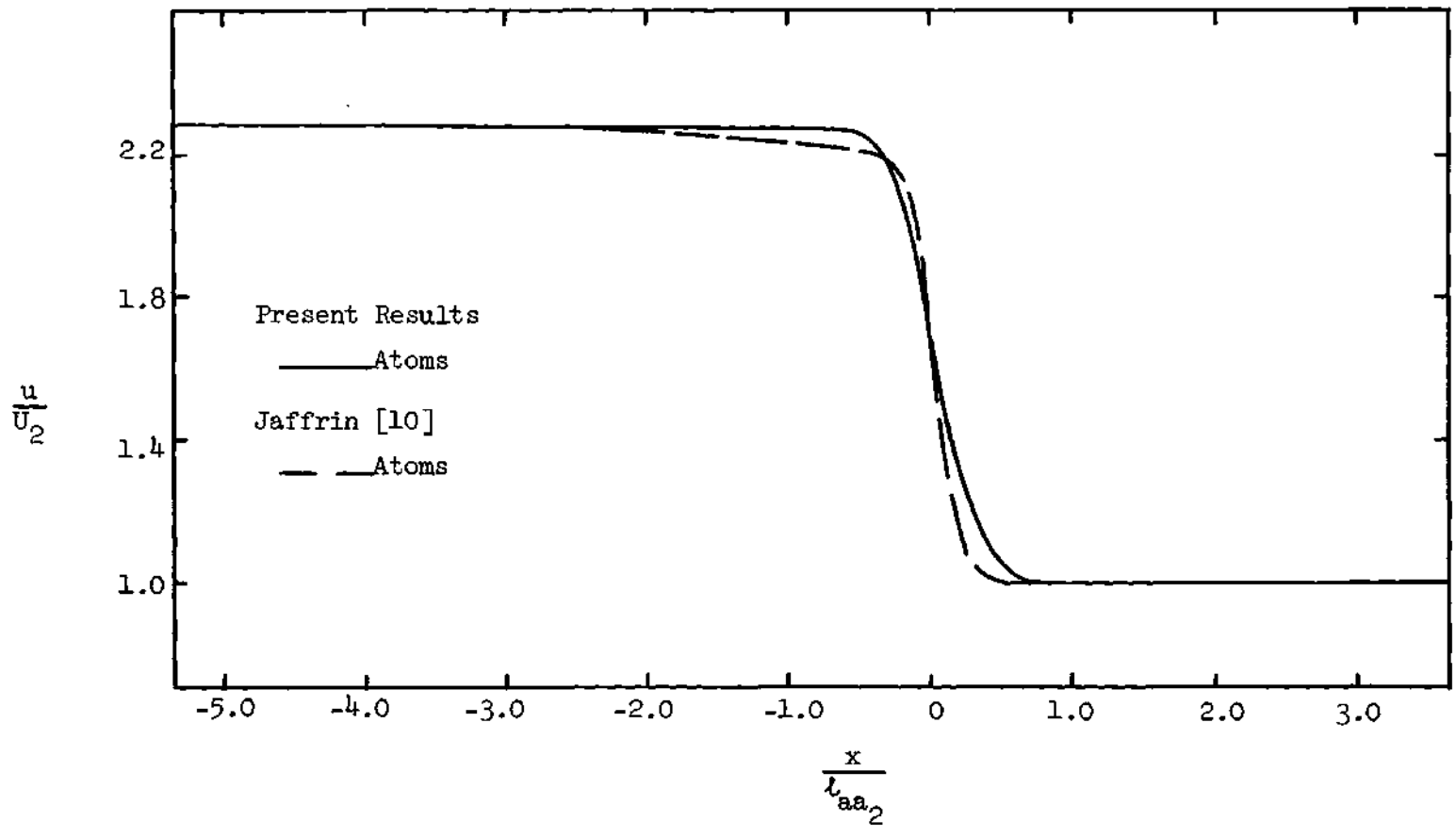

Figure 15. Velocity Profile for $M_1 = 2.0$, $\alpha = 0.1$, $\hat{E} = 0$.

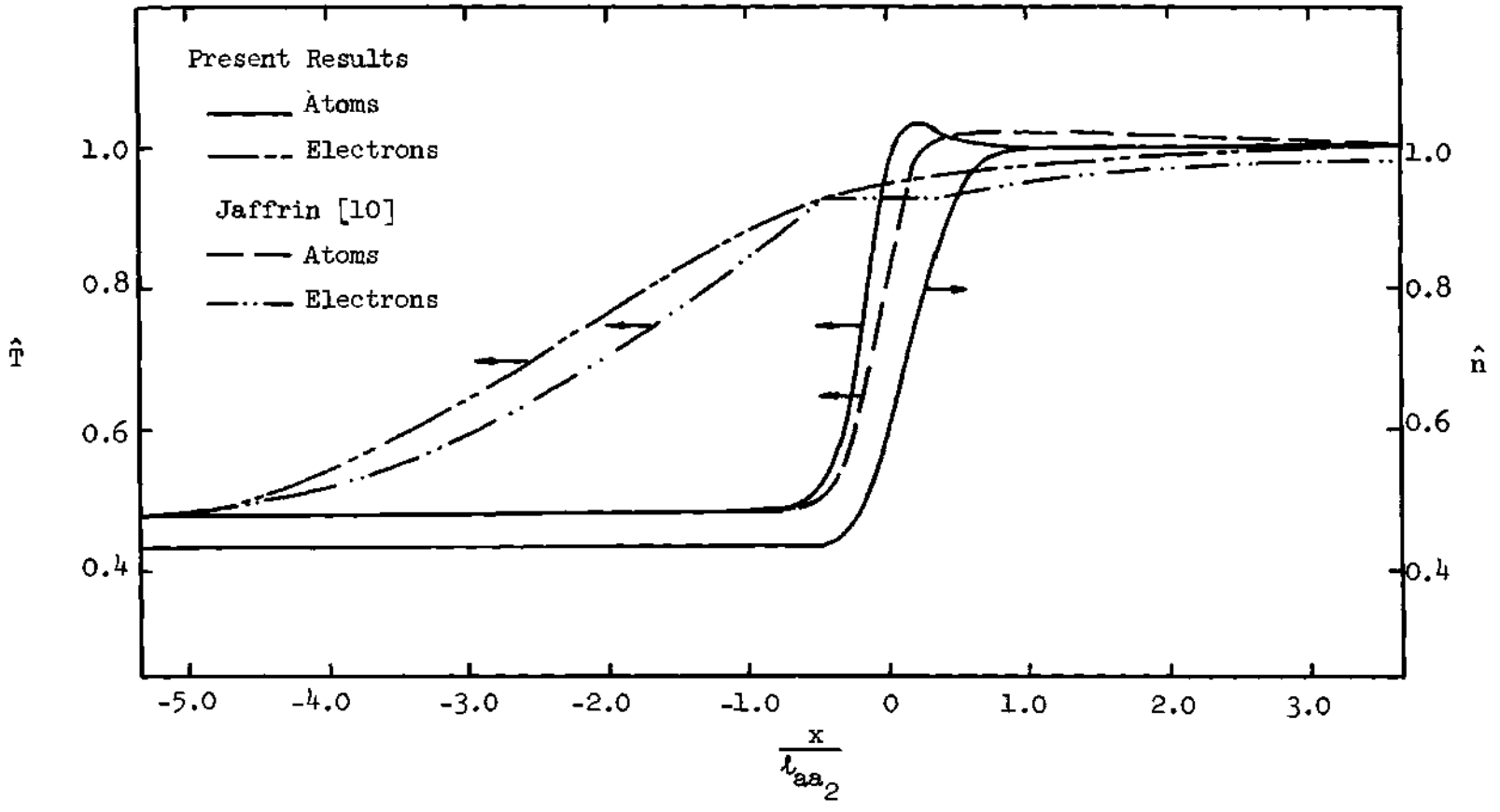

Figure 16. Temperature and Number Density Profiles for $M_1 = 2.0$, $\alpha = 0.1$, $\hat{E} = 0$.

to point out that the ion temperature leads the atom temperature in the upper half of the shock, then the atom temperature takes over the lead for the lower half of the shock. Physically, this phenomenon indicates that the electron-ion interaction is stronger than the electron-atom interaction even though the mass difference between the ion and the atom is so small. This phenomenon can be more obvious as the flow becomes more nonequilibrium in high Mach number conditions. Temperatures of atoms and ions overshoot their downstream values, while the electron temperature is monotonically increasing to its downstream value. The local distribution functions of atoms, ions, and electrons are compared with their local Maxwellian values and are listed in Tables 5, 6, and 7, respectively. The maximum deviations of the local distribution functions of these three species from their local Maxwellian values are all of the order of 10^{-4}.

Figure 17 shows the velocity profile of atoms for $M_1 = 2.0$ and $\alpha = 0.5$. The upstream conditions are the same as those in the previous case. Ion and electron velocity profiles are not shown, because they deviate from the atom velocity profile by only 10^{-4}. The atom velocity takes the early lead until about one-fifth of a ℓ_{aa_2} downstream of the center of the shock. The present results are compared with Jaffrin's results [10]. His profiles have steeper slopes than the present results in the central portion of the shock structure. His ion velocity profile undershoots the downstream value while the present ion velocity is monotonically decreasing to the downstream value. This kind of discrepancy becomes more significant in the comparison of temperature profiles as shown in Figure 18. According to the present results, the differences

Table 5. Comparison of Atom Local Distribution Functions with Local Maxwellian Distribution Functions for $M_1 = 2.0$, $\alpha = 0.1$, $\hat{E} = 0$

I	J	$\hat{g}$	$\hat{G}$
25	38	.68231670-06	.68179074-06
	48	.12710100-01	.12708137-01
	58	.35583150+00	.35584436+00
	68	.14971710-01	.14968751-01
	78	.94673670-06	.94592872-06
50	38	.57233660-05	.42466810-05
	48	.21597280-01	.21365935-01
	58	.34419470+00	.34381872+00
	68	.17604420-01	.17695893-01
	78	.31512070-05	.29130689-05
75	32	.99181110-03	.99180639-03
	42	.11283310+00	.11283287+00
	52	.56398610+00	.56398562+00
	62	.12385800+00	.12385802+00
	72	.11950980-02	.11950990-02

Table 6. Comparison of Ion Local Distribution Functions with Local Maxwellian Distribution Functions for $M_1 = 2.0$, $\alpha = 0.1$, $\hat{E} = 0$

I	J	$\hat{g}$	$\hat{G}$
25	38	.68175590-06	.68119435-06
	48	.12707800-01	.12705643-01
	58	.35584310+00	.35585655+00
	68	.14969030-01	.14966009-01
	78	.94596540-06	.94512605-06
50	38	.57762360-05	.43550641-05
	48	.21703630-01	.21486109-01
	58	.34385830+00	.34345434+00
	68	.17699180-01	.17788043-01
	78	.32805100-05	.29849378-05
75	32	.99180760-03	.99180384-03
	42	.11283300+00	.11283280+00
	52	.56398620+00	.56398571+00
	62	.12385790+00	.12385797+00
	72	.11950950-02	.11950963-02

Table 7. Comparison of Electron Local Distribution Functions with Local Maxwellian Distribution Functions for $M_1 = 2.0$, $\alpha = 0.1$, $\hat{E} = 0$

I	J	$\hat{g}$	$\hat{G}$
25	28	.75166340-05	.88669329-05
	38	.26098270-01	.26720458-01
	48	.32778550+00	.32587735+00
	58	.15600050-01	.16084376-01
	68	.48159540-05	.32128764-05
50	28	.31976630-03	.30944454-03
	38	.54066630-01	.53831990-01
	48	.26955570+00	.26941645+00
	58	.38601920-01	.38791257-01
	68	.15698910-03	.16068291-03
75	28	.14049650-02	.14041426-02
	38	.13601200+00	.13600497+00
	48	.56438030+00	.56437786+00
	58	.10032940+00	.10033600+00
	68	.76370420-03	.76421442-03

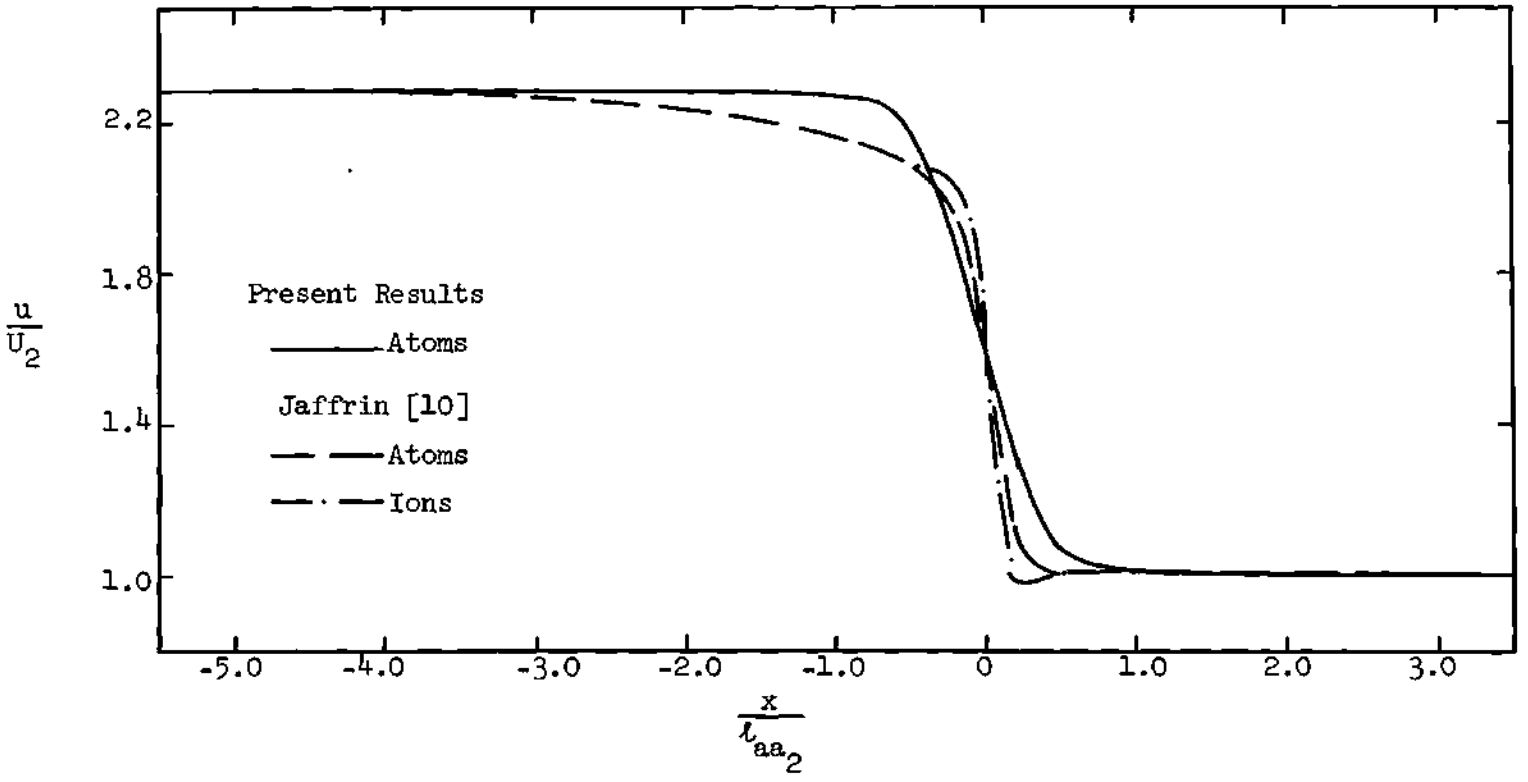

Figure 17. Velocity Profile for $M_1 = 2.0$, $\alpha = 0.5$, $\hat{E} = 0$.

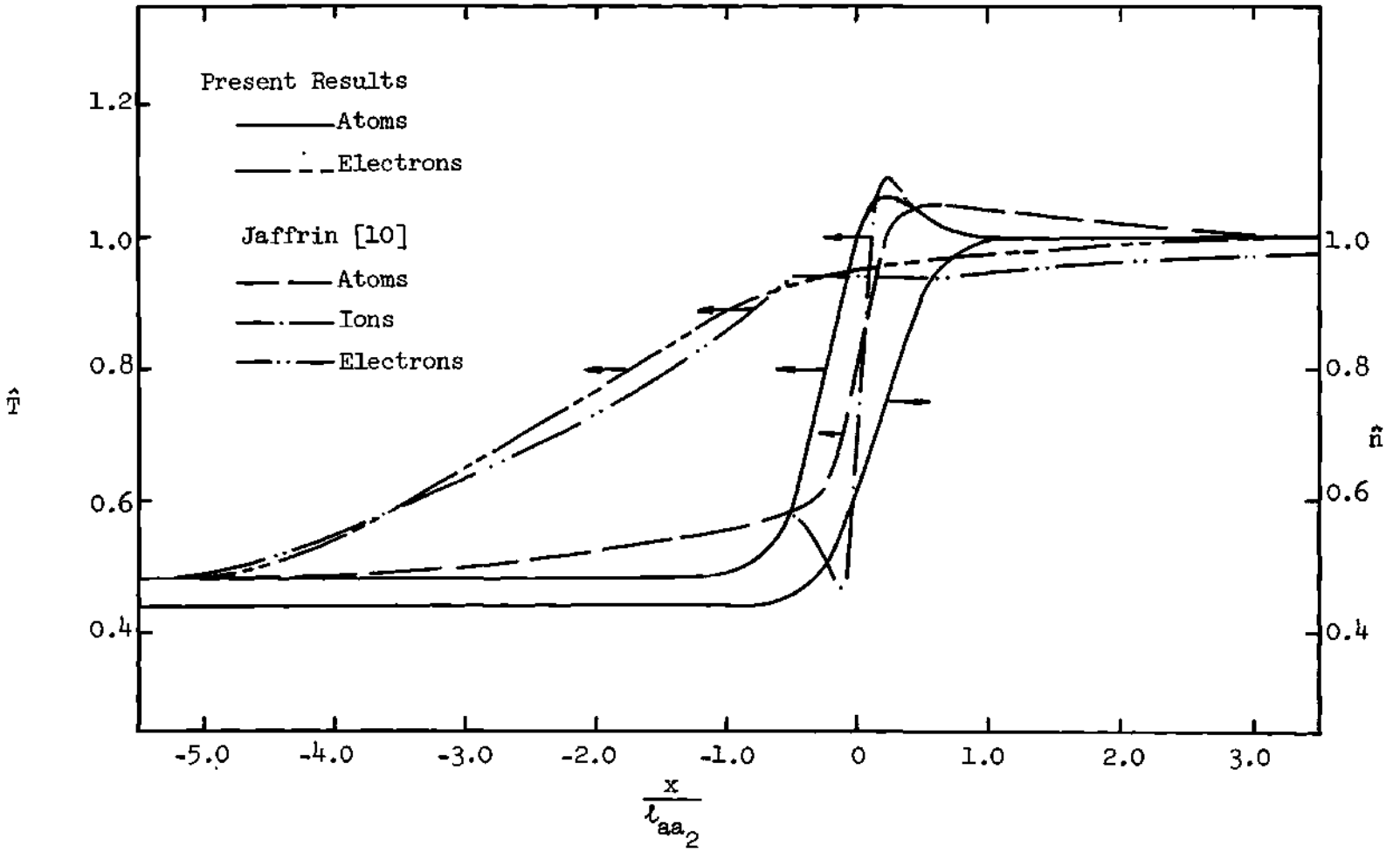

Figure 18. Temperature and Number Density Profiles for M_1=2.0, α = 0.5, $\hat{E}$ = 0.

between ion and atom temperatures are too small to be shown in the figure. Jaffrin's ion temperature undershoots the upstream value. However, the present method does not predict any undershoot. Both methods predict that the temperatures of heavy particles overshoot their downstream temperature. It is noted that the overshoots are greater as the degree of ionization increases. The distribution functions of atoms, ions, and electrons at various locations across the shock are shown in Figure 19, 20, and 21, respectively. These curves are all single-peaked.

For comparison, the case studied by Grewal and Talbot [7] has been investigated. The upstream equilibrium conditions are $n_e = 10^{14}$ cm^{-3}, $n_a = 10^{16}$ cm^{-3}, $T_e = 3500$ °K, $T_a = 700$ °K, and $M_1 = 10$. Figure 22 gives the velocity profiles of atoms and ions. The electron velocity profile is not shown in the figure since it is identical with the ion velocity profile under the assumptions made inthis chapter. It is noted that due to strong electron-ion interactions the ion velocity profile deviates away from the atom velocity profile in the low pressure region of the shock structure. However, in the high pressure region of the shock structure, both velocity profiles tend to merge. The effects of strong electron-ion interactions are also demonstrated in Figure 23. Electrons are heated up much earlier than ions and atoms. Ions tend to move together with electrons, hence their temperature rises earlier than the atom temperature even the difference in mass between the ion and the atom is negligibly small. But this early rise of the ion temperature cannot be seen in the results of Grewal and Talbot [7], because ions and atoms have been grouped into one species. The electron temperatures predicted by both methods are in good agreement. Present atom temperatures agree

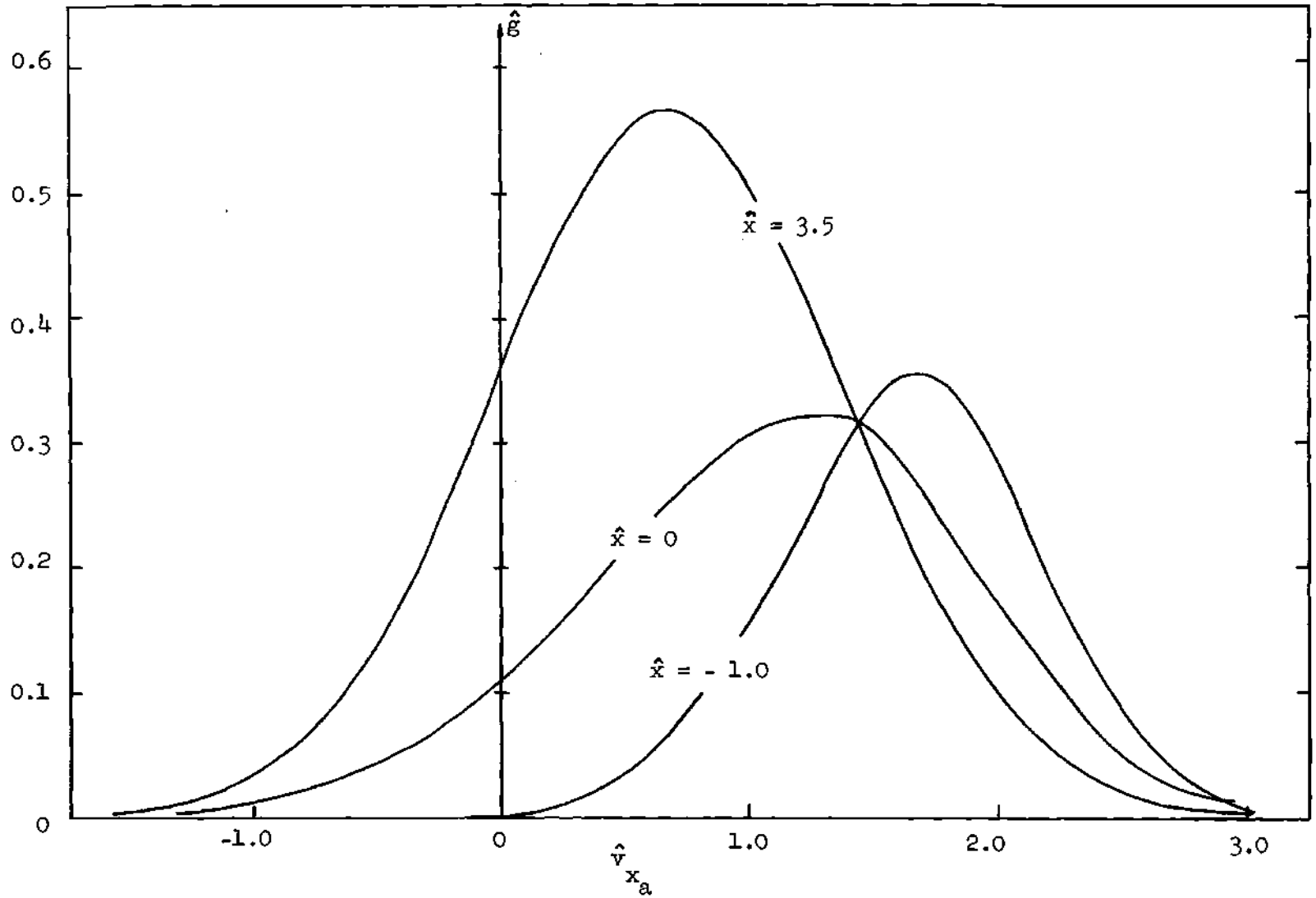

Figure 19. Atom Distribution Functions at Various Locations Across the Shock for $M_1 = 2.0$, $\alpha = 0.5$, $\hat{E} = 0$.

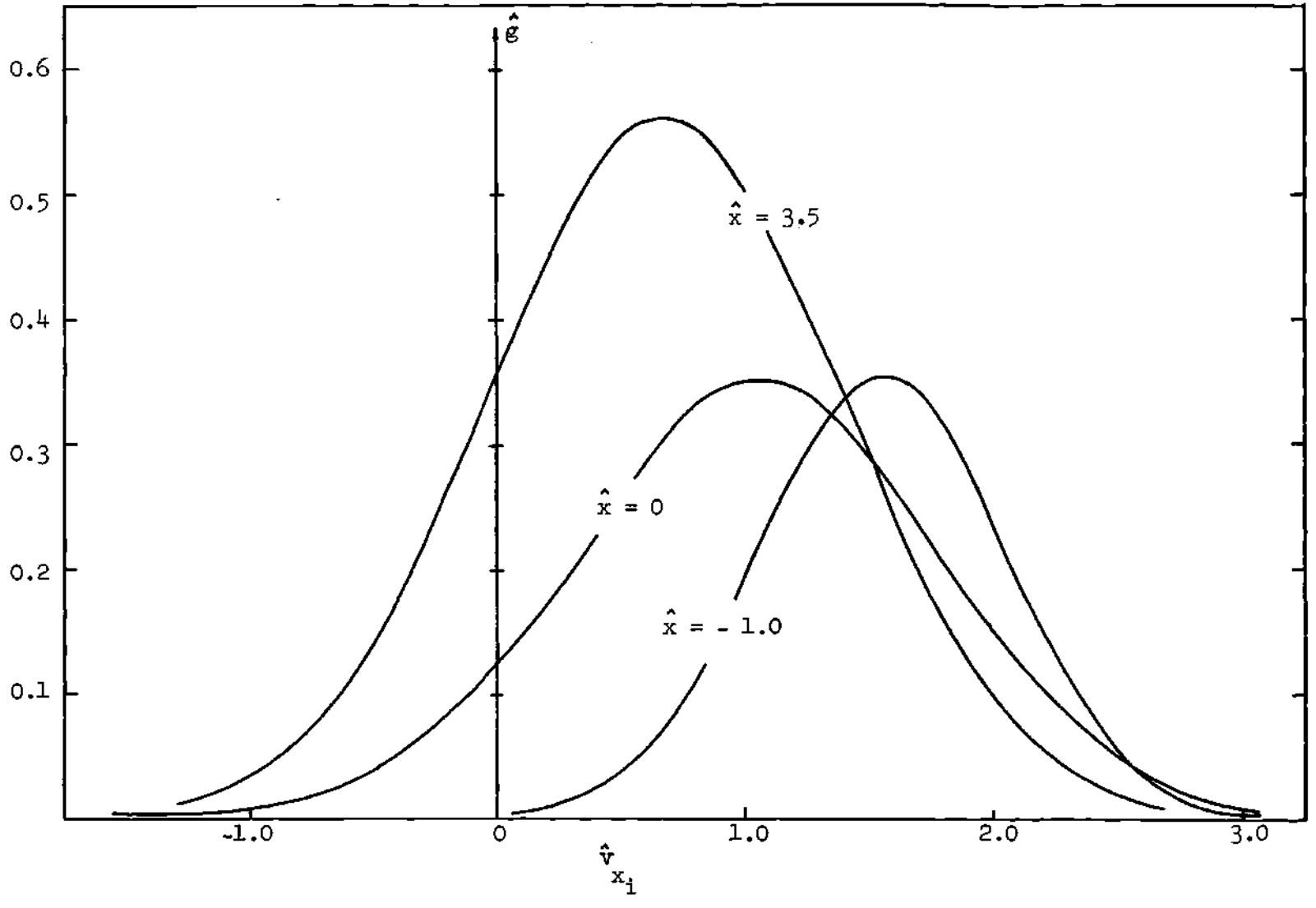

Figure 20. Ion Distribution Functions at Various Locations Across the Shock for $M_1 = 2.0$, $\alpha = 0.5$, $\hat{E} = 0$.

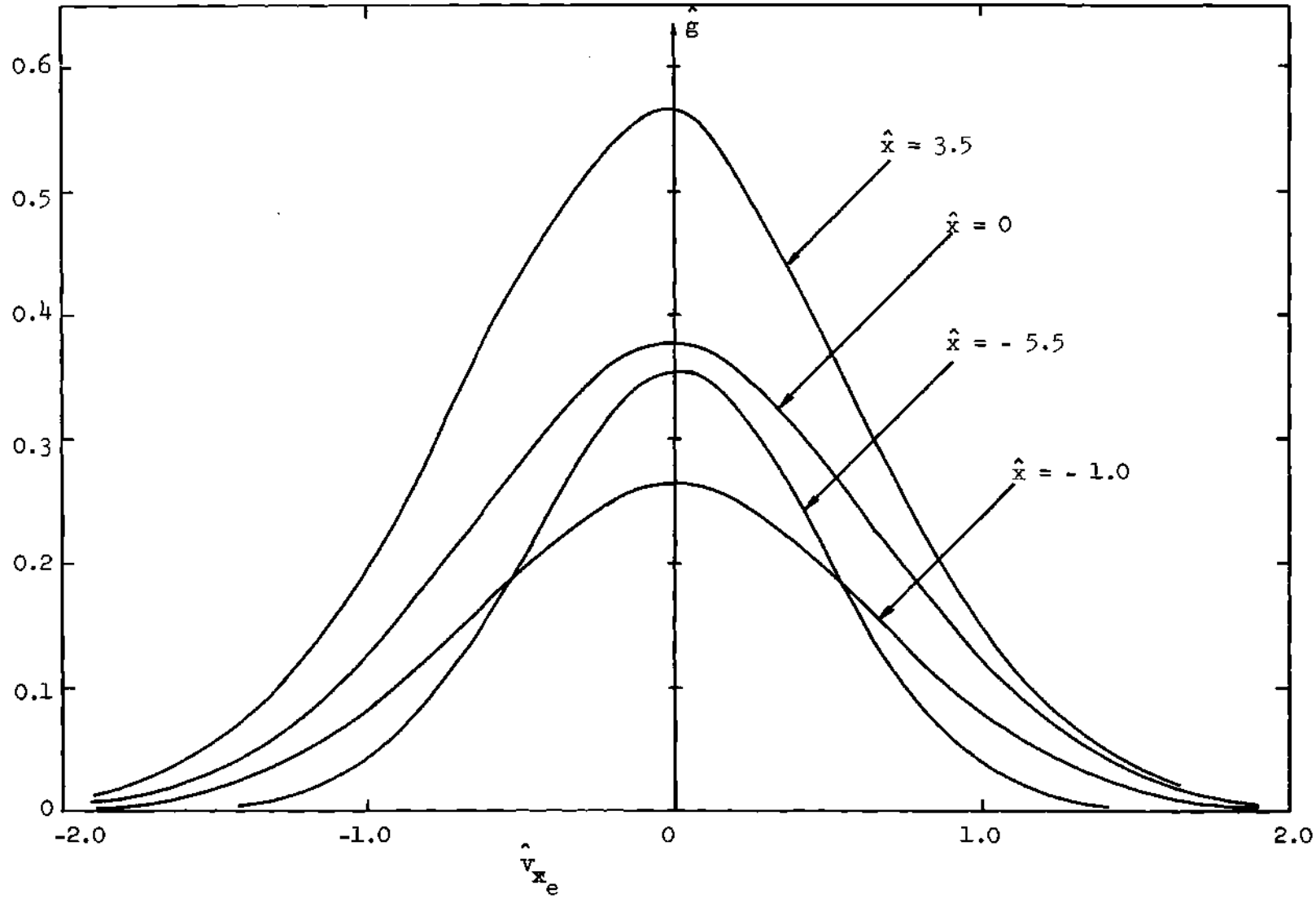

Figure 21. Electron Distribution Functions at Various Locations Across the Shock for $M_1 = 2.0$, $\alpha = 0.5$, $\hat{E} = 0$.

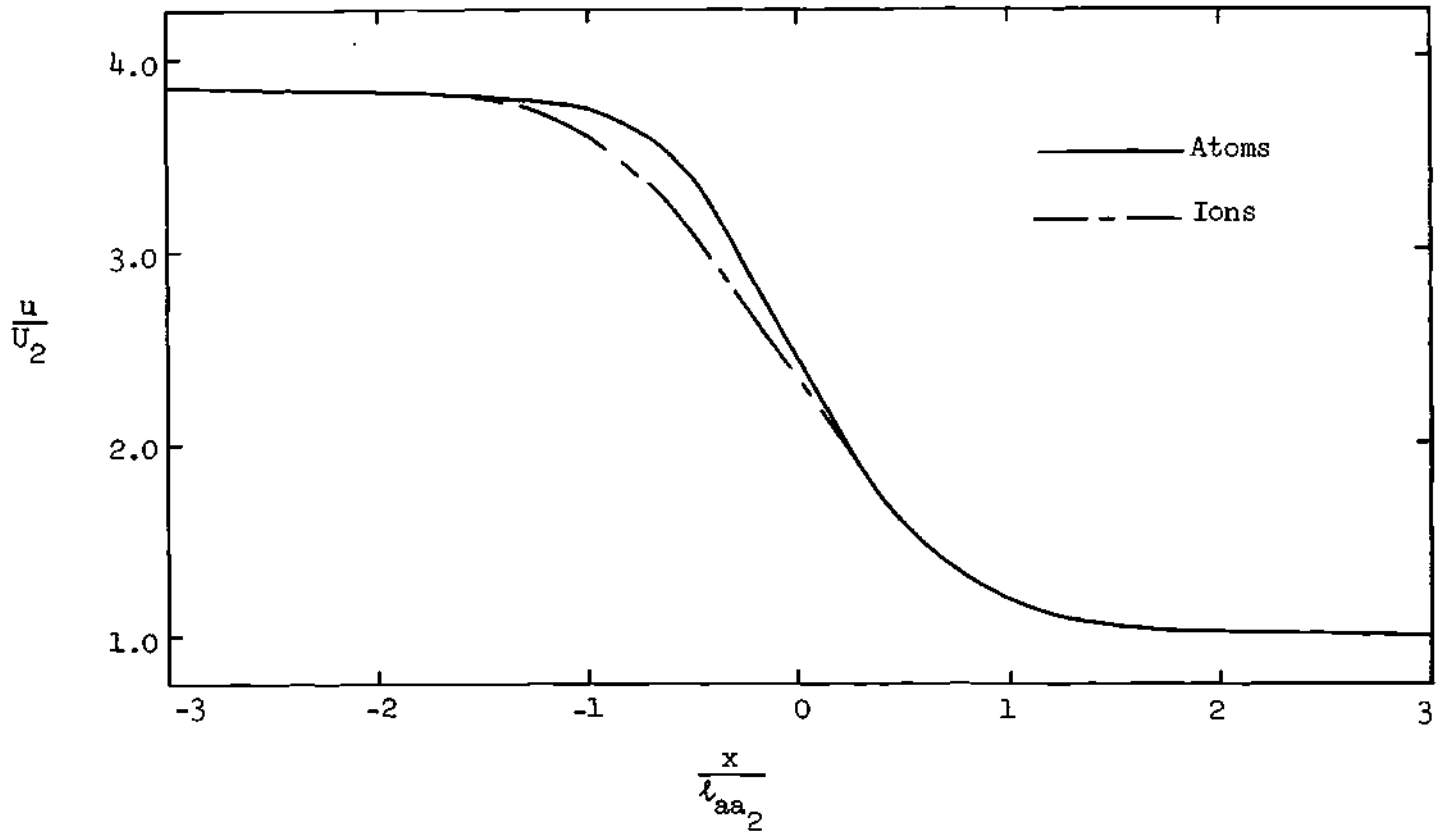

Figure 22. Velocity Profiles of Atoms and Ions at $M_1 = 10$, $\alpha = 0.01$, $\hat{E} = 0$.

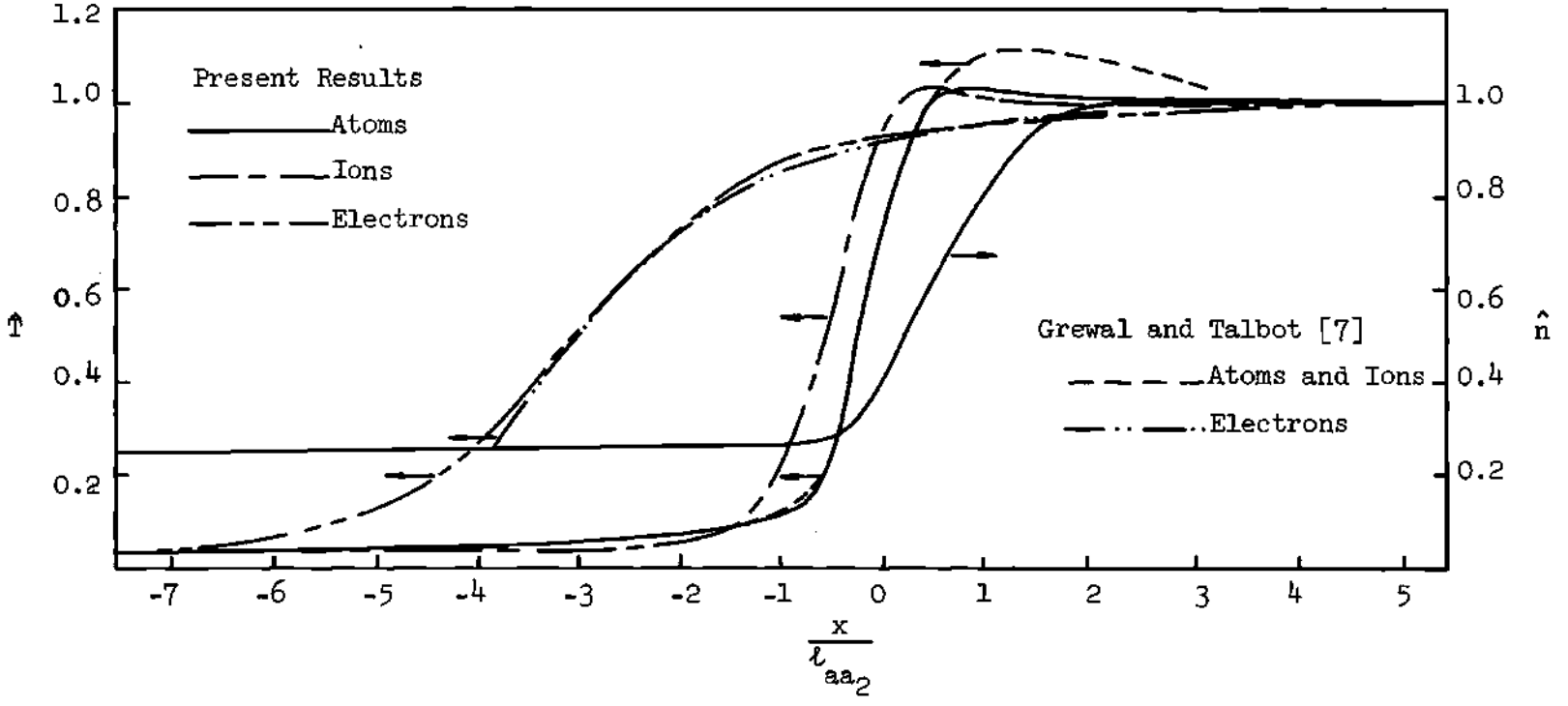

Figure 23. Temperature and Number Density Profiles for $M_1 = 10.0$, $\alpha = 0.01$, $\hat{E} = 0$.

well with their results in the front portion of the shock structure. However, in the high pressure region Reference 7 predicts a higher overshoot in the atom temperature.

It is significant to stress once more that the assumption of grouping atoms and ions into one species of heavy particles can be very misleading, although their difference in mass is so small. Figures 24 and 25 indicate the details of the physical behavior of atoms and ions across the shock structure. Atoms and ions profiles are plotted at the same locations for detailed comparisons. At the location of 1.5 ℓ_{aa_2} upstream of the center of the shock, the ion distribution function is completely different from the atom distribution function both in height and in width. At the center of the shock structure, the atom distribution function appears to be double-peaked and the ion distribution function is single-peaked. Although the areas under these two curves may not have a great difference, yet the physical features of the curves are very different. Under the influence of electrons, ions appear to be less nonequilibrium than neutral particles. It is seen that ions and atoms move according to their own will. Electrons distribution functions at various locations across the shock is shown in Figure 26. The degrees of nonequilibrium of atoms, ions, and electrons are demonstrated in Tables 8, 9, and 10, respectively. It is noted that atoms are in extreme nonequilibrium. The maximum differences between their local distribution function and the corresponding local Maxwellian distribution function is in the order of 0.1. Table 10 shows that the maximum difference between electron local distribution function and electron local Maxwellian distribution function is in the order of 0.01. Therefore the assumption of the local

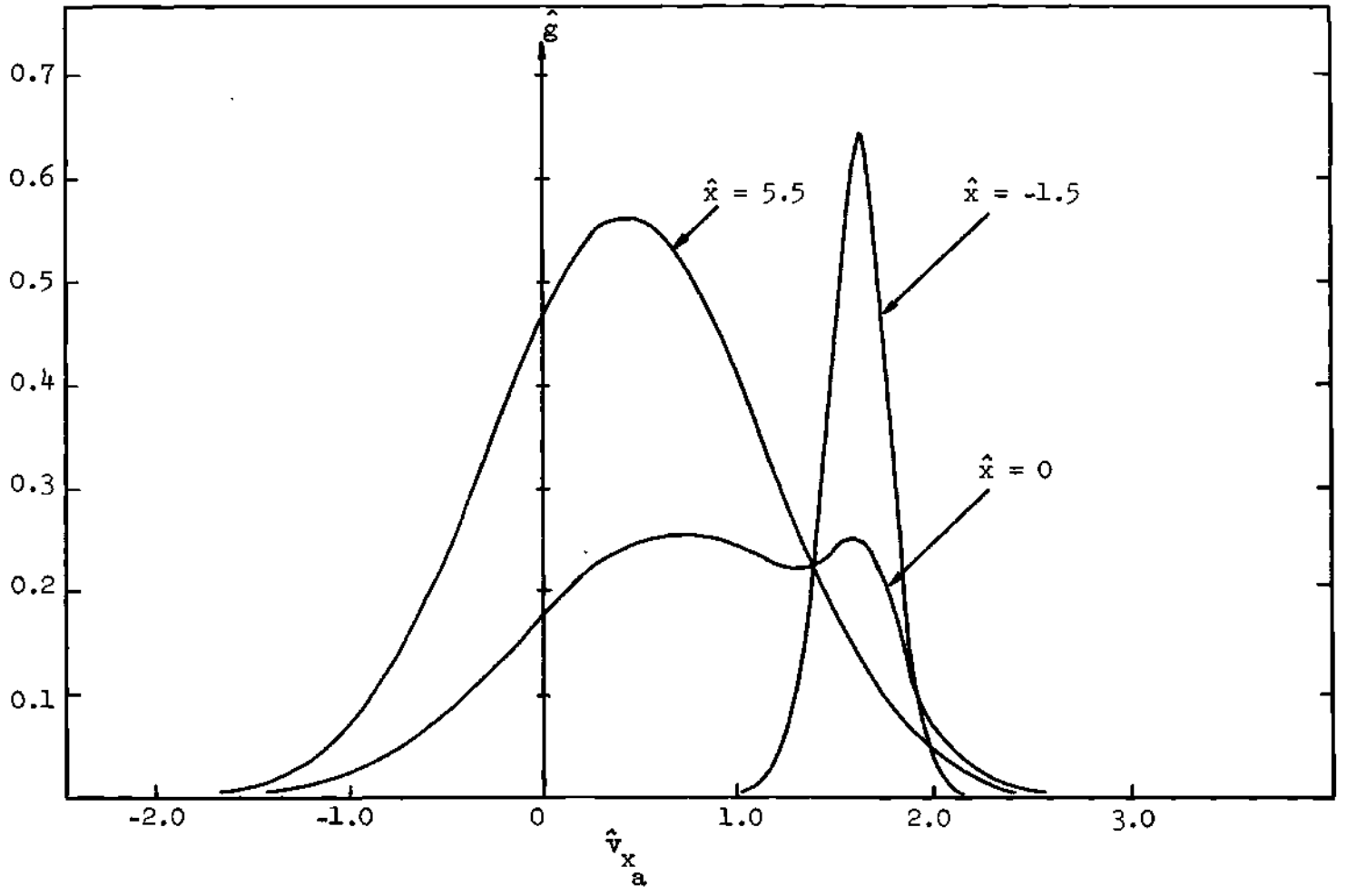

Figure 24. Atom Distribution Functions at Various Locations Across the Shock for $M_1 = 10$, $\alpha = 0.01$, $\hat{E} = 0$.

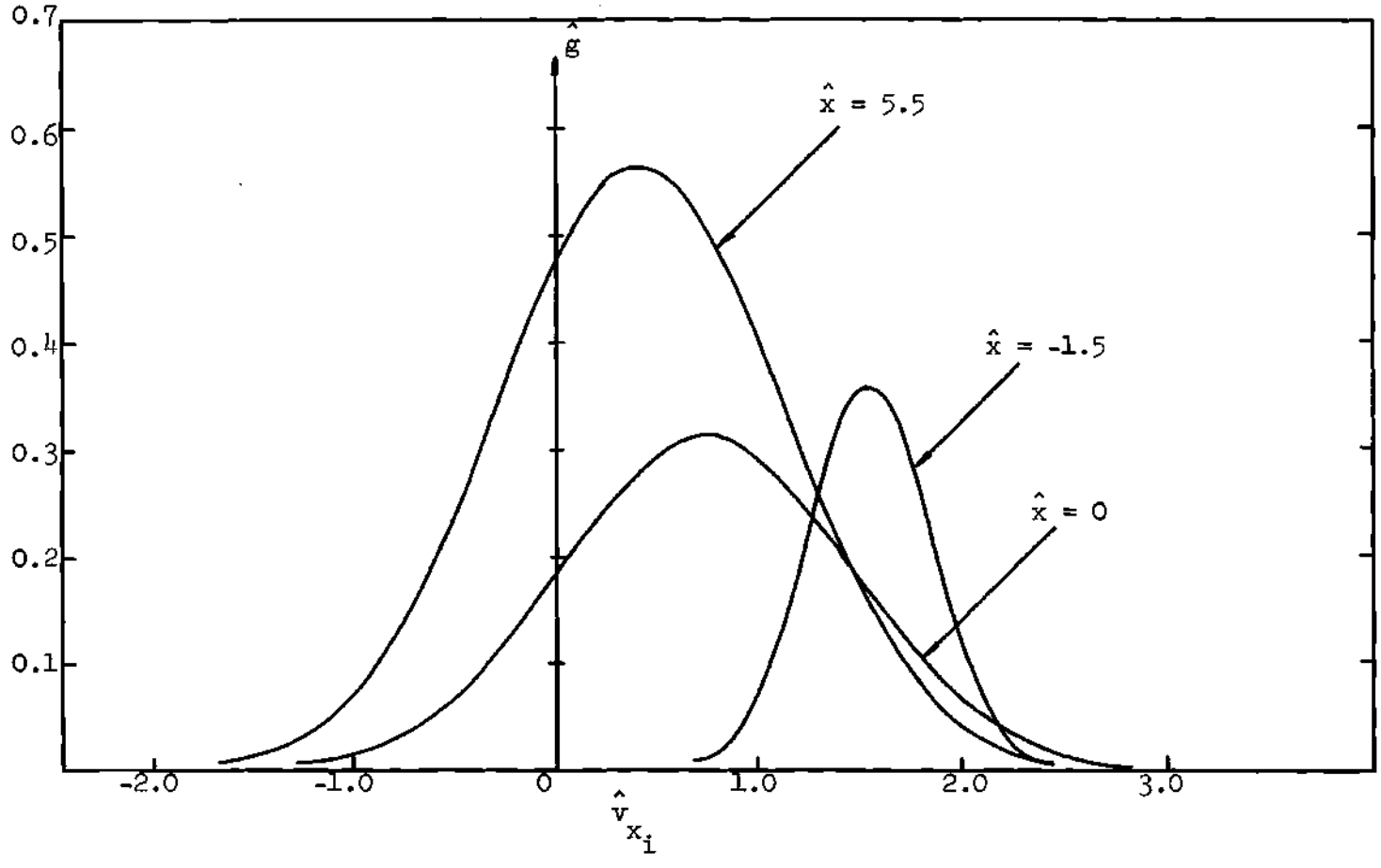

Figure 25. Ion Distribution Functions at Various Locations Across the Shock for $M_1 = 10$, $\alpha = 0.01$, $\hat{E} = 0$.

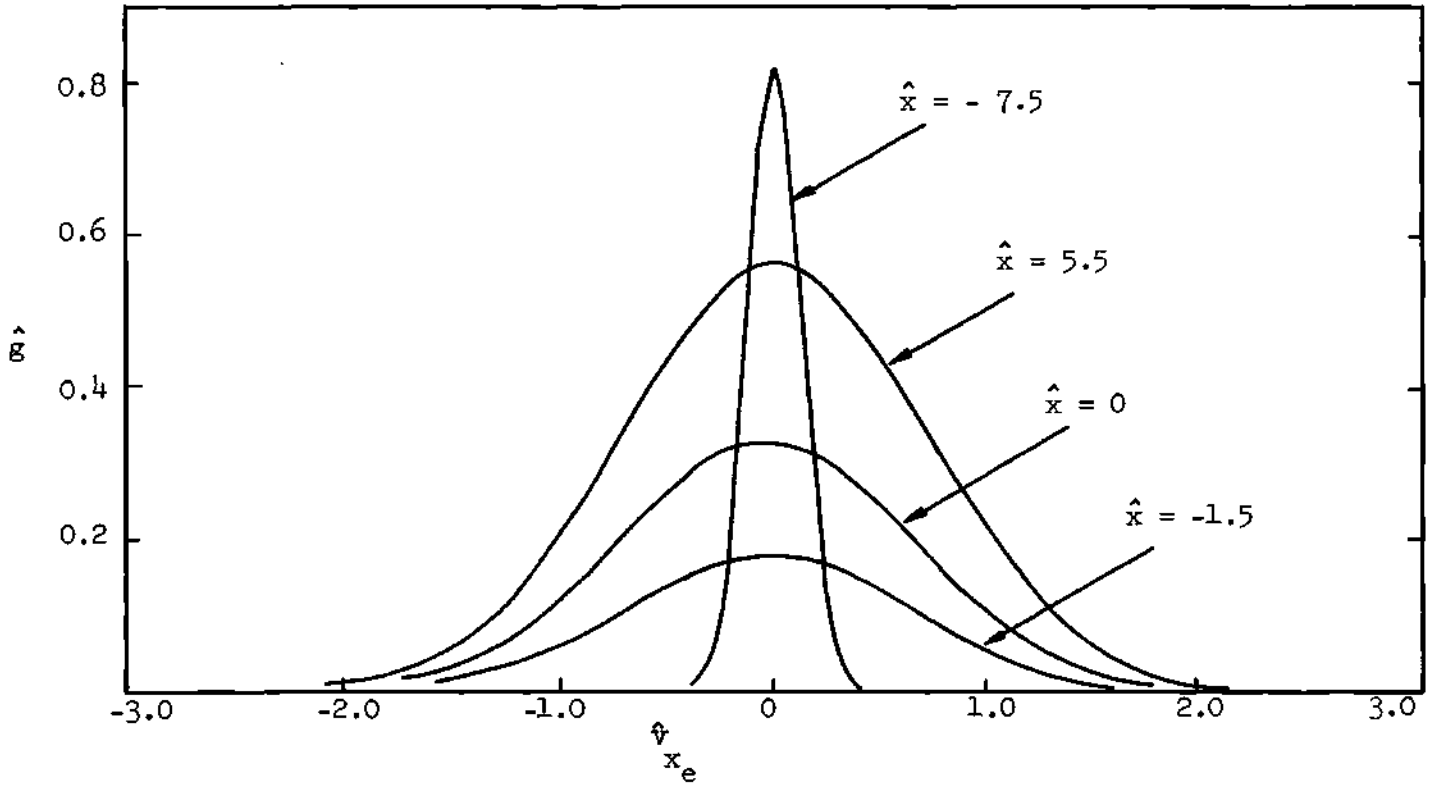

Figure 26. Electron Distribution Functions at Various Locations Across the Shock for $M_1 = 10$, $\alpha = 0.01$, $\hat{E} = 0$.

Table 8. Comparison of Atom Local Distribution Functions with Local Maxwellian Distribution Functions for $M_1 = 10$, $\alpha = 0.01$, $\hat{E} = 0$

I	J	$\hat{g}$	$\hat{G}$
25	50	.62634090-05	0
	89	.34937390-03	0
	120	.18381570-25	.40142972-25
	152	.36667060-04	.31057515-02
	166	.79492880+00	.69030709+00
	180	.64137440-03	.33046748-02
50	50	.27721750-04	.37041113-21
	107	.96375680-02	.38440012-05
	122	.67228150-02	.88450105-03
	166	.48133380+00	.26380547+00
	187	.58843170-02	.18219716-01
	205	.54950930-04	.11515117-03
75	57.	.58965260-03	.59759396-03
	70	.52012660-02	.52512006-02
	88	.53521000-01	.53806543-01
	132	.56591810+00	.56568444+00
	176	.52420650-01	.52275016-01
	194	.50778920-02	.50418195-02

Table 9. Comparison of Ion Local Distribution Functions with Local Maxwellian Distribution Functions for $M_1 = 10$, $\alpha = 0.01$, $\hat{E} = 0$

I	J	$\hat{g}$	$\hat{G}$
25	50	0	0
	89	0	0
	120	.19189900-33	.40905208-36
	152	.29343520-03	.29310439-03
	166	.81835610+00	.81837324+00
	180	.50935930-03	.50922362-03
50	50	.42402640-08	.19944132-09
	107	.40819260-02	.28708999-02
	122	.30231800-01	.28839592-01
	156	.23622080+00	.23491841+00
	187	.35165010-01	.36001551-01
	205	.21528430-02	.23079199-02
75	57	.58201440-03	.58198851-03
	70	.51447060-02	.51445350-02
	88	.53078590-01	.53077523-01
	132	.56377050+00	.56377088+00
	176	.52146620-01	.52146891-01
	194	.50178770-02	.50178894-02

Table 10. Comparison of Electron Local Distribution Functions with Local Maxwellian Distribution Functions for $M_1 = 10$, $\alpha = 0.01$, $\hat{E} = 0$

I	J	$\hat{g}$	$\hat{G}$
25	75	.68154060-04	.23552154-04
	90	.52502770-02	.42993646-02
	105	.99919510-01	.98695710-01
	120	.28505430+00	.28491326+00
	135	.10184920+00	.10343022+00
	150	.39363060-02	.47217462-02
50	75	.17216130-01	.13240861-01
	90	.72763170-01	.59303583-01
	105	.17013230+00	.14608015+00
	120	.22045910+00	.19790058+00
	135	.15797570+00	.14745126+00
	150	.61886590-01	.60422050-01
75	75	.45871940-01	.45769144-01
	90	.18516090+00	.18513044+00
	105	.42821140+00	.42845639+00
	120	.56702060+00	.56736064+00
	135	.42960580+00	.42986844+00
	150	.18609800+00	.18635270+00

Maxwellian distribution is definitely not adequate to be used for electrons in thie case.

The last case to be included in this chapter is the one with the upstream equilibrium conditions $M_1 = 10$, $T_1 = 10^3$ °K, and $n_{a_1} + n_{i_1} = 10^{15}$ cm^{-3}. The frozen degree of ionization is 0.1. Since this case with the effects of E field was previously investigated by Jaffrin [10] using Navier-Stokes equations, his results can be used for comparison with the present results. Figure 27 shows the present results for atoms. Since ion and electron velocities are so close to the atom velocity, they are not shown in the figure. The maximum difference between the ion velocity and the atom velocity is at the center of the shock structure and the value is 0.0464721. Again, due to the assumptions made in this chapter, the electron velocity is equal to the ion velocity. The results of Jaffrin [10] are also shown in the figure for comparison. The slope of the present results in the main part of the shock structure is steeper than the Navier-Stokes solutions of Jaffrin. His ion velocity overshoots the upstream value. However, the present results are continuous. A comparison of his ion temperature and the present results is given in Figure 28. Apparently his ion temperature can not approach the upstream temperature. This difficulty may have connection with his assumption that the electron temperature could be kept constant inside the main part of the atom shock. Both methods predict that electrons are heated up earlier than ions and atoms. However, the initial rise of Jaffrin's electron temperature is sharper than the present electron temperature. The atom and ion temperatures obtained from both approaches overshoot their downstream values. The present overshoots are greater than those of

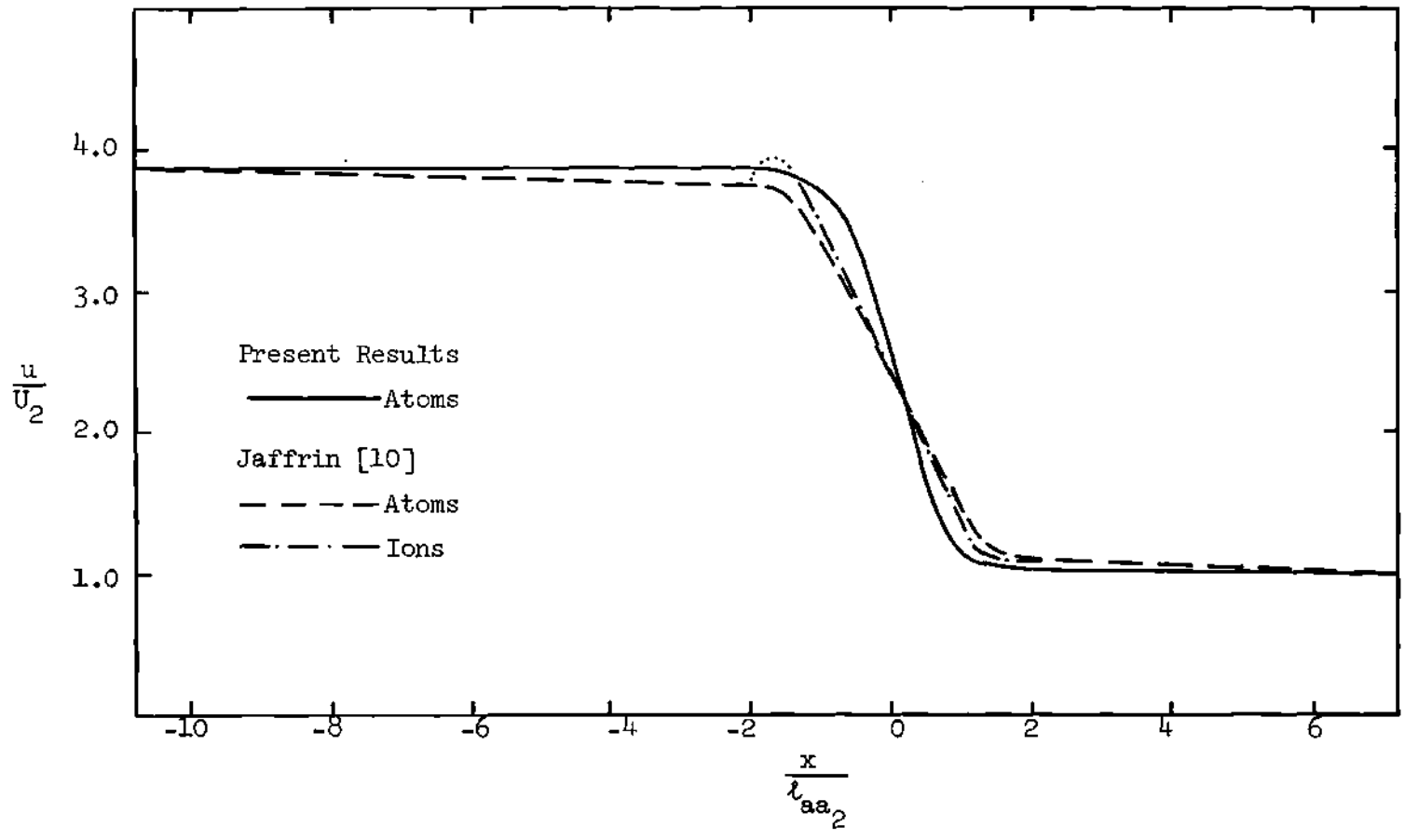

Figure 27. Velocity Profile for $M_1 = 10.0$, $\alpha = 0.1$, $\hat{E} = 0$.

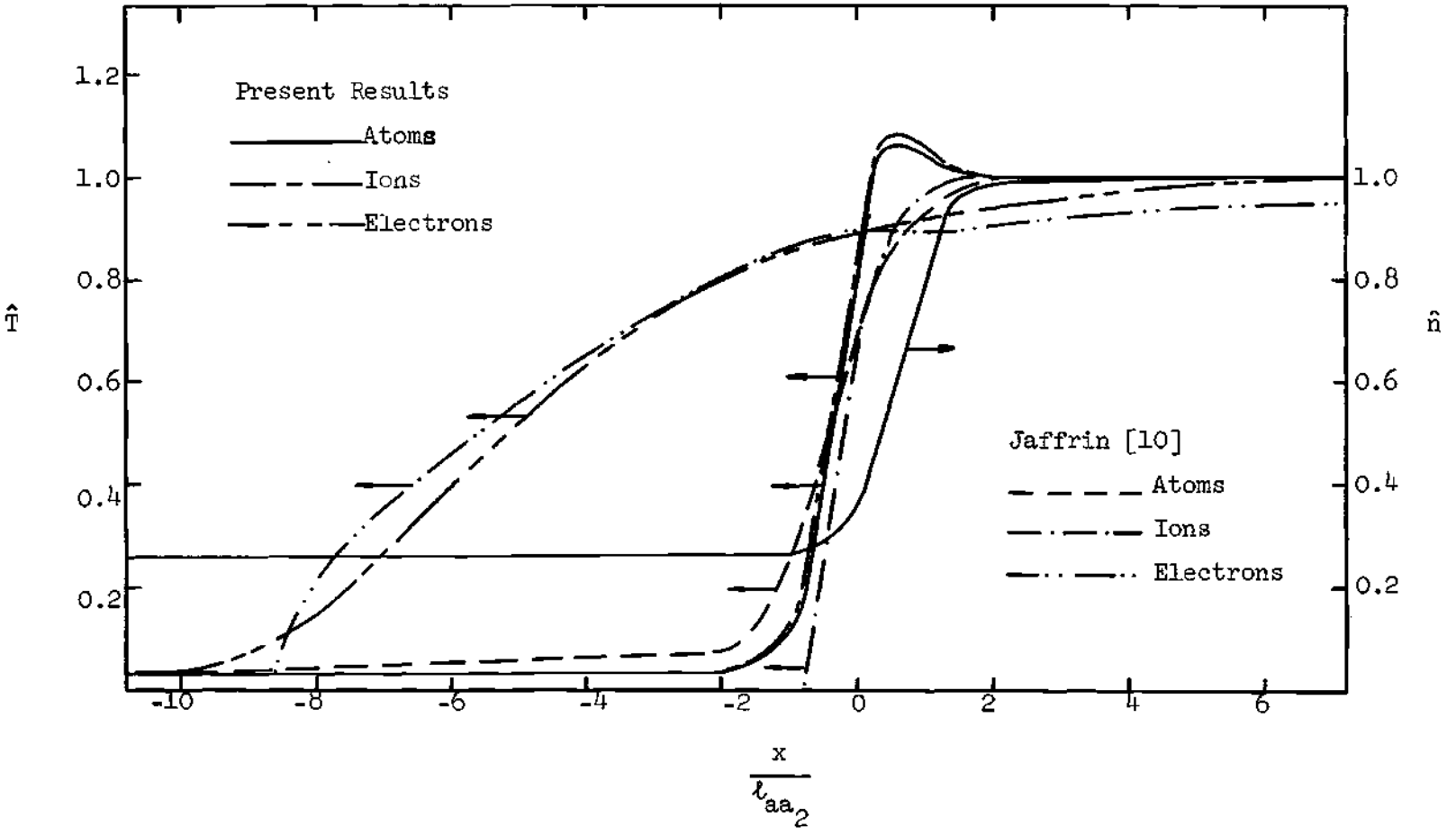

Figure 28. Temperature and Number Density Profiles for $M_1 = 10$, $\alpha = 0.1$, $\hat{E} = 0$.

Jaffrin. The distribution functions of atoms, ions, and electrons are shown in Figures 29, 30 and 31, respectively. For this case, atom distribution functions look similar to ion distribution functions except in a small region upstream of the center of the shock structure where the atom distribution functions contain two peaks. The smaller peak of the atom distribution function at $\hat{x} = -2.0$ has been magnified in order to make it visible in the figure. In general, the case of $\alpha = 0.1$ is less nonequilibrium than the previous case of $\alpha = 0.01$. This equilibrating process can be due to stronger electron effects in a medium with a higher degree of ionization.

From the results shown in this chapter it is noted that the present results for neutral particles and electrons obtained from the discrete ordinate method are generally in fairly good agreement with the Navier-Stokes solutions of Jaffrin [10] at the low Mach number and with the Mott-Smith solutions of Grewal and Talbot [7] at the high Mach number. However, it appears that the discrete ordinate method has the advantage over the other two approacher [7, 10] in obtaining the results for ions. The discrete ordinate method can also provide the detailed descriptions of the behavior of individual species which can not be obtained from the other two approaches [7, 10]. Based on the present results the E field effects on the shock-wave structure, which was included in References [8] and [10], may not be significant.

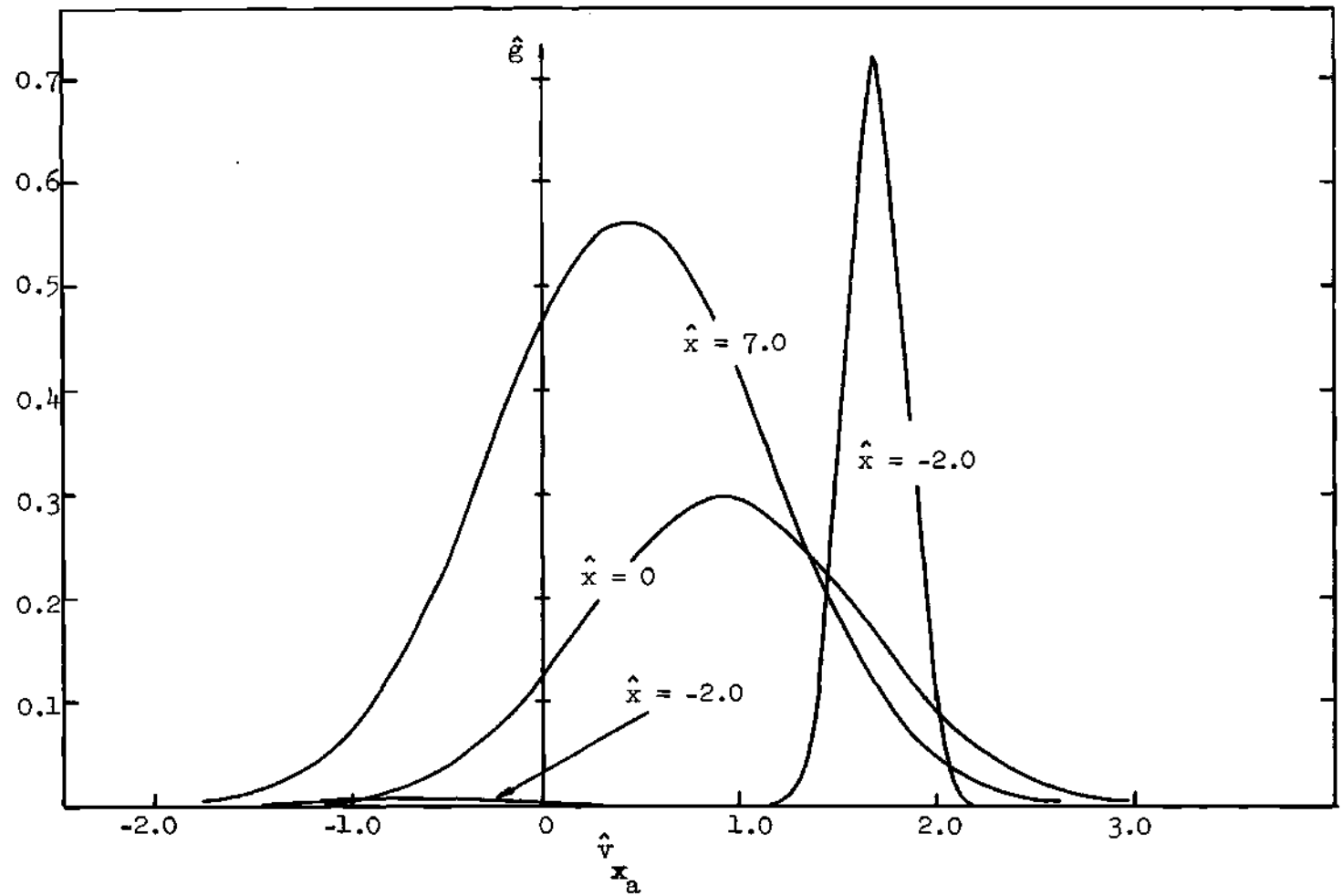

Figure 29. Atom Distribution Functions at Various Locations Across the Shock for $M_1 = 10$, $\alpha = 0.1$, $\hat{E} = 0$.

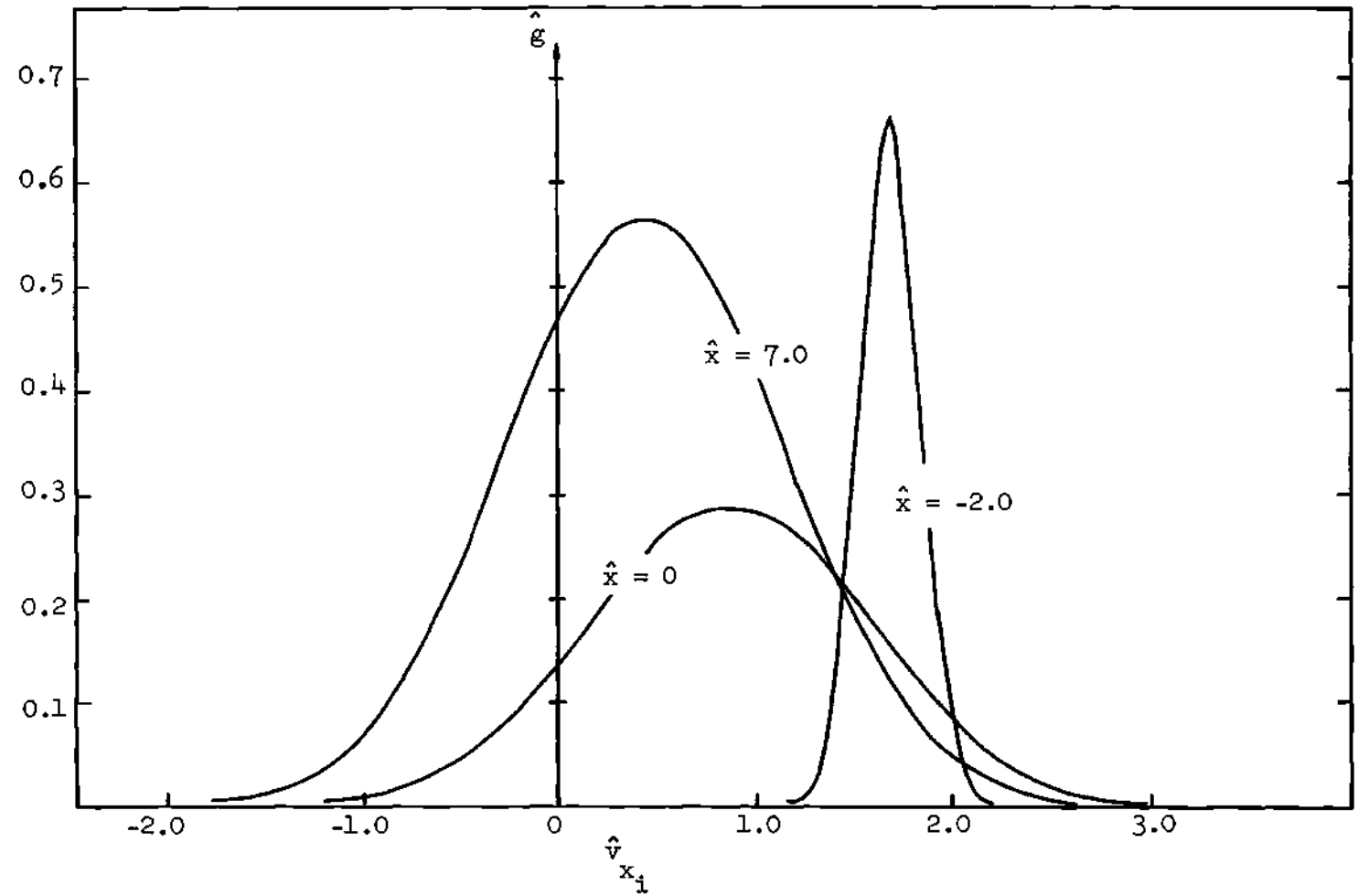

Figure 30. Ion Distribution Functions at Various Locations Across the Shock for $M_1 = 10$, $\alpha = 0.1$, $\hat{E} = 0$.

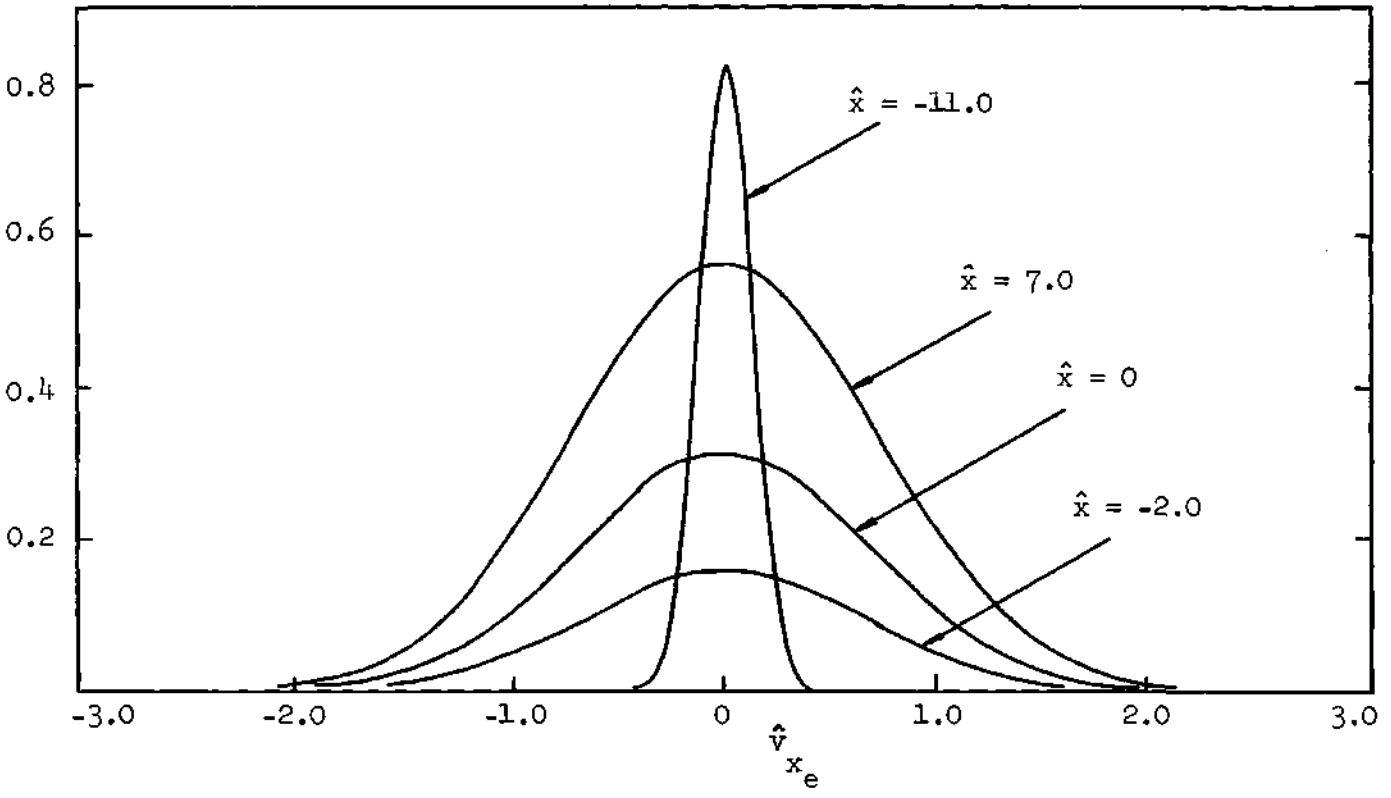

Figure 31. Electron Distribution Function at Various Locations Across the Shock for $M_1 = 10$, $\alpha = 0.1$, $\hat{E} = 0$.

CHAPTER IV

EFFECTS OF INDUCED ELECTRIC FIELD ON SHOCK-WAVE STRUCTURE

Introduction

Under the assumption that the effects of the induced electric field are negligibly small, shock-wave structures in fully and partially ionized argon were investigated in Chapter II and III, respectively, using the discrete ordinate method. The assumption has been made previously by several authors, for examples, Jukes [1] and Tidman [27] for the fully ionized case, and Grewal and Talbot [7] for the partially ionized case.

Results of the discrete ordinate method reported in Chapters II and III have been compared with the Navier-Stokes results of Jaffrin and Probstein [8] for the fully ionized case, and Jaffrin [10] for the partially ionized case. Some discrepancy between the two approaches has been noted. There is a possibility that the disagreement, especially the ion comparison, could be due to the effects of the induced electric field, which was partially taken into account in those results of References [8] and [10].

In a nonequilibrium flow problem of an ionized gas, such as the shock-wave structure, the charged particles in the flow can be caused to separate and as a consequence an electric field can be induced. The electric field in turn interacts with the charged particles and causes them to accelerate or decelerate. When the acceleration or deceleration term in the Boltzmann equation is included, a high degree of numerical

accuracy and a large storage capacity of a computer are needed in order to obtain meaningful solutions.

The purpose of the present chapter is to evaluate the significance of the effects of the induced electric field on the shock-wave structure in an ionized gas with properties encountered in most engineering applications. However, due to the constraints of the numerical accuracy and the capacity limitation of the available computer facility, the subject can only be studied approximately. The difficulties involved will be pointed out in detail as the study proceeds.

Formulation of the Problem

When the induced electric field is included in the analysis, the governing BBGK equations for a steady plane shock wave in a partially ionized gas become

$$v_{x_1}\frac{\partial f_1}{\partial x} + a_{x_1}\frac{\partial f_1}{\partial v_{x_1}} = \frac{n_1}{\sigma_{11}}(F_{11}-f_1) + \frac{n_2}{\sigma_{12}}(F_{12}-f_1) + \frac{n_3}{\sigma_{13}}(F_{13}-f_1), \tag{1}$$

$$v_{x_2}\frac{\partial f_2}{\partial x} + a_{x_2}\frac{\partial f_2}{\partial v_{x_2}} = \frac{n_1}{\sigma_{21}}(F_{21}-f_2) + \frac{n_2}{\sigma_{22}}(F_{22}-f_2) + \frac{n_3}{\sigma_{23}}(F_{23}-f_2), \tag{2}$$

and

$$v_{x_3}\frac{\partial f_3}{\partial x} = \frac{n_1}{\sigma_{31}}(F_{31}-f_3) + \frac{n_2}{\sigma_{32}}(F_{32}-f_3) + \frac{n_3}{\sigma_{33}}(F_{33}-f_3), \tag{3}$$

where the local Maxwellian distributions F_{kl} in Equations (1) - (3) are defined as

$$F_{k\ell} = n_k \left(\frac{m_k}{2\pi K T_{k\ell}} \right)^{3/2} \exp\left\{ - \frac{m_k[(V_x - u_{k\ell})^2 + V_y^2 + V_z^2]}{2K T_{k\ell}} \right\}. \tag{4}$$

Subscripts k, ℓ = 1, 2, 3 stand for electrons, ions, and atoms, respectively.

a_{x_1} and a_{x_2} in Equations (1) and (2) are caused by interactions of the induced electric field and the charged particles. Mathematically,

$$a_{x_1} = \frac{e_1}{m_1} E = - \frac{e_1}{m_1} \frac{d\phi}{dx} \tag{5-a}$$

and

$$a_{x_2} = \frac{e_2}{m_2} E = - \frac{e_2}{m_2} \frac{d\phi}{dx}, \tag{5-b}$$

where E is the induced electric field, e_1 = - e, e is the electric charge, and e_2 = e.

The electrostatic potential is denoted by ϕ and is governed by Poisson's equation. For the present problem the Poisson's equation* becomes

$$\frac{d^2\phi}{dx^2} = - \frac{e}{\epsilon_0} (n_2 - n_1), \tag{6}$$

or in terms of E,

$$\frac{dE}{dx} = \frac{e}{\epsilon_0} (n_2 - n_1), \tag{7}$$

*In this thesis Equation (6) or Equation (7) will be referred to as Poisson's equation.

where ϵ_0 is the permitivity of vacuum.

Equation (1) - (6) form a complete set of the governing equations. They have to be solved simultaneously with appropriate boundary conditions.

The macroscopic flow properties involved in the governing equations can be obtained by taking the moments of the distribution functions as stated in Chapter II. The collision cross sections given in Chapters II and III will be used in this chapter. The reduced distribution functions g_k, h_k, $G_{k\ell}$, and $H_{k\ell}$ are defined as those presented in Chapter II. In addition to the nondimensional quantities defined in Chapters II and III the following nondimensional quantities are introduced

$$\hat{x} = \frac{x}{(L)_2}; \qquad \hat{\nu}_{k\ell} = \frac{(L)_2}{(V_{k\ell})_2}\nu_{k\ell}; \qquad \hat{E} = \frac{eEL^*}{2K(T)_2},$$

$(L)_2$ and L* are characteristic lengths. As examples, $(L)_2$ can be a mean free path, $(\ell_{kk})_2$, and L* can be the Debye length, $(\lambda_D)_2$.

Consequently, the nondimensionalized governing equations and Poisson's equation in discrete ordinate form for a singly ionized gas become

$$\hat{\nu}_{j_1}\frac{\partial \hat{g}_{j_1}}{\partial \hat{x}} - \hat{E}\frac{(L)_2}{L^*}\frac{\partial \hat{g}_{j_1}}{\partial \hat{\nu}_{j_1}} = \hat{\nu}_{j_1}(\hat{G}_{j_{11}} - \hat{g}_{j_1}) + \hat{\nu}_{j_2}(\hat{G}_{j_{12}} - \hat{g}_{j_1}) + \hat{\nu}_{j_3}(\hat{G}_{j_{13}} - \hat{g}_{j_1}), \tag{8}$$

$$\hat{\nu}_{j_2}\frac{\partial \hat{g}_{j_2}}{\partial \hat{x}} + \hat{E}\frac{(L)_2}{L^*}\frac{\partial \hat{g}_{j_2}}{\partial \hat{\nu}_{j_2}} = \hat{\nu}_{j_1}(\hat{G}_{j_{21}} - \hat{g}_{j_2}) + \hat{\nu}_{j_2}(\hat{G}_{j_{22}} - \hat{g}_{j_2}) + \hat{\nu}_{j_3}(\hat{G}_{j_{23}} - \hat{g}_{j_2}), \tag{9}$$

$$\hat{v}_{j_3}\frac{\partial \hat{g}_{j_3}}{\partial \hat{x}} = \hat{\nu}_{31}(\hat{G}_{j_{31}} - \hat{g}_{j_3}) + \hat{\nu}_{32}(\hat{G}_{j_{32}} - \hat{g}_{j_3}) + \hat{\nu}_{33}(\hat{G}_{j_{33}} - \hat{g}_{j_3}), \tag{10}$$

$$\hat{v}_{j_1}\frac{\partial \hat{h}_{j_1}}{\partial \hat{x}} - \hat{E}\frac{(L)_2}{L^*}\frac{\partial \hat{h}_{j_1}}{\partial \hat{v}_{j_1}} = \hat{\nu}_{11}(\hat{H}_{j_{11}} - \hat{h}_{j_1}) + \hat{\nu}_{12}(\hat{H}_{j_{12}} - \hat{h}_{j_1}) + \hat{\nu}_{13}(\hat{H}_{j_{13}} - \hat{h}_{j_1}), \tag{11}$$

$$\hat{v}_{j_2}\frac{\partial \hat{h}_{j_2}}{\partial \hat{x}} + \hat{E}\frac{(L)_2}{L^*}\frac{\partial \hat{h}_{j_2}}{\partial \hat{v}_{j_2}} = \hat{\nu}_{21}(\hat{H}_{j_{21}} - \hat{h}_{j_2}) + \hat{\nu}_{22}(\hat{H}_{j_{22}} - \hat{h}_{j_2}) + \hat{\nu}_{23}(\hat{H}_{j_{23}} - \hat{h}_{j_2}), \tag{12}$$

$$\hat{v}_{j_3}\frac{\partial \hat{h}_{j_3}}{\partial \hat{x}} = \hat{\nu}_{31}(\hat{H}_{j_{31}} - \hat{h}_{j_3}) + \hat{\nu}_{32}(\hat{H}_{j_{32}} - \hat{h}_{j_3}) + \hat{\nu}_{33}(\hat{H}_{j_{33}} - \hat{h}_{j_3}), \tag{13}$$

and

$$\frac{d\hat{E}}{d\hat{x}} = \frac{1}{2}\frac{L^*(L)_2}{(\lambda_D)_2^2}(\hat{n}_2 - \hat{n}_1), \tag{14}$$

where

$$\hat{G}_{j_{kl}} = \frac{\hat{n}_k}{(\pi \hat{T}_{kl})^{1/2}} \exp\left[-\frac{1}{\hat{T}_{kl}}(\hat{v}_j - \hat{u}_{kl})^2\right] \tag{15}$$

and

$$\hat{H}_{j_{kl}} = \hat{T}_{kl}\hat{G}_{j_{kl}},$$

$$(k, l = 1, 2, 3 \; ; \; j = 1, 2, \cdots, n.) \tag{16}$$

The moment equations (Equations (38-a) - (39-b) in Chapter II) can be used to calculate the flow properties.

E Field and Electron Diffusion

It is noted that besides the Poisson equation different expressions relating the E field and flow properties are able to be obtained. Electron diffusion due to the temperature, density, snd pressure gradients in a mixture of electrons and heavy particles has been discussed in details by Chapman and Cowling [37]. They started with the Boltzmann equation and neglected the effects of electron-electron collisions. When a steady state is reached, the relative diffusion velocity between electrons and ions vanishes. In other words, in a steady state condition, there is no net electric current. Under this condition, Chapman and Cowling derived an equation for the E field in terms of the electron temperature gradient, an equivalent velocity and its gradient.

Petschek and Byron [2] have given the physics of the induction of an electric field due to the charge separation. Under the steady state condition as mentioned in the previous paragraph, the Coulomb force from the induced electric field is balanced by the pressure gradient of electrons. As a result, they derived an equation for the E field in terms of the electron temperature and density, and their gradients.

The method of species-momentum transfer has been given in Reference [32]. The ion diffusion velocity is included even though the contribution from the ion is negligible with a small Hall parameter for electrons. The parameter is the product of the electron circular frequency of rotation in a magnetic field and the electron collision time. It is interesting to see that the equation for the total current given in Reference [32] can be reduced immediately to the equation for the E field given by Petschek and Byron [2] if the total current and the magnetic field are

ignored.

Jaffrin and Probstein [8] and Jaffrin [10] used a similar approach as that discussed by Reference [32] to formulate their basic equations. In addition to the assumptions mentioned in Chapter I, they assume that the net current vanished inside the shock structure. Consequently, equations for the E field can be derived and are given in the present notations as follows:

$$\hat{E} = \frac{1}{2} \frac{\lambda_{D_2}}{l_{aa_2}} \hat{T}_e \frac{d \ln \hat{u}_i}{d\hat{x}} \quad \text{, for a partially ionized gas,} \tag{17-a}$$

and

$$\hat{E} = \frac{1}{2} \frac{\lambda_{D_2}}{l_{ii_2}} \hat{T}_e \frac{d \ln \hat{u}_i}{d\hat{x}} \quad \text{, for a fully ionized gas.} \tag{17-b}$$

With the assumption that the net current vanished everywhere in the flow, a subset of equations can be used to serve the purpose of the study of this chapter. Instead of using

$$\hat{n}_1 = \int_{-\infty}^{\infty} \hat{g}_1 \, d\hat{v}_{x_1} \tag{18}$$

$$\hat{n}_2 = \int_{-\infty}^{\infty} \hat{g}_2 \, d\hat{v}_{x_2} \tag{19}$$

and the Poisson equation

$$\frac{d\hat{E}}{d\hat{x}} = \frac{1}{2} \frac{L^*(L)_2}{(\lambda_{D_2})^2} (\hat{n}_2 - \hat{n}_1)$$

for $\hat{n}_1$, $\hat{n}_2$, and $\hat{E}$, another set of equations can be used. Equation (17-a) will be used to obtain $\hat{E}$ for a partially ionized gas, while Equation (17-b) for a fully ionized gas. $\hat{n}_2$ is determined from Equation (19) and $\hat{n}_1'$ can be evaluated by the Poission equation

$$\hat{n}_1' = \hat{n}_2 - Z \frac{(\lambda_D)^2}{L^*(L)_2} \frac{d\hat{E}}{d\hat{x}} \tag{20}$$

It is noted that $\hat{n}_1$ in Equation (18) has been changed to $\hat{n}_1'$ in order to make a distinction from $\hat{n}_1$ in Equation (18).

The subset of equations is valid of $\hat{n}_1'$ obtained from the subset of equations is very close to $\hat{n}_1$ from Equation (18). In other words, the difference between $\hat{n}_1'$ and $\hat{n}_1$ is very small, i.e.,

$$\Delta\hat{n}_1 = \left| \hat{n}_1' - \hat{n}_1 \right| \cong 0 . \tag{21}$$

Computational Procedure and Results

The significance of the effects of the induced electric field due to the charge separation in the shock-wave structure of ionized argon has been investigated. The governing equations for the problem are Equations (8) - (16). It was mentioned that Equation (17-a) or Equation (17-b) can be used to replace the moment equation of $\hat{n}_1$ under the assumptions that the net current vanishes everywhere in the flow and that Equation (21) is satisfied. The boundary conditions are the same as those given in Chapters II and III. The discrete ordinate method is

applied to obtain the solutions. A central difference scheme is used to approximate the derivative with respect to $\hat{x}$, the variable in physical space. The governing equations in finite difference form are rearranged in order that the tridiagonal matrix technique can still be applied. Letting i be the index for variable $\hat{x}$ in physical space and k be the index for species, E uations (8) - (10) can be written as follows:

$$\left(\hat{\nu}_{2_{K1}} + \hat{\nu}_{2_{K2}} + \hat{\nu}_{2_{K3}}\right)\hat{g}_{2,j_K} + \frac{\hat{v}_{j_K}}{2\Delta\hat{x}}\hat{g}_{3,j_K} = \hat{\nu}_{2_{K1}}\hat{G}_{2,j_{K1}} + \hat{\nu}_{2_{K2}}\hat{G}_{2,j_{K2}}$$

$$+ \hat{\nu}_{2_{K3}}\hat{G}_{2,j_{K3}} + \frac{\hat{v}_{j_K}}{2\Delta\hat{x}}\hat{G}_{1,j_{KK}} - \beta_K A_{2,j_K} ,$$

$$\text{for } K = 1, 2, 3 \text{ and } i = 2 ,$$

$$-\frac{\hat{v}_{j_K}}{2\Delta\hat{x}}\hat{g}_{i-1,j_K} + \left(\hat{\nu}_{i_{K1}} + \hat{\nu}_{i_{K2}} + \hat{\nu}_{i_{K3}}\right)\hat{g}_{i,j_K} + \frac{\hat{v}_{j_K}}{2\Delta\hat{x}}\hat{g}_{i+1,j_K} = \hat{\nu}_{i_{K1}}\hat{G}_{i,j_{K1}}$$

$$+ \hat{\nu}_{i_{K2}}\hat{G}_{i,j_{K2}} + \hat{\nu}_{i_{K3}}\hat{G}_{i,j_{K3}} - \beta_K A_{i,j_K}$$

$$\text{for } i = 3, 4, \cdots, N-2 ,$$

and

$$-\frac{\hat{v}_{j_K}}{2\Delta\hat{x}}\hat{g}_{N-2,j_K} + \left(\hat{\nu}_{N-1_{K1}} + \hat{\nu}_{N-1_{K2}} + \hat{\nu}_{N-1_{K3}}\right)\hat{g}_{N-1,j_K} = \hat{\nu}_{N-1_{K1}}\hat{G}_{N-1,j_{K1}}$$

$$+ \hat{\nu}_{N-1_{K2}}\hat{G}_{N-1,j_{K2}} + \hat{\nu}_{N-1_{K3}}\hat{G}_{N-1,j_{K3}} - \frac{\hat{v}_{j_K}}{2\Delta\hat{x}}\hat{G}_{N,j_{KK}} - \beta_K A_{N-1,j_K} ,$$

$$\text{for } i = N-1 ,$$

where,

$$\beta_1 = -(L)_2 / L^* ,$$

$$\beta_2 = (L)_2 / L^* ,$$

$$\beta_3 = 0$$

$$A_{i,1_K} = \hat{E}_i^{\circ} \frac{\hat{g}^{\circ}_{i,2_K} - \hat{g}^{\circ}_{i,1_K}}{\Delta V_K} ,$$

$$A_{i,j_K} = \hat{E}_i^{\circ} \frac{\hat{g}^{\circ}_{i,j+1_K} - \hat{g}^{\circ}_{i,j-1_K}}{2\,\Delta V_K} \quad , \text{ for } j = 2, 3, \cdots, J-1$$

and

$$A_{i,J_K} = \hat{E}_i^{\circ} \frac{\hat{g}^{\circ}_{i,J_K} - \hat{g}^{\circ}_{i,J-1_K}}{\Delta V_K} .$$

$\hat{g}^{\circ}_{i,j_k}$ is the value of $\hat{g}_{i,j_k}$ and $\hat{E}^{\circ}_i$ is the value of $\hat{E}_i$ from the previous iteration.

Similar equations can be written for Equations (11) - (13). The spacing size in both Chapters II and III has been adapted in this study. The results presented in Chapters II and III were used as the initial values for iterative process. Then the tridiagonal matrix technique is applied to obtain the numerical solutions for $\hat{g}_{i,j_k}$ and $\hat{h}_{i,j_k}$ throughout the shock structure at each discrete velocity point. The quadrature of order n = 8 applied in Chapter II and III has been employed to integrate the distribution functions for the flow properties. The convergent criteria are set at 0.0005 for atom and ion number densities at every

physical point between successive iterations.

The case of $M_1 = 2.0$ and $\alpha = 0.5$ presented in Chapter III has been extended to include the effects of the induced electric field. Present results of the E field are given in Figure 32 in comparison with Jaffrin's results [10]. It is seen that the present E field is stronger than Jaffrin's E field. Hence, the effects of the induced E field to the shock structure according to the discrete ordinate method are greater than those predicted by Jaffrin [10]. The present E field was obtained through the subset of equations as mentioned before. The maximum $\Delta \hat{n}_1$ for this case was found to be 0.00005898. Therefore, Equation (21) is approximately satisfied.

Some results of this case using the moment equations of $\hat{n}_1$, $\hat{n}_2$, and Poisson's equation instead of using the subset of equations have been obtained. However, they are not shown in this chapter because their order of magnitude is not reasonable at all. The peak of the induced electric field is about 10^3 times higher than the value predicted by the subset of equations. The causes to the erroneous results have been found.

Usually the acceleration terms are of order 1 at the most, then from Equations (8) - (13) $\hat{E}$ is at the most of order $L^*/(L)_2$. In other words $\hat{E}$ is of order $(\lambda_D)_2/(\ell_{aa})_2$ at the most if L^* is set to be $(\lambda_D)_2$ and $(L)_2$ to be $(\ell_{aa})_2$. From Equation (14), $(\hat{n}_2 - \hat{n}_1)$ is of order $[(\lambda_D)_2/(\ell_{aa})_2]^2$ at the most. For the present investigation and Jaffrin's analysis [10] $(\lambda_D)_2/(\ell_{aa})_2$ is about 10^{-4} and thus $(\hat{n}_2 - \hat{n}_1)$ is of order 10^{-8} at the most. $\hat{E}$ and $(\hat{n}_2 - \hat{n}_1)$ vanish exactly at both upstream and downstream equilibrium conditions.

The accuracy of least 10^{-8} for $(\hat{n}_2 - \hat{n}_1)$ is very difficult to

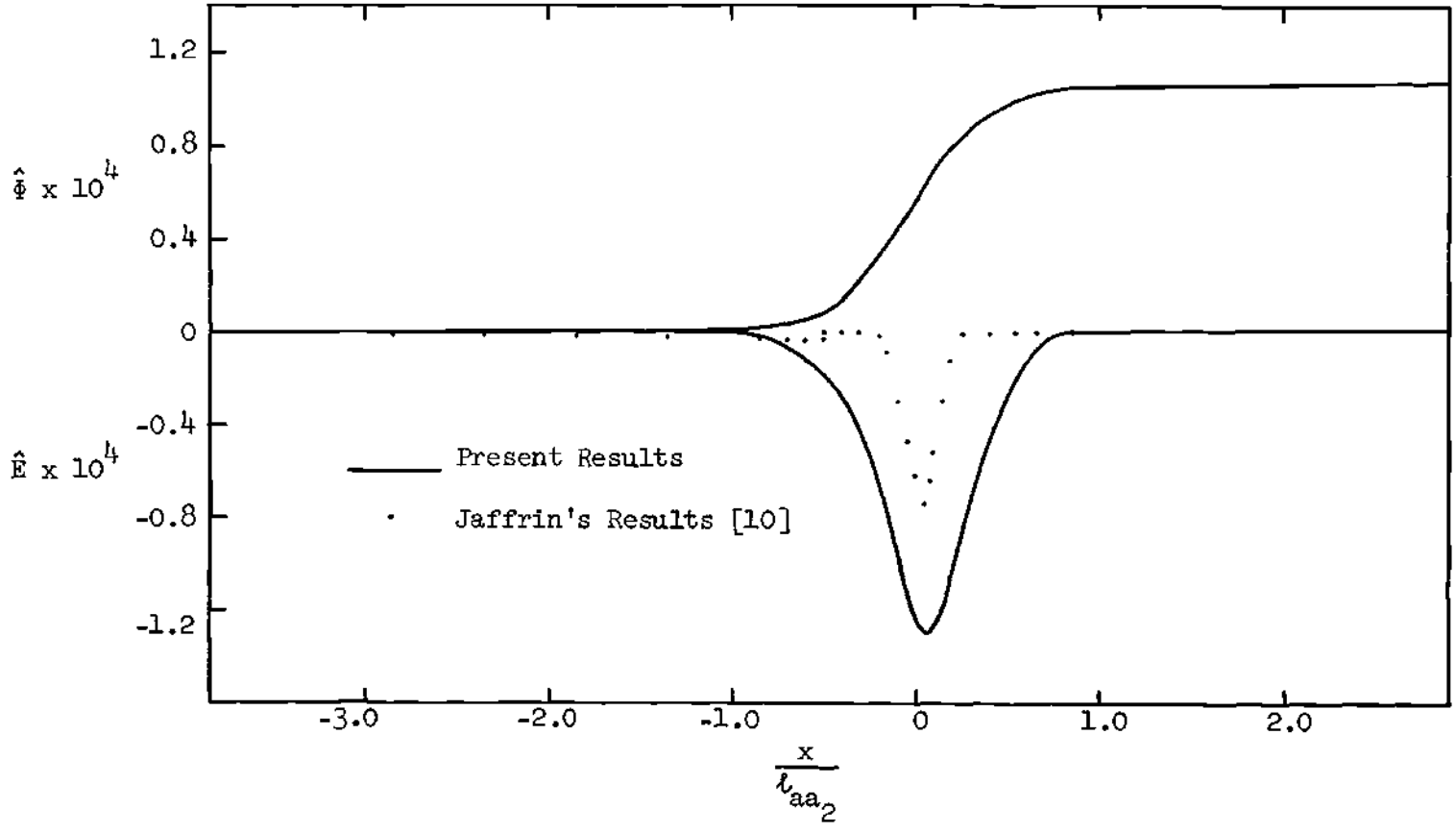

Figure 32. Electric Field and Potential Distributions for $M_1 = 2.0$, $\alpha = 0.5$.

obtain in the actual numerical calculations. Thus fact is responsible for the difficulties encountered when the moment equations of $\hat{n}_1$ and $\hat{n}_2$ were coupled with Poisson's equation. A double precision routine was applied, the accuracy of $(\hat{n}_2 - \hat{n}_1)$ increased from a range of $10^{-4} - 10^{-5}$ to $10^{-5} - 10^{-6}$. Unfortunately, this range of accuracy is still far away from the desired range of 10^{-8}. Immediately from Equation (14) the value of $\hat{E}$ will be predicted at $0(10^3)$ at least. This predicted value of $\hat{E}$ will dominate all other terms in the Boltzmann equation, which are expected to be of $0(1)$. These facts are directly connected with the large values of $\hat{E}$ as mentioned previously and may explain to a certain extent the findings and difficulties in the works of Greenberg, et al.[3] and Greenberg and Tréve [4]. They found that their predicted electric field oscillated throughout the entire shock structure and had large peaks. For Mach numbers greater than 2.19 they could not find continuous solutions. In view of the difficulties just discussed, the results to be presented in this chapter are obtained using the subset of equations mentioned before.

Figure 33 shows the velocity profile of atoms. Ion and electron velocity profiles are not shown, since they deviate from the atom velocity profile by only 10^{-4}. The present results are compared with Jaffrin's results [10]. His profiles have steeper slopes than the present results in the central portion of the shock wave. His ion velocity profile undershoots the downstream value while the present ion velocity is monotonically decreasing to the downstream value. Present temperature profiles are compared with Jaffrin's results in Figure 34. The present ion temperature is not shown in the figure because its deviation from the

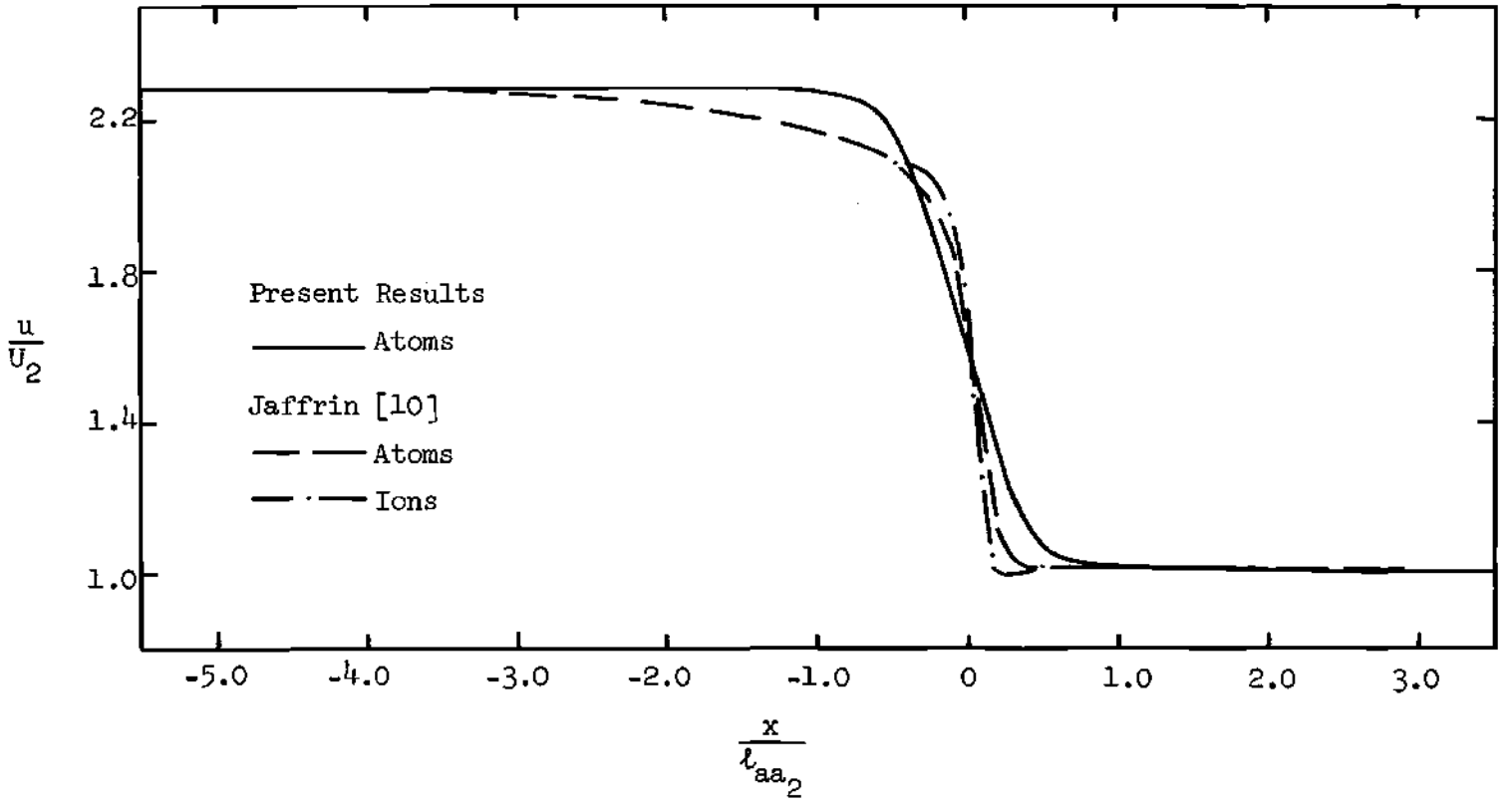

Figure 33. Velocity Profile with $\hat{E}$ Effect for $M_1 = 2.0$, $\alpha = 0.5$.

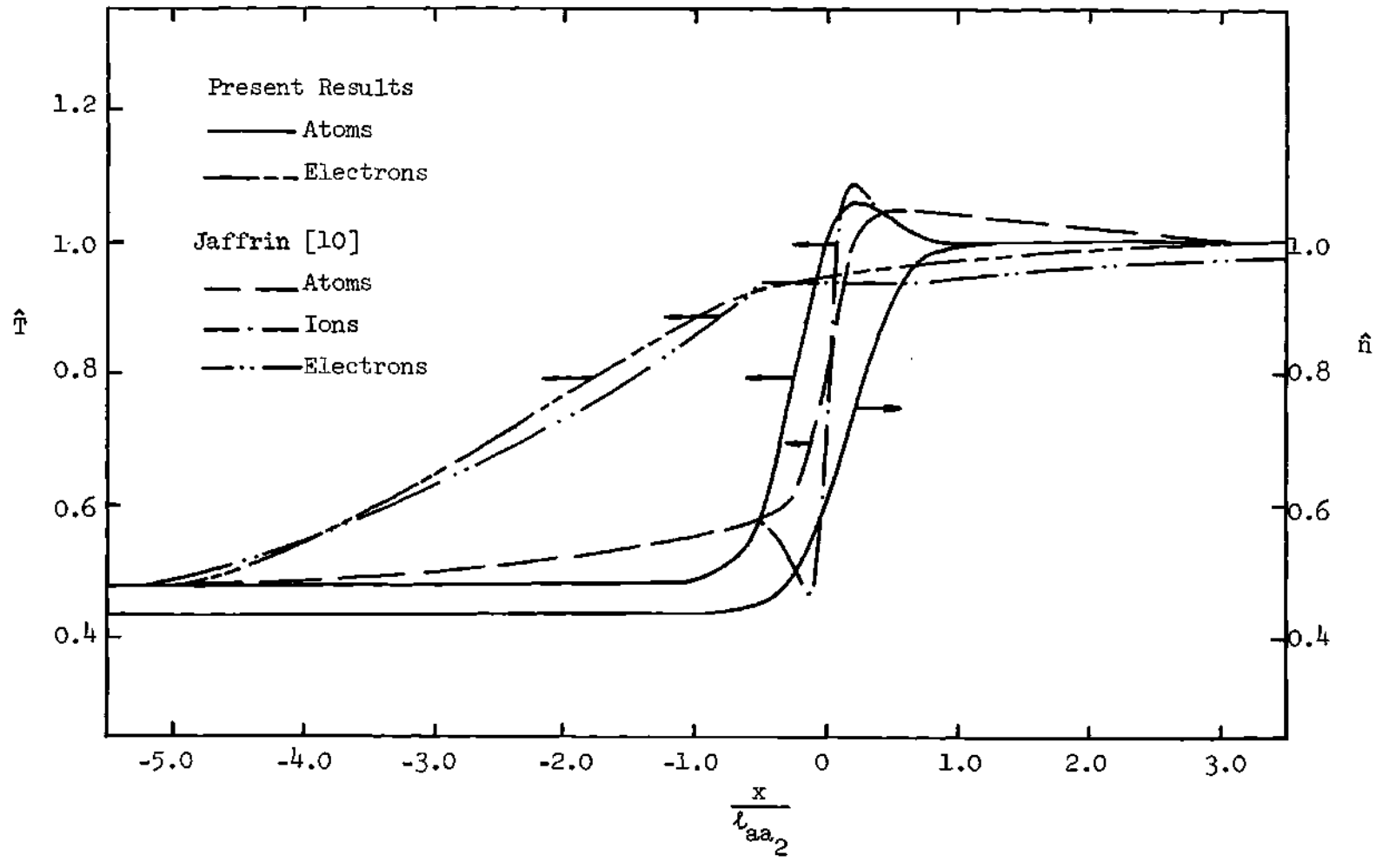

Figure 34. Temperature and Density Profiles with $\hat{E}$ Effect for $M_1 = 2.0$, $\alpha = 0.5$.

atom temperature is too small to be distinguished in the graph. Unlike Jaffrin's ion temperature, the present results do not predict any undershoot. Electron temperatures obtained by both methods are fairly close to each other. Both method predict that the temperatures of heavy particles overshoot their downstream value. Detailed comparisons of the present $\hat{u}$ to the value of $\hat{u}$ without the $\hat{E}$ field effects obtained in Chapter III are listed in Tables 11, 12, and 13 for atoms, ions, and electrons, respectively. The differences are indeed very small. Therefore, the effects of the induced $\hat{E}$ field on the shock structure in this case can be ignored.

The results with the E field effects on a shock wave at $M_1 = 2.0$, $\alpha = 0.1$ have been obtained using the results without the E field effects as the initial values. The present E field is compared with Jaffrin's results [10] in Figure 35. Both methods predict the same order of magnitude for the $\hat{E}$ field. However, unlike the present E field, Jaffrin's results have two discontinuities because the electron temperature was set to be constant inside the main portion of the shock structure. Figure 36 gives a comparison for velocity profiles. Jaffrin's profiles are steeper than the present results in the central portion of the shock structure. His results indicate that there are distinguishable differences between his atom velocity profile and ion velocity profile. Present ion and electron velocity profiles are not shown in the figure, because they deviate from the values of neutral particles by only an order of 10^{-3}. Both methods predict the same general trend in temperature profiles as shown in Figure 37. However, Jaffrin's electron temperature profile contains two discontinuities inside the shock structure. Unlike Jaffrin's

Table 11. Comparison of $\hat{u}_a$ with E to $\hat{u}_a$ without E for $M_1 = 2.0$, $\alpha = 0.5$

I	$\hat{u}_a$ (with $\hat{E}$)	$\hat{u}_a$(without $\hat{E}$)
45	.15434200+01	.15434541+01
47	.15298472+01	.15298733+01
49	.14950654+01	.14950792+01
51	.14135556+01	.14135588+01
53	.12566907+01	.12566928+01
55	.10443348+01	.10443365+01
57	.86156531+00	.86156663+00
59	.75618484+00	.75618609+00
61	.70885520+00	.70885634+00
63	.68999870+00	.68999986+00
65	.68284829+00	.68284948+00

Table 12. Comparison of $\hat{u}_i$ with E to $\hat{u}_i$ without E for $M_1 = 2.0$, $\alpha = 0.5$

I	$\hat{u}_i$ (with $\hat{E}$)	$\hat{u}_i$ (without $\hat{E}$)
45	.15433963+01	.15434300+01
47	.15297888+01	.15298146+01
49	.14949363+01	.14949493+01
51	.14133291+01	.14133323+01
53	.12564573+01	.12564588+01
55	.10442620+01	.10442635+01
57	.86160852+00	.86160997+00
59	.75623212+00	.75623339+00
61	.70888005+00	.70888119+00
63	.69000941+00	.69001048+00
65	.68285234+00	.68285348+00

Table 13. Comparison of $\hat{u}_e$ with E to $\hat{u}_e$ without E for $M_1 = 2.0$, $\alpha = 0.5$

I	$\hat{u}_e$ (with $\hat{E}$)	$\hat{u}_e$(without $\hat{E}$)
45	.57203035-02	.57202744-02
47	.56701111-02	.56697929-02
49	.55413552-02	.55404668-02
51	.52393525-02	.52378941-02
53	.46576119-02	.46565063-02
55	.38704118-02	.38703128-02
57	.31931321-02	.31934553-02
59	.28026247-02	.28028855-02
61	.26272130-02	.26273462-02
63	.25573306-02	.25573888-02
65	.25308312-02	.25308568-02

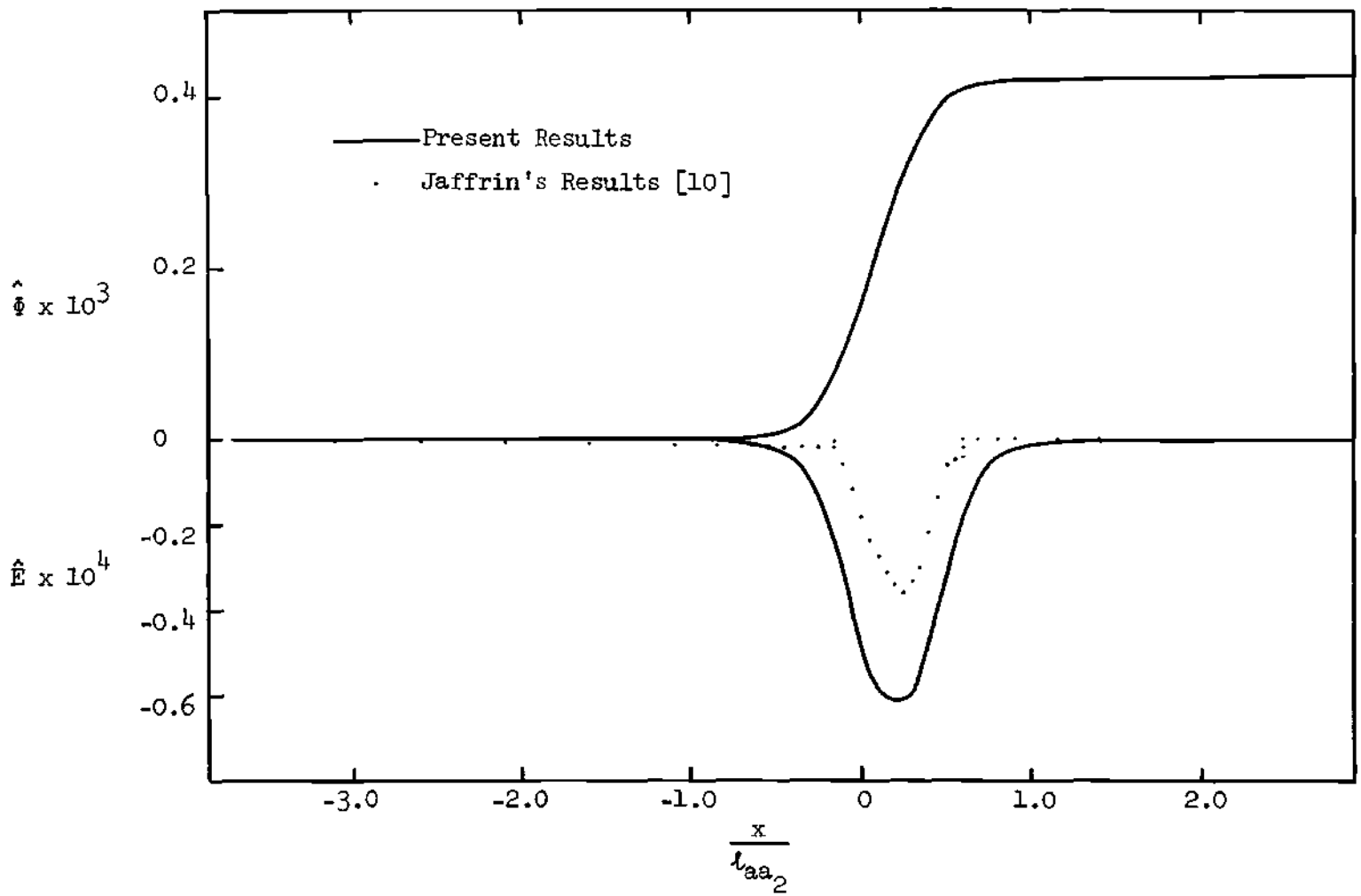

Figure 35. Electric Field and Potential Distributions for $M_1 = 2.0$, $\alpha = 0.1$.

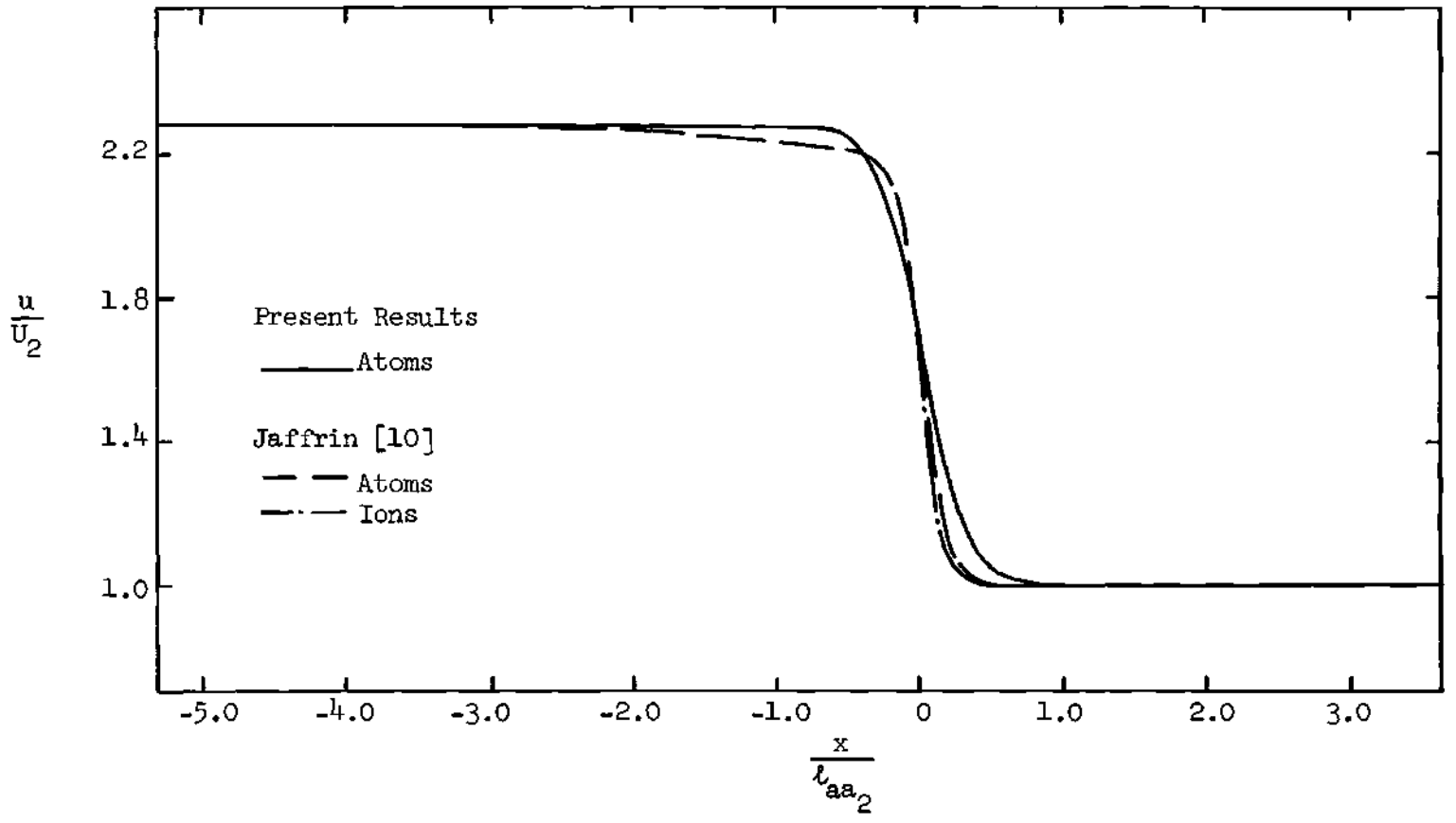

Figure 36. Velocity Profile with $\hat{E}$ Effect for $M_1 = 2.0$, $\alpha = 0.1$.

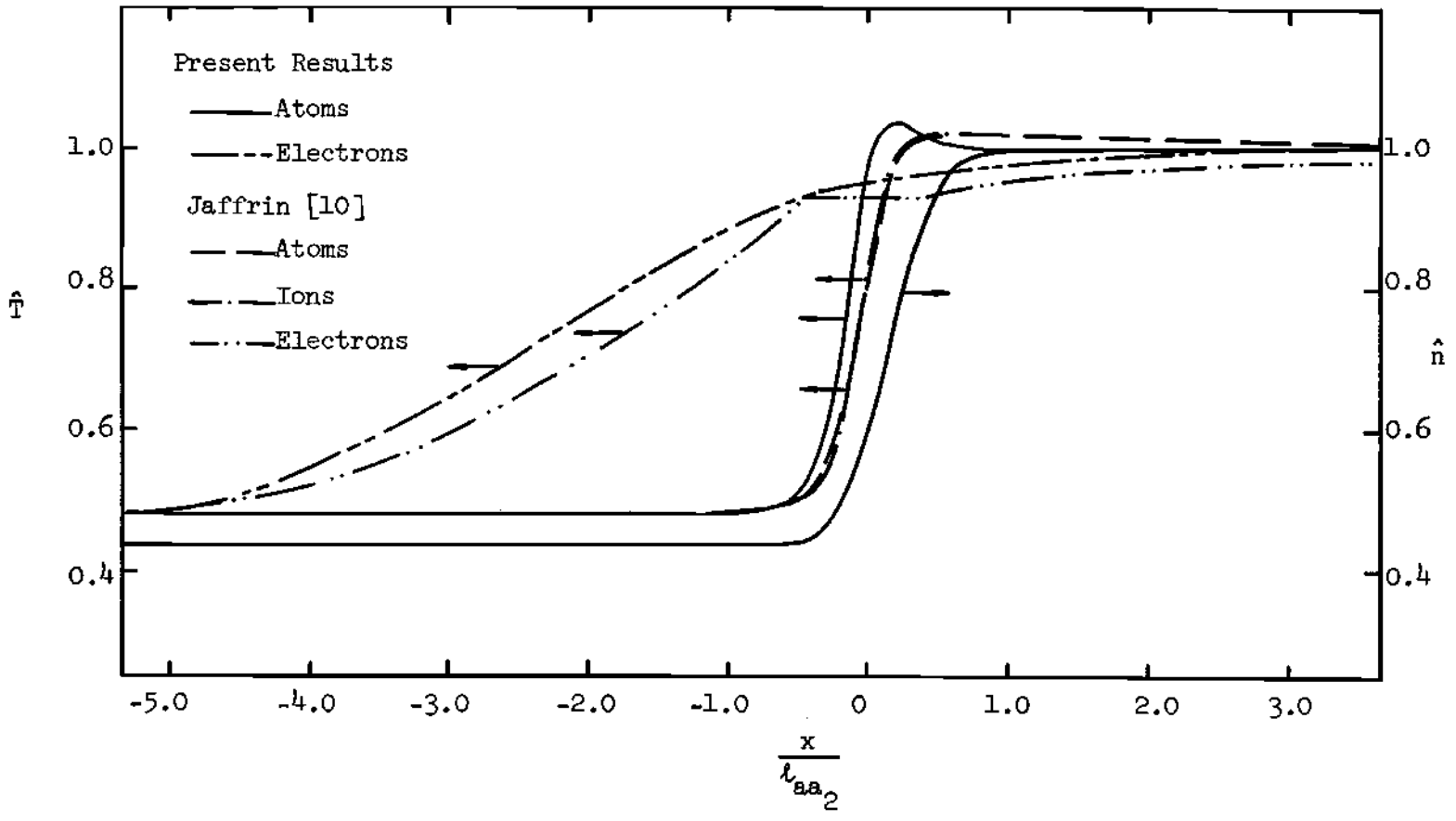

Figure 37. Temperature and Density Profiles with E Effect for $M_1 = 2.0$, $\alpha = 0.1$.

results the differences between the present ion temperature and the atom temperature is in the order of 10^{-3}. Thus, the present ion temperature is not shown in the figure. Detailed comparisons of $\hat{u}$ with the E field effects to $\hat{u}$ without the E field effects for this case are listed in Tables 14, 15, and 16, for atoms, ions, and electrons, respectively. It can be concluded that for this case the effects of the induced electric field on the shock structure can be neglected.

The shock structure with the E field effects at $M_1 = 10$, $\alpha = 0.1$ has been investigated. For this case 240 equally spaced discrete velocity points have been used in order to obtain the desired accuracy. When the E field effects are taken into consideration, all $\hat{g}_{i,j_k}$ and $\hat{h}_{i,j_k}$ have to be stored in the computer. As a result, the storage of a computer becomes a serious problem. The usage of magnetic tapes is helpful. However, the operation procedure and the function at an individual magnetic tape can cause many unexpected troubles. These factors are, in many occasions, beyond the control of reseachers.

For the present case, an alternative iterative process has been adopted in order to avoid the difficulties just mentioned. The initial values of $\hat{E}$, $\hat{G}_{i,j_{11}}$ and $\hat{G}_{i,j_{22}}$ throughout the shock structure were obtained using the final results of the case of $M_1 = 10, \alpha = 0.1$ given in Chapter III. For the first iteration A_{i,j_1} and A_{i,j_2} were evaluated by these $\hat{E}$, $\hat{G}_{i,j_{11}}$ and $\hat{G}_{i,j_{22}}$. Then the tridiagonal matrix technique was applied to obtain $\hat{g}_{i,j_2}$ and $\hat{h}_{i,j_2}$ throughout the shock structure. These newly calculated $\hat{g}_{i,j_2}$ and $\hat{h}_{i,j_2}$ were used to obtain ion flow properties and new A_{i,j_2} with the same $\hat{E}$. This process was repeated five times. Similar procedure was applied to electrons. Then new $\hat{E}$ was evaluated.

Table 14. Comparison of $\hat{u}_a$ with E to $\hat{u}_a$ without E for $M_1 = 2.0$, $\alpha = 0.1$

I	$\hat{u}_a$ (with $\hat{E}$)	$\hat{u}_a$ (without $\hat{E}$)
45	.13271303+01	.13271344+01
47	.13240449+01	.13240491+01
49	.13125665+01	.13125707+01
51	.12720625+01	.12720654+01
53	.11520100+01	.11520101+01
55	.92499420+00	.92499347+00
57	.71815252+00	.71815195+00
59	.62288128+00	.62288077+00
61	.59261627+00	.59261578+00
63	.58420288+00	.58420236+00
65	.58195303+00	.58195256+00

Table 15. Comparison of $\hat{u}_i$ with E to $\hat{u}_i$ without E for $M_1 = 2.0$, $\alpha = 0.1$

I	$\hat{u}_i$ (with $\hat{E}$)	$\hat{u}_i$ (without $\hat{E}$)
45	.13271264+01	.13271306+01
47	.13240311+01	.13240351+01
49	.13125197+01	.13125238+01
51	.12719290+01	.12719321+01
53	.11517849+01	.11517849+01
55	.92491028+00	.92490958+00
57	.71819350+00	.71819285+00
59	.62291166+00	.62291116+00
61	.59262697+00	.59262648+00
63	.58420608+00	.58420558+00
65	.58195393+00	.58195337+00

Table 16. Comparison of u_e with E to u_e with E for $M_1 = 2.0$, $\alpha = 0.1$

I	$\hat{u}_e$ (with $\hat{E}$)	$\hat{u}_e$(without $\hat{E}$)
45	.49187200-02	.49185951-02
47	.49072922-02	.49068274-02
49	.48648305-02	.48634750-02
51	.47149492-02	.47111693-02
53	.42699989-02	.42635147-02
55	.34282311-02	.34269930-02
57	.26615632-02	.26631175-02
59	.23085348-02	.23094875-02
61	.21963933-02	.21967199-02
63	.21652193-02	.21653037-02
65	.21568834-02	.21569090-02

The cycle was repeated until the mentioned convergent criteria were reached.

The results of the E field is shown in Figure 38. Jaffrin's results [10] have been used for comparison. Both methods predict the same order of magnitude. However, the present method does not predict any significant drop of $\hat{E}$ in the region close to the upstream equilibrium conditions. Figure 39 shows the present atom velocity profile. Since ion and electron velocities are very close to the atom velocity, they are not shown in the figure. As examples, at the center of the shock the atom-ion difference in velocity is 0.00424663 and the atom-electron difference is 0.00891254. Jaffrin's results are also shown in the figure for comparison. His ion velocity inside the shock overshoots the upstream value. Present temperature profiles and Jaffrin's profiles are compared in Figure 40. His ion temperature profile is quite different from the present results and can not approach its upstream value. Some detail comparisons of the results with the E field effects to the results without the E field effects are listed in Tables 17 and 18 for ions and electrons, respectively. Since the differences of $\hat{u}$ from both cases are too small, thus the values of the temperature are used. The values of the atom temperature from both cases are almost identical. Table 19 gives comparisons of distribution functions. The results indicate that the induced electric field tends to equilibrate the flow locally. However, the effects of the induced electric field on the shock structure are very small for this case and can be neglected.

The effects of the induced electric field on a fully ionized gas have also been investigated. The results of $\hat{E}$ for the case of $M_1 = 1.1$,

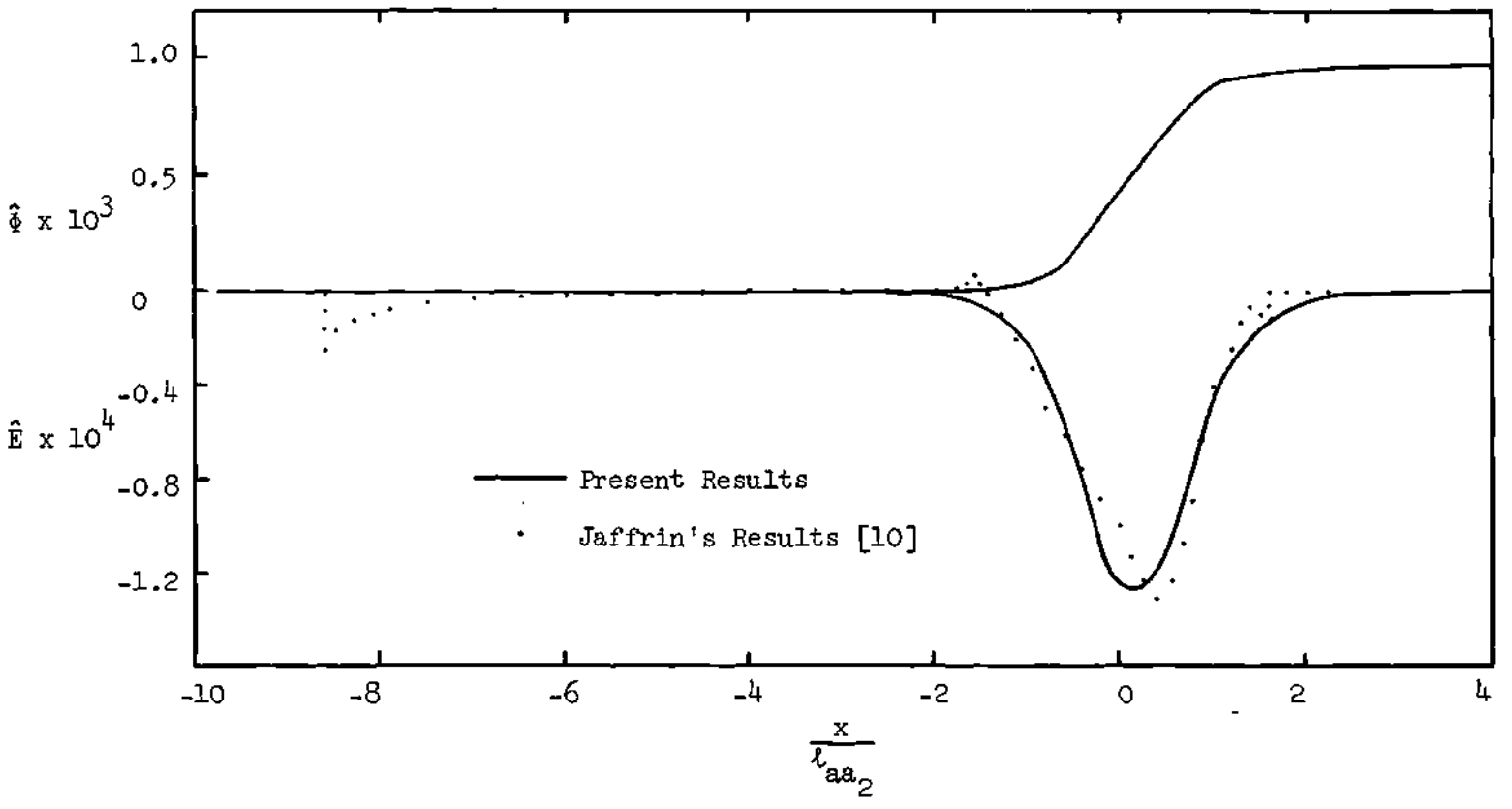

Figure 38. Electric Field and Potential Distributions for $M_1 = 10$, $\alpha = 0.1$.

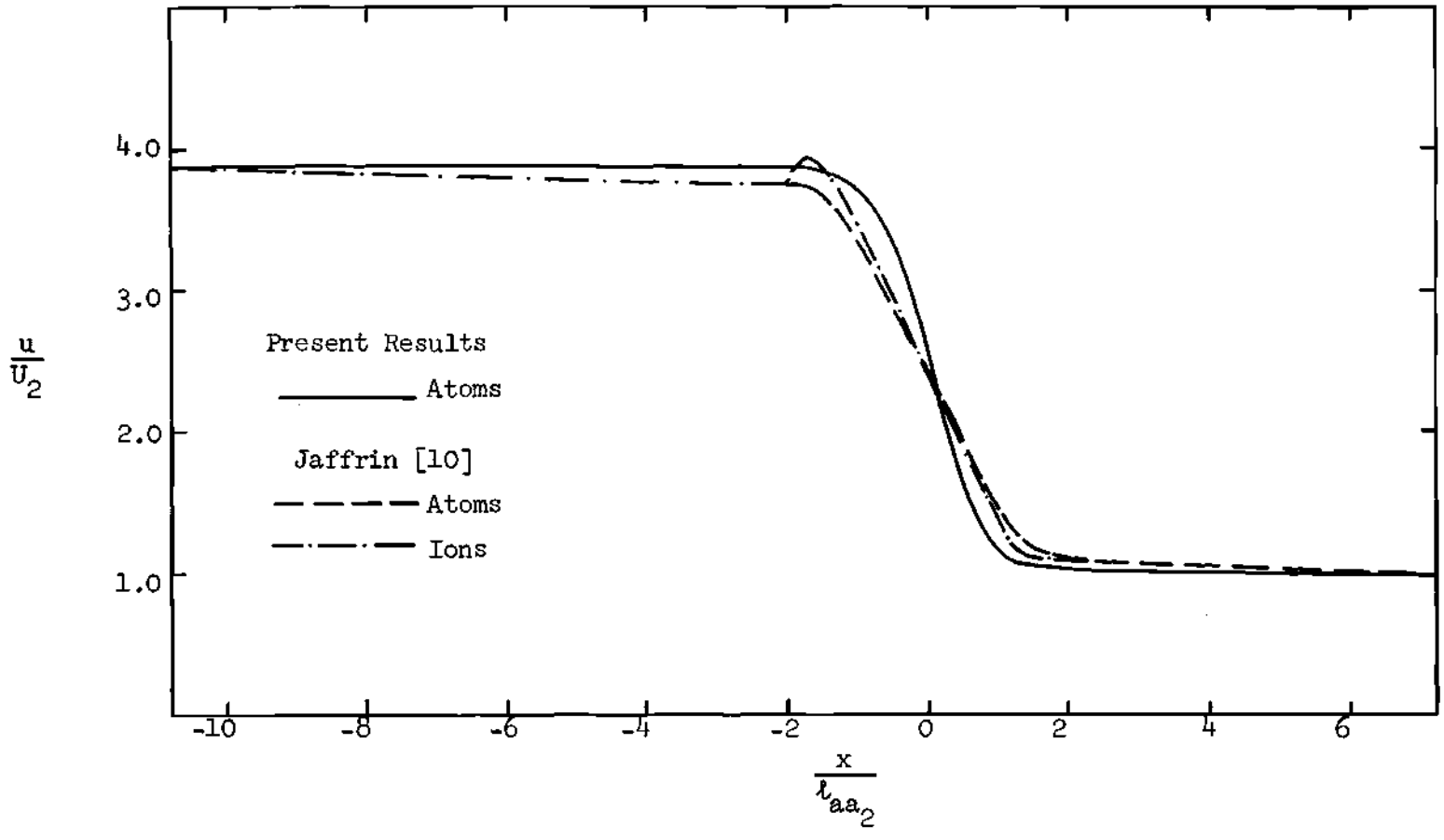

Figure 39. Velocity Profile with $\hat{E}$ Effect, for M = 10.0, α = 0.1 .

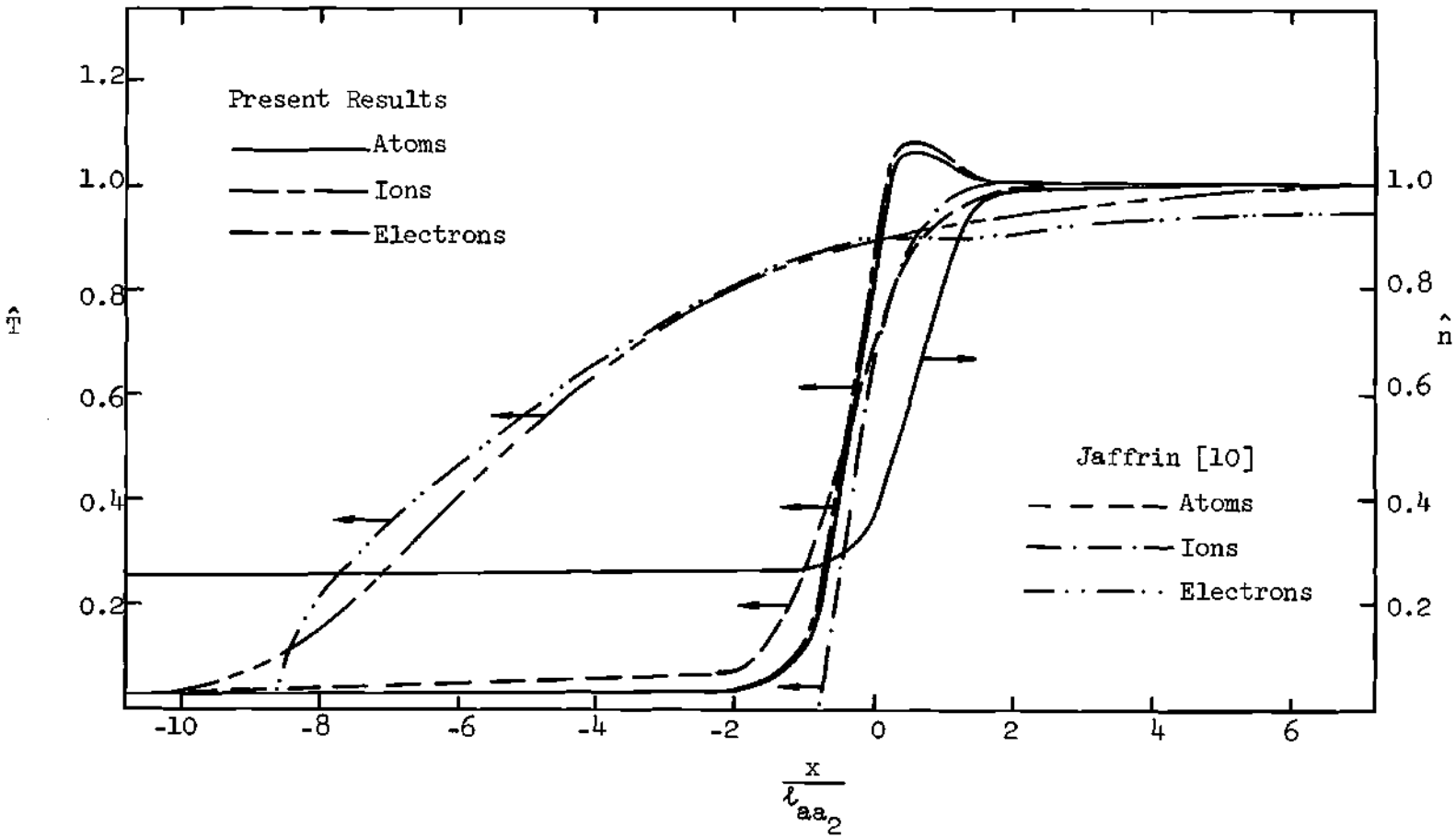

Figure 40. Temperature and Number Density Profiles with $\hat{E}$ Effect, for $M_1 = 10.0$, $\alpha = 0.1$.

Table 17. Comparison of $\hat{T}_i$ with $\hat{E}$ to $\hat{T}_i$ without $\hat{E}$ for $M_1 = 10.0$, $\alpha = 0.1$

I	$\hat{T}_i$ (with $\hat{E}$)	$\hat{T}_i$ (without $\hat{E}$)
45	.49559684-01	.49559637-01
47	.87214503-01	.87214523-01
49	.19483371+00	.19483390+00
51	.45131529+00	.45131531+00
53	.84273698+00	.84273711+00
55	.10812222+01	.10812222+01
57	.10687550+01	.10687551+01
59	.10226515+01	.10226515+01
61	.10062736+01	.10062736+01
63	.10018240+01	.10018241+01
65	.10005527+01	.10005527+01

Table 18. Comparison of $\hat{T}_e$ with $\hat{E}$ to $\hat{T}_e$ without $\hat{E}$ for $M_1 = 10.0$, $\alpha = 0.1$

I	$\hat{T}_e$ (with $\hat{E}$)	$\hat{T}_e$ (without $\hat{E}$)
45	.82928927+00	.82928921+00
47	.84499004+00	.84499005+00
49	.86069526+00	.86069492+00
51	.87640906+00	.87640832+00
53	.89213398+00	.89213277+00
55	.90400191+00	.90400105+00
57	.91200370+00	.91200320+00
59	.92000232+00	.92000214+00
61	.92800172+00	.92800149+00
63	.93600112+00	.93600097+00
65	.94300042+00	.94300042+00

Table 19. Comparison of Distribution Functions with $\hat{E}$ Effect to Distribution Functions without $\hat{E}$ Effect at $\hat{x} = -2$ for $M_1 = 10.0$, $\alpha = 0.1$

J	$\hat{g}_a$ ($\hat{E}$)	$\hat{G}_a$ ($\hat{E}$)	$\hat{g}_a$ ($\hat{E} = 0$)	$\hat{G}_a$ ($\hat{E} = 0$)
75	.98899040-18	0	.98899680-18	0
109	.12721370-16	.53746989-38	.12721440-16	.53737460-38
120	.20208260-26	.53475599-26	.20205500-26	.53469100-26
135	.18832370-06	.30429135-12	.18830720-06	.30427403-12
168	.68362480+00	.67328855+00	.68362560+00	.67328925+00
185	.67065680-03	.88289199-03	.67064590-03	.37451883-03

J	$\hat{g}_i$ ($\hat{E}$)	$\hat{G}_i$ ($\hat{E}$)	$\hat{g}_i$ ($\hat{E} = 0$)	$\hat{G}_i$ ($\hat{E} = 0$)
148	.26920310-04	.32737063-04	.26920000-04	.32736739-04
158	.52482860-01	.54887805-01	.52482740-01	.54887676-01
168	.66244240+00	.65608855+00	.66244280+00	.65608885+00
178	.54134210-01	.55911261-01	.54134080-01	.55911178-01
188	.28641000-04	.33969299-04	.28640680-04	.33969015-04

J	$\hat{g}_e$ ($\hat{E}$)	$\hat{G}_e$ ($\hat{E}$)	$\hat{g}_e$ ($\hat{E} = 0$)	$\hat{G}_e$ ($\hat{E} = 0$)
80	.14776970-01	.14776799-01	.14777000-01	.14776909-01
100	.87897180-01	.87897704-01	.87896900-01	.87898373-01
120	.16038130+00	.16038132+00	.16037990+00	.16038256+00
140	.89766110-01	.89765434-01	.89764800-01	.89766133-01
160	.15411360-01	.15411452-01	.15411040-01	.15411572-01

α = 1.0 are shown in Figure 41. They are in fairly good agreement with the results of Jaffrin and Probstein [8]. Figure 42 gives a comparison for velocity profiles. The present electron velocity deviates from the present ion velocity by an order of 10^{-6}, thus it is not plotted in the figure. The number density of ions is given in Figure 43. The minimum value of $(\hat{n}_2 - \hat{n}_1)$ calculated is $-1.8888282 \times 10^{-12}$ at 0.5 $(\beta x/\ell_{ii_2})$ upstream of the center of the shock and the maximum value of $(\hat{n}_2 - \hat{n}_1)$ is $1.8748385 \times 10^{-12}$ at 0.75 $(\beta x/\ell_{ii_2})$ downstream of the center of the shock. Detail comparisons of $\hat{u}$ with the E field effects to $\hat{u}$ without the E field effects are given in Tables 20 and 21 for ions and electrons, respectively. It can be concluded that for this case the effects of the induced electric field on the shock structure are very small and can be ignored.

The electric field for M_1 = 2.0 and α = 1.0 has been obtained and is shown in Figure 44. The results of Jaffrin and Probstein [8] are used for comparison. The present $\hat{E}$ values are greater than theirs in the main portion of the shock structure. However, their $\hat{E}$ profiles has two discontinuities in slope. Figure 45 shows the velocity profile. In the low-pressure region the present curve deviates significantly from the profile due to Jaffrin and Probstein. In the vicinity of the center of the shock both methods give about the same results. In the high-pressure region the present results again deviate from the results of Jaffrin and Probstein. However, the deviation in the high-pressure region is not as great as that in the low-pressure region. The profiles of temperature and number density are shown in Figure 46. The largest difference between the electron and the ion number densities is in an order of 10^{-8}. The

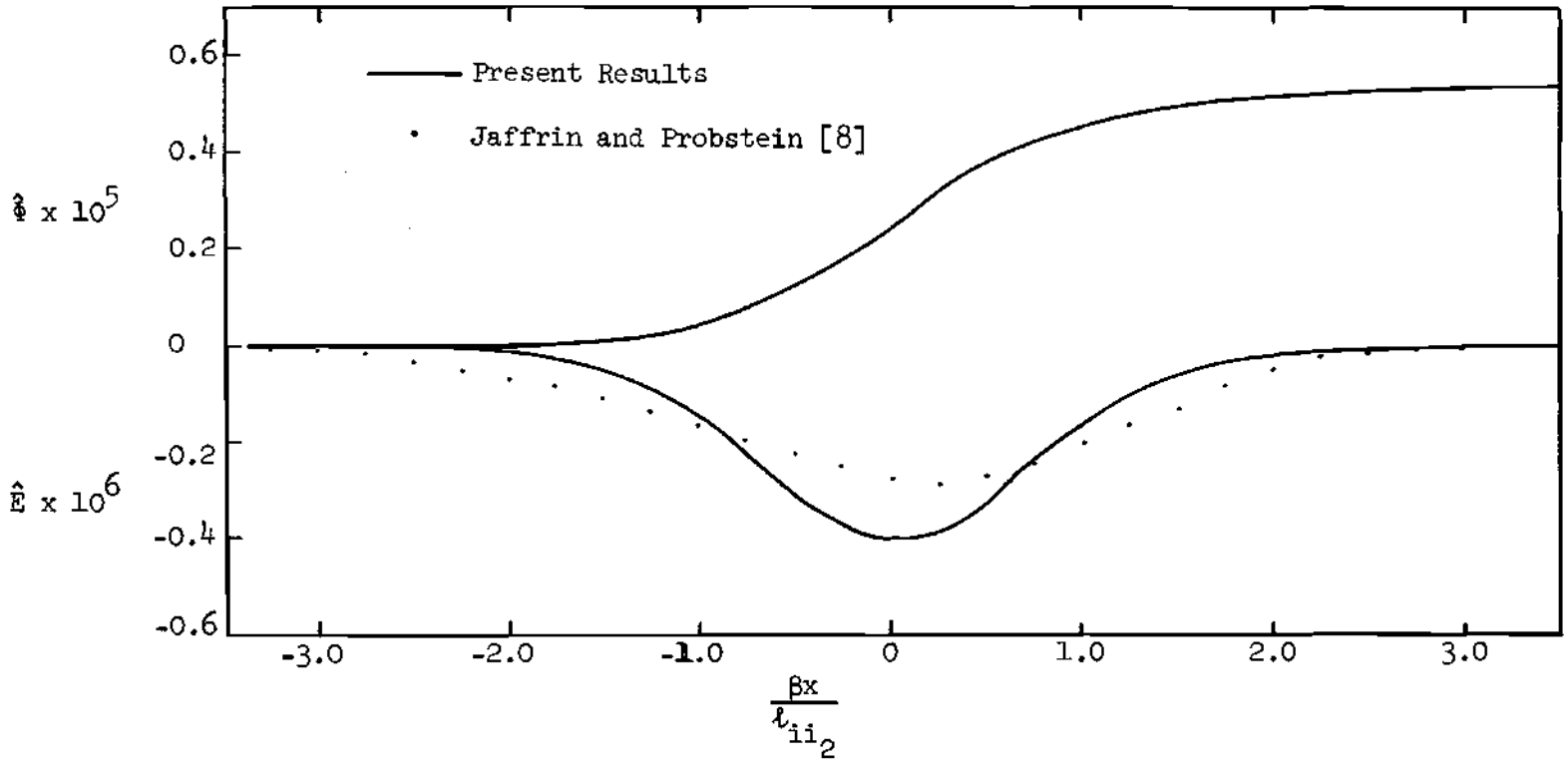

Figure 41. Electric Field and Potential Distributions for $M_1 = 1.1$, $\alpha = 1.0$, $\beta = (m_e/m_i)^{1/2}$.

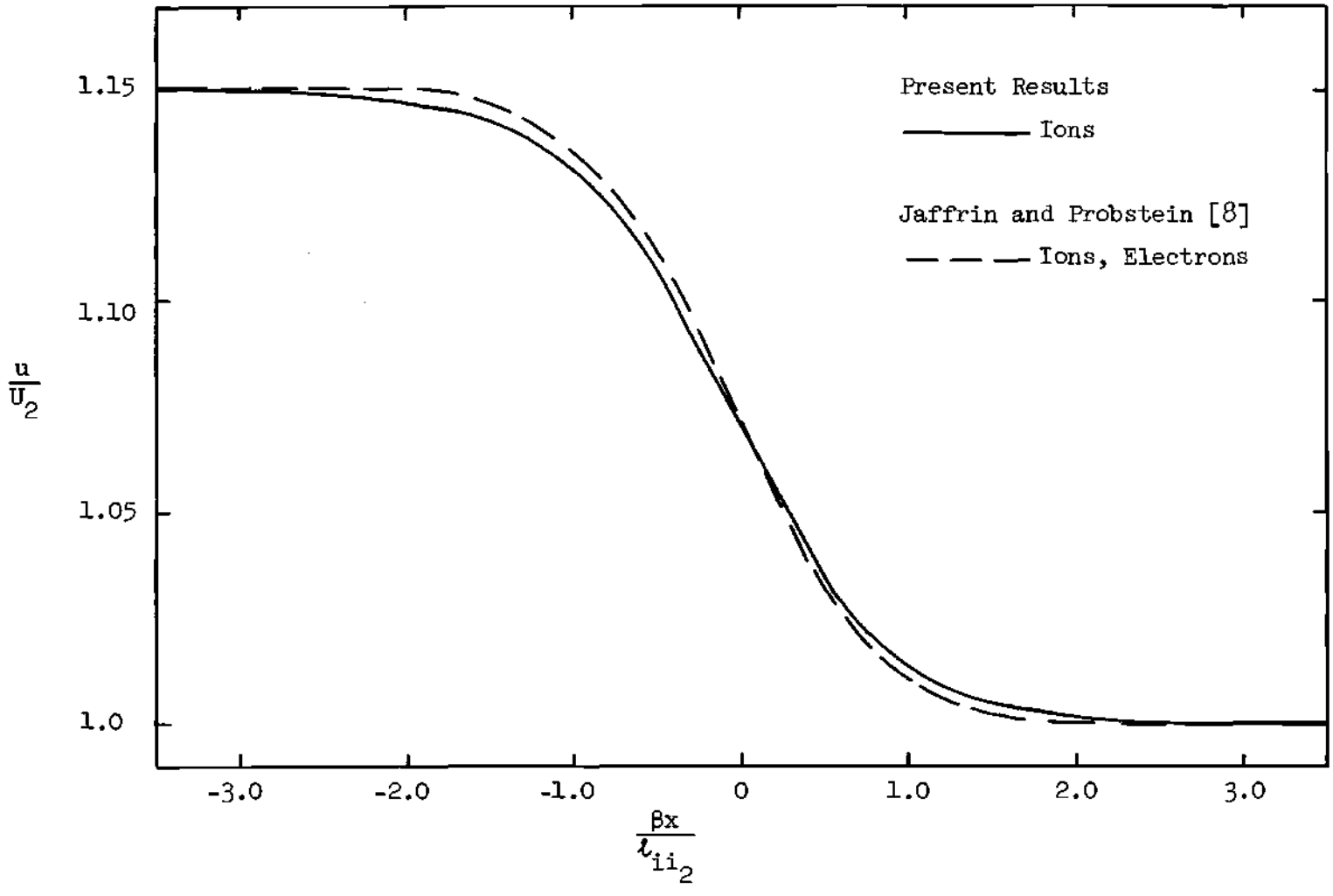

Figure 42. Velocity Profile with $\hat{E}$ Effect for $M_1 = 1.1$, $\alpha = 1.0$, $\beta = (m_e/m_i)^{1/2}$.

Table 20. Comparison of $\hat{u}_i$ with $\hat{E}$ to $\hat{u}_i$ without $\hat{E}$ for $M_1 = 1.1$, $\alpha = 1.0$

I	$\hat{u}_i$ (with $\hat{E}$)	$\hat{u}_i$ (without $\hat{E}$)
45	.13369631+01	.13371857+01
47	.13288024+01	.13291619+01
49	.13179479+01	.13183880+01
51	.13042480+01	.13046490+01
53	.12880381+01	.12882361+01
55	.12702405+01	.12700940+01
57	.12522161+01	.12516825+01
59	.12353884+01	.12345486+01
61	.12208354+01	.12198423+01
63	.12090706+01	.12080708+01
65	.12000775+01	.11991640+01

Table 21. Comparison of $\hat{u}_e$ with $\hat{E}$ to $\hat{u}_e$ without $\hat{E}$ for $M_1 = 1.1$, $\alpha = 1.0$

I	$\hat{u}_e$ (with $\hat{E}$)	$\hat{u}_e$(without $\hat{E}$)
45	.49551601-02	.49559786-02
47	.49249160-02	.49262420-02
49	.48846865-02	.48863125-02
51	.48339104-02	.48353910-02
53	.47738331-02	.47745655-02
55	.47078721-02	.47073278-02
57	.46410699-02	.46390924-02
59	.45787034-02	.45755903-02
61	.45247669-02	.45210869-02
63	.44811641-02	.44774588-02
65	.44478331-02	.44444476-02

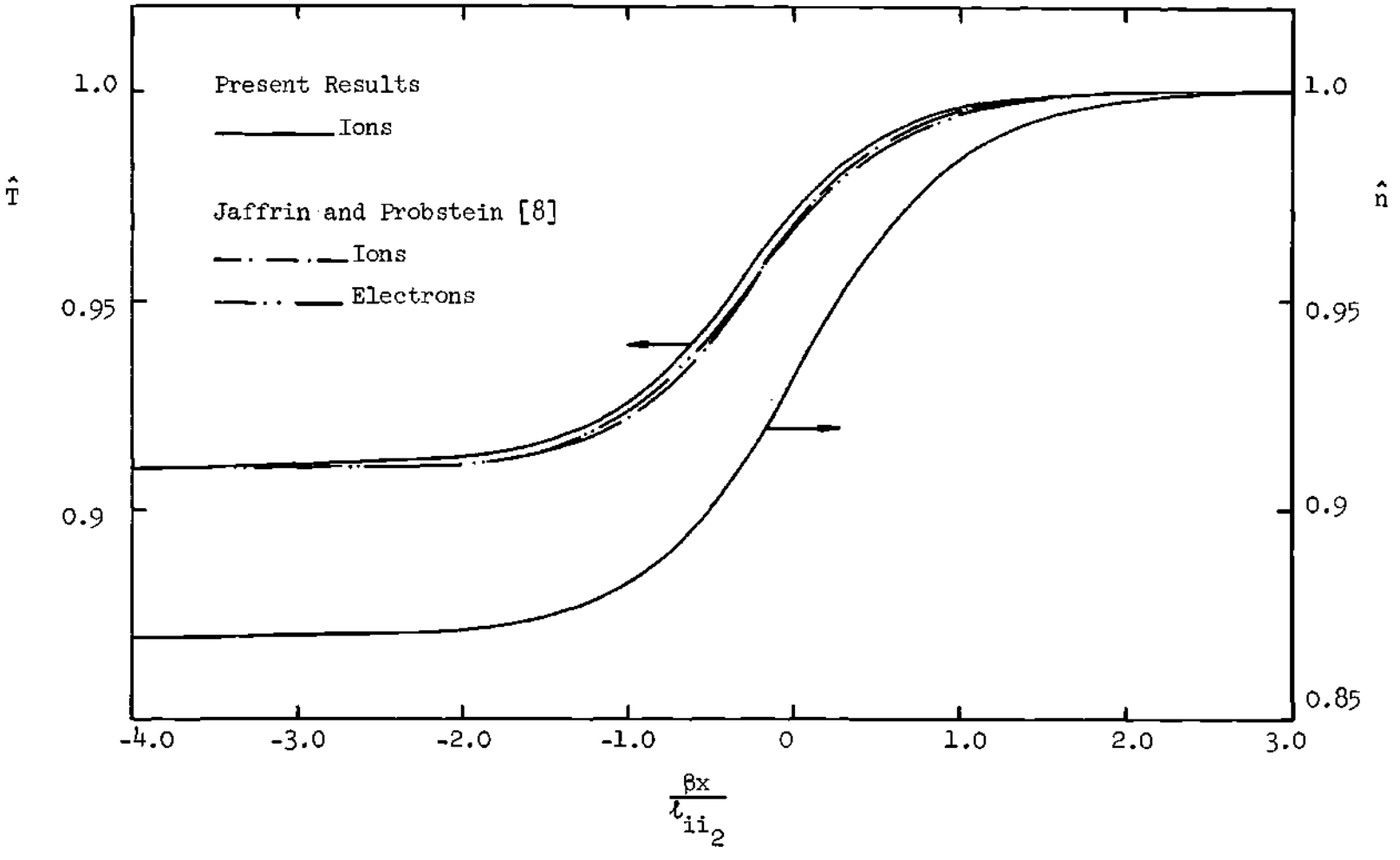

Figure 43. Temperature and Number Density Profiles with $\hat{E}$ Effect for $M_1 = 1.1$, $\alpha = 1.0$, $\beta = (m_e/m_i)^{1/2}$.

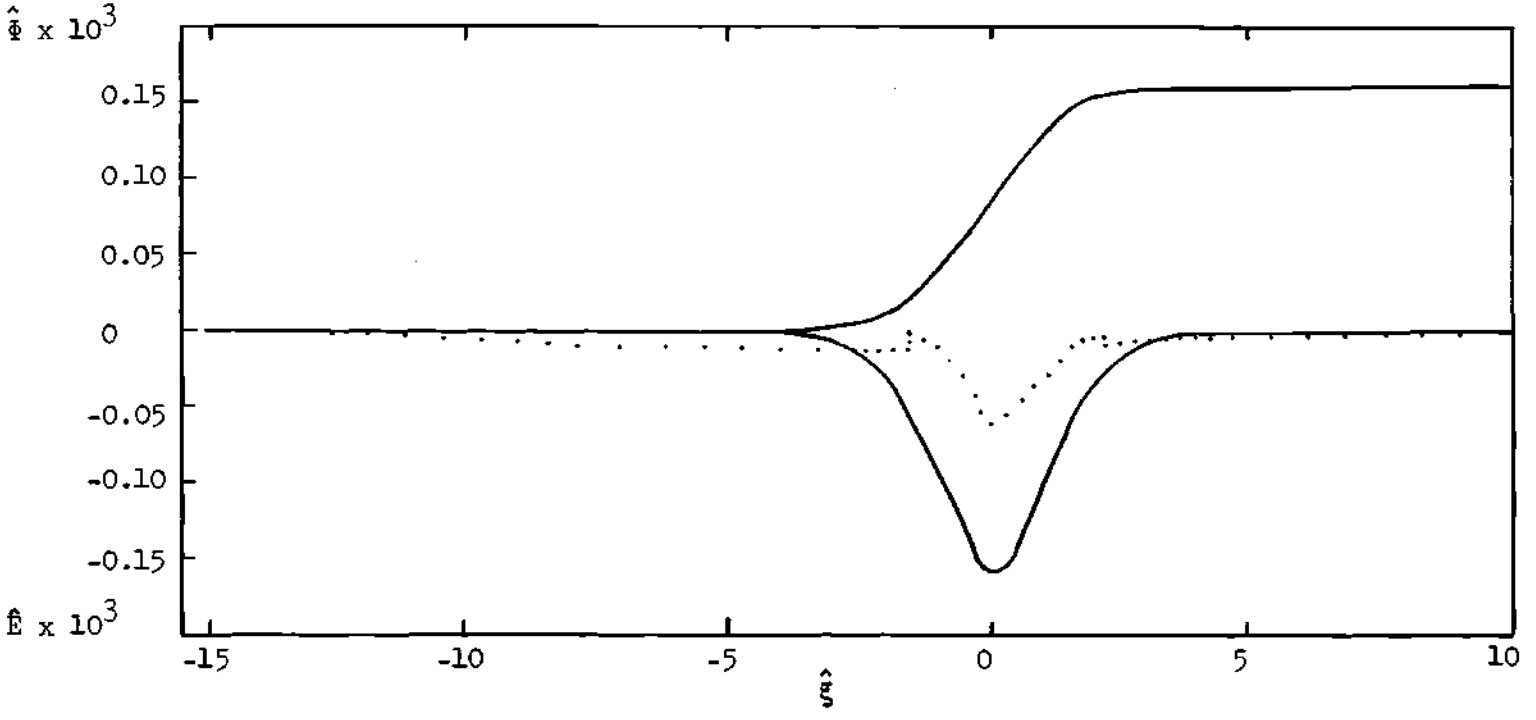

Figure 44. Electric Field and Potential Distributions for $M_1 = 2.0$, $\alpha = 1.0$, $\hat{\xi} = 10x/\ell_{ii_2}$.

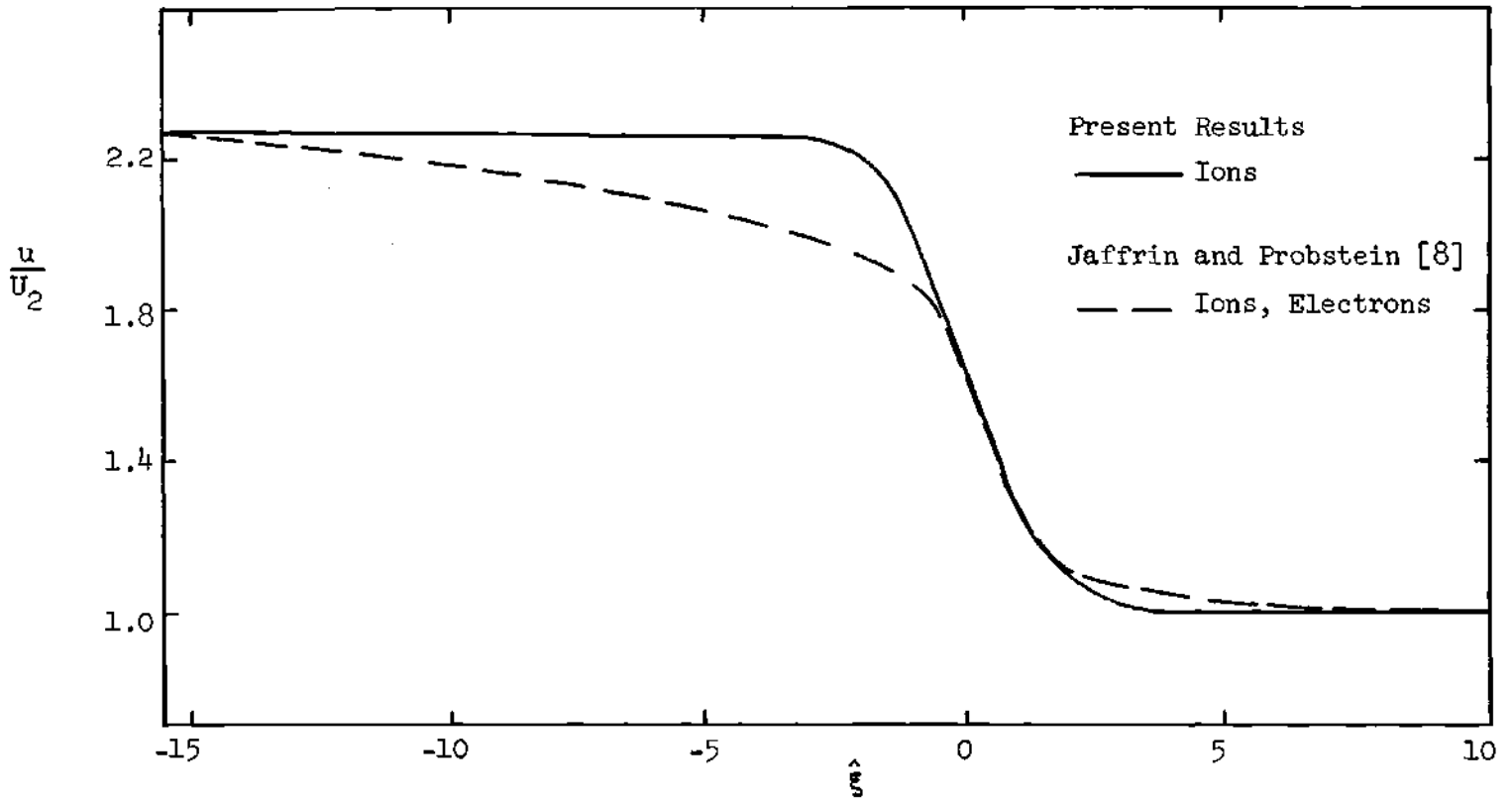

Figure 45. Velocity Profile with $\hat{E}$ Effect for $M_1 = 2.0$, $\alpha = 1.0$, $\hat{\xi} = 10x/\ell_{ii_2}$.

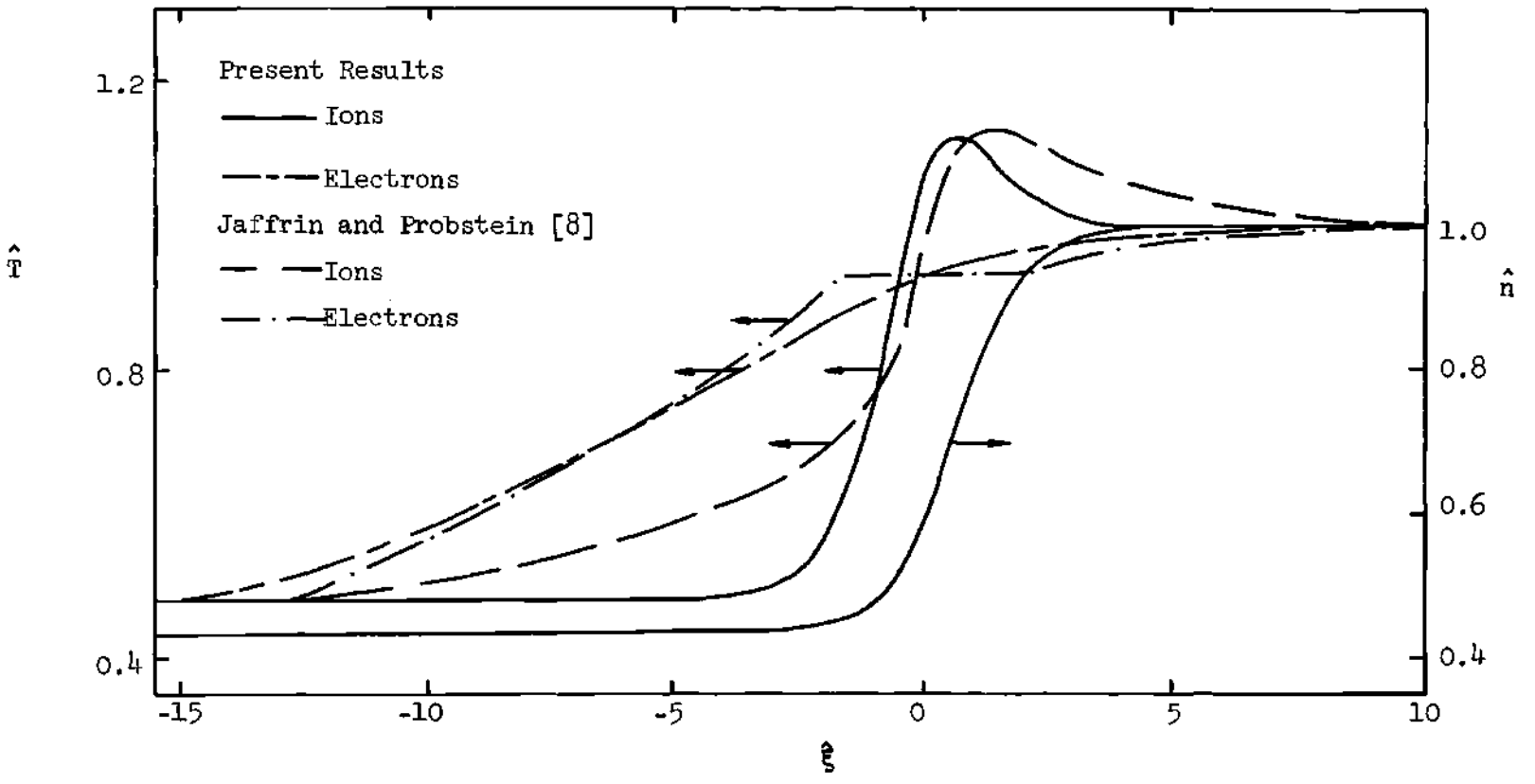

Figure 46. Temperature and Number Density Profiles with $\hat{E}$ Effect for $M_1 = 2.0$, $\alpha = 1.0$.

present ion temperature deviates from the profile of Jaffrin and Probstein except in the vicinity of the center of the shock where both methods yield about the same slope. Both methods also predict about the same value of the maximum ion temperature. Jaffrin and Probstein keep the electron temperature constant in the main portion of the ion shock in their analyses. Detail comparisons of $\hat{u}$ with the E field effects to $\hat{u}$ without the E field effects are listed in Tables 22 and 23 for ions and electrons, respectively. Results indicate that the effects of the induced electric field on the shock structure is very insignificant and can be neglected.

The last case to be investigated is the one with $M_1 = 10$ and $\alpha = 1.0$. The present electric field is compared with the results of Jaffrin and Probstein [8] as shown in Figure 47. In the main portion of the shock structure the profile of Jaffrin and Probstein contains a singularity. The peak of their $\hat{E}$ profile is more negative than the present $\hat{E}$ profile. The present results do not give a "precursor" electric shock layer as they name it. The ion velocity distribution across the shock structure is shown in Figure 48. The results of Jaffrin and Probstein are used for comparison. The difference between the two profiles are more significant in the low-pressure region of the shock than in the high-pressure region. The present electron velocity distribution is not shown in the figure, because its deviation from the present ion velocity profile is only by order of 10^{-5}. The temperature distributions are presented in Figure 49. The present method and the continuous approach of Jaffrin and Probstein predict about the same overshoot of the ion temperature. Their ion temperature profile contains a singularity in the low-pressure region of the shock. Results from both methods do not agree

Table 22. Comparison of $\hat{u}_i$ with $\hat{E}$ to $\hat{u}_i$ without $\hat{E}$ for $M_1 = 2.0$, $\alpha = 1.0$

I	$\hat{u}_i$ (with $\hat{E}$)	$\hat{u}_i$ (without $\hat{E}$)
45	.17638432+01	.17638431+01
47	.17320598+01	.17320599+01
49	.16682524+01	.16682525+01
51	.15531191+01	.15531185+01
53	.13803312+01	.13803312+01
55	.11815034+01	.11815033+01
57	.10120834+01	.10120834+01
59	.90092196+00	.90092197+00
61	.83993713+00	.83993709+00
63	.80972788+00	.80972788+00
65	.79551976+00	.79551980+00

Table 23. Comparison of $\hat{u}_e$ with $\hat{E}$ to $\hat{u}_e$ without $\hat{E}$ for $M_1 = 2.0$, $\alpha = 1.0$

I	$\hat{u}_e$ (with $\hat{E}$)	$\hat{u}_e$(without $\hat{E}$)
45	.65470520-02	.65326735-02
47	.64396899-02	.64115787-02
49	.62154058-02	.61710379-02
51	.57923244-02	.57437766-02
53	.51374674-02	.51084048-02
55	.43815974-02	.43789276-02
57	.37439983-02	.37538216-02
59	.33318329-02	.33422221-02
61	.31080153-02	.31149913-02
63	.29982445-02	.30020556-02
65	.29470526-02	.29489445-02

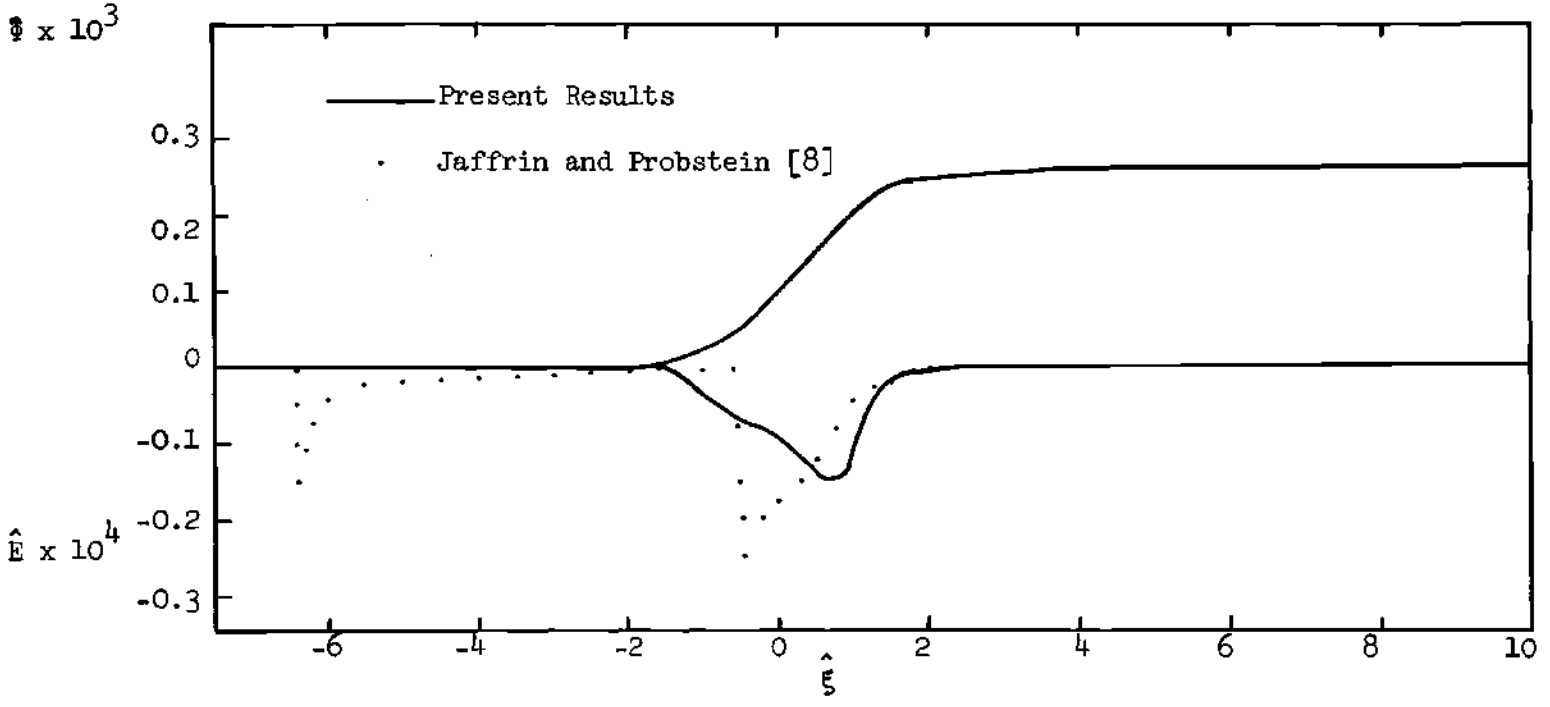

Figure 47. Electric Field and Potential Distributions for $M_1 = 10$, $\alpha = 1.0$, $\hat{\xi} = 10x/\ell_{ii_2}$.

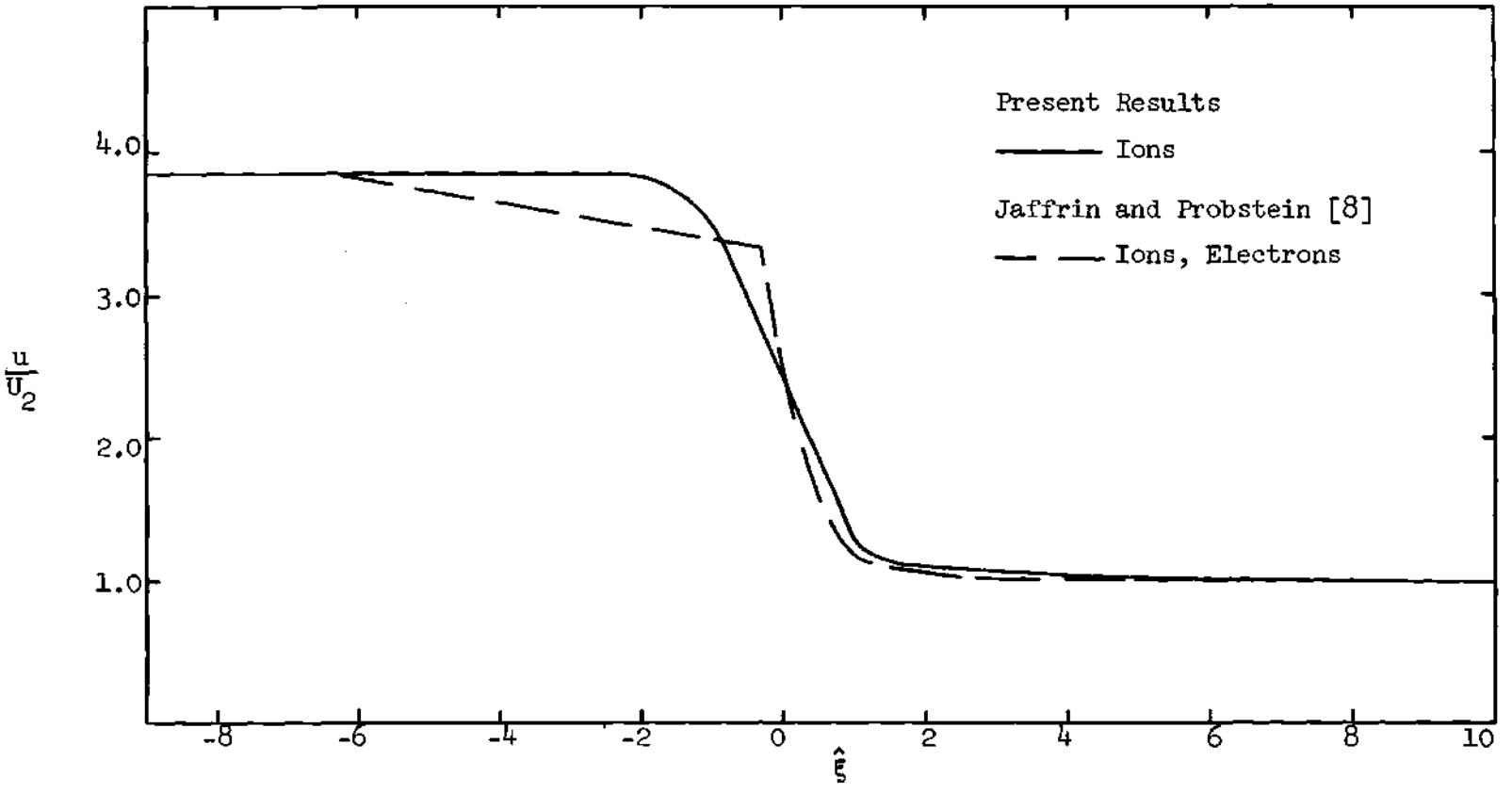

Figure 48. Velocity Profile with $\hat{E}$ Effect for $M_1 = 10.0$, $\alpha = 1.0$, $\hat{\xi} = 10x/\ell_{ii_2}$.

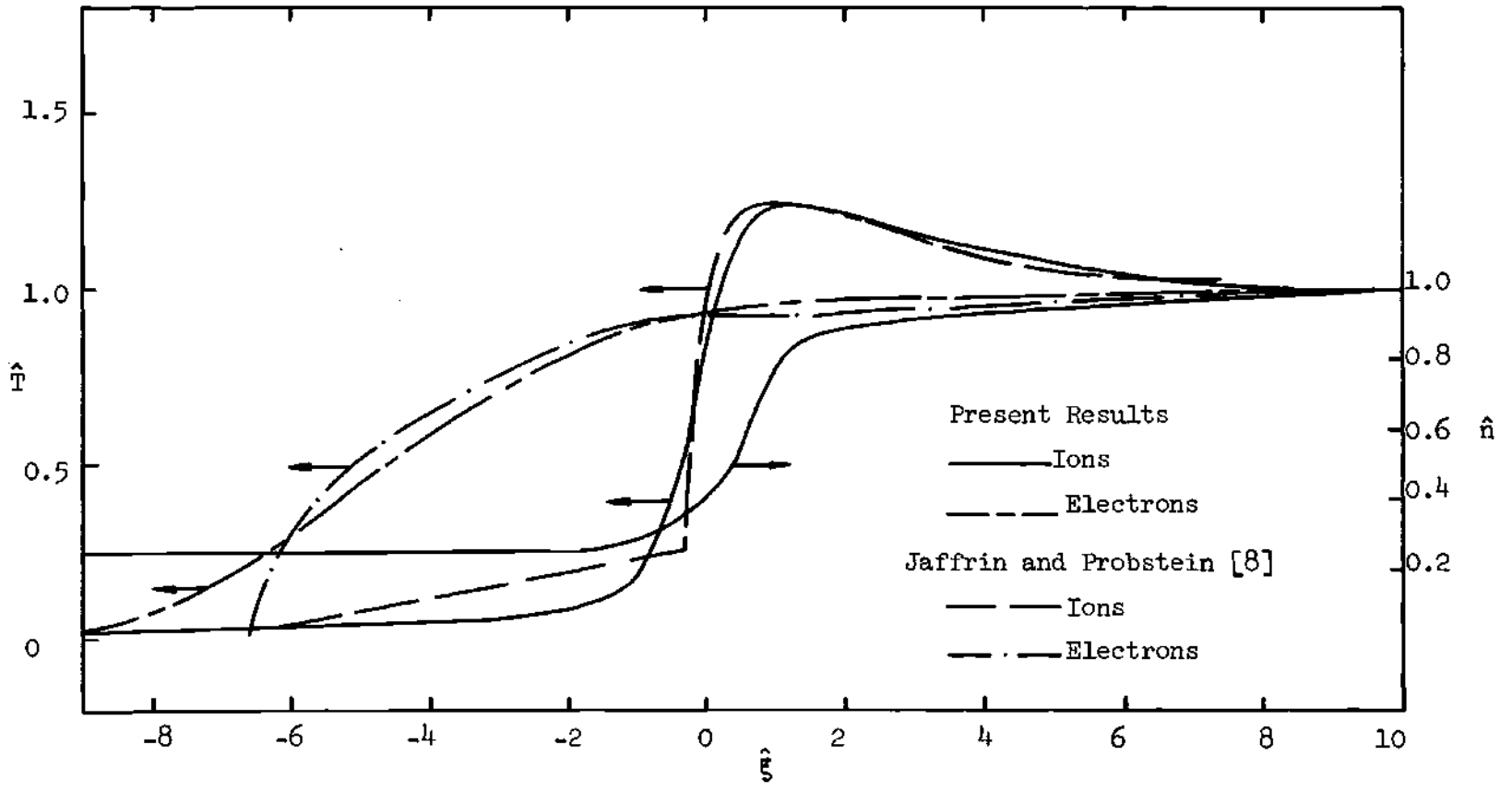

Figure 49. Temperature and Number Density Profiles with $\hat{E}$ Effect for $M_1 = 10.0$, $\alpha = 1.0$, $\hat{\xi} = 10x/\ell_{ii_2}$.

well in the low-pressure region. In general their electron temperature rises more rapidly than the present results. They keep the electron temperature constant in the main portion of the ion shock, thus their electron temperature profile has two singularities. Detailed comparisons of $\hat{u}$ with the electric field effects to $\hat{u}$ without the electric field effects are listed in Tables 24 and 25 for ions and electrons, respectively. Table 26 presents the electric field effects on distribution functions. These results indicate that the electric field effects on this case is very small and can be ignored.

The results presented in this chapter have demonstrated that the discrete ordinate method can be successfully applied to obtain solutions for BBGK equation with the acceleration or deceleration term. It has been observed that the induced electric field due to the charge separation in a shock structure tends to equilibrate the flow locally. However, these effects on the shock structure are very insignificant for all cases investigated and can be neglected. In other words, for all cases studied, the results obtained without the consideration of the effects of the induced electric field yield very good approximations to the results with the E field effects. It has also been experiences that when the E field effects are included in the BBGK equation, the numerical accuracy and the capacity limitation of the available computer facility can cause a great deal of trouble in obtaining numerical solutions.

Table 24. Comparison of $\hat{u}_i$ with $\hat{E}$ to $\hat{u}_i$ without $\hat{E}$ for $M_1 = 10.0$, $\alpha = 1.0$

I	$\hat{u}_i$ (with $\hat{E}$)	$\hat{u}_i$ (without $\hat{E}$)
81	.20968664+01	.20968762+01
83	.19955264+01	.19955364+01
85	.18573647+01	.18573738+01
87	.17192036+01	.17192129+01
89	.15810482+01	.15810632+01
91	.14429080+01	.14429440+01
93	.13047846+01	.13048579+01
95	.11666694+01	.11667878+01
97	.10284729+01	.10285565+01
99	.89027799+00	.89032834+00
101	.77131807+00	.77134473+00

Table 25. Comparison of $\hat{u}_e$ with $\hat{E}$ to $\hat{u}_e$ without $\hat{E}$ for $M_1 = 10.0$, $\alpha = 1.0$

I	$\hat{u}_e$ (with $\hat{E}$)	$\hat{u}_e$(without $\hat{E}$)
81	.77715964-02	.77716468-02
83	.73959989-02	.73960467-02
85	.68839323-02	.68839752-02
87	.63718638-02	.63719024-02
89	.58597999-02	.58598334-02
91	.53477465-02	.53477775-02
93	.48357071-02	.48357344-02
95	.43236771-02	.43237054-02
97	.38115846-02	.38116095-02
99	.32994907-02	.32995110-02
101	.28586593-02	.28586767-02

Table 26. Comparison of Distribution Functions with $\hat{E}$ Effect to Distribution Functions without $\hat{E}$ Effect at $x/\ell_{ii_2} = 0$, for $M_1 = 10.0$, $\alpha = 1.0$

J	$\hat{g}_i(\hat{E})$	$\hat{G}_i(\hat{E})$	$\hat{g}_i(\hat{E}=0)$	$\hat{G}_i(\hat{E}=0)$
121	.20013820-01	.20010012-01	.19996060-01	.19992270-01
141	.13637780+00	.13637378+00	.13635820+00	.13635418+00
161	.26103450+00	.26104315+00	.26107390+00	.26108256+00
181	.14034350+00	.14034330+00	.14034310+00	.14034287+00
201	.21194690-01	.21191855-01	.21181840-01	.21179022-01

J	$\hat{g}_e(\hat{E})$	$\hat{G}_e(\hat{E})$	$\hat{g}_e(\hat{E}=0)$	$\hat{G}_e(\hat{E}=0)$
80	.28932380-01	.28934630-01	.28934750-01	.28932721-01
100	.13932880+00	.13933336+00	.13933680+00	.13202772+00
120	.23654500+00	.23654127+00	.23654680+00	.23653839+00
140	.14157990+00	.14157069+00	.14157010+00	.14156712+00
160	.29874640-01	.29871319-01	.29869490-01	.29869377-01

CHAPTER V

THE STRUCTURE OF THE RELAXATION ZONE OF A SHOCK WAVE

Introduction

In this chapter the discrete ordinate method will be applied to investigate the structure of the relaxation zone which is the region behind the atom-atom shock front. Kinetic model equations will be used as the governing equations. Similar problems have been studied by several other authors using the continuum approach. Petschek and Byron [2] assumed that the electron-atom collisions dominate the ionization process in the relaxation zone. The effects of atom-atom ionization, photoionization, and recombination were neglected. They found that the rate of ionization is relatively insensitive to the inelastic ionization cross-sections for electron-atom collisions. Skalafuris [11] also showed that the electron-atom collisions dominated the ionizing process. Thus, the energy of excitation was not included in his analyses. Morgan and Morrison [9] basically followed the work of Petschek and Byron [2] and included the rate of ionization due to atom-atom collisions in the relaxation zone. It was found that the ionization mechanism was dominated by electron-atom elastic collisions when the degree of ionization began with 10^{-4} for 10^{4}°K and kept increasing with initial temperature of the relaxation zone.

Both atom-atom and electron-atom collisions and recombination were considered by Hoffert and Lien [12]. They treated the atom-atom shock as

a chemically frozen discontinuity. As many other authors, they assumed that atoms and ions had the same temperature and all species moved at the same macroscopic velocity. It was found that for Mach numbers less than 20 only the front portion of the relaxation zone was affected by different initial electron temperatures.

Initial conditions of the relaxation zone were assumed by many authors. For examples, Truitt [6] took the initial degree of ionization as 0.001 and Skalafuris [11] evaluated the initial conditions by shock equations with an assigned degree of ionization. On the other hand, Hoffert and Lien [12] determined the initial conditions by the jump conditions at the downstream of a chemically frozen discontinuity. A similar approach can be found in the study of a normal shock wave in a dissociating gas [39]. Effects of the induced electric field were not included in these investigations.

The contributions from the E field has been found to be small by Chubb [13]. He considered both atom-atom shock and the relaxation zone. In the atom-atom shock a bimodal Mott-Smith velocity distribution [5] was assumed for atoms. Ions and electrons were assumed to be in locally Maxwellian distributions. In the relaxation zone, all three species were assumed to be locally Maxwellian. He observed that for freestream Mach number less than 20 the relaxation zone was much thicker than the atom-atom shock in which only a negligible degree of ionization was generated.

It has been shown in Chapter IV that the effects of the induced electric field on the solution of the shock-wave structure are insignificant. Therefore, the E field effects will be neglected in this chapter. It will be assumed that the electron-atom collisions dominate the

ionization process. The region in front of the relaxation zone can be described approximately by a shock-wave structure with a frozen degree of ionization as discussed in detail in Chapters II through IV.

Formulation of the Problem

Hu and Ziering [16] proposed a set of model equations for three-component plasmas with ionizing effects. In deriving this set of equations, the following basic assumptions are used:

(1) the process of ionization is assumed to be dominated by the electron-neutral collisions;

(2) the plasma is singly ionized and is composed of neutral particles, ions, and electrons;

(3) the collision term in the Boltzmann equation can be replaced by ionizing collisions and non-ionizing collisions;

(4) the non-ionizing collisions are assumed to be elastic and can be represented by the BGK model [14];

(5) dissociation, recombination, and radiation are neglected.

If the upstream Mach number is low enough, the above assumptions are reasonable. Therefore, with this requirement in mind the model equations due to Hu and Ziering [16] will be used in this chapter to investigate the structure of the relaxation zone of an ionizing shock. Neglecting the effects of the induced electric field, the governing equation for this problem are:

$$v_{x_1}\frac{\partial f_1}{\partial x} = \frac{n_1}{\sigma_{11}}(F_{11}-f_1)+\frac{n_2}{\sigma_{12}}(F_{12}-f_1)+\frac{n_3}{\sigma_{13}}(F_{13}-f_1) \tag{1}$$

$$+\frac{P_I n_1'}{\sigma_{13}}F_{31}+\frac{P_I n_3}{\sigma_{13}}[F_{13}'-F_{13}H(v-v_c)],$$

$$v_{x_2}\frac{\partial f_2}{\partial x} = \frac{n_1}{\sigma_{21}}(F_{21}-f_2)+\frac{n_2}{\sigma_{22}}(F_{22}-f_2)+\frac{n_3}{\sigma_{23}}(F_{23}-f_2) \tag{2}$$

$$+\frac{P_I n_1'}{\sigma_{13}}F_{31},$$

and

$$v_{x_3}\frac{\partial f_3}{\partial x} = \frac{n_1}{\sigma_{31}}(F_{31}-f_3)+\frac{n_2}{\sigma_{32}}(F_{32}-f_3)+\frac{n_3}{\sigma_{33}}(F_{33}-f_3)$$

$$-\frac{P_I n_1'}{\sigma_{13}}F_{31}, \tag{3}$$

where P_I is the probability of ionization. The local Maxwellian distribution functions $F_{k\ell}$ in Equations (1) - (3) are defined as

$$F_{k\ell} = n_k\left(\frac{m_k}{2\pi K T_{k\ell}}\right)^{3/2}\exp\left\{-\frac{m_k[(V_x-u_{k\ell})^2+V_y^2+V_z^2]}{2KT_{k\ell}}\right\}. \tag{4}$$

Subscripts k, ℓ = 1, 2, 3 stand for electrons, ions, and atoms, respectively.

The $\sigma_{p\ell}$ are collisions parameters. The quantatities $\frac{n_\ell}{\sigma_{1\ell}}$, $\frac{n_\ell}{\sigma_{2\ell}}$, and $\frac{n_\ell}{\sigma_{3\ell}}$ have the dimensions of a frequency.

The macroscopic properties can be obtained by taking the moments of the distribution functions as mentioned in Chapter II.

In the model equations, Equations (1) - (3), it has been assumed

that the electron-neutral collisions dominate the ionization process and an electron possessing kinetic energy higher than the ionization potential of a neutral particle will ionize the neutral particle at a probability P_I during the collisions.

The last term in Equation (3) is the loss of neutral particles and the corresponding terms in Equation (1) and (2) are the source terms of electrons and ions, respectively.

The local Maxwellian F'_{13} is given as [16]

$$F'_{13} = n'_1 \left(\frac{m_1}{2\pi K T'_{13}} \right)^{3/2} \exp\left\{ - \frac{m_1 [(V_x - u_{13})^2 + V_y^2 + V_z^2]}{2 K T'_{13}} \right\}, \qquad (7)$$

where

$$n'_1 = n_1 \left[\operatorname{erfc}\left(\beta_{13}^{1/2} V_0 \right) + 2 \left(\frac{\beta_{13}}{\pi} \right)^{1/2} V_0 \, e^{-\beta_{13} V_0^2} \right], \qquad (8\text{-a})$$

$$3 n'_1 K T'_{13} = K T_{13} \left[3 n'_1 - 2 n_1 \beta_{13} V_0^2 \operatorname{erfc}\left(\beta_{13}^{1/2} V_0 \right) \right], \qquad (8\text{-b})$$

$$\beta_{13} = \frac{m_1}{2 \pi T_{13}} . \qquad (9)$$

and the complementary error function is defined by

$$\operatorname{erfc}(x) = \frac{2}{\sqrt{\pi}} \int_x^\infty e^{-t^2} dt .$$

Hu and Ziering [16] have assumed that the momentum of the plasma is not changed during the ionization, thus $u'_{13} = u_{13}$.

The Heaviside function $H(v - v_o)$ in Equation (1) is defined as

$$H(v - v_o) = \begin{cases} 1 & \text{for } v > v_o \\ 0 & \text{for } v < v_o \end{cases}$$

where v_o is the electron speed corresponding to the ionization potential.

In Equation (1) the term with $H(v - v_o)$ is the portion of the energetic electrons before they consume their kinetic energy to ionize neutral particles while the term with F'_{13} represents the redistribution of these energetic electrons after they have consumed their kinetic energy. It has been assumed that during the ionizing collisions, both the ionization and relaxation processes take place immediately. The collision cross sections given in Chapters II and III are to be used in this chapter. The reduced distribution functions g_k, h_k, $G_{k\ell}$, and $H_{k\ell}$ are defined as those presented in Chapter II.

If Equations (1) - (3) are multiplied by unity and integrated with respect to v_y and v_z, the following equations are obtained

$$v_{x_1}\frac{\partial g_1}{\partial x} = \nu_{11}(G_{11} - g_1) + \nu_{12}(G_{12} - g_1) + \nu_{13}(G_{13} - g_1)$$

$$+\int_{-\infty}^{\infty}\int_{-\infty}^{\infty}\frac{P_x n_1'}{\sigma_{13}}F_{31}\,dv_y\,dv_z + \int_{-\infty}^{\infty}\int_{-\infty}^{\infty}\frac{P_x n_3}{\sigma_{13}}\left[F'_{13} - F_{13}H(v - v_o)\right]dv_y\,dv_z, \tag{10}$$

$$v_{x_2}\frac{\partial g_2}{\partial x} = \nu_{21}(G_{21} - g_2) + \nu_{22}(G_{22} - g_2) + \nu_{23}(G_{23} - g_2)$$

$$+\int_{-\infty}^{\infty}\int_{-\infty}^{\infty}\frac{P_x n_1'}{\sigma_{13}}F_{31}\,dv_y\,dv_z, \tag{11}$$

and

$$v_{x_3}\frac{\partial g_3}{\partial x} = \nu_{31}(G_{31}-g_3)+\nu_{32}(G_{32}-g_3)+\nu_{33}(G_{33}-g_3)$$

$$-\int_{-\infty}^{\infty}\int_{-\infty}^{\infty}\frac{P_I n_1'}{\sigma_{13}}F_{31}\,dv_y\,dv_z. \tag{12}$$

If the multiplying factor is $v_y^2 + v_z^2$, then the corresponding set of equations yields

$$v_{x_1}\frac{\partial h_1}{\partial x} = \nu_{11}(H_{11}-h_1)+\nu_{12}(H_{12}-h_1)+\nu_{13}(H_{13}-h_1)$$

$$+\int_{-\infty}^{\infty}\int_{-\infty}^{\infty}(v_y^2+v_z^2)\frac{P_I n_1'}{\sigma_{13}}F_{31}\,dv_y\,dv_z$$

$$+\int_{-\infty}^{\infty}\int_{-\infty}^{\infty}(v_y^2+v_z^2)\frac{P_I n_3}{\sigma_{13}}[F_{13}'-F_{13}H(v-v_0)]\,dv_y\,dv_z, \tag{13}$$

$$v_{x_2}\frac{\partial h_2}{\partial x} = \nu_{21}(H_{21}-h_2)+\nu_{22}(H_{22}-h_2)+\nu_{23}(H_{23}-h_2)$$

$$+\int_{-\infty}^{\infty}\int_{-\infty}^{\infty}(v_y^2+v_z^2)\frac{P_I n_1'}{\sigma_{13}}F_{31}\,dv_y\,dv_z, \tag{14}$$

and

$$v_{x_3}\frac{\partial h_3}{\partial x} = \nu_{31}(H_{31}-h_3)+\nu_{32}(H_{32}-h_3)+\nu_{33}(H_{33}-h_3)$$

$$-\int_{-\infty}^{\infty}\int_{-\infty}^{\infty}(v_y^2+v_z^2)\frac{P_I n_1'}{\sigma_{13}}F_{31}\,dv_y\,dv_z. \tag{15}$$

Performing integrations in Equations (10) - (15) gives

$$\int_{-\infty}^{\infty}\int_{-\infty}^{\infty} \frac{P_I n_1'}{\sigma_{13}} F_{31}\, dv_y\, dv_z = \frac{n_1'}{n_3}\, \nu_{13_I} G_{31}$$

where,

$$G_{31} = \frac{n_3}{(2\pi R_3 T_{31})^{1/2}}\, e^{-\frac{(v_x - u_{31})^2}{2R_3 T_{31}}}$$

and

$$\nu_{13_I} = \frac{P_I n_3}{\sigma_{13}} ;$$

$$\int_{-\infty}^{\infty}\int_{-\infty}^{\infty} \frac{P_I n_3}{\sigma_{13}} F_{13}'\, dv_y\, dv_z = \nu_{13_I} G_{13}'$$

where,

$$G_{13}' = \frac{n_1'}{(2\pi R_1 T_{13}')^{1/2}}\, e^{-\frac{(v_x - u_{13})^2}{2R_1 T_{13}'}} ;$$

$$\int_{-\infty}^{\infty}\int_{-\infty}^{\infty} \frac{P_I n_3}{\sigma_{13}} H(v - v_o) F_{13}\, dv_y\, dv_z = \begin{cases} \nu_{13_I} G_{13} & \text{if } |v_x| \geq v_o \\ \nu_{13_I} G_{13}\, e^{-\frac{(v_o^2 - v_x^2)}{2R_1 T_{13}}} & \text{if } |v_x| < v_o . \end{cases}$$

Similarly,

$$\int_{-\infty}^{\infty}\int_{-\infty}^{\infty} (v_y^2 + v_z^2) \frac{P_I n_1'}{\sigma_{13}} F_{31}\, dv_y\, dv_z = \frac{n_1'}{n_3}\, \nu_{13_I} (2R_3 T_{31})\, G_{31}$$

$$= \frac{n_1'}{n_3}\, \nu_{13_I} H_{31} ,$$

where,

$$H_{31} = (2R_3 T_{31})\, G_{31} ;$$

$$\int_{-\infty}^{\infty}\int_{-\infty}^{\infty}(v_y^2+v_z^2)\frac{P_I n_3}{\sigma_{13}}F_{13}'\,dv_y\,dv_z=\nu_{13_I}(2R_1T_{13}')G_{13}'$$

$$=\nu_{13_I}H_{13}',$$

and

$$H_{13}'=2R_1T_{13}'G_{13}';$$

$$\int_{-\infty}^{\infty}\int_{-\infty}^{\infty}(v_y^2+v_z^2)\frac{P_I n_3}{\sigma_{13}}H(v-v_0)F_{13}\,dv_y\,dv_z=\begin{cases}\nu_{13_I}H_{13} & \text{if } |v_x|\geq v_0\\ \nu_{13_I}H_{13}\,e^{-\frac{(v_0^2-v_x^2)}{2R_1T_{13}}}\left[1+\frac{(v_0^2-v_x^2)}{2R_1T_{13}}\right] & \text{if } |v_x|<v_0\end{cases}$$

The following expression for ν_{13_I} which is derived in Appendix III will be used in the governing equations:

$$\nu_{13_I}=5.27665455152\times10^{-16}\sqrt{\pi}\,n_3\left(\frac{n_1}{n_1'}\right)\sqrt{2R_1T_1}\left[1+\frac{2}{\left(\frac{v_0^2}{2R_1T_1}\right)}\right]e^{-\frac{v_0^2}{2R_1T_1}} \tag{16}$$

Equations (10) - (15) become

$$v_{x_1}\frac{\partial g_1}{\partial x}=\nu_{11}(G_{11}-g_1)+\nu_{12}(G_{12}-g_1)+\nu_{13}(G_{13}-g_1)$$

$$+\frac{n_1'}{n_3}\nu_{13_I}G_{31}+\nu_{13_I}(G_{13}'-\bar{G}_{13}), \tag{17}$$

$$v_{x_2}\frac{\partial g_2}{\partial x} = \nu_{21}(G_{21}-g_2) + \nu_{22}(G_{22}-g_2) + \nu_{23}(G_{23}-g_2) + \frac{n_1'}{n_3}\nu_{13_I}G_{31}, \tag{18}$$

$$v_{x_3}\frac{\partial g_3}{\partial x} = \nu_{31}(G_{31}-g_3) + \nu_{32}(G_{32}-g_3) + \nu_{33}(G_{33}-g_3) - \frac{n_1'}{n_3}\nu_{13_I}G_{31}, \tag{19}$$

$$v_{x_1}\frac{\partial h_1}{\partial x} = \nu_{11}(H_{11}-h_1) + \nu_{12}(H_{12}-h_1) + \nu_{13}(H_{13}-h_1) + \frac{n_1'}{n_3}\nu_{13_I}H_{31} + \nu_{13_I}(H_{13}'-\bar{H}_{13}), \tag{20}$$

$$v_{x_2}\frac{\partial h_2}{\partial x} = \nu_{21}(H_{21}-h_2) + \nu_{22}(H_{22}-h_2) + \nu_{23}(H_{23}-h_2) + \frac{n_1'}{n_3}\nu_{13_I}H_{31}, \tag{21}$$

and

$$v_{x_3}\frac{\partial h_3}{\partial x} = \nu_{31}(H_{31}-h_3) + \nu_{32}(H_{32}-h_3) + \nu_{33}(H_{33}-h_3) - \frac{n_1'}{n_3}\nu_{13_I}H_{31}, \tag{22}$$

where

$$\bar{G}_{13} = \begin{cases} G_{13} & \text{if } |v_x| \geq v_c \\ G_{13}\, e^{-\frac{(v_c^2-v_x^2)}{2R_1T_{13}}} & \text{if } |v_x| < v_c \end{cases}$$

and

$$\bar{H}_{13} = \begin{cases} H_{13} & \text{if } |V_x| \geq V_o \\ H_{13}\, e^{-\frac{(V_o^2 - V_x^2)}{2R_1 T_{13}}} \left[1 + \frac{(V_o^2 - V_x^2)}{2R_1 T_{13}} \right] & \text{if } |V_x| < V_o \end{cases}$$

In addition to the nondimensional quantatities defined in Chapters II and III the following nondimensional quantatities are introduced

$$\hat{\nu}_{13_I} = \frac{(\lambda_{33})_2}{(V_1)_2} \nu'_{13_I} ; \qquad \hat{n}_1' = \frac{n_1'}{n_1} .$$

Consequently Equations (17) - (22) in nondimensional forms become

$$\hat{v}_{x_1} \frac{\partial \hat{g}_1}{\partial \hat{x}} = \hat{\nu}_{11} (\hat{G}_{11} - \hat{g}_1) + \hat{\nu}_{12} (\hat{G}_{12} - \hat{g}_1) + \hat{\nu}_{13} (\hat{G}_{13} - \hat{g}_1) + \frac{\hat{n}_1' \hat{n}_1}{\hat{n}_3} \sqrt{\frac{m_3}{m_1}}\, \hat{\nu}_{13_I} \hat{G}_{31} + \hat{\nu}_{13_I} (\hat{G}'_{13} - \bar{\hat{G}}_{13}) , \tag{23}$$

$$\hat{v}_{x_2} \frac{\partial \hat{g}_2}{\partial \hat{x}} = \hat{\nu}_{21} (\hat{G}_{21} - g_2) + \hat{\nu}_{22} (\hat{G}_{22} - \hat{g}_2) + \hat{\nu}_{23} (\hat{G}_{23} - \hat{g}_2) + \frac{\hat{n}_1' \hat{n}_1}{\hat{n}_3} \sqrt{\frac{m_3}{m_1}}\, \hat{\nu}_{13_I} \hat{G}_{31} , \tag{24}$$

$$\hat{v}_{x_3} \frac{\partial \hat{g}_3}{\partial \hat{x}} = \hat{\nu}_{31} (\hat{G}_{31} - \hat{g}_3) + \hat{\nu}_{32} (\hat{G}_{32} - \hat{g}_3) + \hat{\nu}_{33} (\hat{G}_{33} - \hat{g}_3) - \left(\frac{\alpha_2}{1-\alpha_2} \right) \left(\frac{\hat{n}_1' \hat{n}_1}{\hat{n}_3} \right) \sqrt{\frac{m_3}{m_1}}\, \hat{\nu}_{13_I} \hat{G}_{31} , \tag{25}$$

$$\hat{v}_{x_1} \frac{\partial \hat{h}_1}{\partial \hat{x}} = \hat{\nu}_{11} (\hat{H}_{11} - \hat{h}_1) + \hat{\nu}_{12} (\hat{H}_{12} - \hat{h}_1) + \hat{\nu}_{13} (\hat{H}_{13} - \hat{h}_1) + \frac{\hat{n}_1' \hat{n}_1}{\hat{n}_3} \sqrt{\frac{m_1}{m_3}}\, \hat{\nu}_{13_I} \hat{H}_{31} + \hat{\nu}_{13_I} (\hat{H}'_{13} - \bar{\hat{H}}_{13}) , \tag{26}$$

$$\hat{v}_{x_2}\frac{\partial \hat{h}_2}{\partial \hat{x}} = \hat{\nu}_{21}(\hat{H}_{21}-\hat{h}_2)+\hat{\nu}_{22}(H_{22}-\hat{h}_2)+\hat{\nu}_{23}(\hat{H}_{23}-\hat{h}_2) + \frac{\hat{n}_1'\hat{n}_1}{\hat{n}_3}\sqrt{\frac{m_3}{m_1}}\,\hat{\nu}_{13_I}\hat{H}_{31}\,, \tag{27}$$

and

$$\hat{v}_{x_3}\frac{\partial \hat{h}_3}{\partial \hat{x}} = \hat{\nu}_{31}(\hat{H}_{31}-\hat{h}_3)+\hat{\nu}_{32}(\hat{H}_{32}-\hat{h}_3)+\hat{\nu}_{33}(\hat{H}_{33}-\hat{h}_3) - \left(\frac{\alpha_2}{1-\alpha_2}\right)\left(\frac{\hat{n}_1'\hat{n}_1}{\hat{n}_3}\right)\sqrt{\frac{m_3}{m_1}}\,\hat{\nu}_{13_I}\hat{H}_{31}\,, \tag{28}$$

where,

$$\hat{G}_{13}' = \frac{\hat{n}_1'\hat{n}_1}{\sqrt{\pi\hat{T}_{13}'}}\,e^{-\frac{(\hat{v}_x-\hat{u}_{13})^2}{\hat{T}_{13}'}}\,,$$

$$\hat{\bar{G}}_{13} = \begin{cases} \hat{G}_{13} & \text{if } |\hat{v}_x| \geq \hat{v}_c \\ \hat{G}_{13}\,e^{-\frac{(\hat{v}_c^2-\hat{v}_x^2)}{\hat{T}_{31}}} & \text{if } |\hat{v}_x| < \hat{v}_c\,, \end{cases}$$

$$\hat{H}_{13}' = \hat{T}_{13}'\hat{G}_{13}'\,,$$

and

$$\hat{\bar{H}}_{13} = \begin{cases} \hat{T}_{13}\hat{\bar{G}}_{13} & \text{if } |\hat{v}_x| \geq \hat{v}_c \\ \hat{T}_{13}\hat{\bar{G}}_{13}\left[1+\frac{(\hat{v}_c^2-\hat{v}_x^2)}{\hat{T}_{31}}\right] & \text{if } |\hat{v}_x| < \hat{v}_c \end{cases}$$

Equations (8-a) and (8-b) in nondimensional form give

$$\hat{n}_1' = \operatorname{erfc}\left(\sqrt{\frac{\hat{T}_x}{\hat{T}_{13}}}\right)+\frac{2}{\sqrt{\pi}}\sqrt{\frac{\hat{T}_x}{\hat{T}_{13}}}\,e^{-\frac{\hat{T}_x}{\hat{T}_{13}}} \tag{29}$$

and

$$\hat{T}_{13}' = \hat{T}_{13} - \frac{2}{3}\frac{\hat{T}_x}{\hat{n}_1'}\,\mathrm{erfc}\left(\sqrt{\frac{\hat{T}_x}{\hat{T}_{13}}}\right). \tag{30}$$

When the discrete ordinate method is applied, Equations (23) - (28) at the discrete points in velocity space are given as follows

$$\hat{v}_{j_1}\frac{d\hat{q}_{j_1}}{d\hat{x}} = \hat{\nu}_{11}(\hat{G}_{j_{11}} - \hat{q}_{j_1}) + \hat{\nu}_{12}(\hat{G}_{j_{12}} - \hat{q}_{j_1}) + \hat{\nu}_{13}(\hat{G}_{j_{13}} - \hat{q}_{j_1}) + \frac{\hat{n}_1'\hat{n}_1}{\hat{n}_3}\sqrt{\frac{m_3}{m_1}}\,\hat{\nu}_{13_x}\hat{G}_{j_{31}} + \hat{\nu}_{13_x}(\hat{G}_{j_{13}} - \bar{\hat{G}}_{j_{13}}), \tag{31}$$

$$\hat{v}_{j_2}\frac{d\hat{q}_{j_2}}{d\hat{x}} = \hat{\nu}_{21}(\hat{G}_{j_{21}} - \hat{q}_{j_2}) + \hat{\nu}_{22}(\hat{G}_{j_{22}} - \hat{q}_{j_2}) + \hat{\nu}_{23}(\hat{G}_{j_{23}} - \hat{q}_{j_2}) + \frac{\hat{n}_1'\hat{n}_1}{\hat{n}_3}\sqrt{\frac{m_3}{m_1}}\,\hat{\nu}_{13_x}\hat{G}_{j_{31}}, \tag{32}$$

$$\hat{v}_{j_3}\frac{d\hat{q}_{j_3}}{d\hat{x}} = \hat{\nu}_{31}(\hat{G}_{j_{31}} - \hat{q}_{j_3}) + \hat{\nu}_{32}(\hat{G}_{j_{32}} - \hat{q}_{j_3}) + \hat{\nu}_{33}(\hat{G}_{j_{33}} - \hat{q}_{j_3}) - \left(\frac{\alpha_2}{1-\alpha_2}\right)\left(\frac{\hat{n}_1'\hat{n}_1}{\hat{n}_3}\right)\sqrt{\frac{m_3}{m_1}}\,\hat{\nu}_{13_x}\hat{G}_{j_{31}}, \tag{33}$$

$$\hat{v}_{j_1}\frac{d\hat{h}_{j_1}}{d\hat{x}} = \hat{\nu}_{11}(\hat{H}_{j_{11}} - \hat{h}_{j_1}) + \hat{\nu}_{12}(\hat{H}_{j_{12}} - \hat{h}_{j_1}) + \hat{\nu}_{13}(\hat{H}_{j_{13}} - \hat{h}_{j_1}) + \frac{\hat{n}_1'\hat{n}_1}{\hat{n}_3}\sqrt{\frac{m_1}{m_3}}\,\hat{\nu}_{13_x}\hat{H}_{j_{31}} + \hat{\nu}_{13_x}(\hat{H}_{j_{13}}' - \bar{\hat{H}}_{j_{13}}), \tag{34}$$

$$\hat{v}_{j_2}\frac{d\hat{h}_{j_2}}{d\hat{x}} = \hat{\nu}_{21}\left(\hat{H}_{j_{21}} - \hat{h}_{j_2}\right) + \hat{\nu}_{22}\left(\hat{H}_{j_{22}} - \hat{h}_{j_2}\right) + \hat{\nu}_{23}\left(\hat{H}_{j_{23}} - \hat{h}_{j_2}\right)$$

$$+ \frac{\hat{n}_1'\hat{n}_1}{\hat{n}_3}\sqrt{\frac{m_3}{m_1}}\,\hat{\nu}_{13_I}\hat{H}_{j_{31}}, \tag{35}$$

and

$$\hat{v}_{j_3}\frac{d\hat{h}_{j_3}}{d\hat{x}} = \hat{\nu}_{31}\left(\hat{H}_{j_{31}} - \hat{h}_{j_3}\right) + \hat{\nu}_{32}\left(\hat{H}_{j_{32}} - \hat{h}_{j_3}\right) + \hat{\nu}_{33}\left(\hat{H}_{j_{33}} - \hat{h}_{j_3}\right)$$

$$- \left(\frac{\alpha_2}{1-\alpha_2}\right)\left(\frac{\hat{n}_1'\hat{n}_1}{\hat{n}_3}\right)\sqrt{\frac{m_3}{m_1}}\,\hat{\nu}_{13_I}\hat{H}_{j_{31}}, \tag{36}$$

where

$$\hat{G}_{j_{K\ell}} = \frac{\hat{n}_K}{(\pi\hat{T}_{K\ell})^{1/2}}\exp\left[-\frac{1}{\hat{T}_{K\ell}}\left(\hat{v}_j - \hat{u}_{K\ell}\right)^2\right],$$

$$\hat{G}'_{j_{13}} = \frac{\hat{n}_1'\hat{n}_1}{\sqrt{\pi\hat{T}'_{13}}}\exp\left[-\frac{1}{\hat{T}'_{13}}\left(\hat{v}_j - \hat{u}_{13}\right)^2\right],$$

$$\bar{\hat{G}}_{j_{13}} = \begin{cases} \hat{G}_{j_{13}} & \text{if } |\hat{v}_j| \geq \hat{v}_c \\ \hat{G}_{j_{13}}\exp\left[-\frac{1}{\hat{T}_{31}}\left(\hat{v}_c^2 - \hat{v}_x^2\right)\right] & \text{if } |\hat{v}_j| < \hat{v}_c \end{cases},$$

$$\hat{H}_{j_{K\ell}} = \hat{T}_{K\ell}\hat{G}_{j_{K\ell}},$$

$$\hat{H}'_{j_{13}} = \hat{T}'_{13}\hat{G}'_{j_{13}},$$

and

$$\hat{\bar{H}}_{J_{13}} = \begin{cases} \hat{T}_{13}\,\hat{\bar{G}}_{J_{13}} & \text{if } |\hat{v}_j| \geq \hat{v}_0 \\ \hat{T}_{13}\,\hat{\bar{G}}_{J_{13}}\left[1 + \dfrac{(\hat{v}_0^2 - \hat{v}_j^2)}{\hat{T}_{31}}\right] & \text{if } |\hat{v}_j| < \hat{v}_0 \end{cases}$$

$(K, \ell = 1, 2, 3\ ;\ j = 1, 2, \cdots\cdots, n)$.

The moment equations (Equation (38-a) - (39-b) in Chapter II) can be used to calculate the flow properties.

Boundary Conditions

The following Rankine-Hugoniot relations which are derived in Appendix II will be used for the boundary conditions at the downstream equilibrium state of this problem. They are:

$$T_2^* = \frac{\gamma-1}{\gamma}\frac{1}{1+\alpha_2}\left\{\left[1-\left(\frac{1-\alpha_2}{1-\alpha_1}\right)\frac{1}{n_{a_2}^*}\right]u_{a_1}^{*2} + \frac{\gamma}{\gamma-1}(1+\alpha_1) + (\alpha_1-\alpha_2)\,T_0^*\right\}, \tag{37}$$

$$p_2^* = 1 + \frac{2}{1+\alpha_1}u_{a_1}^{*2}\left[1 - \frac{1-\alpha_2}{1-\alpha_1}\frac{1}{n_{a_2}^*}\right], \tag{38}$$

$$n_{a_2}^* = \frac{1+\alpha_1}{1-\alpha_1}\frac{1-\alpha_2}{1+\alpha_2}\frac{p_2^*}{T_2^*}, \tag{39}$$

and the expression for the degree of ionization of argon proposed by Scheibe [40] is

$$\alpha = \frac{1}{\sqrt{\frac{p}{T^{5/2}} \cdot \frac{10^4}{2 + e^{-\frac{2060}{T}}} e^{\frac{182000}{T}} + 1}} \tag{40}$$

where, p is in cm Hg and T is in °K.

By giving the upstream equilibrium conditions, Equations (37) - (40) are to be solved by iterative process to obtain α_2 , T_2^*, p_2^*, and $n_{a_2}^*$. To initiate the iterative process, a degree of ionization at the downstream equilibrium conditions is assumed. Then the shock wave is treated as if it were frozen. Thus, the Rankine-Hugoniot relations for a frozen degree of ionization given in Appendix I can be applied to obtain initial guessed values for T_2, p_2, and n_{a_2}. From Equation (40) a new α_2 can be obtained. With this α_2 , a new set of T_2, p_2, and n_{a_2} can be obtained from Equations (37) - (39). The process is repeated until convergent criteria are satisfied. For the present investigation the criteria are set at 0.001 between two consecutive iterations for both T_2^* and $n_{a_2}^*$.

Computational Procedures

When the discrete ordinate method is applied to Equations (31) - (36), the functions $\hat{g}_k$, $\hat{h}_k$, $\hat{G}_{k\ell}$, and $\hat{H}_{k\ell}$ can be replaced by a series of point functions $\hat{g}_{j_k}$, $\hat{h}_{j_k}$, $\hat{G}_{j_{k\ell}}$, and $\hat{H}_{j_{k\ell}}$, respectively, evaluated at the discrete velocity points $\hat{v}_{j_k}$. A central difference scheme is used to approximate the derivatives with respect to $\hat{x}$, the variable in physical space. Then, the governing equations in finite difference form can

be set up in such a way that the tridiagonal matrix technique can be applied. If i is the index for variable $\hat{x}$ in physical space and k is the index for species, Equations (31) - (33) can be rewritten as follows

$$\left(\hat{\nu}_{2_{K1}} + \hat{\nu}_{2_{K2}} + \hat{\nu}_{2_{K3}}\right)\hat{g}_{2,j_K} + \frac{\hat{v}_{j_K}}{2\Delta\hat{x}}\hat{g}_{3,j_K} = \hat{\nu}_{2_{K1}}\hat{G}_{2,j_{K1}}$$

$$+ \hat{\nu}_{2_{K2}}\hat{G}_{2,j_{K2}} + \hat{\nu}_{2_{K3}}\hat{G}_{2,j_{K3}} + \frac{\hat{v}_{j_K}}{2\Delta\hat{x}}\hat{G}_{1,j_{KK}}$$

$$+ C_K \frac{\hat{n}_{2_1}'\hat{n}_{2_1}}{\hat{n}_{2_3}}\sqrt{\frac{m_3}{m_1}}\,\hat{\nu}_{I_{2,3}}\hat{G}_{2,j_{31}} + D_K\hat{\nu}_{I_{2,3}}\left(\hat{G}'_{2,j_{13}} - \hat{\bar{G}}_{2,j_{13}}\right),$$

for $K = 1, 2, 3$ and $i = 2$,

$$-\frac{\hat{v}_{j_K}}{2\Delta\hat{x}}\hat{g}_{i-1,j_K} + \left(\hat{\nu}_{i_{K1}} + \hat{\nu}_{i_{K2}} + \hat{\nu}_{i_{K3}}\right)\hat{g}_{i,j_K} + \frac{\hat{v}_{j_K}}{2\Delta\hat{x}}\hat{g}_{i+1,j_K} =$$

$$\hat{\nu}_{i_{K1}}\hat{G}_{i,j_{K1}} + \hat{\nu}_{i_{K2}}\hat{G}_{i,j_{K2}} + \hat{\nu}_{i_{K3}}\hat{G}_{i,j_{K3}} +$$

$$C_K \frac{\hat{n}_{2_1}'\hat{n}_{2_1}}{\hat{n}_{2_3}}\sqrt{\frac{m_3}{m_1}}\,\hat{\nu}_{I_{i,3}}\hat{G}_{i,j_{31}} + D_K\hat{\nu}_{I_{i,3}}\left(\hat{G}'_{i,j_{13}} - \hat{\bar{G}}_{i,j_{13}}\right),$$

for $i = 3, 4, \cdots\cdots, N-2$,

and

$$-\frac{\hat{v}_{j_K}}{2\Delta\hat{z}}\hat{g}_{N-2,j_K}+(\hat{v}_{N-1_{K1}}+\hat{v}_{N-1_{K2}}+\hat{v}_{N-1_{K3}})\hat{g}_{N-1,j_K}=\hat{v}_{N-1_{K1}}\hat{G}_{N-1,j_{K1}}$$

$$+\hat{v}_{N-1_{K2}}\hat{G}_{N-1,j_{K2}}+\hat{v}_{N-1_{K3}}\hat{G}_{N-1,j_{K3}}-\frac{\hat{v}_{j_K}}{2\Delta\hat{z}}\hat{G}_{N,j_{KK}}+$$

$$C_K\frac{\hat{n}_{2_1}'\hat{n}_{2_1}}{\hat{n}_{2_3}}\sqrt{\frac{m_3}{m_1}}\hat{v}_{I_{i,3}}\hat{G}_{i,j_{31}}+D_K\hat{v}_{I_{i,3}}(\hat{G}'_{i,j_{13}}-\hat{\bar{G}}_{i,j_{13}}),$$

for $i=N-1$,

where,

$$C_1=C_2=1,$$

$$C_3=-\frac{\alpha_2}{1-\alpha_2},$$

$$D_1=1,$$

and

$$D_2=D_3=0.$$

Similar equations can be written for $\hat{h}_{i,j_k}$.

Proper choices of velocity spacing have to be made in order to insure that the profiles of the calculated distribution functions will accurately describe the actual ones. Sufficient velocity points are

needed to make certain that both ends of the actual distribution functions are well covered. In physical space, sufficient physical points are required so that the equilibrium states can be recovered asymptotically. For the calculations in this chapter, 320 discrete velocity points are used.

The initial values of the macroscopic properties throughout the shock structure are needed in order to initiate the iterative process. Since results obtained by the continuum approach are available in the literature, they will be used as references in assuming the initial forms for profiles of macroscopic properties. All the reduced equilibrium distribution functions throughout the shock can be evaluated with these initial guesses. Systems of equation in finite difference form are solved by the tridiagonal matrix technique to give $\hat{g}_{i,j_k}$ and $\hat{h}_{i,j_k}$ for all i and k at each j. The quadrature of order n = 8 will be used to integrate the distribution functions for the flow properties. The convergent criteria are set at 0.001 for atom and ion number densities at every physical point between successive iterations.

Results

The first case investigated in this chapter is the structure of the relaxation zone of a frozen shock wave at $M_1 = 10.3$, $T_1 = 300\ ^{\circ}K$, and $p_1 = 10$ mm Hg. Figure 50 gives the atom number density in the relaxation zone as a function of time t, which is defined by a distance x behind a frozen shock wave divided by the velocity of the moving shock front. In the beginning of the relaxation zone the atom number density rises slowly until the last one-third of the relaxation zone. The profile of the degree

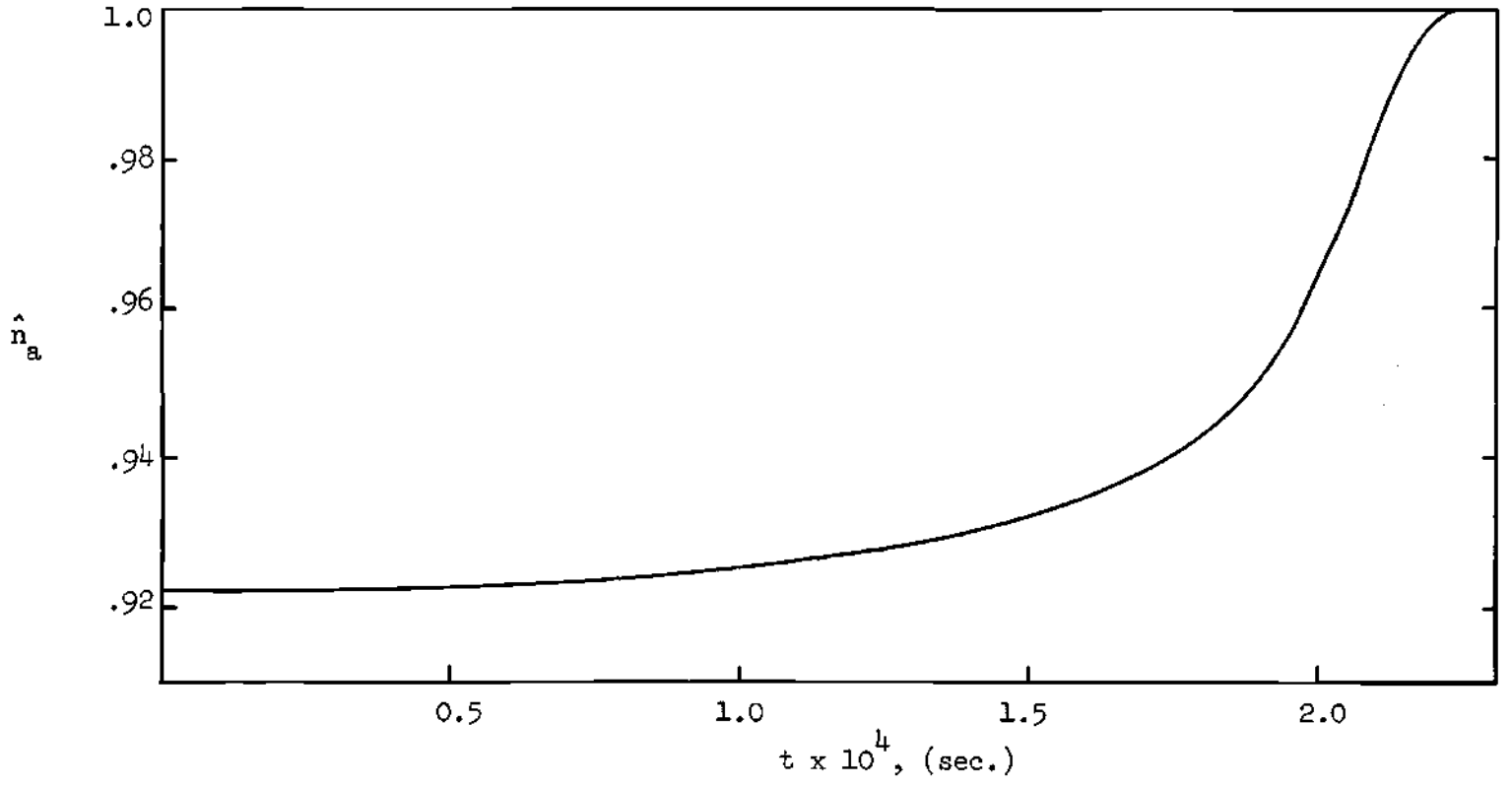

Figure 50. Atom Number Density in Relaxation Zone of Shock Wave at M_1 = 10.3, T_1 = 300°K, and p_1 = 10 mm Hg.

of ionization in the relaxation zone is shown in Figure 51. Very slight ionization is obtained in the early part of the relaxation zone. Ionization increases with time t and approaches the downstream equilibrium value. Figure 52 gives the electron number density distribution throughout the relaxation zone. Electrons are increased sharply in the last one-third of the relaxation zone. In the early part of the relaxation zone the energy transfer between the atom and the electron is not great, thus, the atom temperature drops slightly as indicated in Figure 53. However, the atom temperature decreases sharply in the rear part of the relaxation zone as the electron-atom collisions become more intensive. On the other hand, Figure 54 shows that the electron temperature increases gradually in the early part of the relaxation zone. However, the electron temperature rises sharply in the rear one-third of the relaxation zone and reaches a maximum value while the drop of the atom temperature is most significant. Then the electron temperature decreases quickly as electrons give up their energy for rapid increase of ionization. The ion temperature distribution is not presented since it deviates from the atom temperature by an order of 10^{-5}. The atom velocity distribution is given in Figure 55. The greatest drop of the atom velocity in the relaxation zone occurs in the rear one-third of this region. The ion and electron velocity profiles deviate from the atom velocity profile by an order of 10^{-4}.

The comparison of the present results for $M_1 = 10.3$ to the results of Hoffert and Lien [12] is given in Table 27. The quantity d as defined by Hoffert and Lien is the location where the degree of ionization is equal to $\alpha_2/\sqrt{2}$ in the relaxation zone. The relaxation time, τ, in the laboratory reference frame is defined by d divided by the velocity of the

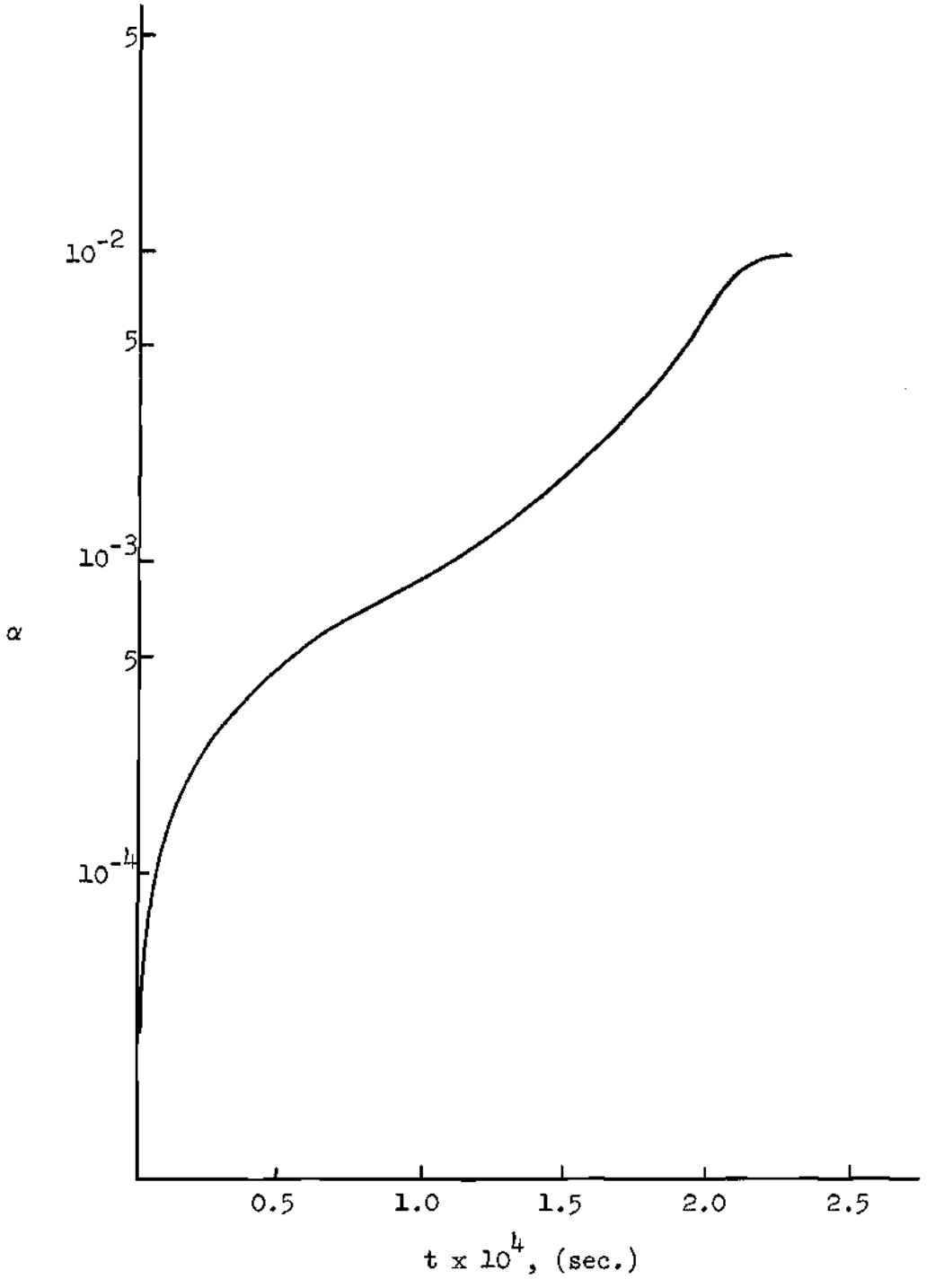

Figure 51. Degree of Ionization in Relaxation Zone of Shock Wave at $M_1 = 10.3$, $T_1 = 300°K$, and $p_1 = 10$ mm Hg .

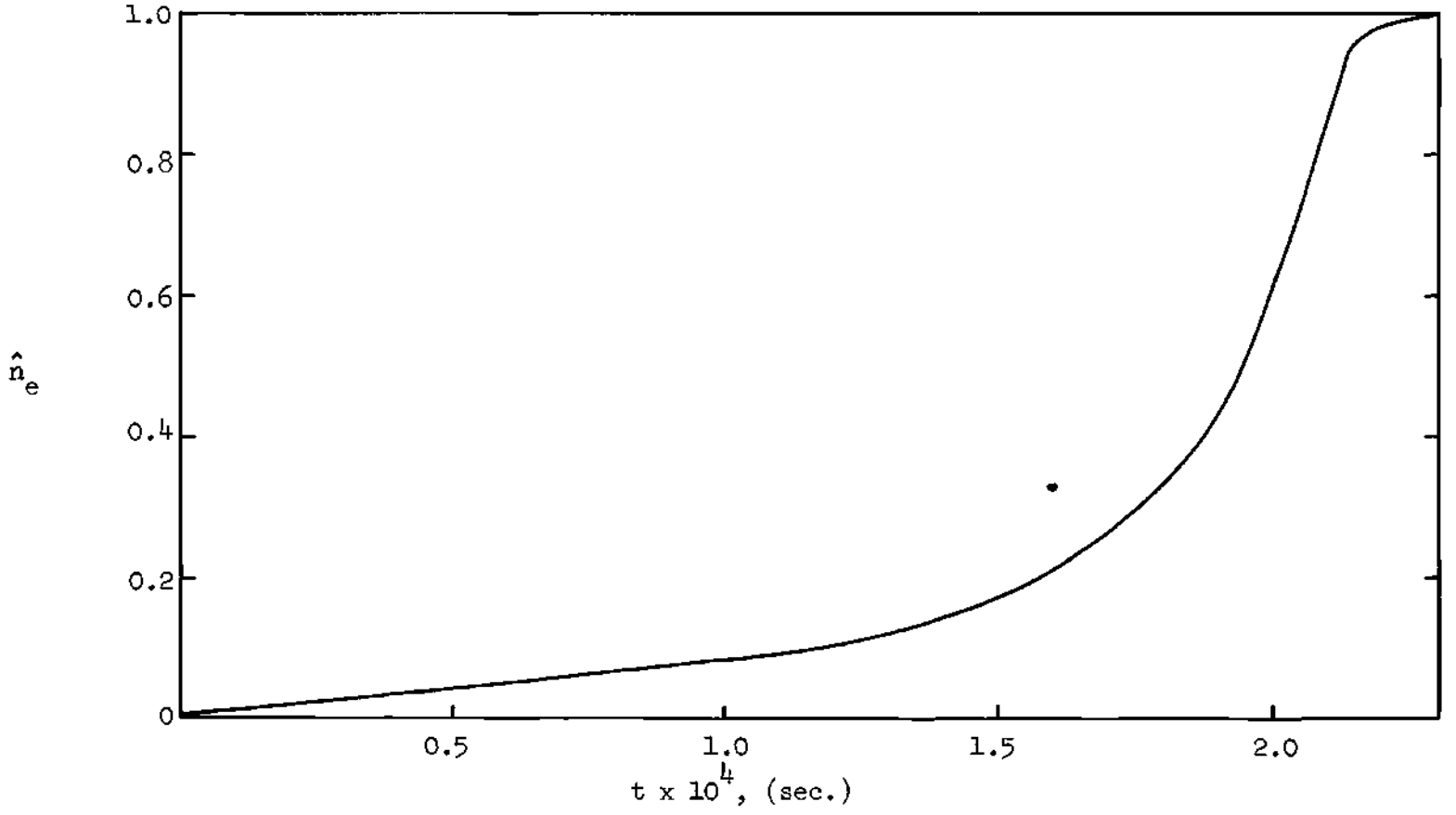

Figure 52. Electron Number Density in Relaxation Zone of Shock Wave at M_1 = 10.3, T_1 = 300°K, and p_1 = 10 mm Hg.

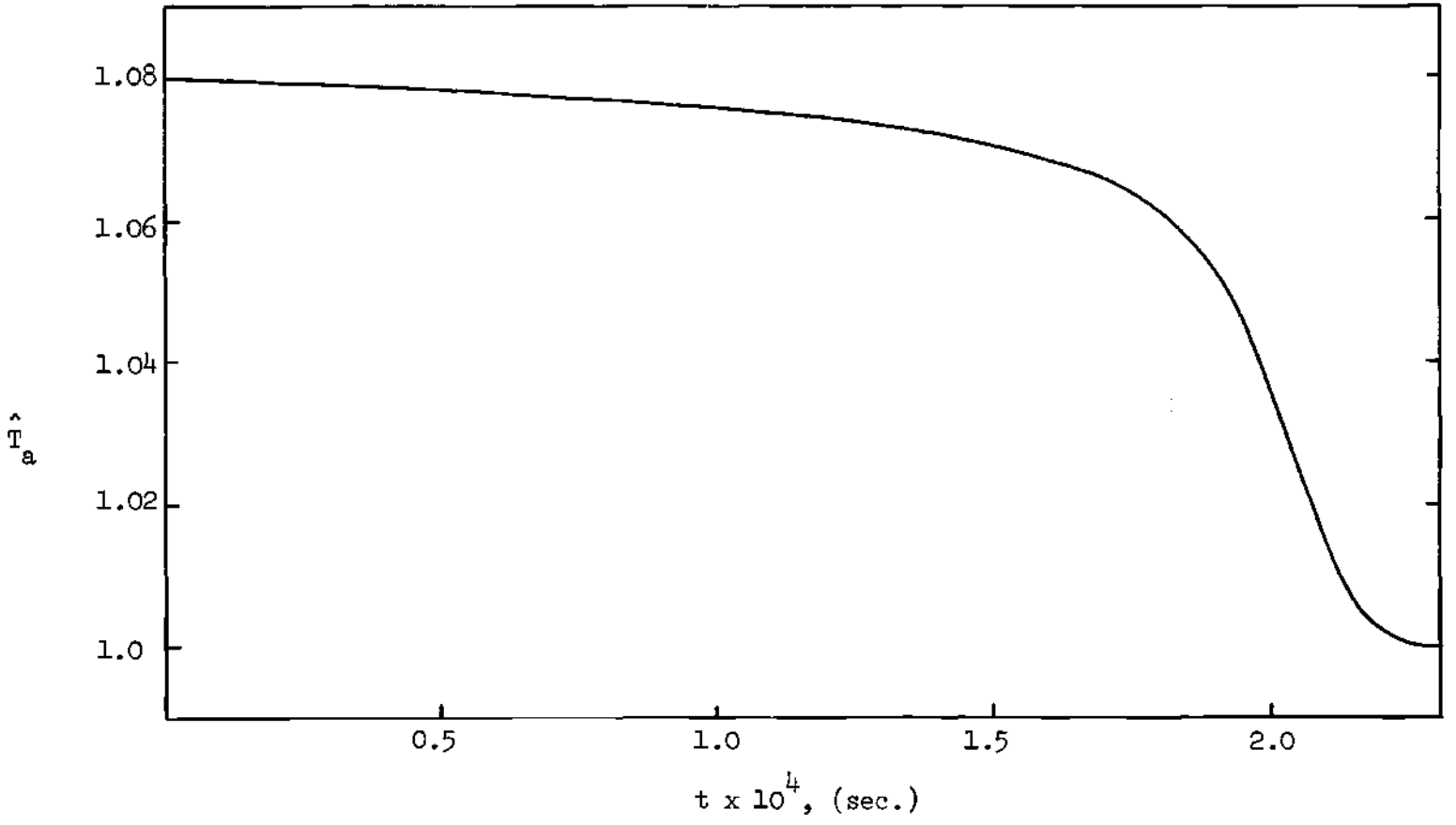

Figure 53. Atom Temperature Profile in Relaxation Zone of Shock Wave at $M_1 = 10.3$, $T_1 = 300^\circ K$, and $p_1 = 10$ mm Hg .

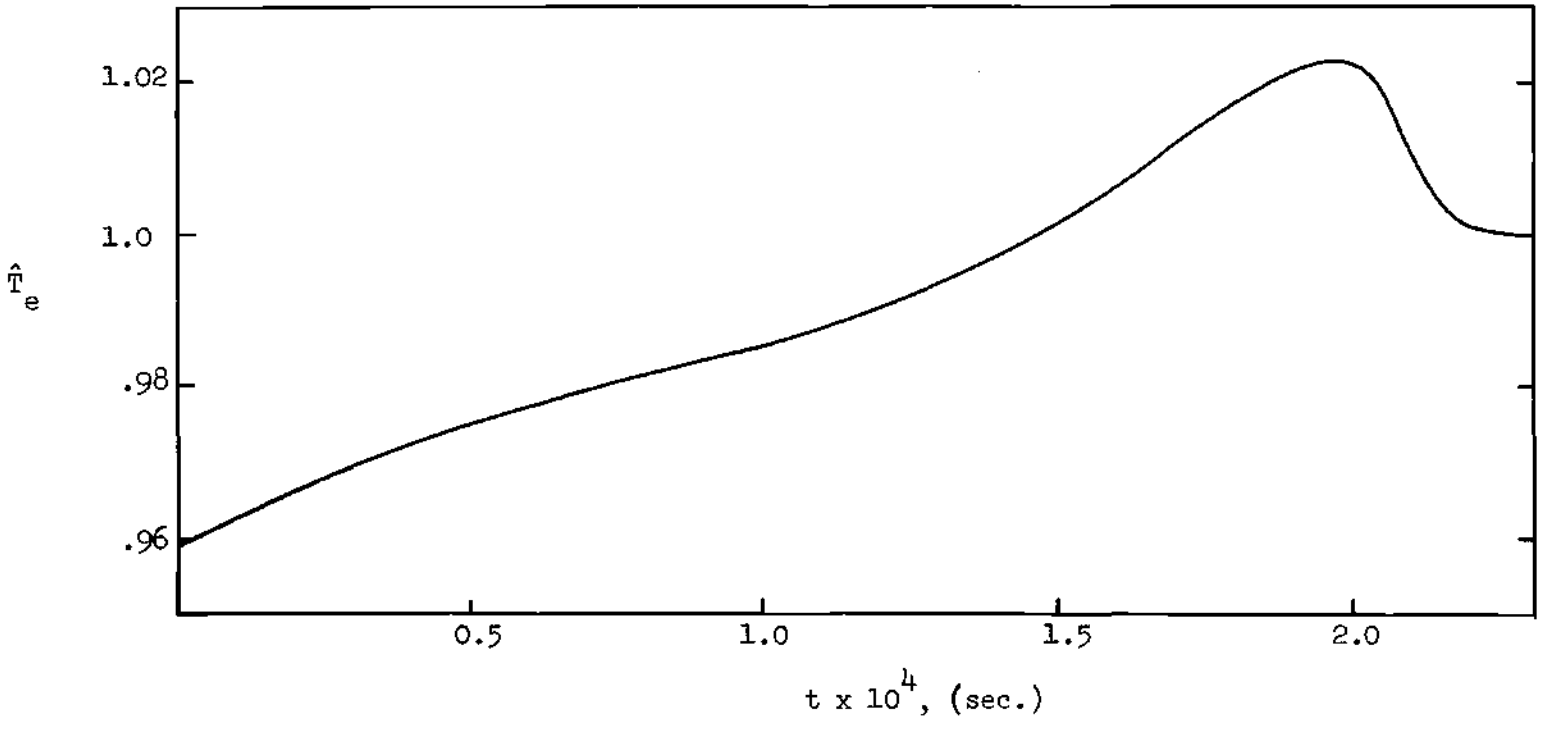

Figure 54. Electron Temperature Profile in Relaxation Zone of Shock Wave at M_1 = 10.3, T_1 = 300°K, and p_1 = 10 mm Hg.

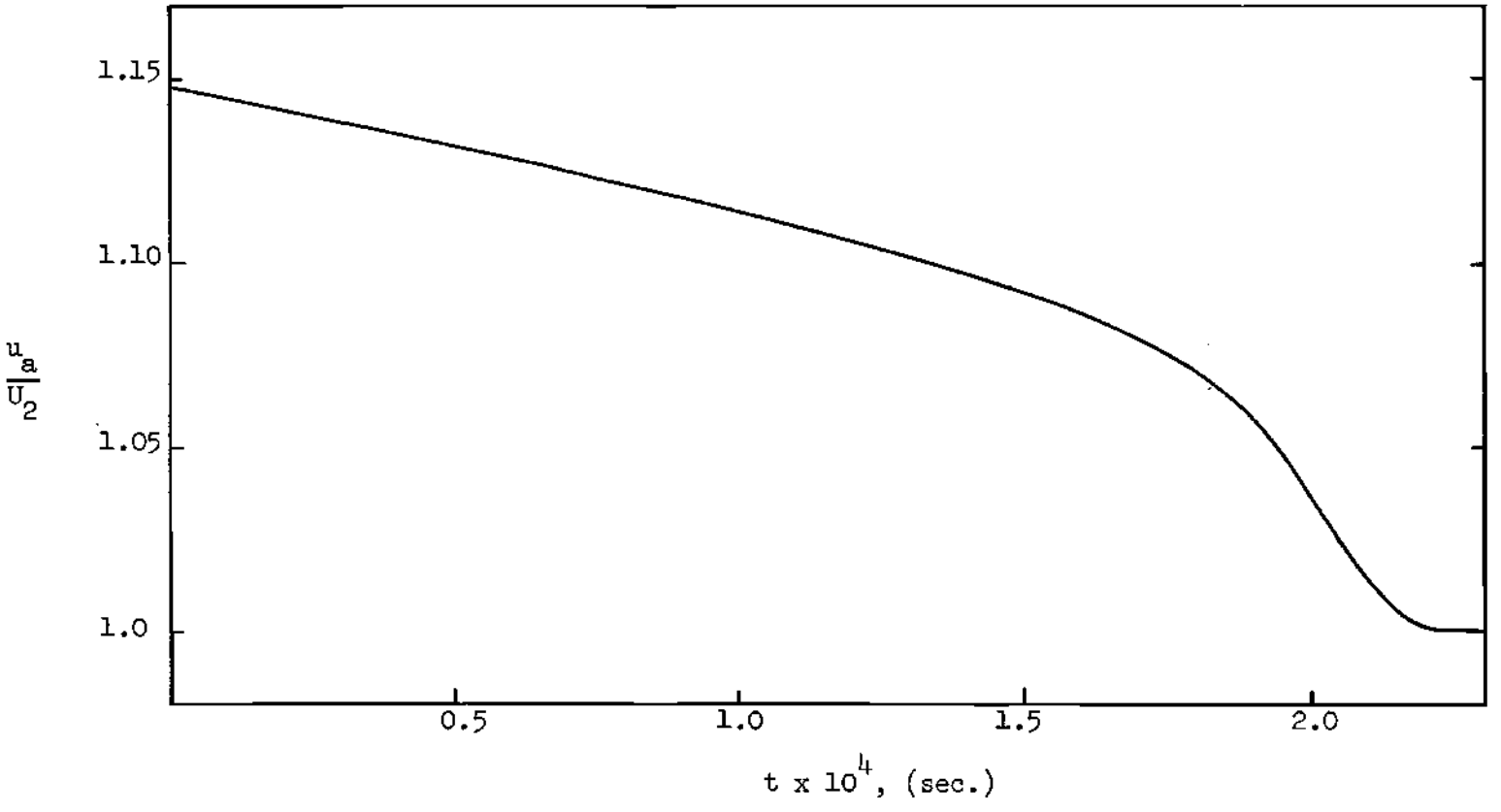

Figure 55. Atom Velocity Distribution in Relaxation Zone of Shock Wave at M_1 = 10.3, T_1 = 300°K, and p_1 = 10 mm Hg.

Table 27. Comparison of Present Results to Results of Hoffert and Lien [12]

	Present		Hoffert and Lien [12]
M_1	8.0	10.3	10.3
T_1(°K)	450	300	300
p_1(mmHg)	1	10	10
α_1	1.1×10^{-4}	3.0×10^{-5}	0
U_1(cm/sec)	3.161×10^{5}	3.323×10^{5}	3.32×10^{5}
$\tau = d/U_1$(sec)	3.1×10^{-3}	2.035×10^{-4}	2.75×10^{-4}
$T_a(0)/T_1$	20.875	34.150	34.0
T_2/T_1	19.075	31.750	31.7
U_2/U_1	0.233	0.236	0.235
α_2	1.175×10^{-2}	9.620×10^{-3}	9.35×10^{-3}

moving shock front. Table 27 indicates that the present results are in good agreement with the results of Hoffert and Lien [12]. Both studies predict almost the same flow properties behind a frozen shock and at the downstream equilibrium condition. The values for $T_a(0)$ obtained from both studies are very close. The present degree of ionization is slightly higher than the value obtained by Hoffert and Lien [12]. The value of τ predicted by the present method is somewhat smaller than theirs. Further comparisons of the present results with experimental data will be presented in Figure 62. A comparison of atom local distribution functions with local Maxwellian distribution functions in the relaxation zone is given in Table 28. It is found that the difference between the local distribution function and the local Maxwellian distribution function is everywhere of an order of 10^{-7} or less. Therefore, the local distribution function can be approximated by the local Maxwellian distribution function for the atom in the relaxation zone. Table 29 indicates that the same conclusion can be drawn for the ion, since the difference between $\hat{g}$ and $\hat{G}$ is everywhere of an order of 10^{-7} or less. From table 30 it is observed that the maximum difference between the electron local distribution function and the corresponding local Maxwellian distribution is of an ordero of 10^{-4}. Therefore, electrons are more nonequilibrium than atoms and ions in the relaxation zone as a result of ionizing effects.

Figure 56 gives the atom number density in the relaxation zone of a shock wave with $M_1 = 8.0$, $T_1 = 450\ ^{\circ}K$, and $p_1 = 1$ mm Hg. The slope of the profile of the atom number density is small in the early part of the relaxation zone. However, the slope becomes steep in the last one-third of this region. The curve of the degree of ionization is shown in Figure 57.

Table 28. Comparison of Atom Local Distribution Functions with Local Maxwellian Distribution Functions in Relaxation Zone of A Shock at $M_1 = 10.3$

I	J	$\hat{g}$	$\hat{G}$
25	112	.76412880-02	.76412541-02
	142	.17203280+00	.17203279+00
	172	.50053440+00	.50053471+00
	202	.18820630+00	.18820599+00
	232	.91456030-02	.91455320-02
50	112	.78308990-02	.78308685-02
	142	.17488890+00	.17488888+00
	172	.50148520+00	.50148588+00
	202	.18462910+00	.18462878+00
	232	.87274970-02	.87273880-02
75	112	.80953160-02	.80952789-02
	142	.18416070+00	.18416105+00
	172	.51889550+00	.51889712+00
	202	.18108530+00	.18108490+00
	232	.78272130-02	.78270964-02

Table 29. Comparison of Ion Local Distribution Functions with Local Maxwellian Distribution Functions in Relaxation Zone of A Shock at $M_1 = 10.3$

I	J	$\hat{g}$	$\hat{G}$
25	113	.46730420-03	.46730238-03
	143	.98280180-02	.98280063-02
	173	.26711810-01	.26711794-01
	203	.93823500-02	.93823342-02
	233	.42588370-03	.42588163-03
50	112	.90566660-03	.90566352-03
	142	.20227730-01	.20227704-01
	172	.58003680-01	.58003661-01
	202	.21354730-01	.21354693-01
	232	.10094010-02	.10093931-02
75	112	.35486690-02	.35486541-02
	142	.80730830-01	.80730751-01
	172	.22747550+00	.22747546+00
	202	.79387310-01	.79387174-01
	232	.34315380-02	.34315186-02

Table 30. Comparison of Electron Local Distribution Functions with Local Local Maxwellian Distribution Functions in Relaxation Zone of A Shock at $M_1 = 10.3$

I	J	$\hat{g}$	$\hat{G}$
25	100	.33345880-03	.33150932-03
	130	.98867630-02	.98579149-02
	160	.30821160-01	.30730117-01
	190	.10172020-01	.10042300-01
	220	.36402150-03	.34402655-03
50	100	.74609000-03	.74295190-03
	130	.21050960-01	.21008779-01
	160	.64452250-01	.64316775-01
	190	.21507310-01	.21317241-01
	220	.79322630-03	.76492879-03
75	100	.31661230-02	.31581170-02
	130	.81055140-01	.80966472-01
	160	.23987050+00	.23957350+00
	190	.82215360-01	.81814238-01
	220	.32789270-02	.32245979-02

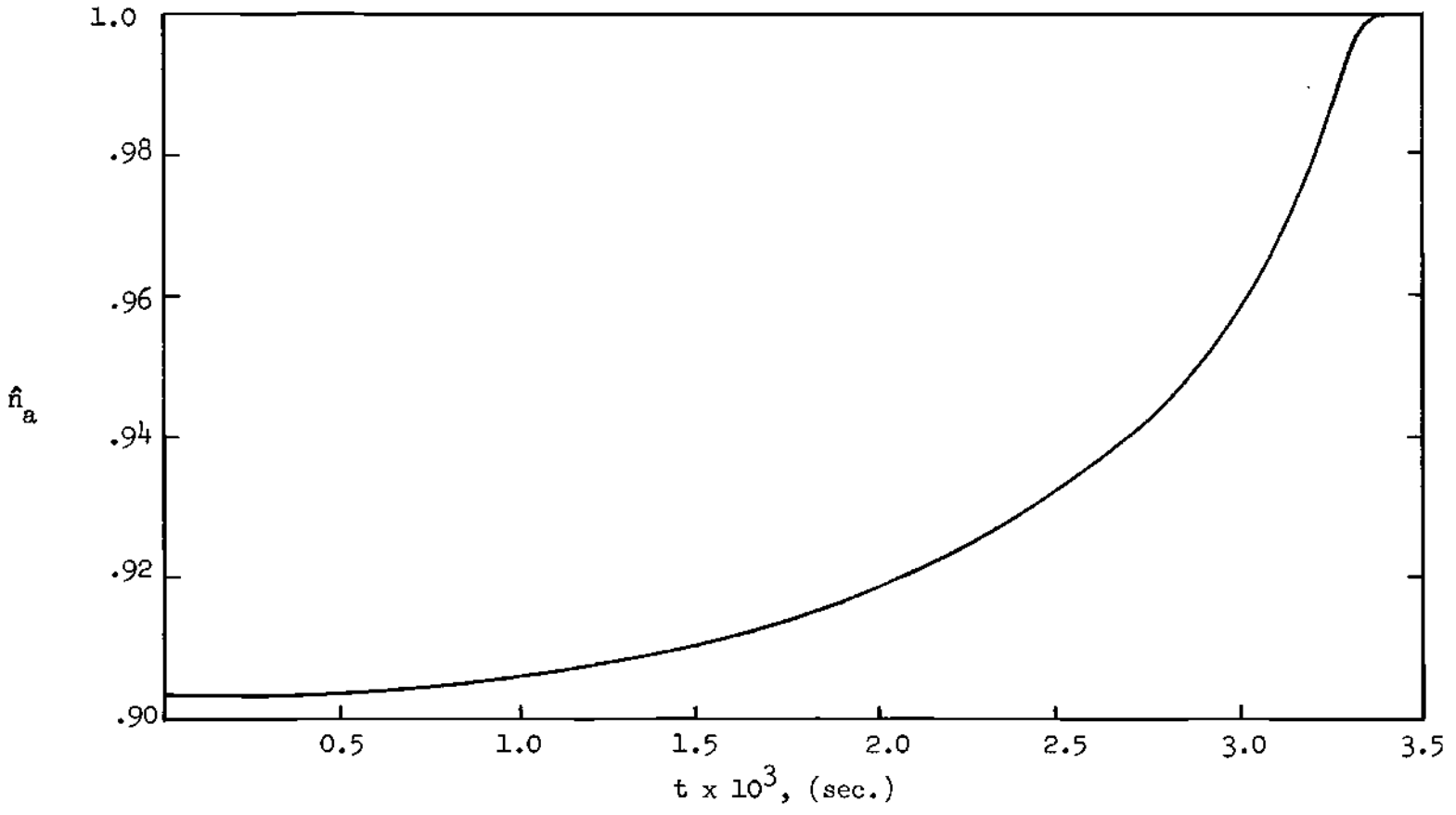

Figure 56. Atom Number Density in Relaxation Zone of Shock Wave at M_1 = 8.0, T_1 = 450°K, and p_1 = 1 mm Hg.

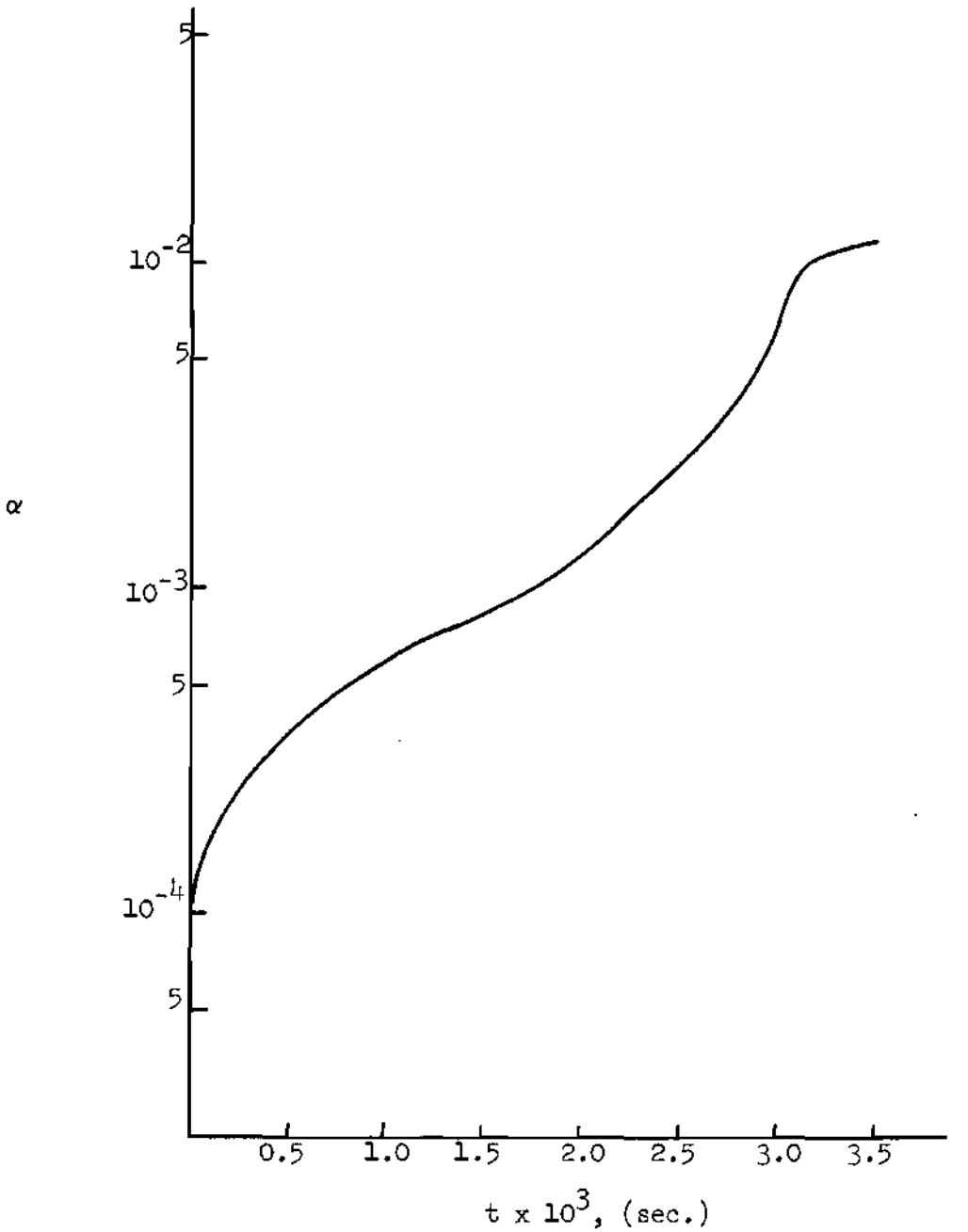

Figure 57. Degree of Ionization in Relaxation Zone of Shock Wave at $M_1 = 8.0$, $T_1 = 450°K$, and $p_1 = 1$ mm Hg.

The profile is in general similar to the one for $M_1 = 10.3$. The electron number density is presented in Figure 58. In the beginning of the relaxation zone the electron number density increases slowly until the last one-third of the relaxation zone. The atom and electron temperature distributions are shown in Figures 59 and 60, respectively. The energy transfer between electrons and atoms in the early part of the relaxation zone is not as great as that in the later part of the relaxation zone. The ion temperature profile is not shown, since its deviation from the atom temperature is only by an order of 10^{-5}. The atom velocity distribution throughout the relaxation zone is given in Figure 61.

The present results for both $M_1 = 8.0$ and $M_1 = 10.3$ in terms of $p_1 \tau$ are compared with experimental data of Petschek and Byron [2] in Figure 62. The comparison indicates that the present results are in reasonable agreement with the experimental data for lower Mach numbers. The number of discrete velocity points must be significantly increased for higher Mach numbers in order to obtain accurate results, especially for electrons. Thus, the present method will require a great deal of computing time.

Tables 31 to 33 give comparisons of local distribution functions with local Maxwellian distribution functions in relaxation zone of a shock at $M_1 = 8.0$ for atoms, ions, and electrons, respectively. The differences between $\hat{g}$ and $\hat{G}$ for both atoms and ions are in an order of 10^{-7} or less everywhere throughout the relaxation zone. Therefore, atoms and ions can be considered as in local Maxwellian distributions. However, the difference between electron $\hat{g}$ and its $\hat{G}$ is in an order of 10^{-5} everywhere in the relaxation zone. Therefore, as in the case of $M_1 = 10.3$,

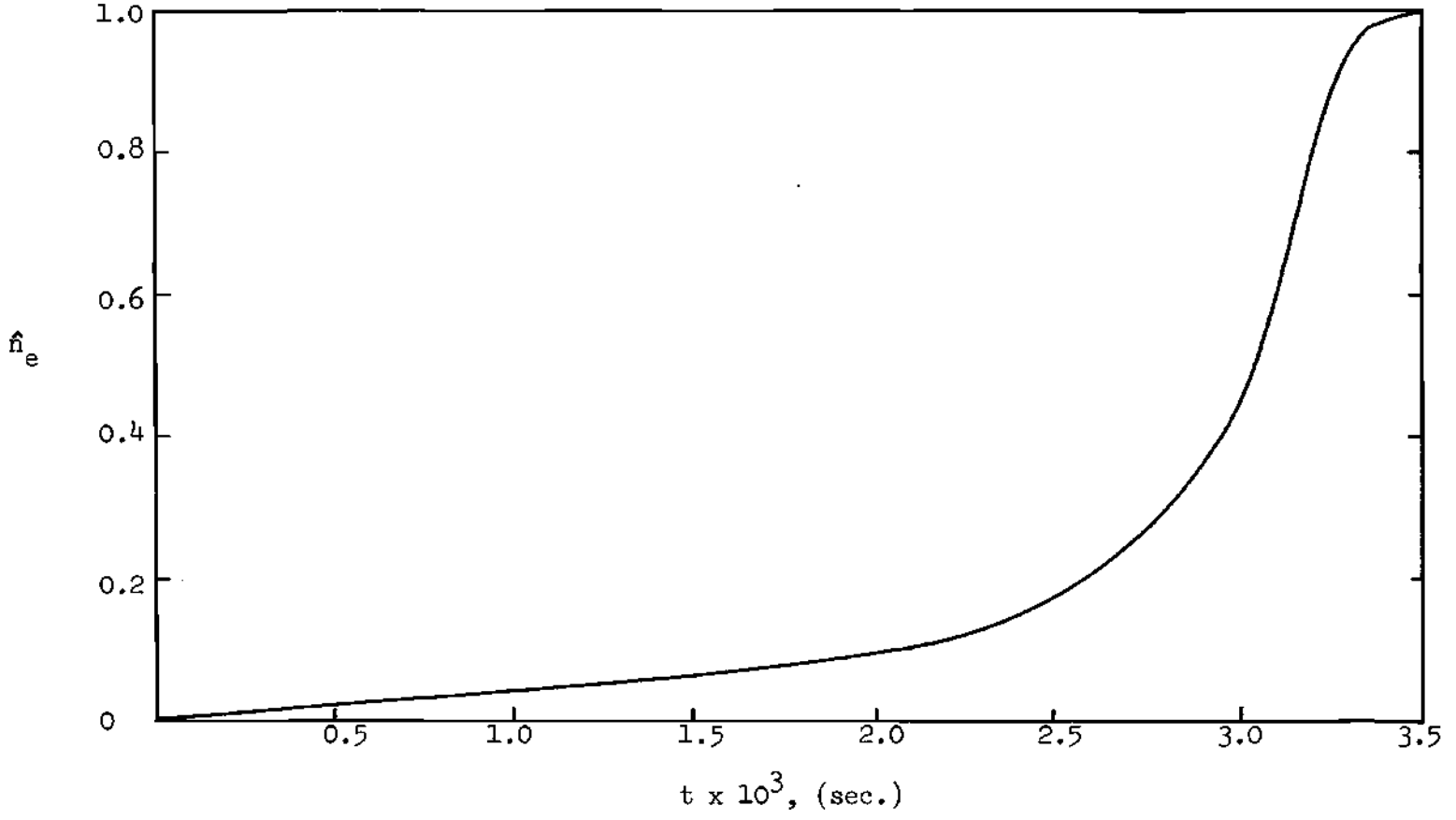

Figure 58. Electron Number Density in Relaxation Zone of Shock Wave at M_1 = 8.0, T_1 = 450°K, and p_1 = 1 mm Hg.

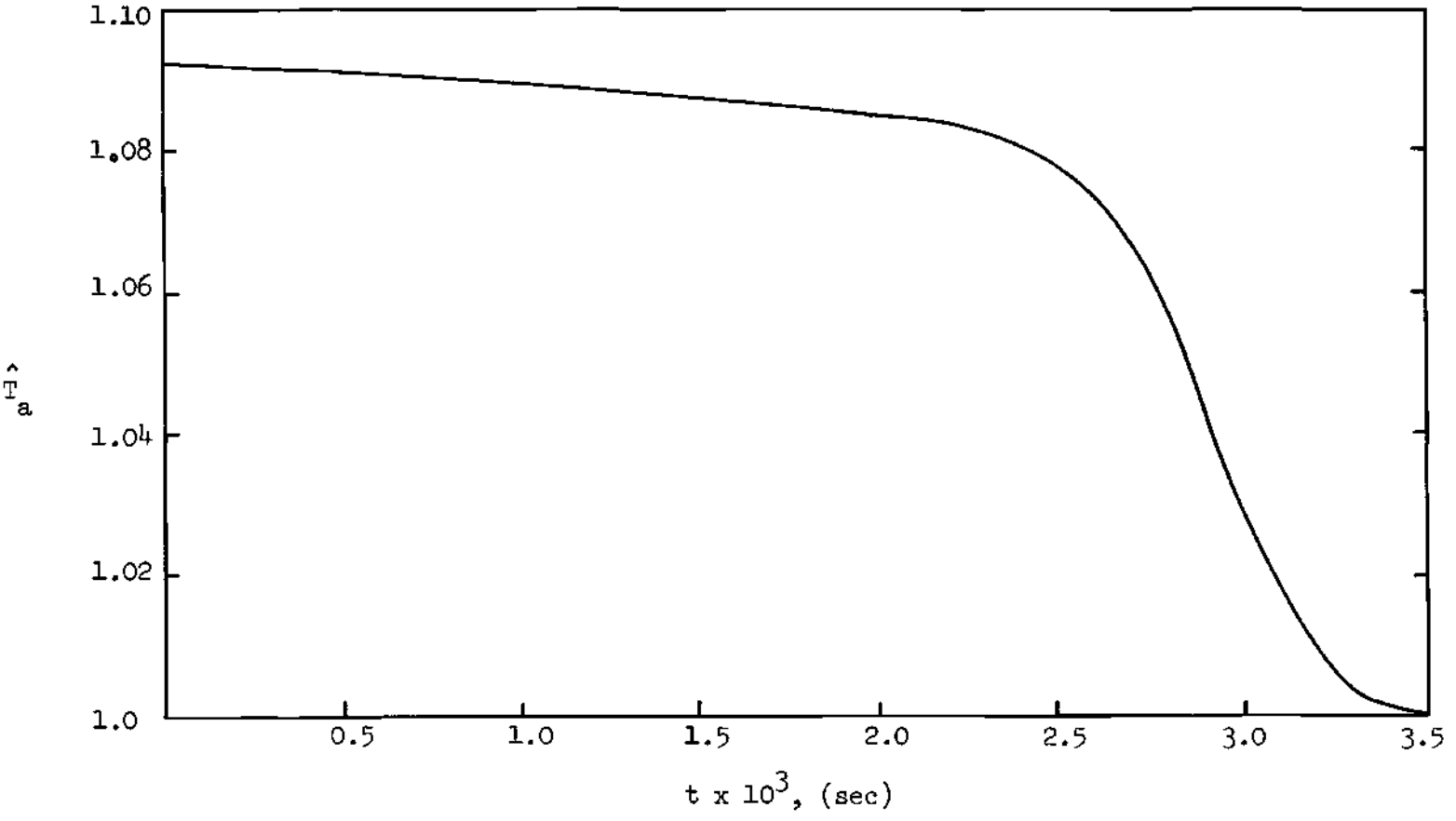

Figure 59. Atom Temperature Profile in Relaxation Zone of Shock Wave at $M_1 = 8.0$, $T_1 = 450^\circ K$, and $p_1 = 1$ mm Hg.

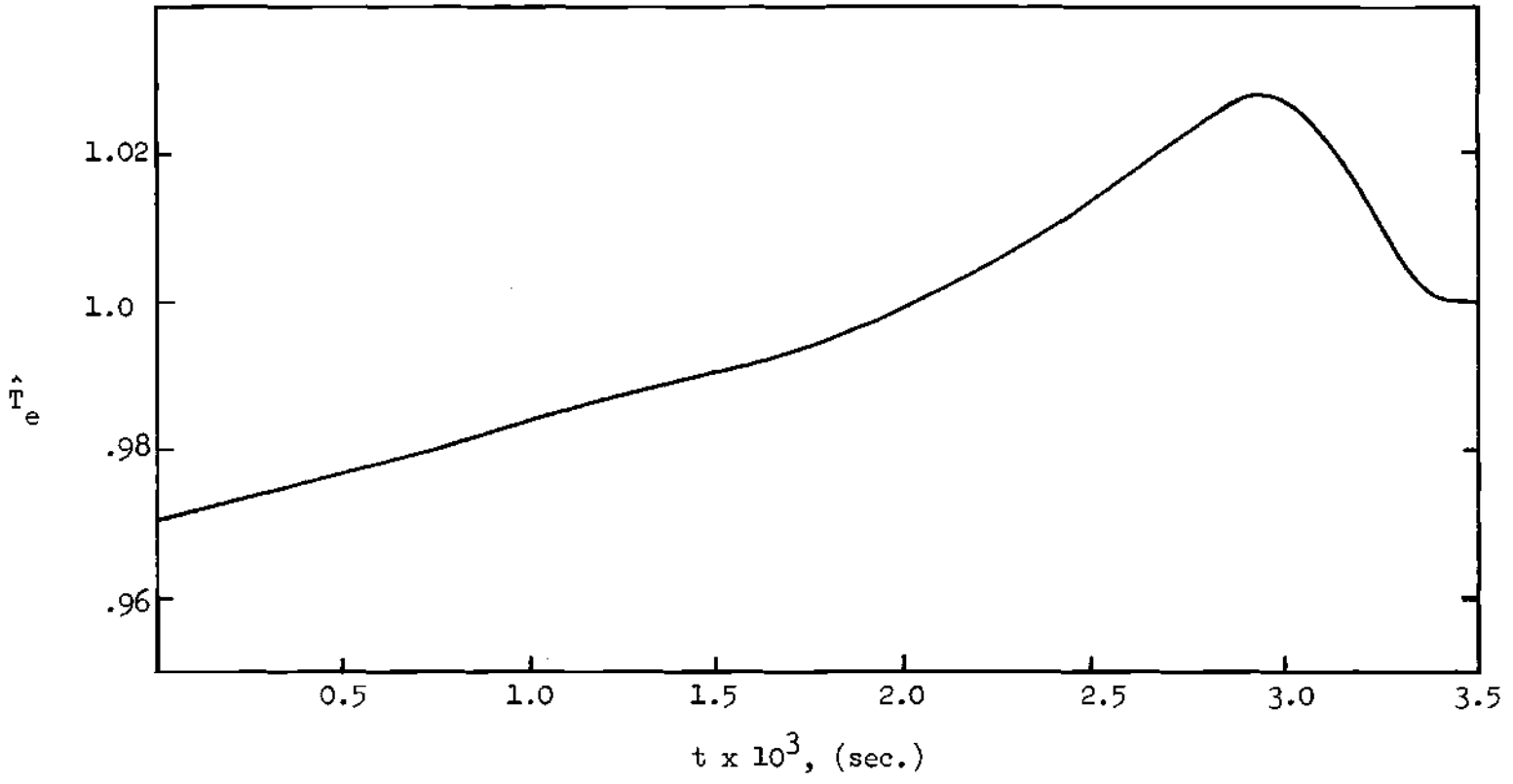

Figure 60. Electron Temperature Profile in Relaxation Zone of Shock Wave at M_1 = 8.0, T_1 = 450°K, and p_1 = 1 mm Hg.

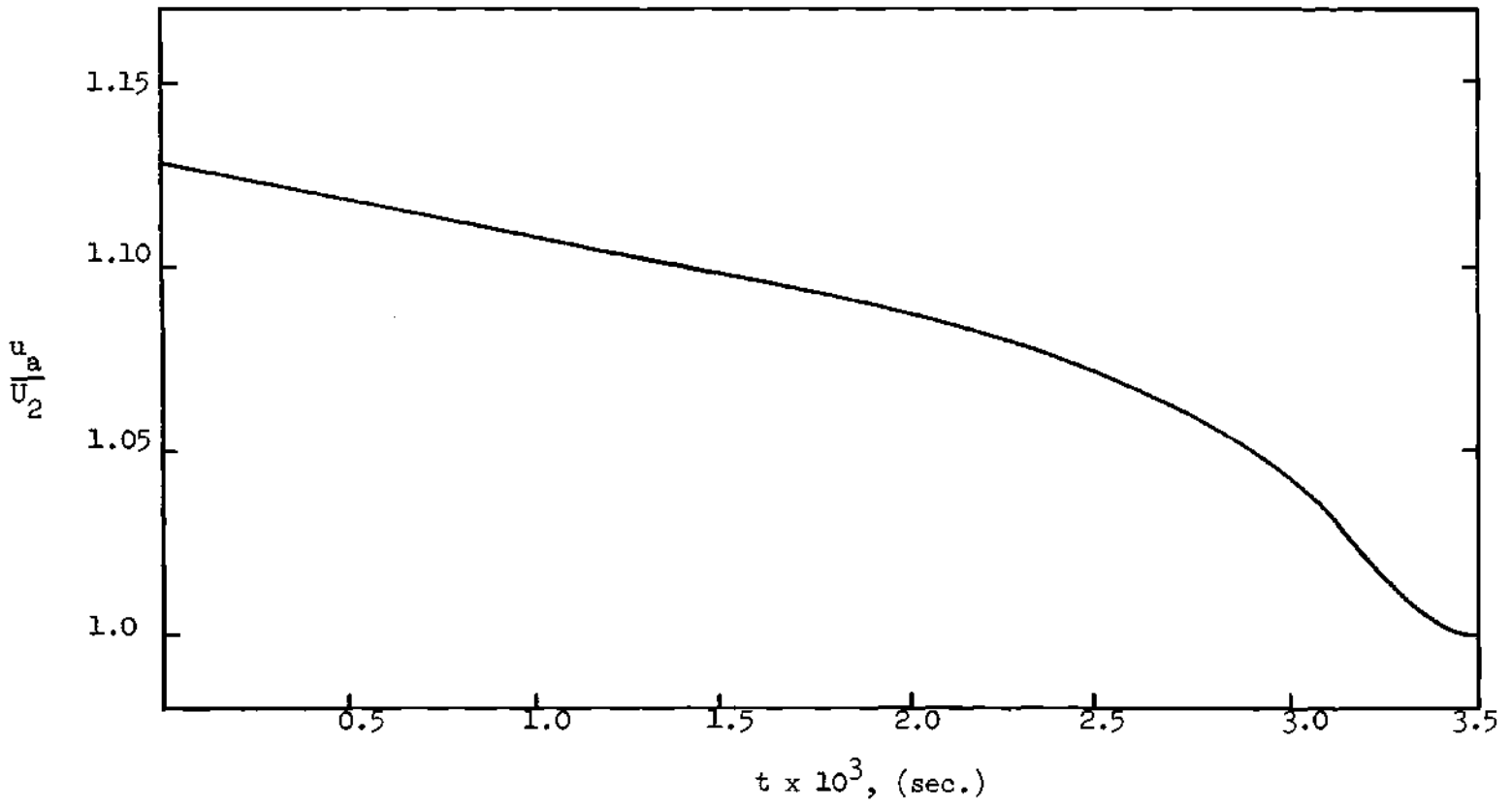

Figure 61. Atom Velocity Distribution in Relaxation Zone of Shock Wave at M_1 = 8.0, T_1 = 450°K, and p_1 = 1 mm Hg.

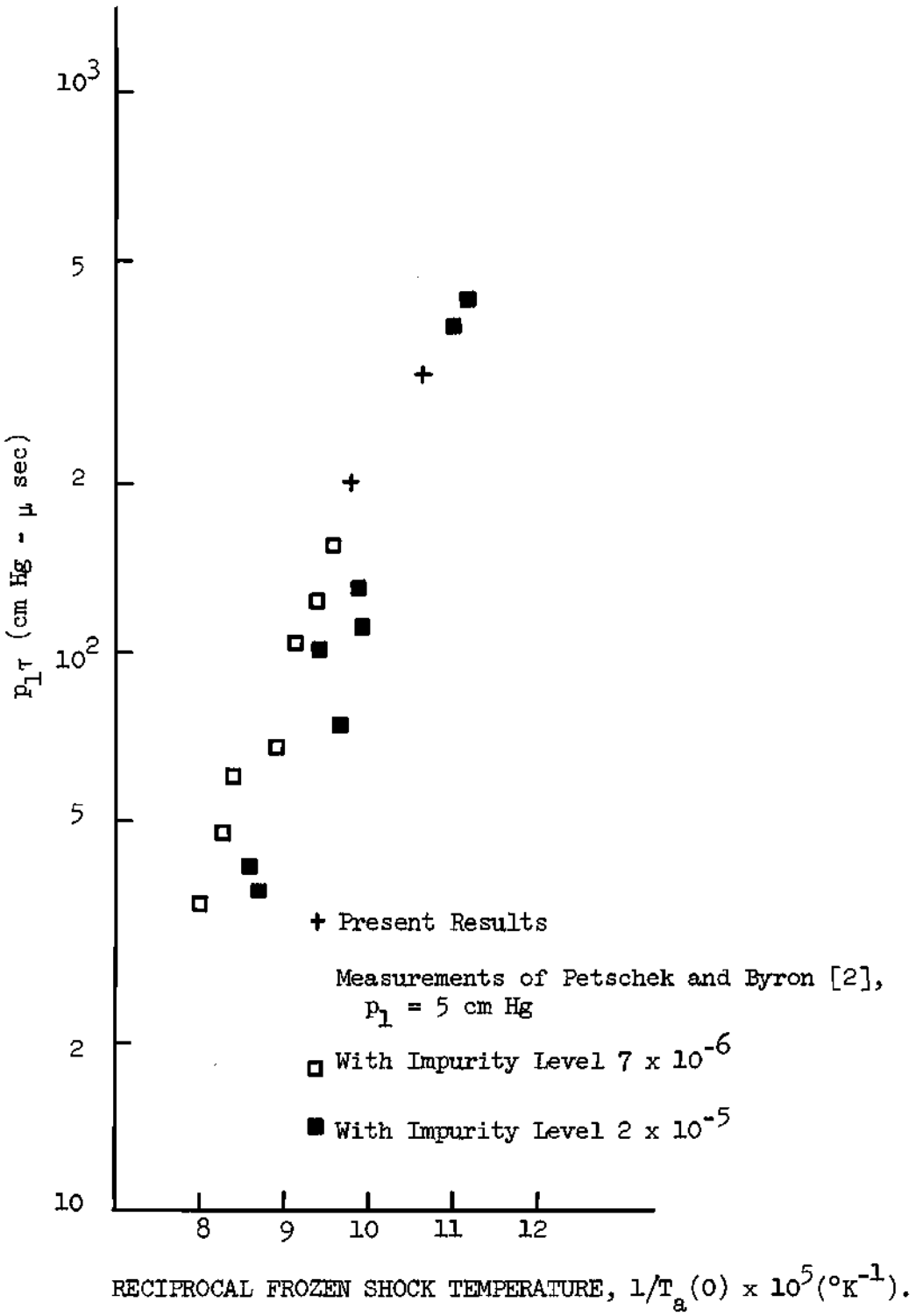

Figure 62. Comparison of Relaxation Times.

Table 31. Comparison of Atom Local Distribution Functions with Local Maxwellian Distribution Functions in Relaxation Zone of A Shock at $M_1 = 8.0$

I	J	$\hat{g}$	$\hat{G}$
25	112	.81523850-02	.81523554-02
	142	.17378090+00	.17378084+00
	172	.48971200+00	.48971202+00
	202	.18243170+00	.18243144+00
	232	.89842360-02	.89841849-02
60	112	.85681130-02	.85680850-02
	142	.18194870+00	.18194854+00
	172	.50346660+00	.50346680+00
	202	.18153120+00	.18153090+00
	232	.85288740-02	.85287950-02
85	111	.68683810-02	.68683514-02
	141	.18317440+00	.18317432+00
	171	.55402260+00	.55402277+00
	201	.19003880+00	.19003849+00
	231	.73928090-02	.73927587-02

Table 32. Comparison of Ion Local Distribution Functions with Local Maxwellian Distribution Functions in Relaxation Zone of A Shock at $M_1 = 8.0$

I	J	$\hat{g}$	$\hat{G}$
25	112	.38281810-03	.38781675-03
	142	.81607280-02	.81607220-02
	172	.22997250-01	.22997246-01
	202	.85670920-02	.85670778-02
	232	.42189220-03	.42188994-03
60	112	.13236530-02	.13236482-02
	142	.28109170-01	.28109132-01
	172	.77778530-01	.77778528-01
	202	.28042070-01	.28042027-01
	232	.13173470-02	.13173356-02
85	111	.61594360-02	.61594110-02
	141	.16426820+00	.16426803+00
	171	.49684040+00	.49684038+00
	201	.17042430+00	.17042398+00
	231	.66297500-02	.66297101-02

Table 33. Comparison of Electron Local Distribution Functions with Local Maxwellian Distribution Functions in Relaxation Zone of A Shock at $M_1 = 8.0$

I	J	$\hat{g}$	$\hat{G}$
25	100	.27335520-03	.27320411-03
	130	.79214900-02	.79193856-02
	160	.24396990-01	.24390692-01
	190	.79903870-02	.79815111-02
	220	.27888600-03	.27750734-03
60	100	.10107750-02	.10104232-02
	130	.27014480-01	.27010330-01
	160	.80963930-01	.80951058-01
	190	.27218400-01	.27200771-01
	220	.10273190-02	.10247217-02
85	100	.62086300-02	.62081432-02
	130	.16636040+00	.16635531+00
	160	.49885310+00	.49883643+00
	190	.16741050+00	.16738871+00
	220	.62880650-02	.62855122-02

electrons are in more nonequilibrium than atoms and ions in the relaxation zone.

In view of the results presented, the kinetic model equations can be applied to the relaxation zone with moderate shock Mach numbers. Atoms and ions are nearly in local Maxwellian distributions in the relaxation zone. However, electrons are more nonequilibrium than atoms and ions due to the ionizing effects in the relaxation zone. For very strong shocks the atom-atom collisions, which are not covered in the present investigation, can make a significant contribution to the ionization process.

CHAPTER VI

CONCLUSIONS

The discrete ordinate method has been applied to the solutions of a shock-wave structure in fully or partially ionized argon and the relaxation zone of a shock-wave. The effects of the electric field induced by the charge separation on the shock-wave structure have also been investigated. The Boltzmann equations with a kinetic model type of collisions have been employed as the governing equations. The present results have been compared with limited experimental measurements and other theoretical treatments, either by continuum approaches or by the Mott-Smith method.

The findings of the present investigation may be summarized as follows:

In the shock structure of a fully ionized gas the ion temperature can exceed their downstream value. The temperature overshoot becomes greater as the Mach number increases. However, in a weak shock the overshoot of the ion temperature was not observed. The electron temperature follows the ion temperature very closely in a weak shock of a fully ionized gas. However, for a strong shock-wave the electron temperature rise preceeds the ion temperature during the compression process of the shock. The overshoot of the electron temperature was not observed in a fully ionized gas. The present results agree well with the results obtained by the continuum approach for weak shocks. The discrete ordinate method gives smooth and continuous results for high Mach numbers. On the other

hand the results from the continuum approach contain discontinuities in slope.

No overshoot of upstream velocity has been observed in the shock structure of a partially ionized gas with a frozen degree of ionization. Although the three species of an ionized gas travel with approximately the same macroscopic velocity, the individual distribution functions can be very different and distinguishable. In a strong shock the atom distribution function may have double peaks, while the ion distribution function has only one peak. The electron local Maxwellian distribution function can be considered as an approximation to its actual local distribution function for weaker shocks in both partially and fully ionized gases. Electrons are heated up much earlier than ions and atoms in a partially ionized gas. Because the interactions of electrons with atoms and with ions are different in nature, the ion temperature can be different from the atom temperature. Thus, it can be very misleading to group atoms and ions as a single species merely on the basis of their insignificant difference in mass. In other words, the contribution from other physical properties can be significant. For all cases investigated no undershoot of the upstream temperature has been found. The present results for neutral particles and electrons are generally in fairly good agreement with the continuum solutions at the low Mach number and with the Mott-Smith solutions at the high Mach number. However, it appears that the discrete ordinate method has the advantage over the Mott-Smith method and the continuum approach in obtaining the results for ions.

The induced electric field due to the charge separation in a shock structure tends to equilibrate the flow locally. However, these effects

on the structure of a shock-wave are very insignificant for all cases investigated and can be neglected. Thus, the results obtained without the consideration of the effects of the induced electric field give very good approximations. It has been experienced that when the E field effects are included in the kinetic model equations, the numerical accuracy and the capacity limitation of the available computer facility can cause a great deal of trouble in obtaining correct solutions.

The discrete ordinate method can yield reasonable results to the kinetic model equations for the structure of the relaxation zone if the shock Mach numbers are not very high. The local Maxwellian distribution functions can be used to approximate the actual local distribution functions of atoms, ions, and electrons in the relaxation zone where electrons are not as equilibrium as atoms and ions due to the ionizing effects. Only very slight ionization is generated in the early part of the relaxation zone, while most ionization occurs in the last one-third of the region. The ion temperature is about the same as the atom temperature in the entire relaxation zone. Both atom and ion temperatures drop sharply in the rear part of the relaxation zone where the electron temperature increases rapidly. The thickness of a frozen shock front is negligibly small in comparison with the thickness of its relaxation zone for the cases investigated.

In view of the results presented in this dissertation it is concluded that the discrete ordinate method has the consistency and the flexibility in dealing with plasmagasdynamic problems.

APPENDICES

APPENDIX I

RANKINE-HUGONIOT RELATIONS OF A NORMAL SHOCK WAVE WITH A FROZEN DEGREE OF IONIZATION

For steady one-dimensional flow without the magnetic field, the plasmagasdynamic equations given in Reference [40] become

$$p = \rho R_p T, \tag{1}$$

$$\frac{d\rho u}{dx} = 0, \tag{2}$$

$$\rho u \frac{du}{dx} + \frac{dp}{dx} - \frac{4}{3}\frac{d}{dx}\left(\mu \frac{du}{dx}\right) = 0, \tag{3}$$

and

$$\rho u \frac{dh_o}{dx} - \frac{4}{3}\frac{d}{dx}\left(\mu u \frac{du}{dx}\right) - \frac{d}{dx}\left(\delta \frac{dT}{dx}\right) = 0, \tag{4}$$

where, ρ, u, p, and T are density, flow velocity, pressure, and temperature of the plasma, respectively. R_p, μ, and δ are the gas constant, viscosity, and thermal conductivity of the plasma, respectively.

$h_o = C_p T + \frac{u^2}{2}$ = stagnation enthalpy and C_p is the specific heat at constant pressure.

Integrating Equations (2) - (4) with respect to x yields

$$\rho u = C_1 \,, \tag{5}$$

$$\rho u^2 + p - \frac{4}{3}\mu \frac{du}{dx} = C_2 \,, \tag{6}$$

and

$$\rho u h_o - \frac{4}{3}\mu u \frac{du}{dx} - \delta \frac{dT}{dx} = C_3 \,, \tag{7}$$

where C_1, C_2, and C_3 are integration constants. Denoting $(\ )_1$ and $(\ )_2$ for upstream and downstream equilibrium states where the differentiation with respect to x vanishes, Equations (5) - (7) become

$$(\rho U)_1 = (\rho U)_2 \,, \tag{8}$$

$$(\rho U^2 + p)_1 = (\rho U^2 + p)_2 \,, \tag{9}$$

and

$$(\rho U h_o)_1 = (\rho U h_o)_2 \,. \tag{10}$$

Applying Equation (8) to Equation (10), then a simpler relation can be obtained, i.e.,

$$(h_o)_1 = (h_o)_2 \,, \tag{10-a}$$

where

$$(h_o)_1 = \frac{1}{2}(U)_1^2 + \frac{\gamma}{\gamma-1}(1+\alpha_1)R_3(T)_1 + \alpha_1 R_3 T_I$$

and

$$(h_o)_2 = \frac{1}{2}(U)_2^2 + \frac{\gamma}{\gamma-1}(1+\alpha_2)R_3(T)_2 + \alpha_2 R_3 T_I ,$$

γ is the specific heat ratio of the plasma; R_3 is the gas constant of neutral particles; α is the degree of ionization.

For a frozen degree of ionization,

$$\alpha_1 = \alpha_2 = \alpha \quad = \text{constant.}$$

Thus,

$$(1+\alpha)R_3 \equiv R_p \quad = \text{constant},$$

and

$$\alpha_1 R_3 T_I = \alpha_2 R_3 T_I = \alpha R_3 T_I \quad = \text{constant.}$$

Then, Equation (10) becomes

$$\frac{1}{2}(U)_1^2 + C_p(T)_1 = \frac{1}{2}(U)_2^2 + C_p(T)_2 , \tag{11}$$

and

$$C_p = \frac{\gamma}{\gamma-1} R_p .$$

It is noted that Equations (1), (8), (9), and (11) are exactly the same as the conservation equations for a normal shock in a perfect neutral gas. Thus, the conventional Rankine-Hugoniot relations can be applied to an

ionized gas with a frozen degree of ionization.

Hence,

$$(\hat{\rho})_1 = \frac{(\rho)_1}{(\rho)_2} = \frac{(\gamma-1)M_1^2 + 2}{(\gamma+1)M_1^2} , \tag{12}$$

$$(\hat{T})_1 = \frac{(T)_1}{(T)_2} = \frac{(\gamma+1)^2 M_1^2}{[2\gamma M_1^2 - (\gamma-1)][(\gamma-1)M_1^2 + 2]} , \tag{13}$$

$$(\hat{p})_1 = \frac{(p)_1}{(p)_2} = \frac{\gamma+1}{2\gamma M_1^2 - (\gamma-1)} , \tag{14}$$

and

$$M_2^2 = \frac{M_1^2 + \frac{2}{\gamma-1}}{\frac{2\gamma}{\gamma-1} M_1^2 - 1} , \tag{15}$$

where,

$$\text{the plasma Mach number} = M \equiv \frac{u}{\sqrt{\gamma R_p T}} ,$$

and u and t are plasma velocity and plasma temperature, respectively.

The plasma density is the sum of the densities of the three species, i.e.,

$$\rho = n_1 m_1 + n_2 m_2 + n_3 m_3 . \tag{16}$$

For singly ionized gases,

$$n_1 = n_2 .$$

If the degree of ionization is defined as

$$\alpha \equiv \frac{n_1}{n_1 + n_3} ,$$

then, Equation (16) becomes

$$\rho = n_1 \left(\frac{m_3 + \alpha m_1}{\alpha} \right) . \tag{17}$$

It is noted that in Equation (17) the difference between m_2 and m_3 is ignored.

$$(\hat{\rho})_1 = \frac{(\rho)_1}{(\rho)_2} = \frac{(\gamma-1) M_1^2 + 2}{(\gamma+1) M_1^2} = \frac{\left[n_1 \left(\frac{m_3 + \alpha m_1}{\alpha} \right) \right]_1}{\left[n_1 \left(\frac{m_3 + \alpha m_1}{\alpha} \right) \right]_2}$$

For a frozen degree of ionization,

$$\alpha_1 = \alpha_2 = \alpha ,$$

then

$$(\hat{n}_1)_1 = \frac{(n_1)_1}{(n_1)_2} = (\hat{n}_2)_1 = \frac{(\gamma-1) M_1^2 + 2}{(\gamma+1) M_1^2} . \tag{18}$$

If $\alpha_1 = \alpha_2$, then

$$(n_1)_1 \left[(n_1)_2 + (n_3)_2 \right] = (n_1)_2 \left[(n_1)_1 + (n_3)_1 \right] .$$

After simplification, one obtains

$$(\hat{n}_3)_1 = (\hat{n}_1)_1 . \tag{19}$$

The definition of Mach number of a mixture gives

$$M_1 = \frac{(U)_1}{(a)_1} \quad ,$$

or

$$(U)_1 = (a)_1 M_1 = \sqrt{\gamma R_p (T)_1}\; M_1 \; .$$

A similar expression can be written for $(U)_2$. From the definition of $(\hat{U}_3)_1$, one obtains

$$(\hat{U}_3)_1 = \sqrt{\frac{\gamma}{2}} \sqrt{\frac{R_p}{R_3}} \sqrt{(\hat{T})_1}\; M_1 \; . \tag{20}$$

Similar expressions can be given to $(\hat{U}_1)_1$, $(\hat{U}_2)_1$, $(\hat{U}_2)_2$, and $(\hat{U}_3)_2$. Since

$$R_1 = \frac{K}{m_1} \quad ,$$

then,

$$\frac{R_p}{R_1} = (1+\alpha)\frac{m_1}{m_3} \; .$$

Similarly,

$$\frac{R_p}{R_2} = (1+\alpha)\frac{m_2}{m_3}$$

and

$$\frac{R_p}{R_3} = 1 + \alpha \; .$$

Thus,

$$(\hat{U}_1)_\ell = (\hat{U}_3)_\ell \sqrt{\frac{m_1}{m_3}} \quad , \quad \text{where} \quad \ell = 1, 2 \quad ,$$

$$(\hat{U}_2)_\ell \approx (\hat{U}_3)_\ell \quad , \quad \text{for } m_2 \approx m_3 \quad ,$$

and

$$(\hat{U}_3)_\ell = \sqrt{\frac{\gamma}{2}}\sqrt{1+\alpha}\sqrt{(\hat{T})_\ell}\,M_\ell\,.$$

APPENDIX II

RANKINE-HUGONIOT RELATIONS OF AN IONIZING NORMAL SHOCK WAVE

This appendix will give the derivations of basic shock relations with a degree of ionization, α , which satisfies the Saha equations. For convenience, a different subscript system will be used.

Continuity Equation

For a mixture of three species

$$\rho_{m_1} U_{m_1} = \rho_{m_2} U_{m_2}$$

or,

$$m_{a_1} n_{a_1} U_{a_1} + m_{i_1} n_{i_1} U_{i_1} + m_{e_1} n_{e_1} U_{e_1} = m_{a_2} n_{a_2} U_{a_2} + m_{i_2} n_{i_2} U_{i_2} + m_{e_2} n_{e_2} U_{e_2} ,$$

where, subscripts, m, a, i, and e stand for mixture, atoms, ions, and electrons, respectively. Subscripts 1 and 2 denote upstream and downstream equilibrium conditions, respectively. If it is assumed that the three species move at the same macroscopic velocity in an equilibrium condition, then

$$(m_a n_{a_1} + m_i n_{i_1} + m_e n_{e_1}) U_{a_1} = (m_a n_{a_2} + m_i n_{i_2} + m_e n_{e_2}) U_{a_2} .$$

For a singly ionized gas,

$$n_i = n_e .$$

Since $m_e << m_i$ and $m_a \simeq m_i$, then

$$(n_{a_1} + n_{i_1}) U_{a_1} = (n_{a_2} + n_{i_2}) U_{a_2} .$$

To nondimensionalize the above equation, the following nondimensional quantities will be introduced:

$$n_a^* = \frac{n_a}{n_{a_1}} \; ; \qquad n_i^* = \frac{n_i}{n_{a_1}} \; ;$$

$$n_e^* = \frac{n_e}{n_{a_1}} \; ; \qquad u_j^* = \frac{u_j}{\sqrt{2 R_j T_1}} \; .$$

Using these nondimensional quantities, the expression for α of a singly ionized gas becomes

$$\alpha = \frac{n_e}{n_a + n_i} = \frac{n_i^*}{n_a^* + n_i^*}$$

and the continuity equation yields

$$(1 + n_{i_1}^*) u_{a_1}^* = (n_{a_2}^* + n_{i_2}^*) u_{a_2}^*$$

or

$$u_{a_2}^* = \frac{(1 + n_{i_1}^*)}{(n_{a_2}^* + n_{i_2}^*)} u_{a_1}^* \; ,$$

where,

$$n_{i_1}^* = \frac{\alpha_1}{1 - \alpha_1}$$

Similarly,

$$n_{i_2}^* = \frac{\alpha_2}{1 - \alpha_2} n_{a_2}^* \; .$$

$$n_{a_2}^* + n_{i_2}^* = \frac{1}{1-\alpha_2}\, n_{a_2}^* .$$

$$1 + n_{i_1}^* = \frac{1}{1-\alpha_1} .$$

The equation for $u_{a_2}^*$ becomes

$$u_{a_2}^* = \frac{1-\alpha_2}{1-\alpha_1}\,\frac{u_{a_1}^*}{n_{a_2}^*} . \qquad (1)$$

For the case that $\alpha_1 \ll 1$, or $n_i^* \approx 0$, then

$$u_{a_2}^* = (1-\alpha_2)\,\frac{u_{a_1}^*}{n_{a_2}^*} .$$

Thermal Equation of State

If the plasma is assumed to follow the perfect gas law, then

$$p = (n_a + n_i + n_e)\,\kappa T .$$

From the definition of the degree of ionization

$$n_e = (n_a + n_i)\,\alpha .$$

Substituting n_e in the perfect gas law gives

$$p = (n_a + n_i)(1+\alpha)\,\kappa T .$$

At the upstream equilibrium condition, then

$$p_1 = (n_{a_1} + n_{i_1})(1+\alpha_1)\,\kappa T_1 .$$

Similarly at the downstream equilibrium condition

$$p_2 = (n_{a_2} + n_{i_2})(1+\alpha_2) K T_2 .$$

Defining

$$p^* = \frac{p_2}{p_1}$$

then,

$$p_2^* = \frac{1+\alpha_2}{1+\alpha_1} \frac{n_{a_2}^* + n_{i_2}^*}{1+n_{i_1}^*} T_2^* .$$

After some manipulation, the following expression for the thermal equation of state can be obtained

$$p_2^* = \frac{1-\alpha_1}{1+\alpha_1} \frac{1+\alpha_2}{1-\alpha_2} n_{a_2}^* T_2^* \qquad (2)$$

If $\alpha_1 <<< 1$, then

$$p_2^* = \frac{1+\alpha_2}{1-\alpha_2} n_{a_2}^* T_2^*$$

Momentum Equation

The conservation of momentum for the plasma gives

$$p_1 + \rho_1 u_{a_1}^2 = p_2 + \rho_2 u_{a_2}^2 .$$

When the mass of electrons is neglected in comparison with the total mass of atoms and ions, then the above equation yields

$$1 + \frac{m_a (n_{a_1} + n_{i_1})}{p_1} u_{a_1}^2 = p_2^* + \frac{m_a (n_{a_2} + n_{i_2})}{p_1} u_{a_2}^2 .$$

Substituting p_1 from the thermal equation of state and performing some

simplification give

$$1 + \frac{2}{1+\alpha_1} u_{a_1}^{*2} = p_2^* + 2 \frac{1-\alpha_1}{1+\alpha_1} \frac{1}{1-\alpha_2} n_{a_2}^* u_{a_2}^{*2} . \qquad (3)$$

If $\alpha_1 \ll 1$, then

$$1 + 2 u_{a_1}^{*2} = p_2^* + \frac{2}{1-\alpha_2} n_{a_2}^* u_{a_2}^{*2} .$$

Energy Equation

The conservation of energy for the plasma gives

$$\frac{1}{2} u_{a_1}^2 + h_1 = \frac{1}{2} u_{a_2}^2 + h_2 ,$$

where,

$$h = \frac{\gamma}{\gamma-1} R_a T (1+\alpha) + \alpha R_a T_o$$

and T_o is the ionization temperature. Substituting h into the energy equation and performing some simplification yield

$$u_{a_1}^{*2} + \frac{\gamma}{\gamma-1}(1+\alpha_1) + \alpha_1 T_o^* = u_{a_2}^{*2} + \frac{\gamma}{\gamma-1}(1+\alpha_2) T_2^* + \alpha_2 T_o^* , \qquad (4)$$

where

$$T_o^* = \frac{T_o}{T_1} .$$

If $\alpha_1 \ll 1$, then

$$u_{a_1}^{*2} + \frac{\gamma}{\gamma-1} = u_{a_2}^{*2} + \frac{\gamma}{\gamma-1}(1+\alpha_2) + \alpha_2 T_o^* .$$

Saha Relation

There are several Saha's relations available in the literature. As an example, Scheibe [40] proposed the following expression for the degree of ionization of argon:

$$\alpha = \frac{1}{\sqrt{\frac{p}{T^{5/2}} \cdot \frac{10^4}{2 + e^{-\frac{2060}{T}}} e^{\frac{182000}{T}} + 1}}, \tag{5}$$

where, p is in cm Hg and T is in °K. Combining E uations (1) and (4) gives

$$T_2^* = \frac{\gamma - 1}{\gamma} \frac{1}{1+\alpha_2} \left\{ \left[1 - \left(\frac{1-\alpha_2}{1-\alpha_1} \right) \frac{1}{n_{a_2}^*} \right] u_{a_1}^{*2} + \frac{\gamma}{\gamma - 1} (1+\alpha_1) + (\alpha_1 - \alpha_2) T_o^* \right\}. \tag{6}$$

Similarly, substituting Equation (1) into Equation (3) yields

$$p_2^* = 1 + \frac{2}{1+\alpha_1} u_{a_1}^{*2} \left[1 - \frac{1-\alpha_2}{1-\alpha_1} \frac{1}{n_{a_2}^*} \right] \tag{7}$$

From thermal equation of state

$$p_2^* = \frac{1-\alpha_1}{1+\alpha_1} \frac{1+\alpha_2}{1-\alpha_2} n_{a_2}^* T_2^*,$$

or

$$n_{a_2}^* = \frac{1+\alpha_1}{1-\alpha_1} \frac{1-\alpha_2}{1+\alpha_2} \frac{p_2^*}{T_2^*}. \tag{8}$$

By given the upstream equilibrium conditions, Equations (5) - (8) have to

be solved simultaneously to obtain α_2 , T_2^*, p_2^*, and $n_{a_2}^*$. Then from the continuity equation and the definition of the degree of ionization, $u_{a_2}^*$ and $n_{i_2}^*$ can be obtained, respectively.

APPENDIX III

DERIVATION OF MEAN IONIZATIONAL COLLISION FREQUENCY DUE TO ELECTRON-ATOM COLLISIONS

The mechanism of ionization in argon by single electron impact has been studied experimentally by Bleakney [41]. The results gave probabilities of argon ionization as a function of the electron velocity. The ionization potential for singly ionized argon was given at 15.7 electron volts. Within the range of the electron velocities which will be considered in Chapter V, the following expression for probabilities of argon ionization can be used

$$P_B = 9.338289962\,92 \left(\frac{v_e^2}{v_o^2} - 1 \right), \tag{1}$$

where, P_B is the probability due to Bleakney [41].

It is noted that P_B has units of numbers of ions per incident electron per cm path per mm pressure at 0 °C. Thus, the ionizational collision cross-section of e - a collisions in argon is given by

$$Q_{ea} = 2.638327275\,76 \times 10^{-16} \left(\frac{v_e^2}{v_o^2} - 1 \right), \quad cm^2, \tag{2}$$

for $v_e \geqslant v_o$.

According to Sutton and Sherman [32] the collision frequency of one electron (at $v_e \geqslant v_o \gg \sqrt{2R_a T_a}$) with argon atoms can be approximated by

$$\nu_{ea} = n_a Q_{ea} v_e . \tag{3}$$

The number of electrons with velocities between v_e and $v_e + dv_e$ is $4\pi v_e^2 f_e \, dv_e$. The average collision frequency of electrons at $v_e \geq v_o$ with argon atoms can be obtained as follows

$$n_e' \nu_{ea_I} = \int_{v_o}^{\infty} \nu_{ea} \left[4\pi v_e^2 f_e \, dv_e \right], \tag{4}$$

where n_e' is the number density of energetic electrons with $v_e \geq v_o$. Using Equations (2) and (3) gives

$$n_e' \nu_{ea_I} = \int_{v_o}^{\infty} n_a Q_{ea} v_e \left[4\pi v_e^2 f_e \, dv_e \right] \tag{5}$$

If it is imagined that a cloud of Maxwellian electrons were colliding with another cloud of argon neutral particles, then

$$n_e' \nu_{ea_I} = \int_{v_o}^{\infty} \left[2.6383272757 6 \times 10^{-16} n_a v_e \left(\frac{v_e^2}{v_o^2} - 1 \right) \right] \cdot \left\{ 4\pi v_e^2 n_e \left(\frac{m_e}{2\pi K T_e} \right)^{3/2} e^{-\frac{m_e v_e^2}{2KT_e}} \, dv_e \right\}. \tag{6}$$

After integration and simplification, there results

$$\nu_{ea_I} = 5.2766545515 2\sqrt{\pi} \, n_a \frac{n_e}{n_e'} \sqrt{2R_e T_e} \left[1 + \frac{2}{\left(\frac{v_o^2}{2R_e T_e} \right)} \right] e^{-\frac{v_o^2}{2R_e T_e}} . \tag{7}$$

BIBLIOGRAPHY*

1. Jukes, J. D., "The Structure of a Shock Wave in a Fully Ionized Gas," J. Fluid Mech., 3, 275 (1957).
2. Petschek, H., and Byron, S., "Approach to Equilibrium Ionization Behind Strong Shock Waves in Argon," Ann. Phys., 1, 270 (1957).
3. Greenberg, O. W., Shen, H. K., and Tréve, Y. M., "Hydrodynamic Model of Diffusion Effects on Shock Structure in a Plasma," Phys. Fluids, 3, 379 (1960).
4. Greenberg, O. W., and Tréve, Y. M., "Shock Wave and Solitary Wave Structure in a Plasma," Phys. Fluids, 3, 769 (1960).
5. Mott-Smith, H. M., "The Solution of the Boltzmann Equation for a Shock Wave," Physical Review, 82, 885 (1951).
6. Truitt, R. W., "Thermal Ionization Behind Strong Shock Waves," J. AIAA, 1, 2175 (1963).
7. Grewal, M. S., and Talbot, L., "Shock-wave Structure in a Partially Ionized Gas," J. Fluid Mech., 16, 573 (1963).
8. Jaffrin, M. Y., and Probstein, R. F., "Structure of a Plasma Shock Waves," Phys. Fluids, 7, 1658 (1964).
9. Morgan, E. J., and Morrison, R. D., "Ionization Rates Behind Shock Waves in Argon," Phys. Fluids, 8, 1608 (1965).
10. Jaffrin, M. Y., "Shock Structure in a Partially Ionized Gas", Phys. Fluids, 8, 606 (1965).
11. Skalafuris, A. J., "The Structure of a Shock Front in Atomic Hydrogen II. The Region of Internal Relaxation," Astrophys. J.,

142, 351 (1965).

12. Hoffert, M. I., and Lien, H., "Quasi-One-Dimensional, Non-equilibrium Gas Dynamics of Partially Ionized Two-Temperature Argon," Phys. Fluids, 10, 1769 (1967).

13. Chubb, D. L., "Ionizing Shock Structure in a Monatomic Gas," Phys. Fluids, 11, 2368 (1968).

14. Bhatnagar, P. L., Gross, E. P., and Krook, M., "A Model for Collision Process in Gases. I. Small Amplitude Process in Charged and Neutral One-Component Systems," Physical Review, 94, 511 (1954).

15. Gross, E. P., and Krook, M., "Model for Collision Processes in Gases: Small-Amplitude Oscillations of Charged Two-Component Systems," Physical Review, 102, 593 (1956).

16. Hu, P. N., and Ziering, S., "Kinetic Model for Three-Component Plasmas with Ionization," Phys. Fluids, 9, 1983 (1966).

17. Chadrasekhar, S., Radiative Transfer, Dover, New York (1960).

18. Huang, A. B., and Giddens, D. P., "The Discrete Ordinate Method for the Linearized Boundary Value Problems In Kinetic Theory of Gases," in Rarefied Gasdynamics, Edited by C. L. Brundin, Academic Press (1967).

19. Huang, A. B., and Giddens, D. P., "Kinetic Theory of the Transient Development of Couette Flow Between Parallel Plates," Physics of Fluids, 11, 446 (1968).

20. Huang, A. B., Giddens, D. P., and Bagnal, C. W., "Rarefied Gas Flow Between Parallel Plates Based on the Discrete Ordinate Method," Phys. Fluids, 10, 498 (1967).

21. Huang, A. B., Giddens, D. P., "The Discrete Ordinate Method for Unsteady Linearized Boltzmann-Bhatnagar-Gross-Krook Equation," Phys. Fluids, 10, 232 (1967).

22. Huang, A. B., and Giddens, D. P., "Rayleigh's Problem at Low Mach Numbers Based on Kinetic Theory," J. AIAA, 5, 1354 (1967).

23. Huang, A. B., "A General Discrete Ordinate Method for the Dynamics of Rarefied Gases," School of Aerospace Engineering, Georgia Institute of Technology, Rarefied Gasdynamics Report No. 4 (1967).

24. Huang, A. B., and Hartley, D. L., "Nonlinear Rarefied Couette Flow with Heat Transfer," Phys. Fluids, 11, 1321 (1968).

25. Huang, A. B., and Hartley, D. L., "Nonlinear Rarefied Rayleigh's Problem," J. AIAA, 6, 2023 (1968).

26. Huang. A. B., and Hwang, P. F., "Nonlinear Rarefied Couette Flow with Heat Transfer in Polyatomic Gas", ASME Winter Annual Meeting, Los Angeles, California (1969).

27. Giddens, D. P., Huang, A. B., and Young, V. Y. C., "Study of the Shock Structure Problem by the Discrete Ordinate Method," the 20th Congress of the International Astronautical Federation, Mar del Plata, Argentina (1969).

28. Giddens, D. P., Barbarika, H. F., and Huang, A. B., "Shock Structure of a Diatomic Gas," the 7th International Symposium on Rarefied Gas Dynamics, Pisa, Italy (1970).

29. Tidman, D. A., "Structure of a Shock Wave in Fully Ionized Hydrogen," Physical Review, 111, 1439 (1958).

30. Morse, T. F., "Kinetic Model Equations for a Gas Mixture," Phys. Fluids, 7, 2012 (1964).

31. Hamel, B. B., "Kinetic Model for Binary Gas Mixtures," Phys. Fluids, 8, 418 (1965).

32. Sutton, G. W., and Sherman, A., Engineering Magnetohydrodynamics, (McGraw-Hill, New York) p. 88 (1965).

33. Rose, D. J., and Clark, M., Jr., Plasma and Controlled Fusion, (MIT Press, Cambridge, Massachusetts), p. 163 (1961).

34. Young, V. Y. C., "A Study of the Shock Structure Problem by the Discrete Ordinate Method," Special Problem for M.S., The School of Aerospace Engineering, The Georgia Institute of Technology (1969).

35. Private communication with P. F. Hwang.

36. Amdur, I., and Mason, E. A., "Properties of Gases at Very High Temperatures," Phys. Fluids, 1, 370 (1958).

37. Shkarofsky, I. P., Bachynski, M. P., and Johnston, T. W., "Collision Frequency Associated with High Temperature Air and Scattering Cross-Sections of the Constituents," Planetary Space Sci., 6, 24, (1961).

38. Chapman, S., and Cowling, T. G., The Mathematical Theory of Non-uniform Gases (Cambridge University Press, London), p. 311 (1964).

39. Vincenti, W.G., and Kruger, C. H., Jr., Introduction to Physical Gas Dynamics (John Wiley and Sons, Inc., New York) p. 282 (1965).

40. Pai, S. I., Magnetogasdynamics and Plasma Dynamics, (Prentice-Hall, N. J.)(1962).

41. Bleakney, W., "Ionization Potentials and Probabilities for the Formation of Multiply Charged Ions in Helium, Neon, and Argon," Physical Review, 36, 1303 (1930).

*Abbreviations used herein follow the form employed by the American Institute of Physics.

VITA

Chien-Shiong Lu was born in Keelung, Taiwan, China on September 3, 1937. His parents are Nien-Wang and Fong-Shiang Lu. On August 20, 1966, he married the former Hue-Shiang Chou of Chia-Yi, Taiwan, China.

After graduation from the An-Lo Elementary School in Keelung, he attended the Taiwan Provincial Keelung Middle School, Pa-Tu, Taiwan where he was graduated in July, 1953. He entered the Taiwan Provincial Taipei Institute of Technology in September, 1953, where he received an honor, and was graduated in Mechanical Engineering in July, 1959. Then he served as a second lieutenant in the Nationalist Chinese Army until February, 1961.

In September, 1961 he entered the Georgia Institute of Technology. The degree of Master of Science in Mechanical Engineering was awarded him in June, 1963. He was an instructor in Mechanical Engineering at Tuskegee Institute during 1962 to 1964. He received a NSF fellowship to attend the Summer Institute of Heat Transfer and Gas Dynamics at the Oklahoma State University, in Summer, 1963. He returned to the Georgia Institute of Technology as a Graduate Research and Teaching Assistant in the School of Mechanical Engineering and the Engineering Experimental Station in 1964. From June, 1965 to September, 1968 he was employed by Lockheed-Georgia Company as an associate scientist in Aerospace Sciences. Then he took an educational leave of absence from Lockheed-Georgia Company and attended the School of Aerospace Engineering, Georgia Tech. He returned to Lockheed-Georgia Company in December, 1970. He is a member of Sigma Gamma Tau, Sigma Xi, and ASEE.